The Use of Sterically Encumbering Ligands for the Stabilisation of Low-Oxidation State Main-Group Element Containing Compounds

Jacques Atkinson-Bodourian

2016–2019

Thesis presented to the School of Chemistry, Monash University, for the degree of Doctor of Philosophy

MONASH University

Declaration

This thesis is an original work of my research and contains no material which has been accepted for the award of any other degree or diploma at any university or equivalent institution and that, to the best of my knowledge and belief, this thesis contains no material previously published or written by another person, except where due reference is made in the text of the thesis.

Signature:

Print Name: Jacques Atkinson-Bodourian

Date: 06/01/2020

In dedication to my grandparents Sydney and Mavis Atkinson, who passed away during the completion of this thesis; and to my beloved dog Coco, who passed away during its writing.

Acknowledgements

The past four years have taught me more about being a scientist than the sum of my prior studies; and if it weren't for the impeccable scientists that grace the Jones research group, this would not be the case. For this, I am forever grateful and hope to take these new founded abilities with me into whatever comes next.

To the sum of the Jones group, thank you for your friendship and support over these last few years; without your assistance, I would never have finished this work. Without your friendship, finishing this work would have been a much more gruelling endeavour.

Specifically, I'd like to thank Dr M Dawkins & Dr J Kelly for their help with X-ray crystallography, as well as their assistance and guidance throughout the PhD. To Juliet Heaton, I thank for her contribution towards the tricyclic and boryl amide projects. To Cory Smith, I'd like to thank for assistance rendered with computational chemistry and providing the middle-lab with some much needed banter. To Dr D Dange, for helping with the bloated administration of the university, and for your general assistance within the labs, thank you. (I'd also like to extend thanks to all those who attended the New Zealand camping trip, "Let's go back to Winnies!")

To my family, I thank you for the support over the past years of study - not just during the PhD but for my entire time at university. Despite the many setbacks we have faced, you have always gotten me back on track. I hope this work and accomplishment gives some solace for the sacrifices made for my education.

And last, but most importantly, I give my sincerest thanks to Professor C Jones for allowing me to conduct this research and obtain my PhD. Without your tutelage, I would not be the scientist I am today nor had the opportunity to meet so some many brilliant scientists. Thank-you!

Abstract

Chapter 1: General Trends in Heavy Main-Group Chemistry

Introduces the fundamental aspects of low-oxidation state main-group chemistry, with an emphasis on group 14 (tetrel chemistry). The consequences of these fundamental aspects are characterised with examples from the literature, with a small section focusing on the reactivity of low-oxidation state group 14 element compounds to exemplify the utility of this chemistry.

Chapter 2: Ligand Design and Synthesis for Low-Oxidation State Main-Group Chemistry

Provides a brief introduction into the aspects of monodentate and bidentate ligand design, focusing on a new classification system to define the factors which allow these ligands to kinetically stabilise low-oxidation state main-group compounds. The chapter goes on to present the pro-ligands developed throughout the PhD candidature, providing both theoretical and experimental data. These results are split into two sections: (1) Tricyclic motif containing amines and (2) boryl amines.

Chapter 3: The Utilisation of Monodentate Ligands Containing Tricyclic Substituents for the Stabilisation of Group 14 Element Complexes

With the utility of low-oxidation state group 14 element chemistry and the pro-ligands established, this details the work conducted using tricyclic containing ligands in group 14 element chemistry. The introduction of said chapter presents the typical coupling/ligation of these ligands to main-group element centres, before discussing the little work done with such ligand systems, focusing on the work of Matsuo and co-workers. The conversion of tricyclic motif containing amines into amides for coupling to group 14 element centres is discussed, as well as our attempts to form low-oxidation state group 14 element compounds.

Chapter 4: The Utilisation of Boryl Amides, Amidinates, and Nacnacs for the Stabilisation of Low-Oxidation Group 14 Complexes

A brief overview of published and unpublished work from within the group, which utilised boryl amines in low-oxidation state group 14 chemistry. Within this overview is contained a summary of amidinate and beta-dikitiminate ligands for the stabilisation of group 14 element compounds. The results sequentially go through the ligands from mono to bidentate, following a similar format to chapter 3: coupling of ligands to element centres followed by the attempted reductions to form low-oxidation state group 14 element compounds.

Chapter 5: The Utilisation of Boryl Amides as Monodentate Ligands for Low-Oxidation State Group 15 Chemistry

The final chapter changes tack and discusses the work accomplished in the area of low-oxidation state group 15 element chemistry. A brief introduction explains the tenants of this chemistry, drawing upon the fundamentals discussed in chapter 1. This introduction details prior and similar work done within this field whilst drawing upon the typical ligand-element coupling reactions discussed in chapter 3, before moving on to discuss the low-oxidation state chemistry of the group 15 elements. Results and discussion cover the previously reported ligands utilised for this project (i.e. boryl amides and benzhydrol based monodentate amides) and the ligation of these ligands to group 15 elements. A focus is given toward the low-oxidation state group 15 element compounds synthesised; primarily, an anionic bismuth cluster stabilised by magnesium cations.

Contents

3 The Utilisation of Monodentate Ligands Containing Tricyclic Substituents for the Stabilisation of Group 14 Element Complexes 96

Abbreviations

9-BBN: 9-borabicyclo[3.3.1]nonan-9-yl

Ac: acetyl/CO_2CH_3

acac: acetylacetonyl

Ad: adamantyl

An: anthracene/anthryl

Ar*: 2,6-$(Ph_2CH)_2$-4-Me-C_6H_2

Ar: aryl group/$C_6H_nR_m$ (n/m: 5-0)

Ar': 2,3,4-Me_3-6-^tBu-C_6H

Ar†: 2,6-$(Ph_2CH)_2$-4-^iPr-C_6H_2

Ar^X: 1,1,4,4,5,5,6,6,8,8-octamethyl-1,2,3,4,5,6,7,8-octahydroanthryl

BBP: boron bis(pyrollidine)/Py_2B

br: broad

bV%: percentage buried volume

C: Celsius

ca.: circa/approximately

cal: calorie (1 kcal = 4.184 J)

cat.: a catalytic amount

cf.: confer/compare with

CycHex/Cyc: cyclohexyl, C_6H_{11}

C1: (R)-(+)-alpha-methylbenzyl

C2: (R)-(+)-1-(1-Naphthyl)ethyl

d: doublet (NMR)

D: donor ligand/Lewis base

d^8-Tol: deuterated toluene/C_7D_8

DAB: Diazobutadiene/{CHN(R)}$_2$

DCM: dichloromethane/CH_2Cl_2

decomp.: decomposed/decomposition

DIBAl-H: diisobutylaluminium hydride/$^iBu_2AlH$

DMAP: p-dimethylaminopyridine

Dep: diethylphenyl/2,6-Et_2-C_6H_3

Dipp: diisopropylphenyl/2,6-$^iPr_2$-C_6H_3

{(^{Dipp}DAB)B}: {CHN(Dipp)}$_2$B

e.g.: *exemplī grătiā*/for example

etc.: *et cetera*/and others

E: element

Et: ethyl/C_2H_5

HBcat: catechol borane

HBpin: pinacol borane

HMDS: hexamethyldisilazane/$(TMS)_2NH$

HOMO: highest occupied molecular orbital

Hz: hertz, s^{-1}

i.e.: *id est*/it is, in other words

^{i}Bu: isobutyl

^{i}Pr: isopropyl, $(CH_3)_2HC$

IPr: 1,3-$Dipp_2$-imidazol-2-ylidene

IR: infrared

Imid: 1-methylimidizole

Ind^R: 1,1,3,3,5,5,7,7-R/R'$_8$-s-hydrindacen-4-ylane

in vacuo: in a vacuum/under vacuum

J: Joule

K: Kelvin

KC$_8$: Potassium graphite

L-Selectride: (^{s}Bu)$_3$BHLi

L: generic ligand

LDA: lithium diisopropyl amide/^{i}Pr$_2$NLi

LUMO: lowest unoccupied molecular orbital

M$^+$: parent molecular ion (M.S.)

M.S.: mass spectrometry

M.p.: melting point

M: generic metal

m: mulitplet (NMR), medium (IR)

M: molar, mol L$_{-1}$

Me: methyl, CH$_3$

mes: mesityl/2,4,6-Me$_3$-C$_6$H$_2$

^{Mes}nacnac: {HC(^{Mes}NCMe)$_2$}

MHz: megahertz, 106 Hz

Mg(I): [({^{Mes}nacnac}Mg)$_2$]

mL: millilitre/1 x 10^{-3} L

MO: Molecular Orbital

mol: mole

nacnac: β-diketonate/HC(RNR')$_2$

NBS: N-bromosuccinimide

^{n}Bu: n-butyl, C$_4$H$_9$

^{n}BuLi: n-butyl lithium

NHC: N-heterocyclic carbene

^{n}j$_{E-E'}$: coupling constant between E and E' separated by n bonds in Hz

NMR: nuclear magnetic resonance spectroscopy

p: principle (orbital)

Ph: phenyl/C$_6$H$_5$

Pn: pnictogen **ppm**: parts per million

PPy: 4-pyrrolidinopyridine

Py: pyrollidine/(C^{2}H^4)^{2}NH

q: quartet (NMR)

R: general organic moiety

s: singlet (NMR), strong (IR)

s: sharp (orbital)

^{s}Bu: sec-butyl

SOJT: second-order Jahn-Teller effect

^{t}Bu: tert-butyl, (CH$_3$)$_3$C

^{t}BuLi: tert-butyl lithium

^{t}Oct: tert-octyl, (CH$_3$)CCH$_2$C(CH$_3$)$_2$

^{t}OctLi: tert-butyl lithium

THF: tetrahydrofuran/(C$_2$H$_4$)$_2$O

TIPS: triisopropylsilyl/(^{i}Pr)$_3$Si

TMC: tetramethyl carbene/1,3,4,5-Me$_4$-imidazol-2-ylidene

TMEDA: tetramethylethylenediamine

TMP-Li: lithium 2,2,6,6-tetramethyl piperidide

TMS: trimethylsilyl/Me$_3$Si

Tbb: 2,6-{(TMS)$_2$CH}$_2$-4-^{t}Bu-C$_6$H$_2$

Tbt: 2,4,6-{(TMS)$_2$CH}$_3$-C$_6$H$_2$

t: triplet (NMR)

UV: ultra violet

v.: very

vide infra: see below

vide supra: see above

viz.: *videlicet (videre licet)*/namely

VT: variable temperature

X: halide/F, Cl, Br, or I

Xyl: 2,6-Me$_2$-C$_6$H$_3$

w: weak (IR)

Å: Angström, 1 x 10^{-10} m

$\Delta_{s \rightarrow t}$: singlet-triplet energy gap

δ: chemical shift in NMR spectroscopy in ppm

η: hapticity

μ: denotes a ligand is bridging

ν/cm^{-1}: wavenumber

$\Delta_{\text{HOMO-LUMO}}$: HOMO-LUMO energy gap

Σ: summation

Chapter 1

General Trends in Heavy Main-Group Chemistry

The chemistry of the main-group elements (s- and p block elements) was somewhat overlooked for the better part of 20th century. Predominantly, this was the consequence of chemists' belief that the main-group elements were locked into few discrete oxidation states (unlike the transition metals: the d-block elements).[1] Because of this, main-group chemistry was underdeveloped and only recently have these beliefs been quelled, allowing for low-oxidation state main-group chemistry to emerge as an expanding field of inquiry.[2,3] One of the most promising current areas of main-group chemistry is the pursuit of low-oxidation state group 14 compounds.

This thesis seeks to focus on low-oxidation state heavy group 14 chemistry; however, some of the principles presented are universal across all of low-oxidation state main-group chemistry.

The purpose of this introduction is to present the background behind low-oxidation state heavy group 14 chemistry and contextualise with examples of low-oxidation state group 14 compounds and their unusual reactivity, essentially, providing a brief overview of low-oxidation, state group 14 chemistry from its realisation to the present.

1.1   Low-Oxidation State Main-Group Chemistry

Low-oxidation state main-group chemistry is dominated by elements stabilised and, or, utilised in their low-oxidation states (oxidation states not typically stable or common for the element). In the case of the group 14 elements, which are typically found in the +4 oxidation state (or sometimes +2 for the heavier congeners: germanium (Ge), tin (Sn),

and lead (Pb)), the $+2$ and $+1$ oxidation states are deemed as being low-oxidation states[i]. Characteristically, group 14 compounds in their low-oxidation states can possess element-element multiple bonds, e.g. alkenes and alkynes; but, it has only been recently that this characteristic has been likened with the heavier group 14 elements (Si, Ge, Sn and Pb).

For a long time, it was the paradigm that the heavier main-group elements would oligomerise upon reduction: a theorem brought about by the double-bond rule which states 'elements having a principal quantum number greater than two should not be able to form π-π bonds to themselves or with other elements' – essentially limiting multiple element-element bonding to the lighter main-group elements (B, C, N, O etc.).[4] This expectation has long since been refuted, with multiple examples reported of low-oxidation state main-group element compounds containing multiple element-element bonds (many containing the heavier group 14 elements).[5] However, some of the principles of the double-bond rule remain true: it is a fact that the heavier main-group elements form stronger σ bonds than π bonds, and hence multiple element-element bonding is less favourable for these elements than it is for them to oligomerise (with E-E single bonds).[6,7] It is because of this that carbon-carbon multiple bonds are far more prevalent in chemistry (alkene, alkynes etc.) than analogous silicon, germanium, tin and lead multiple bonds.

To circumnavigate these issues, chemists can kinetically stabilise the heavy main-group elements in their low-oxidation states by using sterically hindering substituents (sterically encumbering ligands) – essentially 'trapping' the element into a unstable/non-preferred electronic arrangement. By 'physically' blocking the element's coordination sites via their bulk, these ligands slow the rate of reaction at the main-group centre from undergoing olgiomerisation and decomposition (viz disproportionation), which are thermodynamically favourable.

Thermodynamic stabilisation of low-oxidation state main-group compounds is achieved in concert with kinetic stabilisation (the degree of thermodynamic stability afforded is dependent on the donor element of the ligand and its denticity, discussed in chapter 2). It is inherently difficult to solely stabilise these compounds thermodynamically as they are most stable in their higher oxidation states, consequently, kinetic stability is the major stabilising factor. However, sterically encumbering ligands do influence the thermodynamic preference for which product will be formed during the reduction of the precursor to its low-oxidation state congener. Furthermore, thermodynamically stabilisation reduces their reactivity, theoretically – this will be discussed in greater detail throughout this chapter.

The range of ligands produced to capture these low-oxidation state main-group compounds is as eclectic as those for the transition metals, but all share the characteristic of sterically hindering the element centre through their bulk. Some of the more commonly utilised ligand classes are shown in **figure 1.1**.[8–11]

---

[i]For Ge, Sn and Pb, whilst the $+2$ oxidation state is stable and somewhat common, compounds containing a $+2$ oxidation state Ge, Sn or Pb centre are still considered low-oxidation state group 14 element compounds.
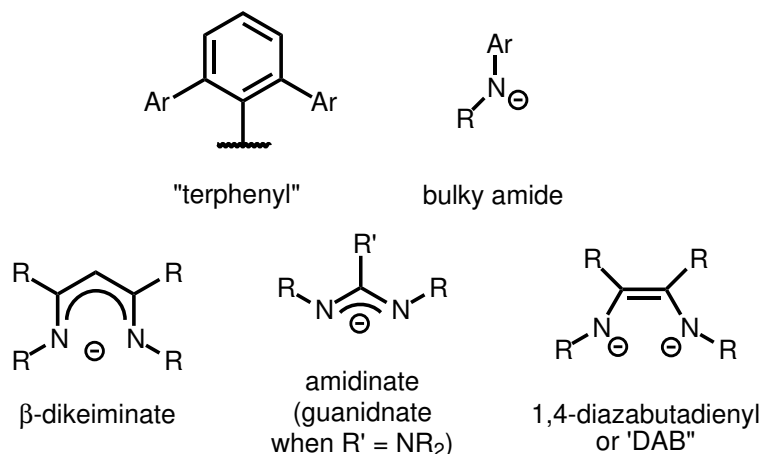
Figure 1.1: Structure and colloquial names of some commonly used sterically encumbering (bulky) ligands.

The very nature of low-oxidation state main-group chemistry limits what ligands can be used in relation to the periodic group and oxidation state being targeted. It is therefore, a constant challenge for low-oxidation state main-group chemists to produce ligands which provide enough kinetic protection, meet the requirements for the low-oxidation state compound being targeted, and which provide the required electronic environment. The ligands employed in low-oxidation state heavy group 14 chemistry will be discussed in greater detail in **chapter 2**, but some examples are presented throughout the rest of this introductory chapter.

1.2   Low-Oxidation State Chemistry of the Heavy Group 14 Elements

The genesis of low-oxidation state group 14 heavy element chemistry was in the 1970's with the synthesis of the first low-oxidation state organotin compound by Lappert and co-workers. This discovery began to erode the concepts preserved by the double-bond rule.[12,13] Termed a distannene **i-1a** (a heavy alkene analogue), it is a dimeric tin compound that readily dissociates to give the monomeric stannylene **i-1b** (a heavy carbene analogue) (**scheme 1.1**).[14] As the first multiply bonded heavy group 14 compound isolated, **i-1** heralded an epoch for low-oxidation state main-group chemistry. However, due to the dissociation of the tin-tin multiple bonds in solution the double-bond rule was not completely supplanted at this stage. But, upon the discovery and isolation of the first stable silene **i-1c** (Si=C containing compound) the double-bond theorem was discredited.[15]
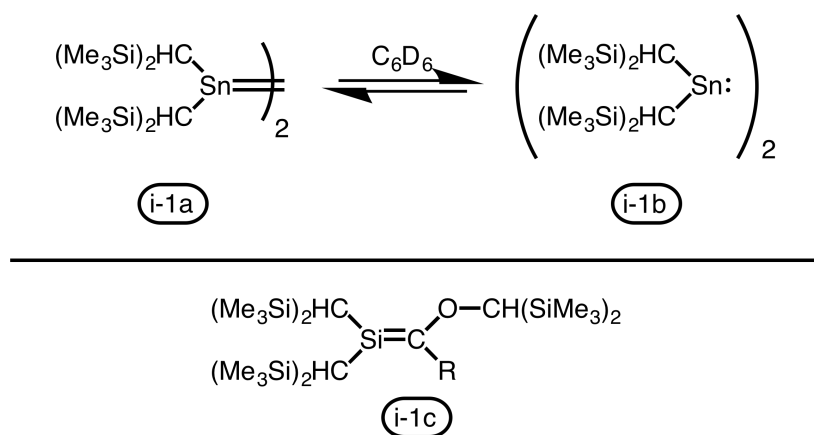
Scheme 1.1: *First reported distannene **i-1a** and dissociation to the stannylene **i-1b** (top); First stable silenes **i-1c** (where R =^{t}Bu/CEt$_3$/1-adamantyl) (bottom).*

Following these discoveries, multiple examples of other low-oxidation state main-group complexes begun to be synthesised and reported – including low-oxidation state silicon, germanium, tin, and lead compounds in the +2 and +1 oxidation states[ii] (**figure 1.2**).[16,17]
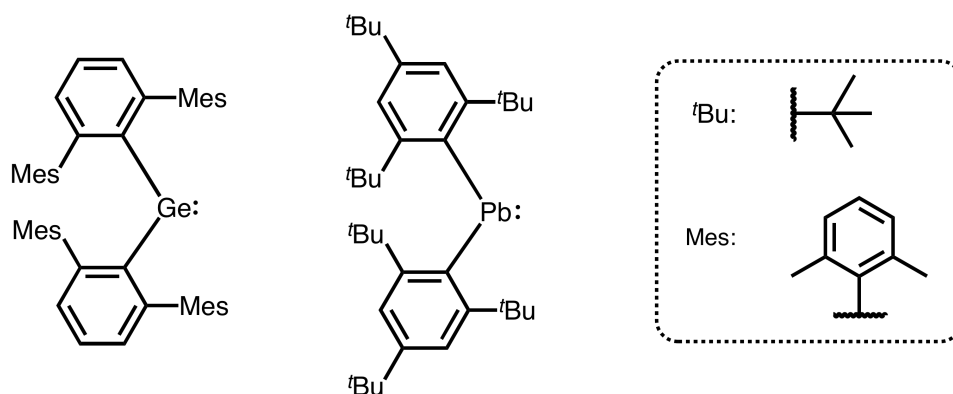
Figure 1.2: *Two examples of low-oxidation state heavy group 14 element compounds: a germyleme (left) and plumbylene (right).*

Chemists moved from isolating the group 14 elements in their +2 oxidation state to the +1 oxidation state – pushing the boundaries of the time – and with the turn of the century the first heavy alkyne analogue was isolated, a diplumbyne (**scheme 1.2**).[18] Subsequently disilynes, digermynes and distannynes followed, highlighting unique chemical property trends as the group is descended.[19–21]   The synthesis of these compounds highlights a common route to these low-oxidation state species, the reduction of halide 'precursors'.

[ii]Generally speaking, low-oxidation state group 14 compounds can be divided into three categories: (I) heavy alkene analogues, where the element centre is in the +2 oxidation state(–ylenes for monomeric, and -enes for dimeric); (II) heavy alkyne analogues, where the element centre is in the +1 oxidation state (-yne for monomeric, and di-yne for dimeric); and (II) radical species.
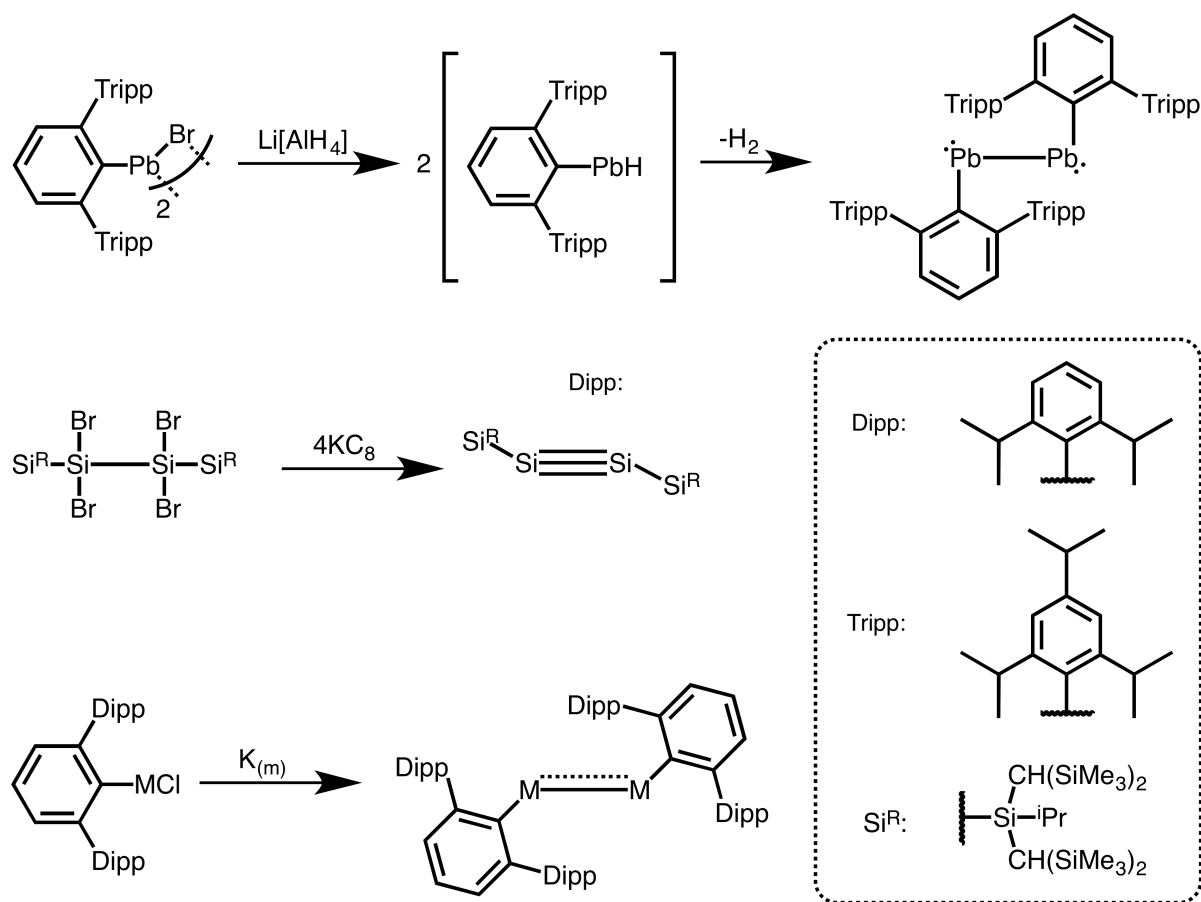
Scheme 1.2: Synthesis of heavy alkyne analogues: dipumbyne (top), disilyne (middle), and digermyne/distannyne (where M = Ge, Sn).

The isolation of the heavy alkyne analogues illustrated the unique element-element 'trans-bent' bonding motif, a characteristic that increases upon descent of the group, and indicates the unique electronic configuration of the element centres within this class of compounds.

1.2.1   Bonding In Heavy Alkene and Heavy Alkyne Analogues

The bonding geometry of alkenes ($R_2C=CR_2$), and alkynes ($RC\equiv CR$), are linear and planar: a characteristic that does not conform to the bonding geometries displayed for the heavier analogues.[22] For the heavy alkene and alkyne analogues, an increased bond angle at the group 14 element is observed as the group is descended: the bonds are said to 'bend' and it is most pronounced within the heavy alkyne analogues (**figure 1.3**). It is a phenomenon called trans-bending and is intrinsic to the low-oxidation state group 14 element compounds.
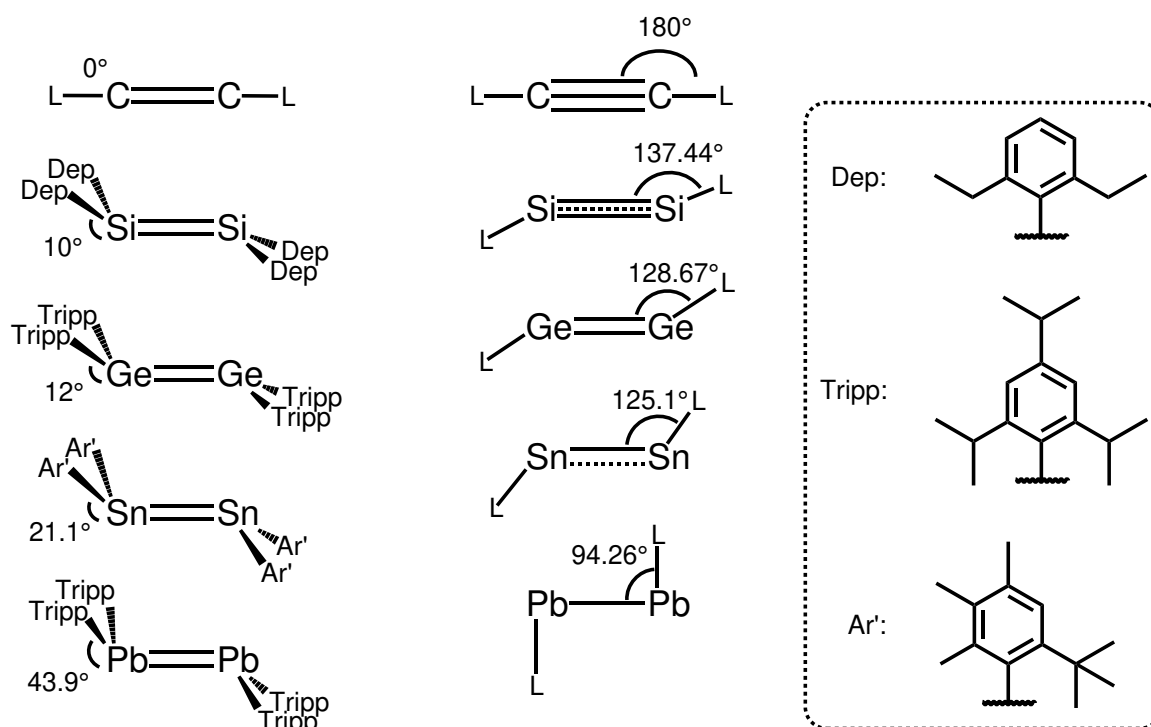
Figure 1.3: L-M-M bond angles of group 14 double bonded compounds (left), and triple bonded compounds (right). (where Dep = 2,6-Et$_2$-C$_6$H$_3$, and Ar'= 2,3,4-Me$_3$-6-^{t}Bu-C$_6$H).[23–26]

The phenomenon of trans-bending is a result of a variety of factors which are intricately connected and amplify as the group is descended, but can be compartmentalised into the following: (I) an increase in the $s{:}p$ orbital size ratio and orbital diffusiveness; (II) the inert pair effect; and (III) poorer orbital hybridisation. The magnitude of these factors strengthen as the group is descended. Overarching, it is (III) that leads to trans-bending but itself is a consequence of (I) and (II) which will be discussed here.

Before continuing, it is to be noted that the following factors also influence the tendency for the heavier group 14 elements to become increasingly stable in the +2 oxidation state over the +4 oxidation state i.e. Ge, Sn, and Pb are found to be relatively stable in +2 oxidation state whilst C and Si are not. This is important for future reference: the extent of kinetic stabilisation required for the heavier elements is somewhat lessened and so some sterically encumbering ligands can stabilise Ge, Sn, and Pb in the +2 oxidation state but not necessarily Si. Please note, this is a generalised/practical statement, the actual situation for this compound class is more complex.

(I) When going down group 14 there is an increase in the s:p orbital size ratio, where the p orbitals increase in size at a higher rate than the s orbitals.[27] Due to this contrast in s:p orbital size, hybridisation becomes more difficult in the heavier elements. In the case of

carbon, the s and p orbitals are similar in size allowing for hybridisation compared to the heavier elements that bond with higher p orbital character leaving two non-bonding electrons with higher s orbital character as a lone pair. This is best exemplified by comparing carbene (CH_2) and carbyne (CH) with the heavier analogues (EH_n, E = Si, Ge, Sn, or Pb; n = 1 or 2)(**figure 1.4**).
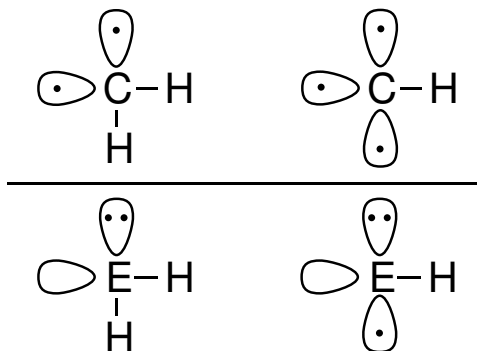
Figure 1.4: Carbene in a triplet state and carbyne in a quartet state (top, left to right respectively); the heavy group 14 analogues of a carbene in a singlet state and carbyne in a doublet state (bottom, left and right respectively) (where E = Si, Ge, Sn or Pb).

Hybridisation of the s and p orbitals allows carbenes and carbynes to adopt a triplet and a quartet electronic configuration, respectively. The reduced hybridisation of the heavier analogues leads to the adoption of a singlet and doublet electronic configuration, respective to the carbene and carbyne analogues (**figure 1.4**). This exhibited reduced hybridisation is amplified by the inert pair effect (II).

(II) The inert pair effect states that for the p block elements, when going down the group, that the n-2 oxidation state (n = max valency for a group, i.e. for group 14, 4 is the max valency) is predominantly more stable with two s orbital electrons remaining localised in the s orbital as a lone pair.[28] For germanium and tin, this effect is attributed to the d-block contraction: the poor electron shielding provided by the electron filled d-orbitals leads to a higher effective nuclear charge on the valence s orbital electrons, binding them more strongly to the nucleus and hence rendering them inert.[29] For lead, the d-block contractions is combined with the f-block contraction (where like the d-block contraction, the f-block contraction leads to a greater effective nuclear charge felt by the valence s electrons), and relativistic effects which are discussed here.

The special theory of relativity states that the faster an object moves the heavier it becomes, reaching an infinite mass at the speed of light. With 82 protons in its nucleus, the electrons of the lead atom are subjected to a high degree of electrostatic attraction[iii]. To

---

[iii]In fact, lead is the second-to-last stable element on the periodic table – the electrostatic attraction of the lead nucleus is only surpassed by that of bismuth.

compensate for this incredible electrostatic attraction, the electrons of the 1s-orbital move at a greater velocity, maintaining sufficient kinetic energy to not "fall-into" the nucleus. This increase in velocity leads to an increase in mass and induce a contraction of the 1s-orbital. This induction leads to a stabilisation of the valence s orbital electrons, which is why lead is found to be stable in the +2 oxidation state.

(III) The combination of p orbital diffusiveness (I) and the inert pair effect (II) lead to poorer orbital hybridisation (III) which in turn leads to trans-bending as the s orbital electrons lay lower in energy. The unique multiple element-element bonding motif that occurs in the heavy group 14 elements is explained as being a result of dative bonds – or more accurately described by molecular orbital (MO) theory.

Dative Bond Explanation

For the formation of an alkene, the two carbon monomers are electronically configured in the triplet state, leaving two unpaired electrons in the p and sp^2 orbitals; the two monomers approach allowing the unpaired electrons to pair to their counterparts forming a σ bond and a π bond. For the heavier alkene analogues, due to poor hybridisation the two monomer centres conceptually adopt a singlet electronic configuration, leaving a lone pair of electrons within the sp^2 orbitals and a free p orbital. When the two monomers approach electrostatic repulsion occurs (caused by the lone pair of electrons on each centre) and to alleviate this repulsion the monomers rotate divergently, allowing the lone pairs to form two dative π bonds, leading to a trans-pyramidal structure. The sp^2 orbital lone pair electrons donate into the empty p orbital on the opposite monomer. The same occurs on the formation of the heavier alkynes (**figure 1.5**).
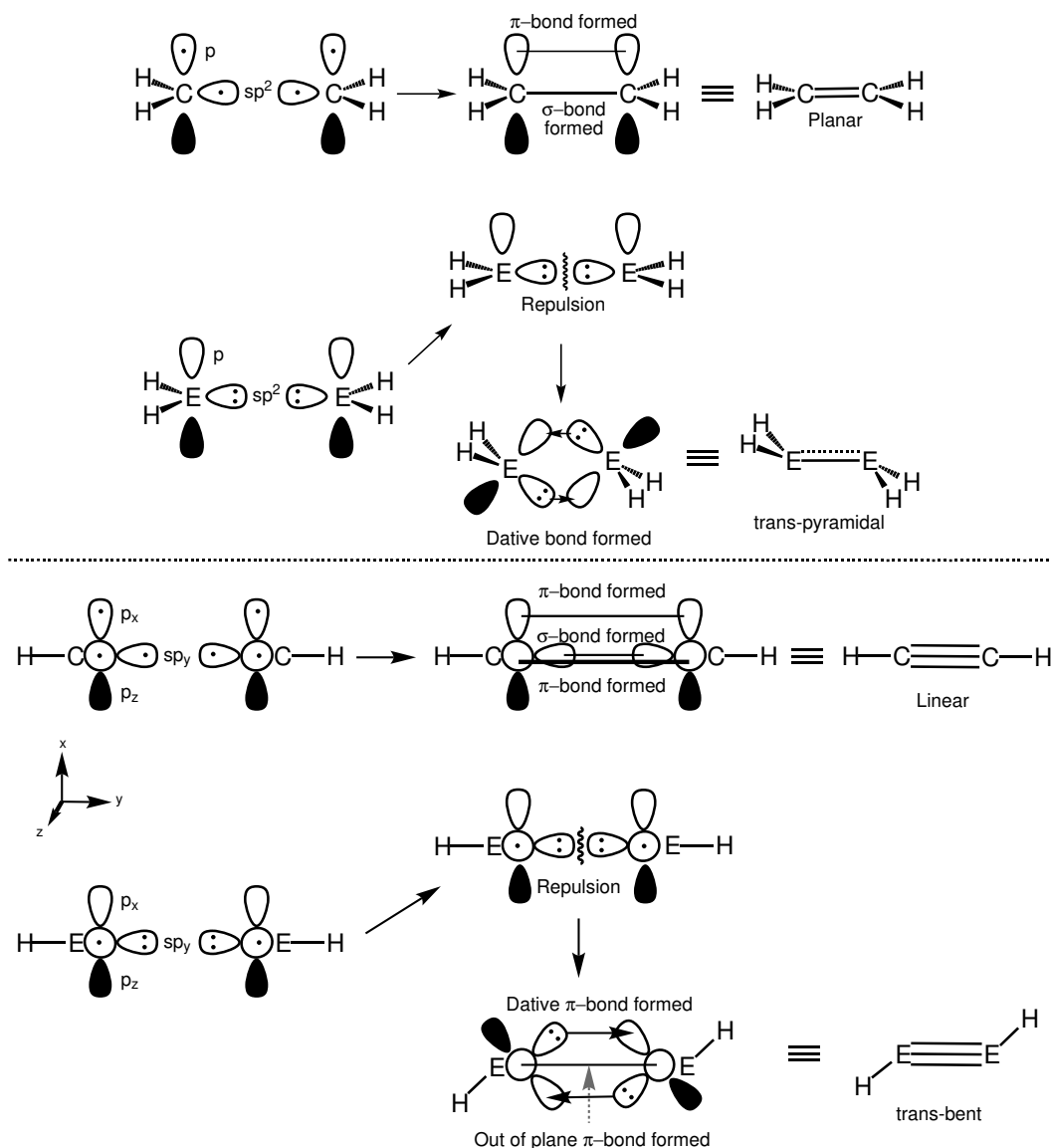
Figure 1.5: Comparison of the formation of double bonds (top) and triple bonds (bottom) between carbon and the heavy group 14 elements (where E = Si, Ge, Sn, or Pb).

The formation of the alkyne occurs in the same manner as for the alkene, however in this case the electronic configuration adopts a quartet state[iv] which leads to the formation of a σ bond and two π bonds. In the formation of the heavy alkynes the monomers adopt a doublet state: a lone pair of electrons in the sp orbital and an unpaired electron in the p_z-orbital. Repulsion between the lone pair sp orbital electrons of the two monomers occurs leading to the formation of two dative bonds, while unpaired electrons located within the p_z-orbitals of each monomer form a π bond, giving one π bond and two dative π bonds.

This explanation is supported by MO theory, which covers the bonding in even greater depth.

[iv]The quartet state is low enough in energy that the electron promotion energy from the doublet to the quartet state (16.7 kcal mol^{-1}) is offset by the formation of the triple bond.[30]

9

Molecular Orbital Theory Explanation

Molecular orbital (MO) theory describes trans-bending as a consequence of bonding and anti-bonding orbitals mixing based on their symmetry. This mixing is favourable for the heavier group 14 elements, but not for carbon – the lightest group 14 element – and is a consequence of the electronic states of the heavier group 14 elements.

In the case of heavy alkenes, the higher energy π orbitals of the heavy group 14 elements are energetically 'close' to their symmetrically equivalent (b_u) σ^* orbital which allows orbital mixing to occur. This is also the case for the π orbital which mixes with the π^*-orbital, both having a_g symmetry. As a result, the $1b_u$, $2a_g$, and $2b_u$ mixed orbitals decrease in energy whilst the $1a_g$ orbital increases in energy[v]; and overall, this mixing is energetically favourable as the total energy of the system decreases. The bent geometry is, therefore, more stable. For carbon, this mixing does not occur as the energy increase of the $1a_g$-orbital is too large to be compensated by the decrease in energy of the other orbitals; therefore, the bent geometry is less stable than the planar geometry. This is exemplified in **figure 1.6** which shows the MOs of ethylene and digermene (the digermene MO diagram is analogous to similar tin and lead derivatives).[22]
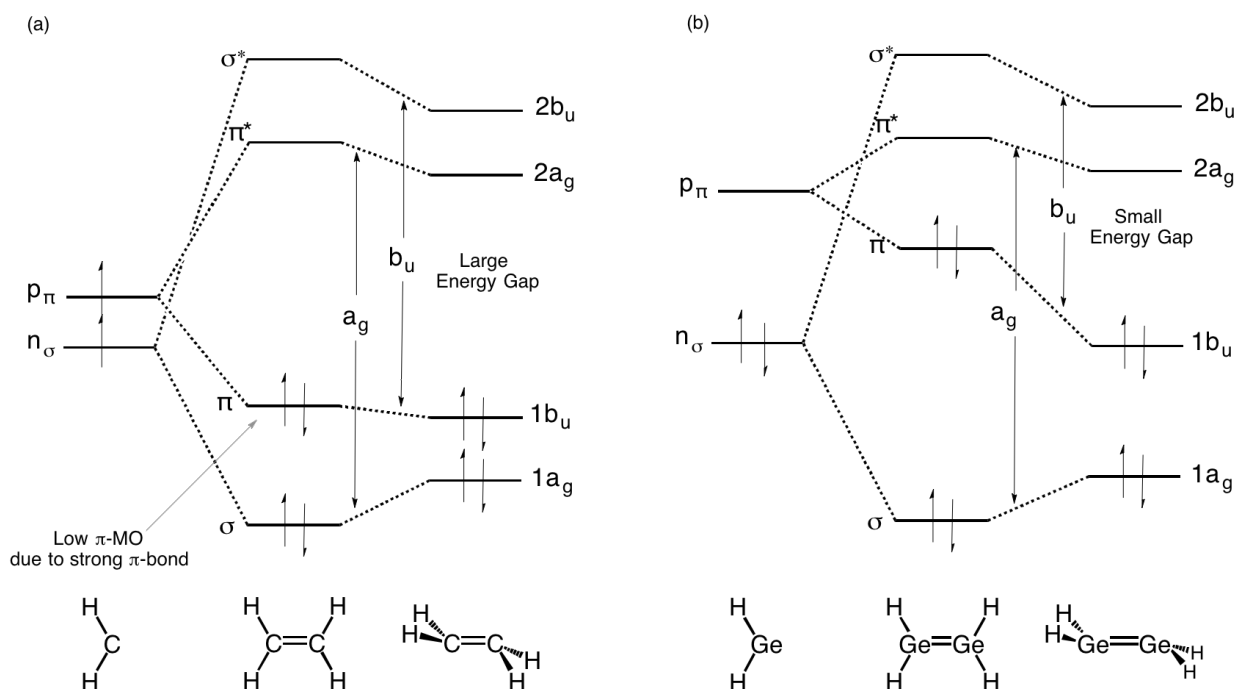
Figure 1.6: Molecular orbital diagrams for ethylene (a) and digermene (b) going from a planar to trans-pyramidal geometry.

---

[v]In the digermene the energy lost vs. gained is -0.47 eV to +0.32 eV, as a consequence of this mixing (**figure 1.7**).

The increased molecular orbital mixing in digermene is due to the smaller energy gap between the π and π^* molecular orbitals, compared to ethylene. The disparity between (a) and (b) is a consequence of the increased n_σ and p_π (these orbitals refer to the parent germylene (b)) energy gap, and the high energy π orbital. The high energy π orbital is due to the weak π bonding experienced by the heavy group 14 elements.

This type of orbital mixing is referred to as the second-order Jahn-Teller effect (SOJT). This mixing occurs when there is a high-energy occupied MO close in energy to a low-lying unoccupied MO (in this case the π and σ^* orbital respectively).[31] This type of mixing can be used to explain the bonding in heavy alkyne analogues. Similar to the SOJT mixing seen for the heavy alkene analogues, mixing occurs between symmetrically equivalent bonding and anti-bonding orbitals: σ and π^*-orbitals, π orbitals and σ^* orbitals. As this mixing occurs the π orbital (which mixes with the σ^* orbital) begins to gain more lone pair character - the bond that forms is referred to as a slipped π orbital (**figure 1.7**).[32] SOJT mixing occurs for the heavy group 14 elements because the bonding and anti-bonding orbital energy gap is much smaller compared to carbon.[33]
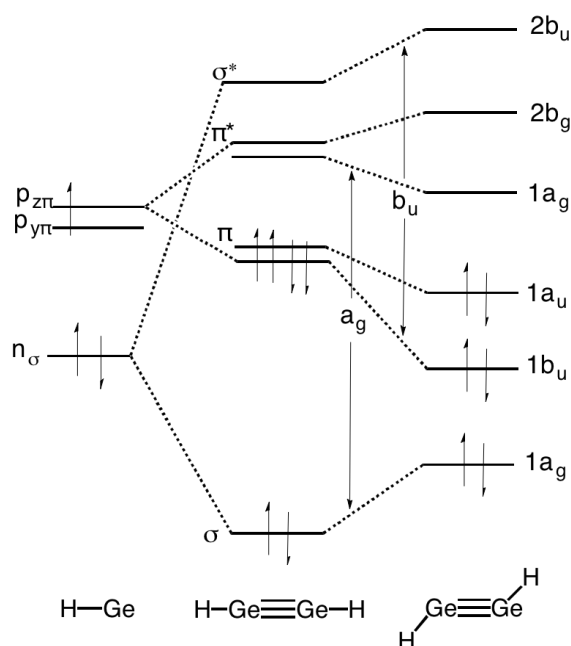
Figure 1.7: Molecular orbital diagram of digermyne in a linear (middle) and trans-bent (right) geometry.

The weaker bonds formed by the heavy alkenes and alkynes can lead to dissociation in solution to give their monomeric counterparts (called tetrylenes or heavy carbene analogues for the +2 oxidation state). These tetrylenes can be isolated in the solid state by adopting the appropriate substituents on the ligands.

1.3 Chemistry of Tetrelyenes (Heavy Carbene Analogues)

Tetrelyenes are neutral compounds containing a two-coordinate group 14 element centre in the +2 oxidation state and are classified as being cyclic or acyclic. **Figure 1.8** illustrates the first examples of stable tetrelyenes: the cyclic silylene and the acyclic germ/stann/plumb-ylenes.[34]
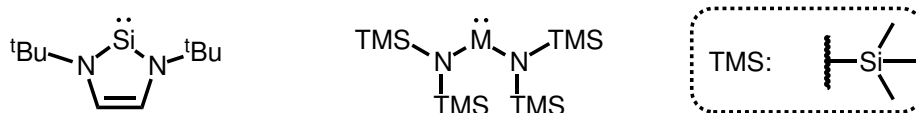
Figure 1.8: The first stable silylene (left) and germ/stann/plumb-ylene (right) (where M = Ge, Sn, Pb).

The tetrelyenes electronic configuration is either in the singlet or triplet state and the energy between these two states influences the chemistry of the tetrelyenes. This singlet-triplet energy gap is intrinsic to these heavy group 14 element compounds and can be altered by substituent effects.

1.3.1 Intrinsic Singlet-Triplet Energy Gap of the Heavy Tetrelyenes

Adopting the same electronic configurations as carbenes, tetrelyenes can exist in the singlet or triplet state.[35] In the singlet state, the valence electrons reside in the n-orbital forming a lone pair, leaving an empty p orbital. For the triplet state, there is one unpaired electron in the n-orbital and another in the p orbital. Whether tetrelyenes adopt a singlet or triplet state is centred upon the energy difference between these n- and p orbitals (the singlet-triplet energy gap: $\Delta_{s \to t}$) being lesser or greater than electron repulsion energy: if electron repulsion of the lone pair is lesser than the $\Delta_{s \to t}$ then the singlet state is favoured, if it is greater than the triplet state is favoured.

The trend seen within the group 14 elements is that the singlet state becomes more stable with increasing weight of the group 14 element (**figure 1.9**).[36–38] This trend is explained by two factors: (1) as the orbitals becomes larger and there is less electron repulsion within these orbitals, stabilising the singlet state; (2) decreased orbital hybridisation and the inert pair effect increases the s character of the n-orbital, lowering its energy and stabilising the singlet state. This is most profound when comparing the parent tetrelyenes H_2Si and H_2C. The lone pair of H_2Si has 89% s character whilst the lone pair of H_2C has 52% s character.[39]
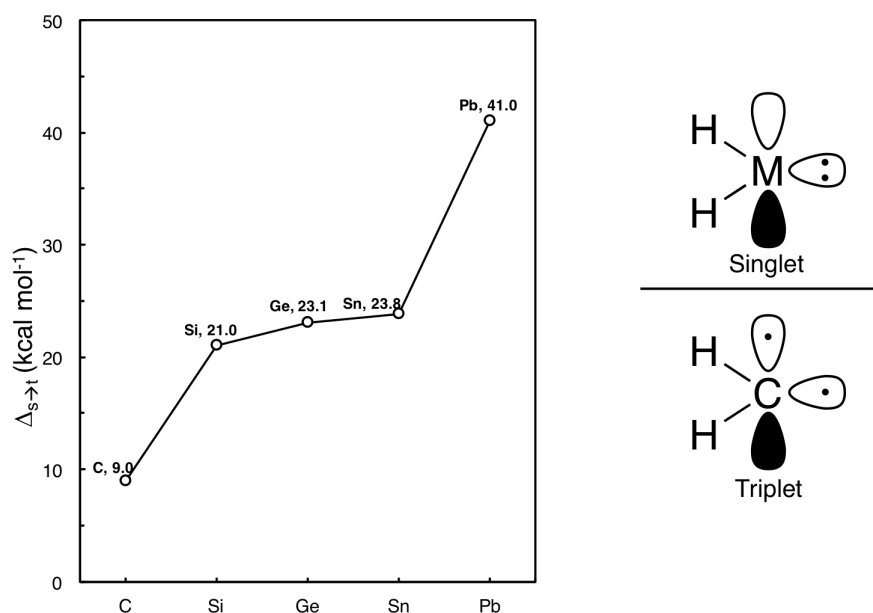
Figure 1.9: The singlet-triplet energy gap $\Delta_{(s \to t)}$ of the parent tetrelylenes (H_2E, E: C to Pb), indicating an increase in singlet stability with an increase in weight of the group 14 element (left); and representations of a singlet and triplet state, top and bottom respectively (right).

The electronegativity of the group 14 element and of the substituents bound to it affects the $\Delta_{s \to t}$. According to Bent's rule, more electronegative elements bind to orbitals with greater p character whilst electropositive elements bind to orbitals with greater s character.[40] Again, using the parent tetrelylenes (H_2M, M = Si, Ge, Sn, or Pb) as an example, when this is applied to the heavier tetrelylenes, the M-H bond is polarised due to the higher electronegativity of the hydrogen, so the M-H bond will have more p character and the lone pair on the group 14 element will have more s character, lowering its energy. The stability of the singlet state is, therefore, increased when group 14 elements bond with electronegative substituents e.g. organic ligands.

1.3.2   Substituent Effects on the Singlet-Triplet Gap of Heavy Tetrelyenes

The singlet-triplet energy gap ($\Delta_{s \to t}$) is not an absolute value for the group 14 elements and can be changed by altering the substituents on the tetrel centre's via electronics (I) and, or steric effects (II). The effects of substituents on the $\Delta_{s \to t}$ can be examined using UV-visisble spectroscopy[vi], where the absorption analysed is the excitation of one electron from the non-bonding orbital to the vacant p orbital.[41]

[vi]An increase in the $\Delta_{s \to t}$ produces a blue shift, whilst a decreased $\Delta_{s \to t}$ produces a red shift.

(I) The electronics of the substituents bound to the group 14 element centre influence the $\Delta_{s \to t}$. Primarily, it is the donor atom of the substituent that has the greatest influence (although, this donor atom is in turn influenced by its own substituents – a domino effect of influence towards the group 14 element, so-to-speak). Most substituents have both a σ and π donating or withdrawing electronic influence on the group 14 element's n- and p orbitals.

Through induction, σ donation causes an increase of the n-orbital's (the lone pair electrons) energy whilst σ withdrawal decreases the energy: electronegative substituents are σ withdrawing and stabilise the singlet state (e.g. F and CF_3) whilst electropositive substituents are σ donating and destabilise the singlet state (e.g. SiH_3). The stabilisation of the singlet state is amplified when electronegative substituents are bound to the group 14 element. Electronegative moieties will bond with more p character and increase the p orbital energy.

π donation and withdrawal has the same influence over the p orbital as σ donation has over the n-orbital: the p orbital energy is raised on electron donation, lowered on withdrawal. This is achieved through the use of n-donor ligands and ligands that have π orbitals which can donate into the p orbital (as described by Bent's rule).

As an example, amides are n-donor ligands – they donate their lone pair electrons – so they increase the p orbital energy, but as they are of a higher electronegativity than the heavy group 14 elements, they are partially σ withdrawing groups, lowering the n-orbital energy of the group 14 element: both influence an increase in $\Delta_{s \to t}$ (**figure 1.10**).
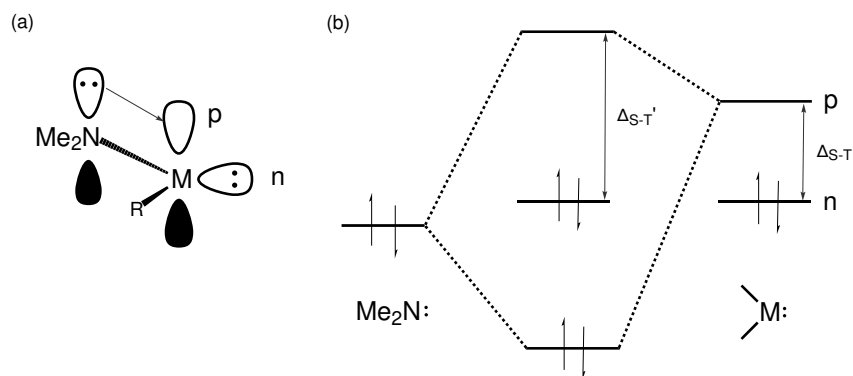
Figure 1.10: Orbital (a) and molecular orbital diagram (b) of n-donor ligands on heavy tetrelylenes (M = Si, Ge, Sn, Pb).

The electronic influence of substituents containing a π orbital can become more complicated, as is the case for vinyl and aryl ligands. Based on what has been said, it would be expected that vinyl and aryl ligands would increase the $\Delta_{s \to t}$ as they can donate electron density into the empty p orbital from their π orbital, but this is not the case.[42] Orbital mixing occurs between the low-lying anti-bonding orbitals of the unsaturated substituent and the 'newly-formed' high-energy anti-bonding orbitals leading to a decrease in the $\Delta_{s \to t}$. This process is

best explained as a two-step process using **figure 1.11**.
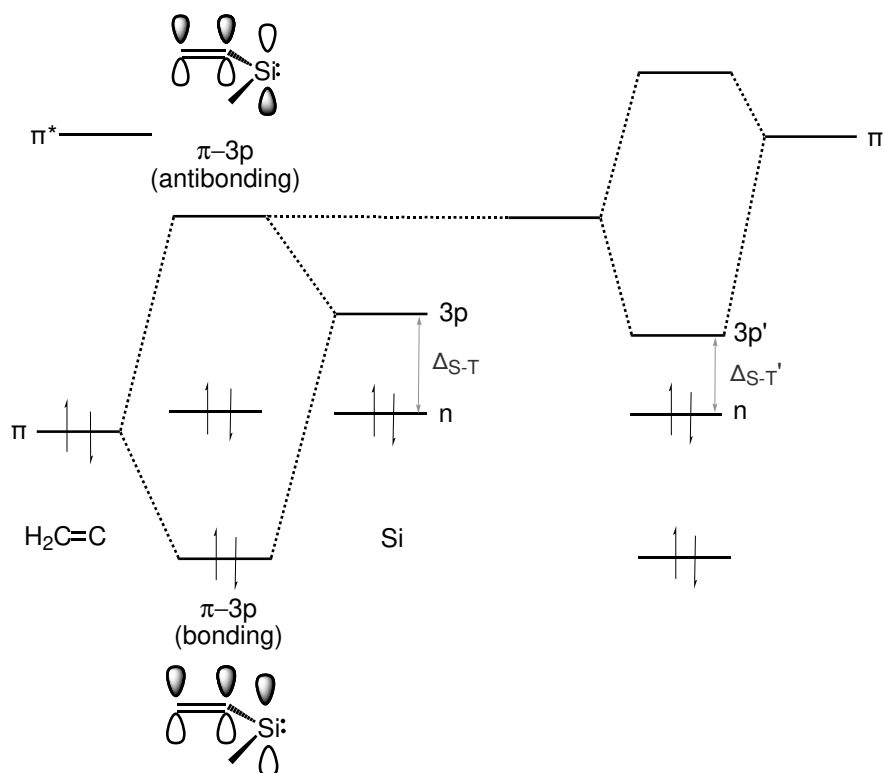
Figure 1.11: Molecular orbital diagram depicting the two-step orbital interaction leading to the decreased $\Delta_{s \rightarrow t}$.

Figure 11 shows the bonding situation between a silylene and an unsaturated substituent (a vinyl group). First, the occupied π orbital of the vinyl group interacts with the $3p$ orbital at the silicon centre, this produces bonding and anti-bonding π $3p$ orbitals. This anti-bonding π $3p$ orbital is high enough in energy to mix with the π^*-orbital of the vinyl ligand, lowering the energy of the $3p$ orbital (termed $3p$' in **figure 11**). This leads to an overall decrease in $\Delta_{s \rightarrow t}$.

(II) Steric factors also affect the $\Delta_{s \rightarrow t}$ of the group 14 element centre. Predominantly, it is the forced bond angle of the substituents about the element centre that lead to an increased or decreased $\Delta_{s \rightarrow t}$. When the bond angle is increased the lone-pair electrons (n-orbital) gains more p character, increasing in energy – the opposite occurs when the bond angle is decreased. This occurs as increasing the bond angle destabilising the n-orbital, and therefore $\Delta_{s \rightarrow t}$ decreases.[43]

This can be seen experimentally by altering the steric encumbrance of the substituents around the silicon centre (**figure 1.12**) – on increasing the steric hindrance there is a shift towards longer wavelengths which indicates a reduced $\Delta_{s \rightarrow t}$.[44]
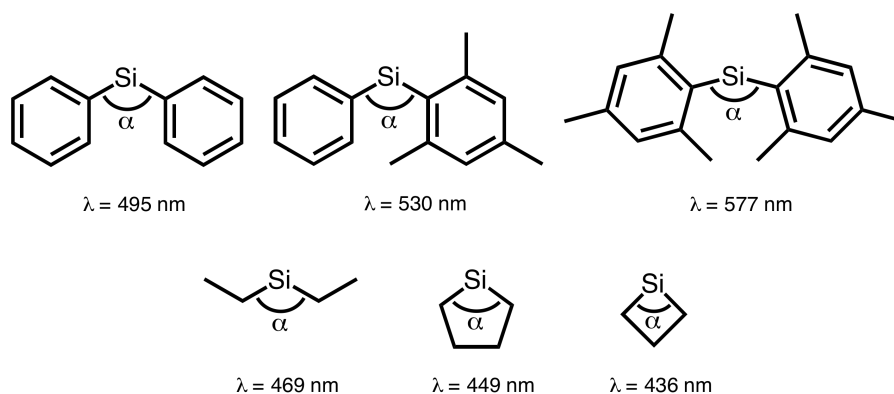
Figure 1.12: A series of silylenes with differing subsitutents and their corresponding λ_{max} (Ph$_2$Si, Ph(Mes)Si, Mes$_2$Si; top, left to right) (Et$_2$Si, cyclo-C$_5$H$_{10}$Si and cyclo-C$_4$H$_8$Si; bottom, left to right).

1.4   Reactivity of Low-Oxidation State Heavy Group 14 Element Compounds

The reactivity of low-oxidation state heavy group 14 compounds is mimetic to transition metal chemistry. This is due to the orbital interactions that arise from SOJT orbital mixing which leaves an empty orbital, capable of accepting electrons, and an orbital containing a lone-pair of electrons, which can be donated. Termed amphiphilic (nucleophilic and electrophilic), it is this electronic characteristic which has led to their use in small molecule activation (e.g. H-H bond activation), bond activation (e.g. C-X bond activation), reversible activation, and reductive elimination (**figure 1.13**).
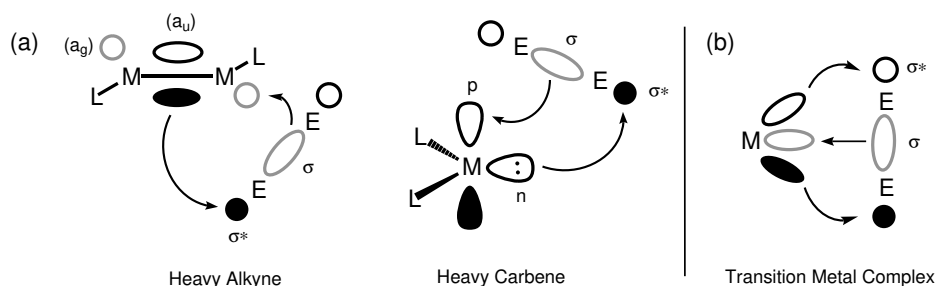
Figure 1.13: Diagram depicting the orbital interactions between a small molecule (e.g. H$_2$,H$_2$C=CH$_2$) with heavy alkyne/ carbene analogues (a) (M= Si, Ge, Sn, Pb) and transition metal complexes (b) (M = transition metal).

1.4.1   Cleavage of σ Bonds at Group 14 Centres

The cleavage of σ bonds (i.e. H-H, N-H, C-X) is an important event in most catalytic cycles. Until recently, this has remained within the domain of transition metal complexes, but recent

advances have shown the capacity of low-oxidation state group 14 compounds to activate these bonds.[45]

First reported in 2005, Power et al. disclosed the reaction of dihydrogen with the digermyne **i-1d** to give a mixture of hydrogenated digermanes and germanes.[46,47] This constituted the first example of un-catalysed activation of dihydrogen by a main-group molecule at room temperature (**scheme 1.3**).
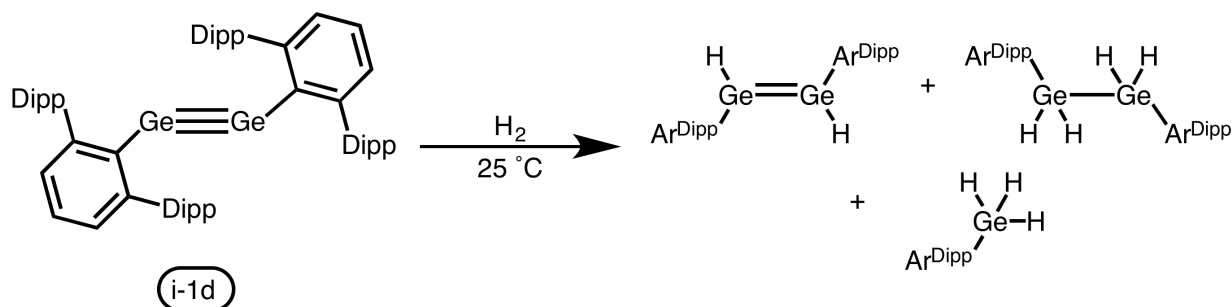
*Scheme 1.3: Un-catalysed activation of dihydrogen by Power's digermyne **i-1d**.*

This unprecedented main-group compound reactivity is due to the high energy (pseudo) lone pair electrons and the available empty orbital (π^*-orbital) i.e. the a_u and a_g molecular orbitals which act as electron donors/acceptors, respectively. **Figure 1.14** illustrates this electronic configuration and should be considered as the base-model orbital situation for heavy alkyne bond activation.
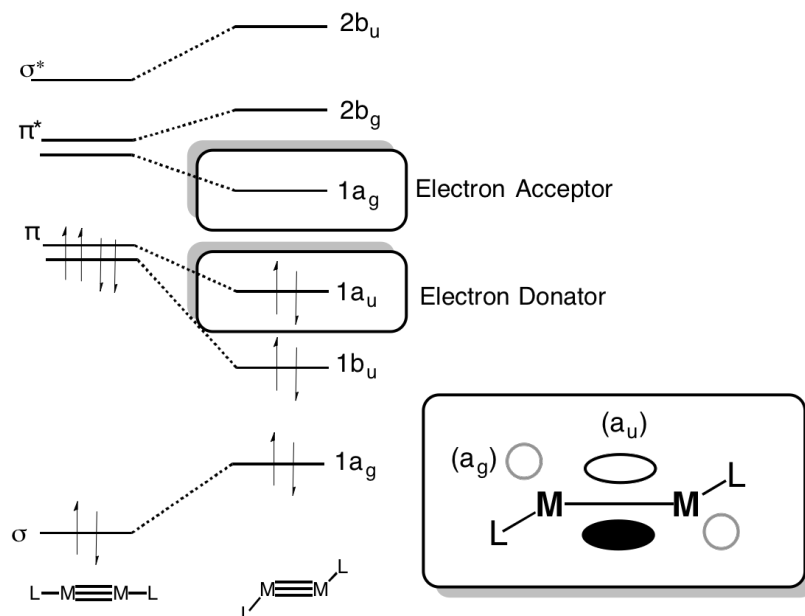
Figure 1.14: Molecular orbital diagram of heavy alkyne analogues, highlighting the electron donor ($1a_u$: pseudo lonepair) and acceptor ($1a_g$: π^*-orbital) orbitals.

The discovery of **i-1d** to activate dihydrogen inspired chemists to explore the ability of low-oxidation state group 14 compounds to activate other small molecules and their ability to activate strong C-X bonds (X = halogen). All the compounds act in a similar fashion to **i-1d**, having available electron density to donate and empty orbitals which can accept electron density.

The following sections will explore σ bond cleavage at heavy carbenes and heavy alkyne group 14 centres[vii].

H-H Bond Activation

Aldridge, Jones, and Mountford reported the silylene **i-1e** (where silicon is in the + 2 oxidation state), which activates dihydrogen to give the corresponding dihydrosilane **i-1f** (**scheme 1.4**).[47] **i-1e**'s reactivity is due to the increased p character of the lone pair electrons, a result of the strong σ-donor group and increased bond angle (obtuse) at silicon[viii]. Both these factors increase the n-orbital energy and lower the HOMO-LUMO energy gap (also known as the singlet-triplet energy gap: $\Delta_{s\rightarrow t}$)
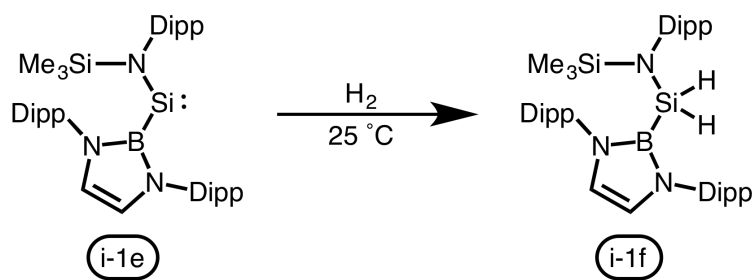
Scheme 1.4: First reported activation of dihydrogen by a silylene compound.

More recently, Inoue et al. reported the activation of dihydrogen by the 'masked silylene'/silepin **i-1g** (**scheme 5**). **i-1g** is in equilibrium with the 'un-masked silylene' **i-1h** which can undergo hydrogenation to form the dihydrosilane **i-1i** at elevated temperatures. Like **i-1e**, the un-masked silylene **i-1h** contains an imine-like ligand which is a strong σ-donor group; this combined with the donating silyl ligand decreases the HOMO-LUMO gap allowing for this reactivity[ix].[49]

[vii]Nikonov, G.I. and Chu, T. provide an excellent review of main-group reactivity in the paper titled: 'Oxidative Addition and Reductive Elimination at Main-Group Element Centers'.[45]

[viii]For comparison, the B-Si-N bond-angle seen in **i-1e** is 118.1(1)°vs 90.52°to 100.05(2)°for S-Si-S in (ArS)2Si; the HOMO-LUMO gap is 1.96 eV for **i-1e** vs. 4.26 eV for $(ArS)_2Si$.[48]

[ix]These 'masked' low-oxidation state main-group element compounds may be a new area of study; the silepin is not sensitive overtly sensitive to oxygen or moisture allowing it to be handled in non-inert atmospheric conditions, unlike the low-oxidation state silylenes reported to date.
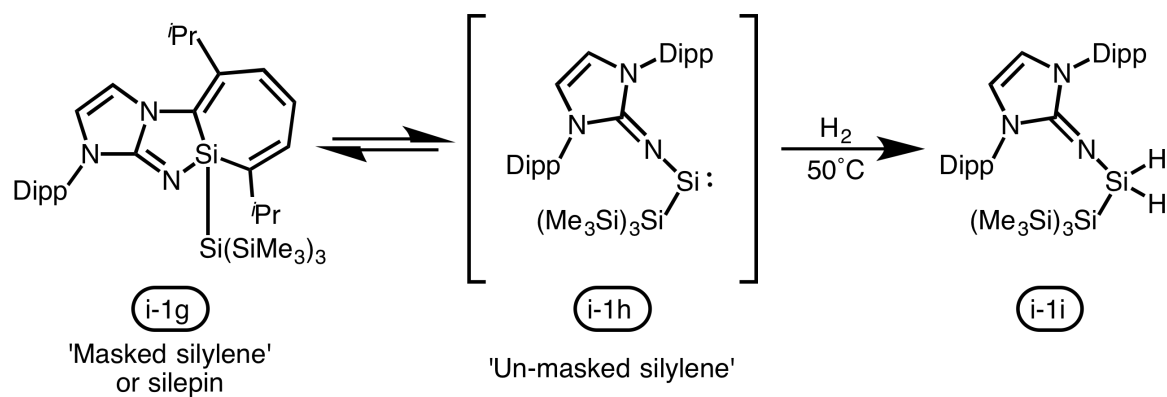
Scheme 1.5: The equilibrium of the masked silylene and un-masked silylene. The un-masked silylene can undergo hydrogenation at elevated temperatures to produce the dihydrosilane.

Computational studies suggest that dihydrogen activation is not favourable for cyclic-silylenes or any silylenes with an increased HOMO-LUMO energy gap (viz. acyclic bis(arylthio)-subsituted silylenes); however, the same studies have indicated silylenes' greater facility towards dihydrogen activation than in comparison to its heavier group 14 element neighbours.[50]

The activation of dihydrogen is not limited to germanium(I) compounds. Power et al. reported the hydrogenation of the germylene **i-1j** to give the dihydrogermane **i-1k**: here, germanium was reacting from the +2 oxidation state. Interestingly, unlike the digermyne **i-1d**, the germylene required elevated temperatures to cleave the σ bonds of dihydrogen (**scheme 1.6**).[51]
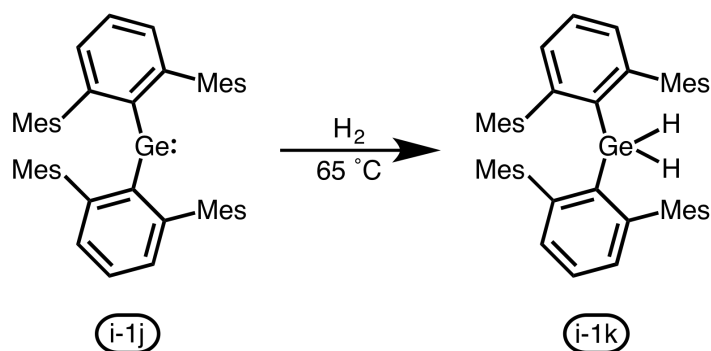
*Scheme 1.6: Hydrogenation of the germylene **i-1j** to form the dihydrogermane **i-1k**.*

Calculations revealed the reaction between **i-1j** and dihydrogen likely proceeded via interactions of the σ orbital of dihydrogen with the valence p orbital of **i-1** with concomitant back-donation from the lone-pair (n-orbital) to the σ^* orbital of dihydrogen.

The tin carbene **i-1l** and alkyne **i-1m** analogues have also been shown to activate dihydrogen (**scheme 1.7**). Comparing the reaction conditions of **i-1l** and **i-1m** highlights the increased reactivity of the heavy alkyne compound which underwent hydrogenation to

cleanly form the bridged Sn(II) hydride **i-1n** at room temperature.[52,53]
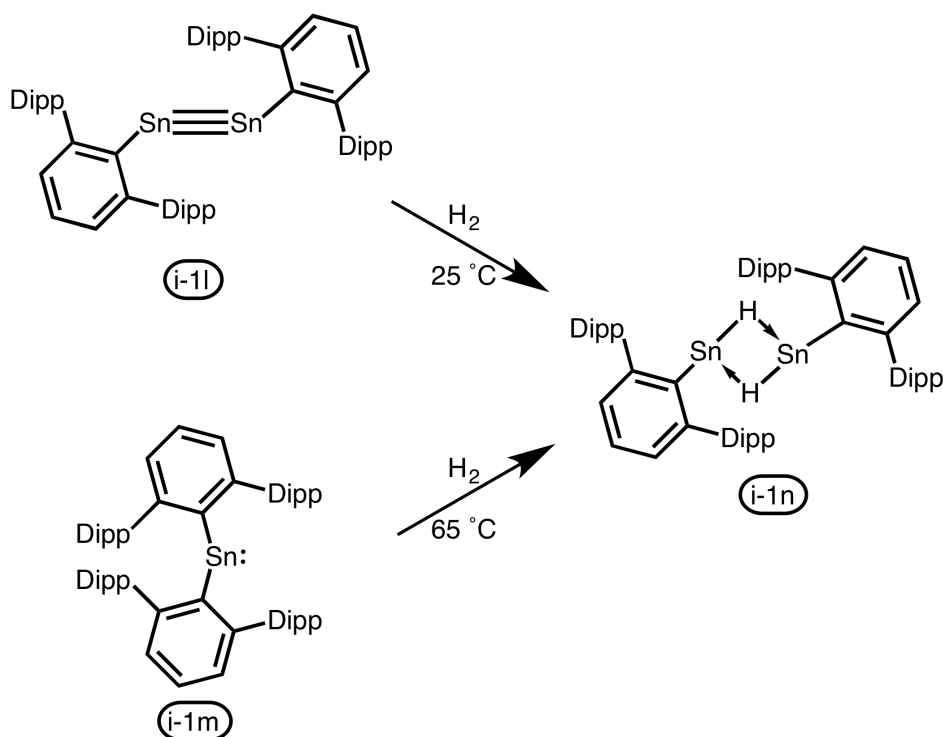
*Scheme 1.7: The two hydrogenation pathways by a tin heavy alkyne **i-1l** (top) and tin heavy carbene **i-1m** (bottom) to from the same hydrogenated product: the tin(II) hydride **i-1n**.*

To date, there are no reports of a plumbylene or plumbyne that have successfully activated dihydrogen. This is most likely due to the magnitude of the inert pair effect and compounded by relativistic effects which create a much large HOMO-LUMO gap for these compounds, rendering them less reactive towards small molecules.

N-H Activation

The activation of N-H bonds is a challenge for transition metals due to their tendency to form classical Werner-type complexes[x]. In contrast, low-oxidation state main-group compounds have been much more successful at such chemical transformations: great strides in the field were accomplished in 2007 by Bertrand and co-workers utilising nucelophillic carbenes to activate ammonia[xi].[55,56]

Today, ammonia's N-H bonds have been activated by a multitude of low-oxidation state group 14 compounds such as those shown in **Figure 1.15**.[57–59] The common feature across these compounds is their ambiphilicity i.e. their ability to accept and donate electrons.

---

[x]Lewis acid-base adducts; because of this, it wasn't until 1991 that a transition metal complex was used to successfully activate ammonia.[54]

[xi]This seminal work clearly described the necessity for the nucleophillic character of the carbene; however, later studies have shown that electrophilic activation of N-H bonds is also credible.

This feature allows these compounds to activate the N-H bonds of activated and deactivated amines (electron rich or poor, respectively). This is achieved by the concerted acceptance of the nitrogen's lone-pair electrons into the empty p orbital of the tetrel centre, and then activation of the N-H σ bond of the amine, and *vice versa*. Pointedly, this ambiphilicity creates a competitive pathway against the formation of Werner-type complexes, and hence N-H bond cleavage can occur "smoothly".[55]
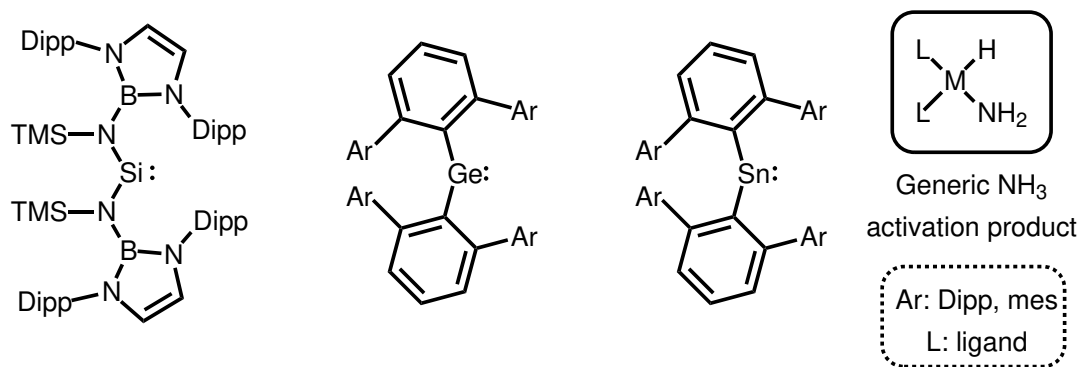
Figure 1.15: Quintessential examples of some low-oxidation state group 14 compounds (in the +2 oxidation state) which are capable of activating ammonia's N-H bonds.[57–59]

C-X Bond Activation

The activation of C-X bonds varies in difficulty based on the X substituent: the bonds formed between carbon and fluorine (C-F bonds) are the strongest at 116 Kcal mol^{-1}, and so these will be the primary focus. C-F bond activation has been achieved with carbenes and recent reports have shown the successful reproduction of said activation utilising silylenes. An example of such reactivity is shown with compounds **i-1o** and **i-1p**, both being three-coordinate tetreylenes with bidentate amidinate ligands for stabilisation; both compounds are capable of C-F activation under mild-conditions (**scheme 1.8**).[60,61]
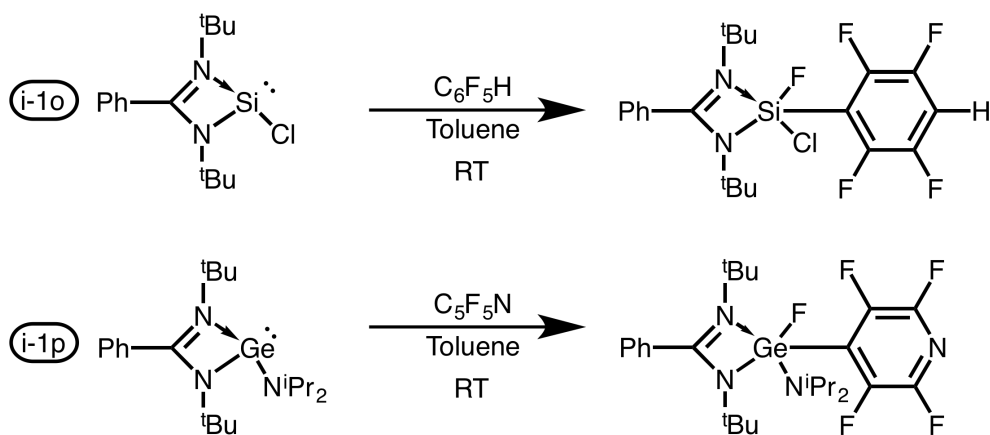
*Scheme 1.8: A silylene (**i-1o**) and germylene (**i-1p**) capable of activating C-F bonds.*

It should be unsurprising that the C-F bond activation by tetreylenes is a consequence of their ambiphilicity. They are able to accept electron density into their formally vacant p orbital (presumably from fluorine), polarising the C-F bond, followed by donation of the silicon lone-pair of electrons towards the positive fragment (the carbon fragment). In this way they could be thought of to be nucleophilic activators[xii].

Of the heavier tetrels only silicon and germanium have shown the capacity to activate C-F bonds. For decades low-oxidation state Si, Ge, and Sn compounds have been observed to activate C-X bonds (where X = Cl, Br, I).[62,63] It is postulated that the lower energy s orbital electrons (the formal lone-pair electrons of low-oxidation state group 14 congeners) are the main reason for this observation, in contrast to the higher energy s orbital electrons observed in the lighter tetrels (C, Si, and, to an extent, Ge).

Reversible Activation and Reductive Elimination

The eclectic reactivity of low-oxidation state main-group compounds has already been compared to transition metals, but there is an aspect of transition-metal chemistry which is still challenging to mimic: reversible activation and reductive elimination, two incredibly important steps in catalysis.[45] The transition metals can easily "jump" between high and low-oxidation states, in contrast to main-group compounds which require a lot of energy to be forced into their lower-oxidation states. This difficulty is further aggravated by the harsh chemical conditions required to prepare low-oxidation state main-group compounds (discussed in greater detail in **chapter 3**). In spite of these challenges there have been some, but few, reports of low-oxidation state group 14 element compounds which can conduct this chemistry [xiii]

Unsurprisingly, many of the examples that are presented within this subsection have already been mentioned. The masked silylene **i-1h** (**scheme 1.5**) can reversibly activate aromatic C-C bonds of its ligand-substituent to form **i-1g**.[49] As shown in **figure 16**, the germylene **i-1j** (previously found to undergo hydrogenation, *vide supra*) and analogous stannylene **i-1q** are capable of activating GaR$_3$ and ZnMe$_2$, whilst **i-1j** can also activate AlMe$_3$ and reversibly activate white phosphorus.[64,65] The reversible activation of white phosphorus has not been achieved with any other molecular metal system to this date.[66]

[xii]As proposed for cyclic(alkyl)(amino)carbenes (CAACs) by Bertrand and co-workers.[55]

[xiii]Again not all examples of such chemistry are presented here. For further reading, it is suggested that one seeks the review by Nikonov et al.[45]
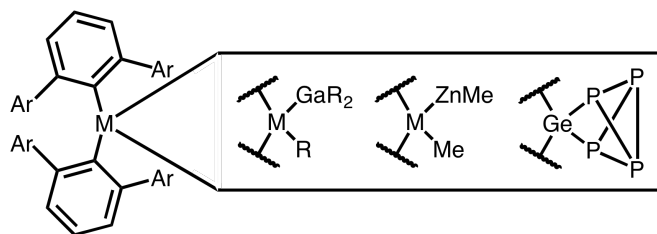
*Figure 1.16: The stannylene **i-1q** can reversibly activate GaR_3 and $ZnMe_2$ to furnish the corresponding substituted compounds under mild reaction conditions; germylene **i-1j** can also activate AlR_3 and reversibly activate white phosphorus.*

Aside from the examples already mentioned, there are few main-group compounds left which show reversible activation, and even fewer low-oxidation state group 14 element compounds which display the ability to reductively eliminate. Two of these compounds are the organotin hydride **i-1r** and the chloro stannylene **i-1s**, which both require "assistance" to reductively eliminate dihydrogen (**scheme 1.9**).[67,68]
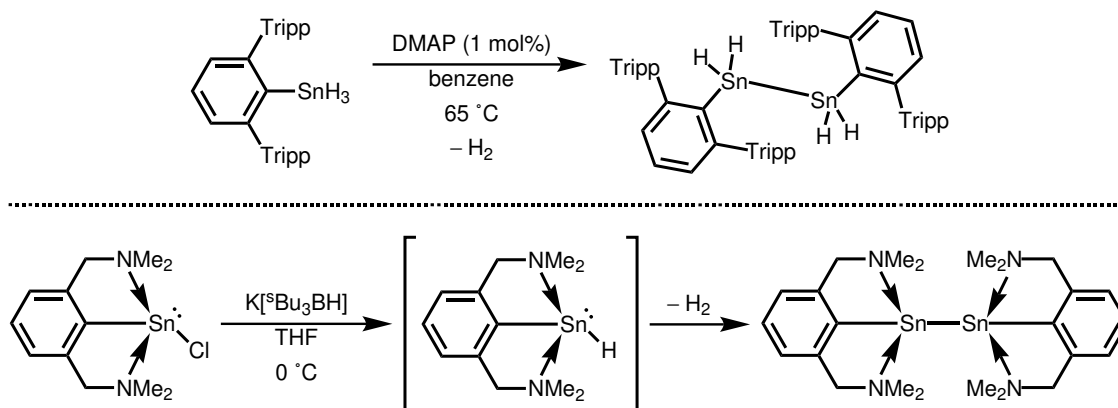
*Scheme 1.9: Top: **i-1r** - with the assistance of the lewis base DMAP - reductively eliminates hydrogen to form the distannane;[67] Bottom: In situ, **i-1s** is converted into the transient pincer-supported stannylene which reductively eliminates dihydrogen to form the distannyne.[68]*

1.5 A Paradigm Shift Towards Main-Group Catalysis

As a species, we face a unique challenge: how do we maintain a healthy environment? With our planet becoming an increasingly undesirable place to live - predominantly due to humanity's continued efforts to use and discard all the resources at our disposal - we are required to explore new renewable systems for our production needs. Collectively, society is moving to reduce our one-use mentality and beginning to consider the affect the resources we use has on our environment.

One such problematic area of abuse is the use of low-abundant and toxic elements, viz. transition metals; another is the continued use of inefficient chemical processes. Both of these issues can be tackled with exploration into new catalysts. In comes the main-group elements, a previously un-investigated area of chemistry, bringing along a new, abundant, non-toxic, and cheap chemical tool-box, which provides us a route to continue production and maintain a healthy eco-system.

With these elements, scientists have shown their ability to mimic the chemistry of the transition metals, and in-so-doing have opened up new areas of exploration. Further to this, the area of main-group chemistry offers fundamental knowledge: our ability to understand the reactivity, the electronics and kinetics of catalytic cycles, is transferable to other fields of chemistry[xiv].

It is both an area of immediate reward and future potential, not limited in its chemical scope nor in application, and because of this is an area worthy of pursuit.

[xiv]The fundamental concepts of steric encumbrance, discussed in **chapter 2**, gives us greater insight into the physical properties of chemical electronics and furthers the area of physical chemistry.

Bibliography

[1] C. Jones and G. A. Koutsantonis, "Modern Main Group Chemistry: From Renaissance to Revolution," *Australian Journal of Chemistry*, vol. 66, no. 10, pp. 1115–1117, 2013.

[2] S. K. Ritter, "Main Grouping," *Chemical & Engineering News*, vol. 82, no. 19, pp. 39–42, 2004.

[3] G. Bertrand, "Introduction to Main Group Chemistry," *Chemical Reviews*, vol. 110, no. 7, p. 3851, 2010.

[4] W. E. Dasent, *Nonexistent Compounds; Compounds of Low Stability*. Dekker, 1965.

[5] P. Jutzi, "New Element-Carbon (p-p) π Bonds," *Angewandte Chemie International Edition in English*, vol. 14, no. 4, pp. 232–245, 1975.

[6] M. C. Kuchta and G. Parkin, "Terminal Chalcogenido Complexes of Group 13 and 14 Elements," *Coordination Chemistry Reviews*, vol. 176, no. 1, pp. 323–372, 1998.

[7] R. S. Mulliken, "Overlap Integrals and Chemical Binding1," *Journal of the American Chemical Society*, vol. 72, no. 10, pp. 4493–4503, 1950.

[8] P. Smie, "Publikationen," *Angewandte Chemie International Edition in English*, vol. 58, no. 2019, pp. 716–721, 2018.

[9] H.-J. Himmel and J. Vollet, "Probing the Reactivity of Aluminum (I) Compounds: the Reaction of Pentamethylcyclopentadienyl-Aluminum, Al $[C_5(CH_3)_5]$, Monomers with Dihydrogen in a Solid Ar Matrix to Give the New Aluminum Hydride Molecule H_2Al $[C_5(CH_3)_5]$," *Organometallics*, vol. 21, no. 26, pp. 5972–5977, 2002.

[10] M. Asay, C. Jones, and M. Driess, "N-Heterocyclic Carbene Analogues with Low-Valent Group 13 and Group 14 Elements: Syntheses, Structures, and Reactivities of a New Generation of Multitalented Ligands," *Chemical Reviews*, vol. 111, no. 2, pp. 354–396, 2010.

[11] D. L. Kays, "Extremely Bulky Amide Ligands in Main Group Chemistry," *Chemical Society Reviews*, vol. 45, no. 4, pp. 1004–1018, 2016.

[12] J. D. Cotton, P. J. Davison, D. E. Goldberg, M. F. Lappert, and K. M. Thomas, "Coordination Chemistry of Heavy-Atom Group IV Donors, and the Crystal and Molecular Structure of $[(Me_3Si)_2CH]_2SnCr(CO)_5$," *Journal of the Chemical Society, Chemical Communications*, no. 21, pp. 893–895, 1974.

[13] D. E. Goldberg, D. H. Harris, M. F. Lappert, and K. M. Thomas, "A New Synthesis of Divalent Group 4B Alkyls M $[CH(SiMe_3)_2]_2$ (M= Ge or Sn), and the Crystal and Molecular and Molecular Structure of the Tin Compound," *Journal of the Chemical Society, Chemical Communications*, no. 7, pp. 261–262, 1976.

[14] P. J. Davidson, D. H. Harris, and M. F. Lappert, "Subvalent Group 4B Metal Alkyls and Amides. Part I. The Synthesis and Physical Properties of Kinetically Stable Bis[Bis (Trimethysilyl)Methyl]-Germanium (II),-Tin (II), and-Lead (II)," *Journal of the Chemical Society, Dalton Transactions*, no. 21, pp. 2268–2274, 1976.

[15] A. Brook, S. Nyburg, F. Abdesaken, B. Gutekunst, G. Gutekunst, R. Krishna, M. Kallury, Y. C. Poon, Y. M. Chang, and W. N. Winnie, "Stable Solid Silaethylenes," *Journal of the American Chemical Society*, vol. 104, no. 21, pp. 5667–5672, 1982.

[16] R. S. Simons, L. Pu, M. M. Olmstead, and P. P. Power, "Synthesis and Characterization of the Monomeric Diaryls M{C_6H_3-2, 6-Mes$_2$}2 (M= Ge, Sn, or Pb; Mes= 2, 4, 6-Me$_3$C$_6$H$_2$-) and Dimeric Aryl-Metal Chlorides [M (Cl){C_6H_3-2, 6-Mes$_2$}]$_2$ (M= Ge or Sn)," *Organometallics*, vol. 16, no. 9, pp. 1920–1925, 1997.

[17] M. Stürmann, M. Weidenbruch, K. W. Klinkhammer, F. Lissner, and H. Marsmann, "New Plumbylenes and a Plumbylene Dimer with a Short Lead-Lead Separation," *Organometallics*, vol. 17, no. 20, pp. 4425–4428, 1998.

[18] L. Pu, B. Twamley, and P. P. Power, "Synthesis and Characterization of 2,6-Trip$_2$H$_3$C$_6$PbPbC$_6$H$_3$-2,6-Trip$_2$ (Trip= C$_6$H$_2$-2,4,6-^{i}Pr$_3$): a Stable Heavier Group 14 Element Analogue of an Alkyne," *Journal of the American Chemical Society*, vol. 122, no. 14, pp. 3524–3525, 2000.

[19] A. D. Phillips, R. J. Wright, M. M. Olmstead, and P. P. Power, "Synthesis and Characterization of 2,6-Dipp$_2$-H$_3$C$_6$SnSnC$_6$H$_3$-2,6-Dipp$_2$ (Dipp= C$_6$H$_3$-2,6-^{i}Pr$_2$): A Tin Analogue of an Alkyne," *Journal of the American Chemical Society*, vol. 124, no. 21, pp. 5930–5931, 2002.

[20] M. Stender, A. D. Phillips, R. J. Wright, and P. P. Power, "Synthesis and Characterization of a Digermanium Analogue of an Alkyne," *Angewandte Chemie International Edition in English*, vol. 41, no. 10, pp. 1785–1787, 2002.

[21] A. Sekiguchi, R. Kinjo, and M. Ichinohe, "A Stable Compound Containing a Silicon-Silicon Triple Bond," *Science*, vol. 305, no. 5691, pp. 1755–1757, 2004.

[22] G. Trinquier and J. P. Malrieu, "Nonclassical Distortions at Multiple Bonds," *Journal of the American Chemical Society*, vol. 109, no. 18, pp. 5303–5315, 1987.

[23] S. Masamune, S. Murakami, J. T. Snow, H. Tobita, and D. J. Williams, "Molecular Structure of Tetrakis (2,6-Diethylphenyl) Disilene," *Organometallics*, vol. 3, no. 2, pp. 333–334, 1984.

[24] H. Schäfer, W. Saak, and M. Weidenbruch, "Azadigermiridines by Addition of Diazomethane or Trimethylsilyldiazomethane to a Digermene1," *Organometallics*, vol. 18, no. 16, pp. 3159–3163, 1999.

[25] M. Weidenbruch, H. Kilian, K. Peters, H. G. V. Schnering, and H. Marsmann, "Compounds of Germanium and Tin, 16. A Tetraaryldistannene with a Long Tin—Tin Multiple Bond and Differing Environments at the Tin Atoms," *Chemische Berichte*, vol. 128, no. 10, pp. 983–985, 1995.

[26] M. Stürmann, W. Saak, H. Marsmann, and M. Weidenbruch, "Tetrakis (2, 4, 6-Triisopropylphenyl) Diplumbene: A Molecule with a Lead–Lead Double Bond," *Angewandte Chemie International Edition in English*, vol. 38, no. 1-2, pp. 187–189, 1999.

[27] S. Nagase, K. Kobayashi, and N. Takagi, "Triple Bonds Between Heavier Group 14 Elements. A Theoretical Approach," *Journal of Organometallic Chemistry*, vol. 611, no. 1-2, pp. 264–271, 2000.

[28] N. V. Sidgwick, *Some Physical Properties of the Covalent Link in Chemistry*, vol. 11. Cornell University Press, 1933.

[29] P. Pyykko, "Relativistic Effects in Structural Chemistry," *Chemical Reviews*, vol. 88, no. 3, pp. 563–594, 1988.

[30] K.-P. Huber, "Constants of Diatomic Molecules," *Molecular Spectra and Molecular Structure*, 1979.

[31] R. G. Pearson, "The Second-Order Jahn-Teller Effect," *Journal of Molecular Structure: THEOCHEM*, vol. 103, pp. 25–34, 1983.

[32] P. P. Power, "Interaction of Multiple Bonded and Unsaturated Heavier Main Group Compounds with Hydrogen, Ammonia, Olefins, and Related Molecules," *Accounts of Chemical Research*, vol. 44, no. 8, pp. 627–637, 2011.

[33] P. P. Power, "Bonding and Reactivity of Heavier Group 14 Element Alkyne Analogues," *Organometallics*, vol. 26, no. 18, pp. 4362–4372, 2007.

[34] M. Denk, R. Lennon, R. Hayashi, R. West, A. V. Belyakov, H. P. Verne, A. Haaland, M. Wagner, and N. Metzler, "Synthesis and Structure of a Stable Silylene," *Journal of the American Chemical Society*, vol. 116, no. 6, pp. 2691–2692, 1994.

[35] V. Y. Lee and A. Sekiguch, *Organometallic Compounds of Low-Coordinate Si, Ge, Sn and Pb: From Phantom Species to Stable Compounds*. Wiley, 2010.

[36] Y. Apeloig, R. Pauncz, M. Karni, R. West, W. Steiner, and D. Chapman, "Why is Methylene a Ground State Triplet while Silylene is a Ground State Singlet?," *Organometallics*, vol. 22, no. 16, pp. 3250–3256, 2003.

[37] J. Berkowitz, J. Greene, H. Cho, and B. Ruščić, "Photoionization Mass Spectrometric Studies of SiH n (n= 1–4)," *The Journal of Chemical Physics*, vol. 86, no. 3, pp. 1235–1248, 1987.

[38] K. Balasubramanian, "Breakdown of the singlet and triplet nature of electronic states of the superheavy element 114 dihydride (114h2)," *The Journal of Chemical Physics*, vol. 117, no. 16, pp. 7426–7432, 2002.

[39] B. Luke, J. Pople, M. Krogh-Jespersen, Y. Apeloig, J. Chandrasekhar, and P. v. R. Schleyer, "A Theoretical Survey of Singly Bonded Silicon Compounds. Comparison of the Structures and Bond Energies of Silyl and Methyl Derivatives," *Journal of the American Chemical Society*, vol. 108, no. 2, pp. 260–269, 1986.

[40] H. A. Bent, "An Appraisal of Valence-bond Structures and Hybridization in Compounds of the First-row elements.," *Chemical Reviews*, vol. 61, no. 3, pp. 275–311, 1961.

[41] Y. Apeloig and M. Karni, "The Effect of Substituents on the First Transition in the Visible spectra of Silanediyls (Silylenes)," *Journal of the Chemical Society, Chemical Communications*, no. 15, pp. 1048–1049, 1985.

[42] Y. Apeloig, M. Karni, R. West, and K. Welsh, "Electronic Spectra of Ethynyl- and Vinylsilylenes: Experiment and Theory," *Journal of the American Chemical Society*, no. 21, pp. 9719–9729, 994.

[43] Y. Apeloig and Z. Rappoport, *The Chemistry of Organic Silicon Compounds Vol. 2*. Wiley, 1998.

[44] M. Michalczyk, M. Fink, D. DeYoung, C. Carlson, K. Welsh, R. West, and J. Michl, *Silicon, Germanium, Tin, Lead Compounds*. Springer, 1986.

[45] T. Chu and G. I. Nikonov, "Oxidative Addition and Reductive Elimination at Main-Group Element Centers," *Chemical Reviews*, vol. 118, pp. 3608–3680, 04 2018.

[46] G. H. Spikes, J. C. Fettinger, and P. P. Power, "Facile Activation of Dihydrogen by an Unsaturated Heavier Main Group Compound," *Journal of the American Chemical Society*, vol. 127, pp. 12232–12233, 09 2005.

[47] A. V. Protchenko, K. H. Birjkumar, D. Dange, A. D. Schwarz, D. Vidovic, C. Jones, N. Kaltsoyannis, P. Mountford, and S. Aldridge, "A Stable Two-Coordinate Acyclic Silylene," *Journal of the American Chemical Society*, vol. 134, pp. 6500–6503, 04 2012.

[48] B. D. Rekken, T. M. Brown, J. C. Fettinger, H. M. Tuononen, and P. P. Power, "Isolation of a Stable, Acyclic, Two-Coordinate Silylene," *Journal of the American Chemical Society*, vol. 134, pp. 6504–6507, 04 2012.

[49] D. Wendel, A. Porzelt, F. A. D. Herz, D. Sarkar, C. Jandl, S. Inoue, and B. Rieger, "From Si(II) to Si(IV) and Back: Reversible Intramolecular Carbon–Carbon Bond Activation by an Acyclic Iminosilylene," *Journal of the American Chemical Society*, vol. 139, pp. 8134–8137, 06 2017.

[50] Y. Wang and J. Ma, "Silylenes and Germylenes: The Activation of H–H bond in Hydrogen Molecule," *Journal of Organometallic Chemistry*, vol. 694, no. 16, pp. 2567–2575, 2009.

[51] Y. Peng, J.-D. Guo, B. D. Ellis, Z. Zhu, J. C. Fettinger, S. Nagase, and P. P. Power, "Reaction of Hydrogen or Ammonia with Unsaturated Germanium or Tin Molecules under Ambient Conditions: Oxidative Addition versus Arene Elimination," *Journal of the American Chemical Society*, vol. 131, pp. 16272–16282, 11 2009.

[52] Y. Peng, M. Brynda, B. D. Ellis, J. C. Fettinger, E. Rivard, and P. P. Power, "Addition of H_2 to Distannynes under Ambient Conditions," *Chemical Communications*, no. 45, pp. 6042–6044, 2008.

[53] Y. Peng, B. D. Ellis, X. Wang, and P. P. Power, "Diarylstannylene Activation of Hydrogen or Ammonia with Arene Elimination," *Journal of the American Chemical Society*, vol. 130, pp. 12268–12269, 09 2008.

[54] R. Koelliker and D. Milstein, "Evidence for an Unprecedented Ir (H)(NH$_3$) $\rightleftharpoons$ Ir (H$_2$)(NH$_2$) Equilibrium and Hydrogen Exchange between NH and CH bonds," *Journal of the American Chemical Society*, vol. 113, no. 22, pp. 8524–8525, 1991.

[55] G. D. Frey, V. Lavallo, B. Donnadieu, W. W. Schoeller, and G. Bertrand, "Facile Splitting of Hydrogen and Ammonia by Nucleophilic Activation at a Single Carbon Center," *Science*, vol. 316, no. 5823, pp. 439–441, 2007.

[56] J. P. Moerdyk, G. A. Blake, D. T. Chase, and C. W. Bielawski, "Elucidation of Carbene Ambiphilicity Leading to the Discovery of Reversible Ammonia Activation," *Journal of the American Chemical Society*, vol. 135, no. 50, pp. 18798–18801, 2013.

[57] T. J. Hadlington, J. A. Abdalla, R. Tirfoin, S. Aldridge, and C. Jones, "Stabilization of a Two-Coordinate, Acyclic Diaminosilylene (ADASi): Completion of the Series of Isolable Diaminotetrylenes: E (NR$_2$)$_2$ (E= Group 14 Element)," *Chemical Communications*, vol. 52, no. 8, pp. 1717–1720, 2016.

[58] Y. Peng, J.-D. Guo, B. D. Ellis, Z. Zhu, J. C. Fettinger, S. Nagase, and P. P. Power, "Reaction of Hydrogen or Ammonia with Unsaturated Germanium or Tin Molecules under Ambient Conditions: Oxidative Addition versus Arene Elimination," *Journal of the American Chemical Society*, vol. 131, no. 44, pp. 16272–16282, 2009.

[59] Y. Peng, B. D. Ellis, X. Wang, and P. P. Power, "Diarylstannylene Activation of Hydrogen or Ammonia with Arene Elimination," *Journal of the American Chemical Society*, vol. 130, no. 37, pp. 12268–12269, 2008.

[60] A. Jana, P. P. Samuel, G. Tavcar, H. W. Roesky, and C. Schulzke, "Selective Aromatic C-F and C-H Bond Activation with Silylenes of Different Coordinate Silicon," *Journal of the American Chemical Society*, vol. 132, no. 29, pp. 10164–10170, 2010.

[61] P. P. Samuel, A. P. Singh, S. P. Sarish, J. Matussek, I. Objartel, H. W. Roesky, and D. Stalke, "Oxidative Addition Versus Substitution Reactions of Group 14 Dialkylamino Metalylenes with Pentafluoropyridine," *Inorganic chemistry*, vol. 52, no. 3, pp. 1544–1549, 2013.

[62] W. Atwell and D. Weyenberg, "Divalent Silicon Intermediates," *Angewandte Chemie International Edition in English*, vol. 8, no. 7, pp. 469–477, 1969.

[63] M. J. Gynane, M. F. Lappert, S. J. Miles, and P. P. Power, "Ready Oxidative Addition of an Alkyl or Aryl Halide to a Tin (II) Alkyl or Amide; Evidence for a Free-Radical Pathway," *Journal of the Chemical Society, Chemical Communications*, no. 7, pp. 256–257, 1976.

[64] J. D. Erickson, J. C. Fettinger, and P. P. Power, "Reaction of a Germylene, Stannylene, or Plumbylene with Trimethylaluminum and Trimethylgallium: Insertion into Al–C or Ga–C Bonds, a Reversible Metal–Carbon Insertion Equilibrium, and a New Route to Diplumbenes," *Inorganic Chemistry*, vol. 54, no. 4, pp. 1940–1948, 2015.

[65] J. D. Erickson, R. D. Riparetti, J. C. Fettinger, and P. P. Power, "Molecular Zinc Species with Ge–Zn and Sn–Zn Bonds: A Reversible Insertion of a Stannylene into a Zinc–Carbon Bond," *Organometallics*, vol. 35, no. 12, pp. 2124–2128, 2016.

[66] J. W. Dube, C. M. Graham, C. L. Macdonald, Z. D. Brown, P. P. Power, and P. J. Ragogna, "Reversible, Photoinduced Activation of P4 by Low-Coordinate Main Group Compounds," *Chemistry–A European Journal*, vol. 20, no. 22, pp. 6739–6744, 2014.

[67] C. P. Sindlinger and L. Wesemann, "Hydrogen Abstraction from Organotin Di- and Trihydrides by N-Heterocyclic Carbenes: A New Method for the Preparation of NHC Adducts to Tin (II) Species and Observation of an Isomer of a Hexastannabenzene Derivative $[R_6Sn_6]$," *Chemical Science*, vol. 5, no. 7, pp. 2739–2746, 2014.

[68] R. Jambor, B. Kašná, K. N. Kirschner, M. Schürmann, and K. Jurkschat, "[{2, 6-$(Me_2NCH_2)_2C_6H_3$} Sn]$_2$: An Intramolecularly Coordinated Diorganodistannyne," *Angewandte Chemie International Edition in English*, vol. 47, no. 9, pp. 1650–1653, 2008.

Chapter 2

Ligand Design and Synthesis for Low-Oxidation State Main-Group Chemistry

Low-oxidation state main-group chemistry relies on the use of sterically encumbering ligands to stabilise a main-group element centre in its reactive low-oxidation states. The imparted steric encumbrance of the ligand towards the main-group element suppresses decomposition, i.e. disproportionation, by physically preventing the formation of homoleptic complexes etc.

The design of these ligands plays an important role relative to the chemistry which can occur at the element-centre-of-interest (ECOI): the denticity of a ligand effects the number of coordination sites available on the surface of the ECOI; the donor element influences the electronic character of the ECOI; and there is a balance between the kinetic stabilisation and reactivity of the ECOI allowed for by the ligand.

Within the field of low-oxidation state tetrel chemistry there has been a shift towards monodentate ligands due to the heightened reactivity observed in monodentate stabilised low-oxidation state group 14 element compounds. However, multidentate ligands are still heavily utilised as they provide greater kinetic and thermodynamic stabilisation.

It is the purpose of this chapter to highlight the advancements made in sterically-encumbering ligand design, before discussing the ligands synthesised as part of this project. Within the introduction section, an inductive proposal is presented which defines a qualitative system for the steric characterisation of molecules. The system suggests and provides definition for the steric terminology used throughout the thesis: bulk, flexibility, and proximal bulk.

2.1 An Aside: Defining Chelation and Denticity

Until now it has been a focus of this thesis to emphasise the principle that sterically encumbering a main-group element kinetically stabilises it, allowing access to its low-oxidation states. Another equally important factor in stabilisation is the chelation effect.

Chelation is the thermodynamic stability afforded to a compound via the saturation of its coordination sphere by the fewest number of ligands[i]. This saturation, or increased coordination, about the ECOI is both a thermodynamically and kinetically stabilising phenomenon. Thermodynamically, multidentate ligands are favourable as they increase disorder (entropy): by displacing more constituents (solvents, ligands, ions etc.) bound to the ECOI, they produce a net increase in entropy. Kinetically, the increase in coordination about the ECOI blocks/occupies the coordination-sites of the ECOI, physically preventing interactions between it and other molecules and consequently preventing decomposition, but also suppressing reactivity.[1,2]

Chelation is an incredibly important form of stabilisation, one widely understood in transition-metal chemistry and adopted by main-group chemists. Main-group chemists can manipulate chelation by adopting ligands which can multiply-bind to a main-group ECOI. Ligands are catergorised based on their ability to multiply bind to an ECOI, by their denticity: they can be mono or multidentate (where multidentate can be broken down into bi/tri/tetradentate etc.).

Multidentate ligands increase chelation and therefore the overall stability of the compound, and the reverse holds for monodentate ligands. However, with increased denticity there is a decrease in the coordination sites around the ECOI and as a consequence reactivity decreases.

2.2 Bidentate Ligands

Bidentate ligands are useful in low-oxidation state main-group chemistry as they provide chelation (thermodynamic stability) and (typically) greater steric encumberance than monodentate ligands.

There is a vast number of bidentate ligands reported within the literature, so this section focuses on two classes: amidinates and β-dikitiminates (nacnacs). Both of these ligand classes are the nitrogen analogues of oxygen congeners (carboxylates & β-diketonates, respectively) and are ubiquitous throughout the literature, both in transition-metal chemistry and main-group chemistry.[3]

---

[i]It is the enhanced affinity of a multidentate ligand towards a ECOI in comparison to similar non-chelating ligands.

Bidentate ligands when bound to an ECOI form a bite angle, which is the ligand-ECOI-ligand angle of the closed-ringed-system when the ligand is chelated to the ECOI. An important consideration to be made when adopting a bidentate ligand is this potential bite angle relative to the preferred geometry of the ECOI: for stability, the choice of ligand should allow for the optimal geometry about the ECOI i.e. the bite angle should mimic the geometry obtained when monodentate ligands are employed[ii]; for reactivity, chelating ligands that enforce a well-defined bite angle can enforce a certain ECOI geometry, influencing the reactivity and reaction pathways[iii](refer to **chapter 1, section 1.3.2**.)[4]

Technically speaking, a ligand is a molecule or anion which is bound to the ECOI/metal centre. The following amine-type "ligands" are actually the protonated ligand (pro-ligand) derivative, and when bound to a ECOI are amides-type ligands. Conversion of the amine to the amide, the coupling of the ligand to the ECOI, will be discussed in **chapter 3**. For the interim discussion, the term ligand is used to refer to the pro-ligand when discussing amine-type ligands.

2.2.1   Amidinates

Amidinates are bidentate, monoanionic, nitrogen donors which form four-memembered rings upon complexation to an element-centre. Being first synthesised in 1973, their continued use in main-group and transition-metal chemistry is partly due to their ease of synthesis and easy modification.[7]

There is a variety of ways in which amidinates are synthesised, today. The most general of these syntheseses is the reaction of a metal amide with a carbodiimide (**scheme 2.1, a**); to isolate and form the pro-ligand the synthesis is as shown in **scheme 2.1, b**.

[ii]Metal complexes with chelating ligands preferring a bite angle of 90°stabilise square planar geometries, for example.[4]

[iii]The affects of bite angle and the reactivity of complexes which contain diphosphine bidentate ligands has been extensively explored, highlighting the influence of bite angle and reactivity.[5,6]
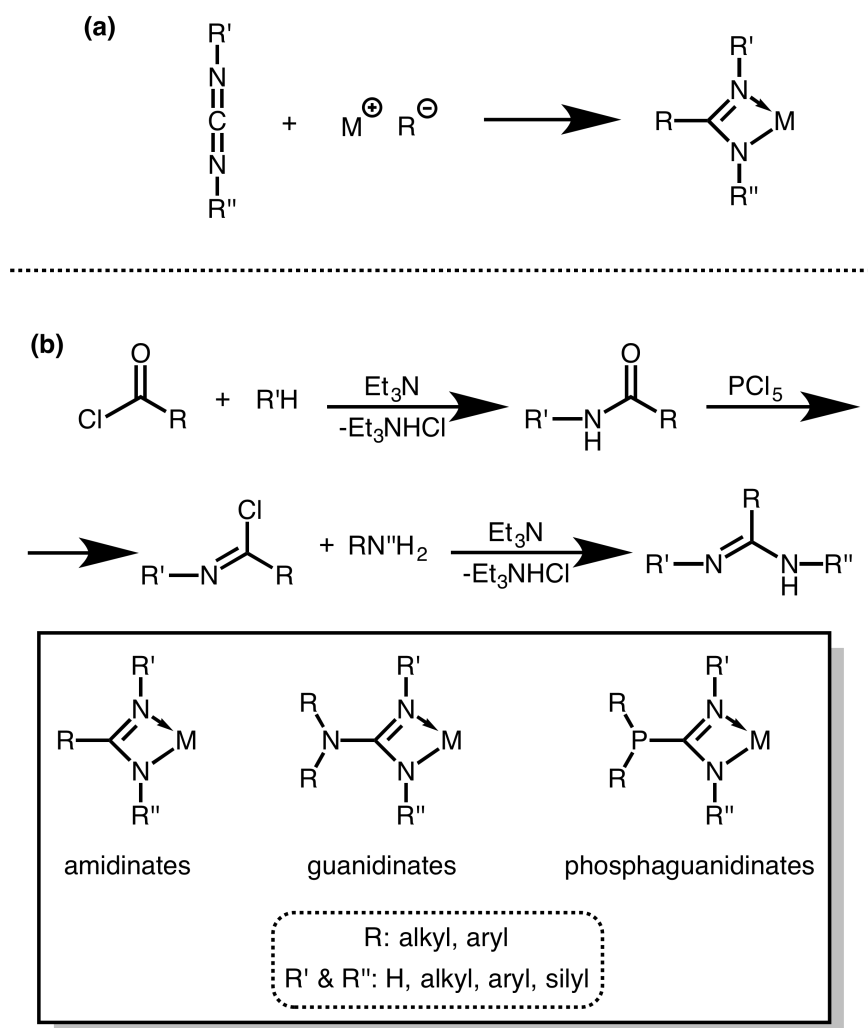
Scheme 2.1: General syntheses and Lewis structure of amidinates, guanidinates, and phosphaguanidinates.

Amidinates provides the majority of their potential steric encumbrance via flanking[iv] aryl or alkyl moieties, which can be modified to alter the steric profile of the ligand. The backbone R groups can be altered to enhance the electronic properties of the ligand, though these groups also affect the bite angle of the ligand and consequently their steric profile (in most cases, the R groups are modified to alter the crystallinity of the compound). One of the most significant modifications to these ligands is achieved by substituting the backbone R-group with a nitrogen or phosphorus moiety to form a guanidinate or phosphaguanidinates (**scheme 2.1**).

One of the major downsides of using amidinates in group 14 element chemistry is the formation of a four-membered ring upon complexation, which are inherently less stable than six-membered tetrel ring motifs, a consequence of the heavy tetrel elements preferred

---

[iv]'Flanking' groups are those which are less than perpendicular to the ECOI. In this case, the aryl or alkyl substituents upon the nitrogen are angled less than 90° towards the ECOI.

tetrahedral geometry.

2.2.2 β-dikitiminates, the Nacnacs

β-dikitiminates, the nacnacs, are monoanionic, nitrogen donor ligands, which form six-memebered rings upon complexation to an element centre. Over the past two decades, these ligands have allowed for the formation and isolation of a range of novel low-oxidation state main-group element compounds: the first magnesium(I) and monomeric aluminium(I) compounds were isolated due to the kinetic stabilisation afforded by nacnac type ligands.[8,9]

Nacnacs can be prepared in a one-step synthesis: the condensation of aryl/alkylamines with 1,3-diketones, though there are other ways of synthesizing more elaborate nacnacs (**scheme 2.2**).[10,11] In recent times, aryl containing nacnacs are primarily used in main-group chemistry and hence will be the focus hereon-in.
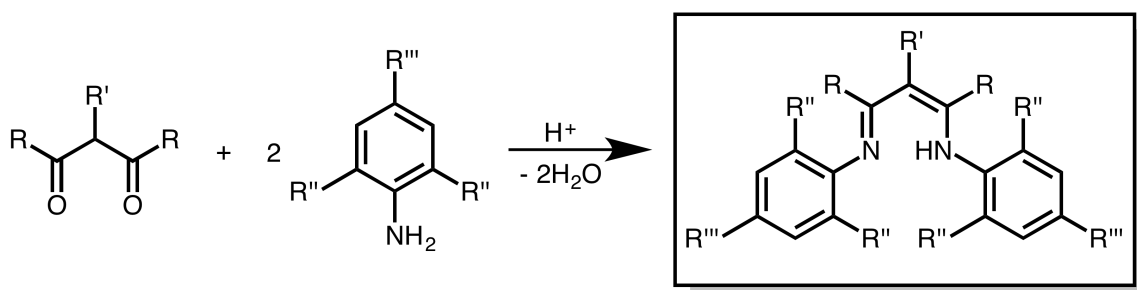
Scheme 2.2: Synthesis and general structure of β-diketiminate (nacnac) ligands.

Like amidinates, the nacnac's Ar and backbone R groups can be modified to tune the steric and electronic profile. The simplest of these changes comes by way of the Ar group: larger aromatic groups are used in order to increase potential steric encumbrance; also, changing the Ar functional groups can have some effect on the overall ligand's electronics. For the R groups, the story becomes more complicated. The R group can be modified to alter the electronics of the ligand[v] and to affect the bite angle upon complexation: larger R groups create steric repulsion upon the Ar functional groups and force them towards the bound ECOI, creating a smaller bite angle. The opposite holds true for smaller R groups[vi].[13]

The formation of a six-membered ring upon complexation with a tetrel element lends further stability to the resulting compounds: increased flexibility in the degree of bonding between the ligand and tetrel element achieves closer to optimal geometry about the tetrel

---

[v]Similar to aromatic chemistry, electron withdrawing and donating groups decrease or increase the donor ability of the ligand.[12]

[vi]The affects of modification upon nacnacs is well documented; a particularly good review is provided by Holand and co-workers, titled *Tuning Steric and Electronic Effects in Transitionmetal β-Diketiminate Complexes*, which covers nacnacs in relation to transition-metals, though the principles in ligand design still apply to main-group chemistry.

element centre i.e. tetrahedral, with bond angles closer to 109.5°.

2.3   Monodentate ligands

The desire to use monodentate ligands stems from chemists' understanding of the relationship between stability vs. reactivity: the more stable a compound the less reactive it is and *vice versa*. Monodentate ligands bind to a single point of an element, taking up one position of the coordination sphere and, therefore, the ECOI is coordinatively unsaturated. This "freeing up" of the coordination sphere heightens the potential reactivity of these compounds: the increased surface area and binding potential at the main-group element centre increase the opportunity for substrates to bind, react, and then be released (obviously, the release/elimination stage is an important step in the case of catalysis). However, this increased reactivity comes at the cost of kinetic stabilisation and these compounds may become prone to decomposition.

Monodentate ligands forgo the inherent chelating stabilisation of multidentate ligands and heavily rely on their steric encumbrance as the preventative force against decomposition and instability of the complexes formed. This is a major challenge as monodentate ligands must be incredibly encumbering whilst only forming one point of bonding between the donor atom and a main-group ECOI. Further difficulties arise due to limitations in monodentate ligand design and where the bulk of the ligand can be placed relative to the main-group element centre; in contrast, multidentate ligands often have multiple proximal points to the ECOI, which can be modified to increase or decrease the steric encumbrance provided about the main-group centre.

An example of these issues is noted with monodentate amide ligands. These ligands, whilst having the potential to create incredible sterically encumbering environments, have the majority of their sterically encumbering constituents directed away from the main-group element centre, a consequence of nitrogens bonding geometry [vii]. To overcome such issues it is typical that larger and larger substituents are placed upon the donor-nitrogen element so that the the majority of the potential steric-encumbrance offered by the ligand "wraps" back towards the sphere of the main-group element centre (**figure 2.1**). As in bindentate ligands, altering the bulk of a ligand at position further away from the ECOI can influence the rigidity and directionality of the substituents closest to the ECOI. Larger substituents at positions further away from the ECOI may concertedly influence the preferred orientation

---

[vii]The nitrogen element geometry is often observed as being trigonal planar, not the expected pyramidal geometry. This is due to the steric environment forced upon the nitrogen atom by its substituents, conforming to the less spatially demanding geometry: trigonal planar. The substituents upon the nitrogen are spatially removed from each-other by approximately 120° from one another rather than 109.5° as would be the case if nitrogen adopted it's usual pyramidal geometry.

of the ligand, influencing the steric profile[viii]. This is discussed in greater detail *vide supra*.
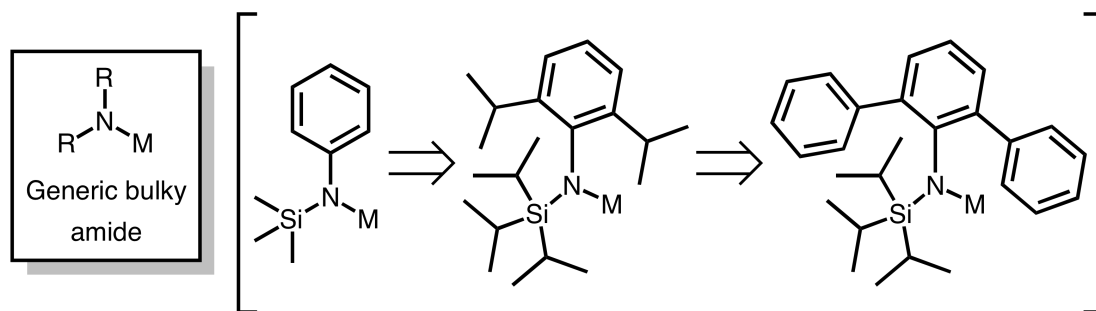
Figure 2.1: Increasing the bulk of the ligand at non-proximal positions relative to the ECOI (M) can lead to an increase in steric encumbrance. Adding bulk increases steric congestion and may eventuate in kinetic stabilisation of the ECOI as the bulk conforms about it's sphere, or compound fission could ensure. An increase in size/bulk of the nitrogen substituents leads to a closer-to trigonal planar nitrogen geometry.

The monodentate ligands discussed in this section are either carbon or nitrogen donors. In contrast to nitrogen donors, carbon donors are generally strong σ-donors and form stronger bonds to a main-group centre than their nitrogen counterparts; however due to the strength of C-H bonds they are also more easily hydrolysed back to their protonated-ligand (pro-ligand).

2.3.1   Terphenyls

The 2,6-bis(aryl)-phenyl ligands, more commonly referred to as terphenyls, are a carbon-donor monodentate ligands which have seen incredible success in stabilising a wide variety of main-group elements in their low-oxidation state (some exemplary low-oxidation state group 14 element compounds are described in **chapter 1**).

The modern-day synthesis of terphenyls is as shown in **scheme 2.3**.[14,15] The versatility/scope of this synthesis allows for the production of a range of terphenyls with alternative steric and electronic profiles. The modification of these ligands into their bulky amide analogues is discussed *vide infra*.

[viii]This could also be considered to be an affect of steric congestion, which eventually leads to the bulk of a ligand being forced to encompass an ECOI or fission of the compound.
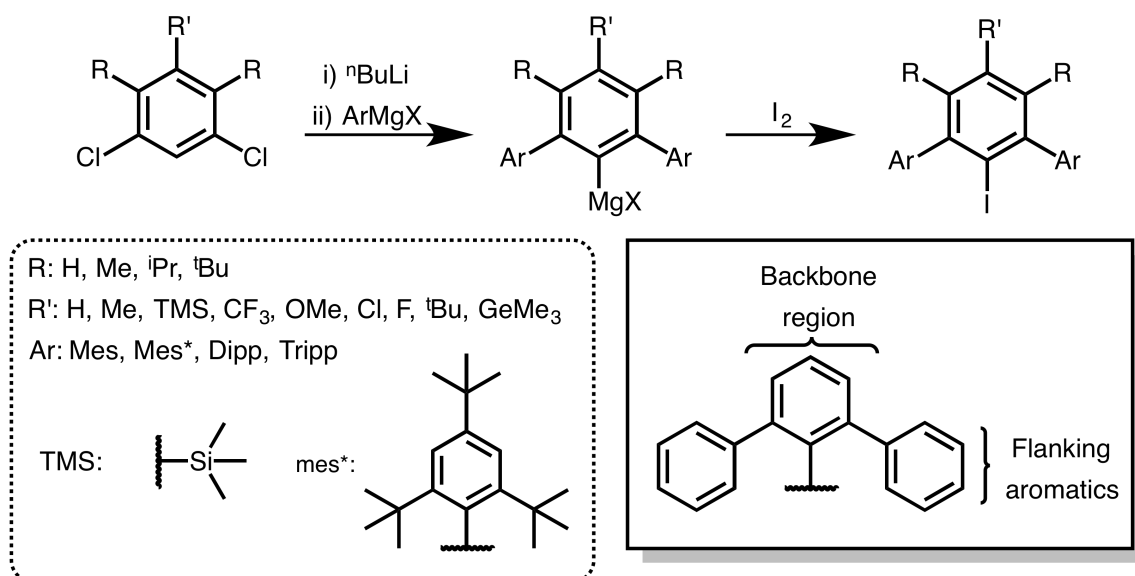
Scheme 2.3: Synthesis of terphenyl-based ligands.

The majority of these ligands' encumbrance is provided through the flanking aromatic moieties, and these can be substituted allowing for modification of the ligands steric profile. The added boon of these ligands is their rigidity: the flanking aromatics can only rotate about the carbon-carbon axial bonds connecting it to the central aromatic. This rotation may be hindered upon the formation of dimeric low-oxidation state main-group element compounds due to steric effects. Furthermore, the backbone region of the central aromatic can also be modulated, which has shown some influence on the electronic properties of these ligands.[16,17]

2.3.2   Terphenyl and Benzhydrol-Like Amines/Amides

Amide ligands have been used extensively in main-group chemistry, starting with smaller ligands such as bis(silyl)amide ($\{(TMS)_2N\}^-$), and moving towards larger amines such as the terphenyl and benzhydrol-like bulky amines (**schemes 2.4 & 2.5**). These larger amines predominantly rely on the steric encumbrance afforded by their aromatic moieties, either from the flanking aromatics or those possessed by the benzhydrol-like functional group. Added steric encumbrance is supplied from the secondary nitrogen subsistent: an alkyl, aryl, boryl, or silyl group.

The majority of the bulky-amine/amide synthesis is involved in the formation of the terphenyl or benzhydrol-like substituted central aniline. For the boryl and silyl derivatives, salt-metathesis can be used to couple the aniline to a silyl or boryl substituent: the bulky aniline is lithiated and quenched with a boryl or silyl halide of choice resulting in the final pro-ligand (**scheme 2.4 & 2.5**).[18,19] Buchwalk-Hartwig amination is the primary route to synthesise the aryl or alkyl derivatives (as shown in **scheme 2.8**, *vide infra*).[20–24]
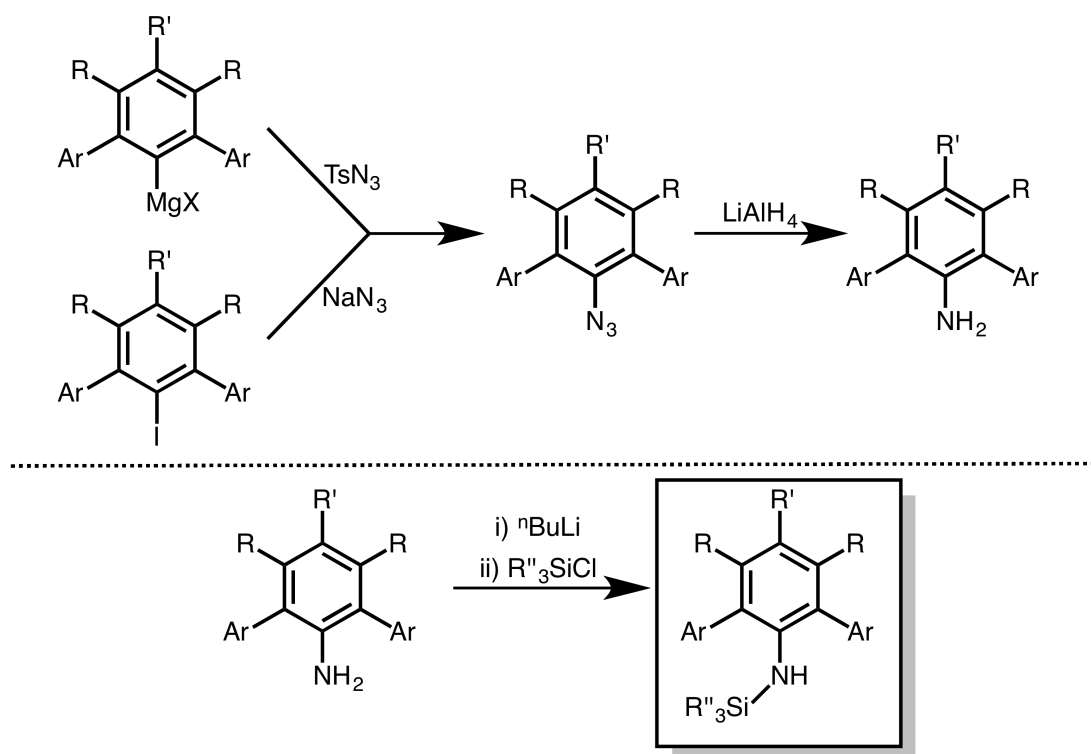
Scheme 2.4: Synthesis of terphenyl bulky amines.

Ar* = R: Me, R': H

Ar† = R: ^{i}Pr, R': H

Ar$^\Omega$ = R: OMe, R': H

Ar' = R: CHPh$_2$, R': H

Ar'' = R: CPh$_3$, R': H

Ar$^\partial$ = R: ^{i}Pr, R': ^{t}Bu

Ar$^\Delta$ = R: NMe$_2$, R': H

R'': Me, ^{i}Pr, Ph, O^{t}Bu
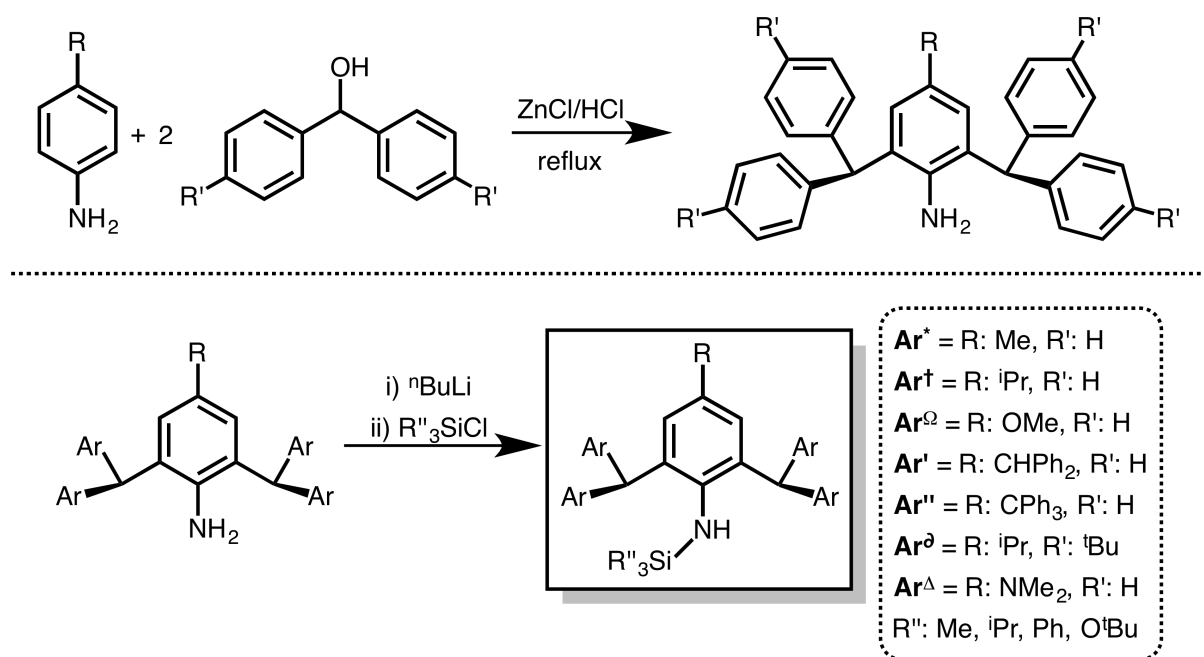
Scheme 2.5: Synthesis of benzhydrol-like bulky amines.

The modularity of these bulky amines/amides means this ligand class is highly tuneable in relation to its steric and electronic profile: the initially used aniline determines the backbone R positions, which has shown some electronic impact in the final compounds; alteration of

the secondary (non-aryl) nitrogen substituent can decrease or increase the potential steric encumbrance provided by the ligand towards the ECOI, as well as significantly altering the electronic character of the nitrogen donor.[23]

For the benzhydrol-like bulky amines/amides, the kinetic stability (steric encumbrance) they afford towards an ECOI can be compromised. Typically, the aryl rings of the benzhydrol-like functional groups flank the ECOI and provide a high degree of steric encumbrance; however, these functional groups can conform/orientate in such a way that the steric encumbrance they provide is reduced. Bond rotation between the tertiary carbon (of the benzhydrol-like moiety) and aromatic carbon (2, 6 positions) allows the aryl rings to 'flip'/point away from the ECOI and instead the tertiary carbon's proton is orientated towards the ECOI. Howbeit, upon complexation it has been noted that aryl interactions with the ECOI may decrease the level of flexibility in the ligand and - like terphenyls - the allowance of rotation and flexibility is limited when forming dimeric low-oxidation state tetrel element compounds due to steric clash.[23–26] On few occasions, the relatively acidic benzhydrol-like tertiary proton (CHPh$_2$) has been observed to be C-H activated upon reduction, leading to decomposition and undesirable products.[26]

The effectiveness of terphenyl substitued bulky amides in stabilising low-oxidation state group 14 element compounds has been lacklustre[ix] ; no further chemistry has been successful with these ligands in the field of low-oxidation state main-group chemistry. Primarily, it is believed that due to the incredible steric encumbrance about the nitrogen donor - the steric repulsion between the aromatic moiety and ECOI causes cleavage of the bond between donor and main-group centre: in layman's terms, there is not enough area about the nitrogen donor atom to allow heavy another element to bind sufficiently.

2.3.3 Bulky Boryl-Amines/Amides: {(^{Dipp}DAB)B}(R)NH Amines/Amide

A class of bulky amine/amide, the bulky boryl-amide ligand {(^{Dipp}DAB)B}(SiR$_3$)N}$^-$ ({(^{Dipp}DAB)B}(R)NH for the amine, where DAB = (DipNCH)$_2$, Dipp = C$_6$H$_3$Pr$^i_2$-2,6)) offers an alternative steric and electronic environment for the ECOI. This is primarily due to the DAB moiety, which influences the directionality of the flanking aromatics and alters the electronics of the nitrogen donor.[27]

^{Dipp}DAB is synthesised by the imination of glyoxal with two equivalents of diisopropyyl aniline, this is then followed by multiple salt-methatheses to form the desired compound as shown in **scheme 2.6**.[27,28]

[ix]Some success has been achieved in stabilising low-oxidation state main-group compounds utilising the terphenyl anilines.[15]
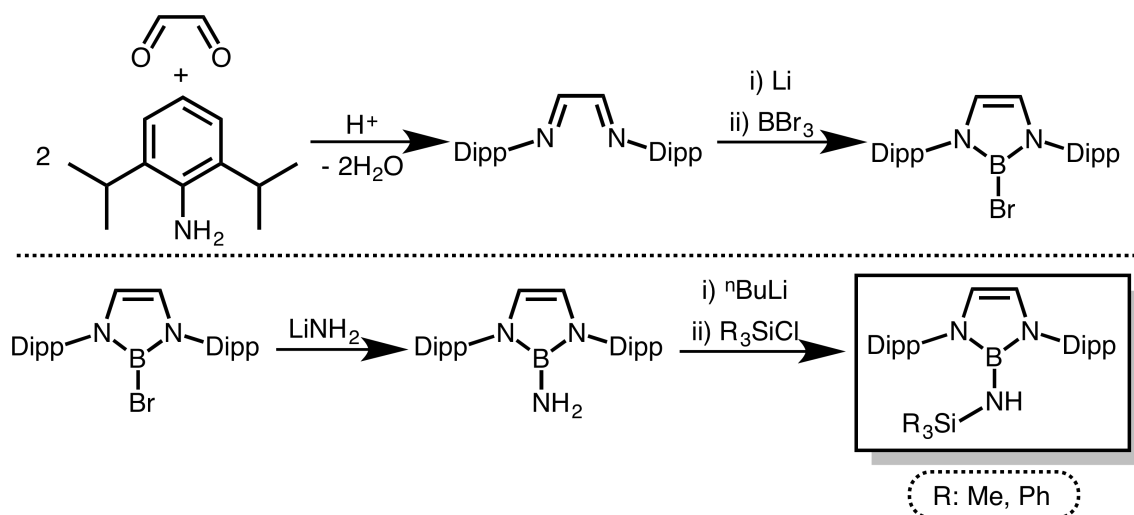
Scheme 2.6: General synthesis of {(^{Dipp}DAB)B}(R)NH species.

{(^{Dipp}DAB)B}(R)NH relies on its aromatic moiety to provide the majority of steric en-cumbrance towards a ECOI[x]. The benefit of this ligand-class is both electronic and steric; electronically, the boron allows some degree of nitrogen lone-pair back bonding, which has a concerted electronic effect on the low-oxidation state main-group element it stabilises and hence changing the reactivity at the main-group element centre; sterically, it is a rigid system, potentially equivalent to the rigidity of the aromatics in terphenyls.

2.3.4   Saturated Indacenes

The last of the monodentate ligands discussed are the carbon-donor 1,1,3,3,5,5,7,7-octa-R-substituted s-hydrindacenyl groups, or saturated indacene ligands, reported by Matsuo and co-workers.[29] Rigid, sterically demanding, and modular, this ligand class has quickly seen success in the realm of main-group chemistry; primarily, their success in stabilising low-oxidation state main-group element compounds has been attributed to their rigid s-hydrindacenyl skeleton which maintains a consistent orientation and steric environment about the ECOI ("freeze-rotation").[30,31]

Shown in **scheme 2.7**, the synthesis of these saturated indacenes requires multiple steps which are generally low-yeilding, creating a pseudo-barrier for further interest in these lig-ands: the synthesis is arduous including grignard coupling, chlorination, followed by an intramolecular double Friedel-Crafts alkylation, and, lastly, bromination. The halide com-pounds (the bromide containing compounds) acts as the precursor to the ligand lithium salt. The synthesis allows for modification to the positioning of the R groups: the R/R' groups can be situated as to have the R groups placed on the side of the halide (side of bonding),

---

[x]The degree to which the flanking aryl substituents of the nitrogen atoms (of DAB) protect the ECOI is somewhere between that observed in similar amidinates and nacnacs.

reversed so that the R groups are facing towards the halide, or crossed producing mix of these two environments and creating a pseudo-asymmetric spatial environment about the ECOI.
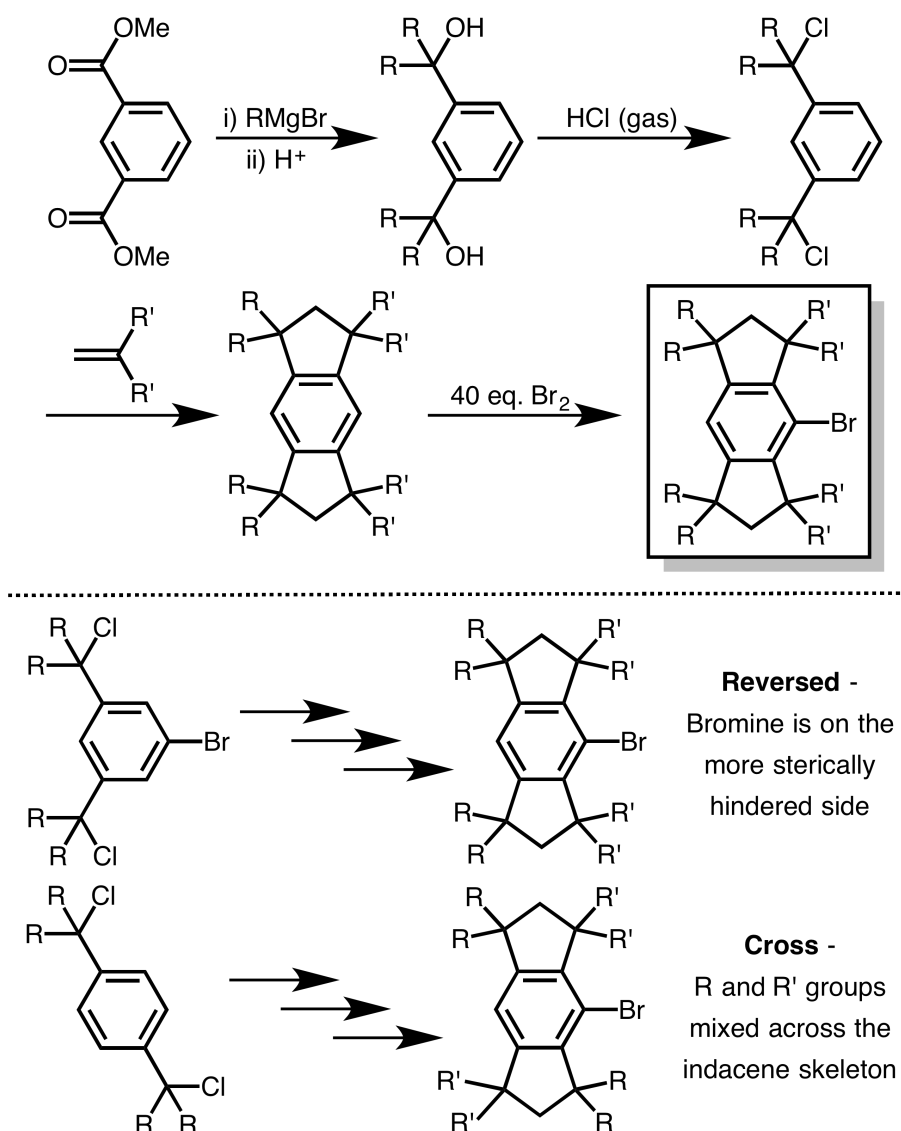
Scheme 2.7: General synthesis of saturated indacenes (top); and the conformations of R groups upon the indacene framework (bottom).

Unlike most of the examples presented, the steric encumbrance provided by these ligands is not predominantly created by the aromatic fragment but often by cyclic and non-cyclic alkyl groups (R). The proximity of the tricyclic-indacene body and the R substituents upon the four benzylic positions relative to the ECOI creates a steric pocket which is both consistent and proximal. This is compounded by their rigidity - their "freeze-rotation" - creating an kinetically stabilising environment.

2.4   Steric Terminology: Bulk, Flexibility, and Proximity

Kinetic stabilisation of an ECOI can only be accomplished when a molecule or ligand with the appropriate spatial and physical qualities are utilised. These spatial and physical qualities culminate in the ability of a ligand to provide a sterically encumbering environment for the ECOI i.e. provide kinetic stabilisation. These are also generally referred to as steric effects. The steric effects of the ligand, combined with the electronic effects, influence the properties of the complex and reactivity of the ECOI.[32] Coille and co-workers suggested the following equation to illustrate this relationship (**equation 2.1**). The nature of low-oxidation state main-group chemistry and its reliance on kinetic stabilisation puts an emphasis on understanding these steric effects.

$$Complex\ property = A(unknown) + B(sterics) + C(electronics) \tag{2.1}$$

A ligand's spatial and physical qualities, which influence its steric profile, have been discussed within the literature, but often the terminology used to describe the steric profile of a ligand is not uniform or focuses on one class of ligand.[32] Consequently, the transferability of these assessments becomes limited to a specific field of chemistry. Another issue is the over simplification of sterics; typically a ligand is described as being bulky[xi] and so can be (or is) sterically encumbering.[33] This simplification of steric concepts leads to oversight: if the steric parameters which enable kinetic stabilisation are not articulated they are not considered in the future design of ligands. The aforementioned steric effects are not only related to a ligand's size (bulk) but also its shape, conformation, and orientation.[33]

A computationally derived qualitative approach to characterise the steric profile of ligands is beneficial. It is proposed that the major steric parameters are: bulk, flexibility, and proximity[xii]. Bulk, though the most commonly expressed steric parameter, is the least important factor to describe steric encumbrance and should be considered a secondary steric factor. The more important, primary steric factors which should be considered are the flexibility (rigidity) and proximity (distality[xiii]) of the ligand's bulk.

The theorem established here is best exemplified and relies on computational methods. What is provided henceforth is an attempted crude/rudimentary theoretical approach[xiv] but nonetheless one which provides some indication that more than bulk (size) should be considered when describing a ligand's steric properties. To establish this approach, **figure**

[xi]An ellipsis is employed: bulk typically refers to steric bulk, which is the broad term used to describe sterics hindrance within a molcule.

[xii]These parameters have been suggested before. However, as stated *vide supra*, their inconstant use and the lack of uniformity in terminology have made their use in-consistent and non-transferable.

[xiii]Derived from the word distal.

[xiv]The methodology is provided in the **experimental** of this chapter and an explanation as to the utility of the method is offered within that section.

2.2 illustrates the base/foundation motif of some commonly utilized monodentate ligands within low-oxidation state main-group chemistry.
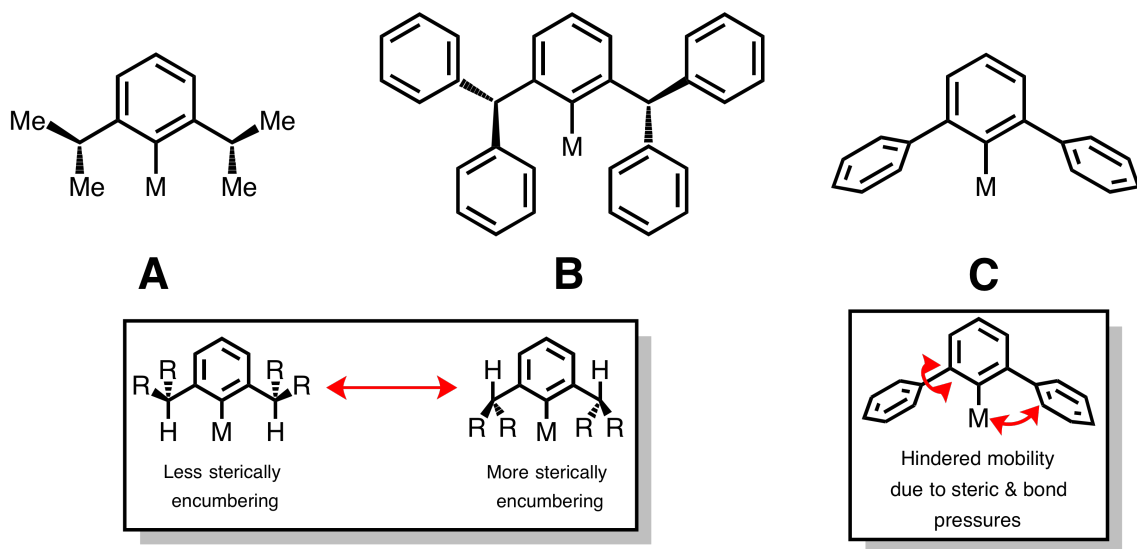
Figure 2.2: An illustration for the potential flexibility ligands can experience when not in the solid-state.

From **figure 2.2**, what should be immediately apparent is the contrasting bulk between examples **A** and **B**; obviously **B** is much bulkier (it has a greater surface area). From this most would deduce an increase in steric encumbrance when **B** is employed, and based on the steric mapping this seems to be a reasonable expectation (*vide infra*). Let us now consider example **C**, here we have a ligand that based on intuitive deduction is smaller in bulk than **B**, and so it shouldn't be unreasonable to expect less steric encumbrance, which is what is observed, **C** having a buried volume (bV%) of 36.7% (**table 2.1**). Lastly, let us make a slight tweak to **B** - "giving" the system a small quanta of energy we could expect rotation and movement of its parts - and flip the benzhydrol-like substituents away from the ECOI; now, the bound element's steric protection has been drastically compromised. This rotation is not something that is experienced within the solid-state but can/does occur in the solution state[xv]. The inherent flexibility in **A** and **B** befuddles the steric profile/data and are not always going to provide the most sterically encumbering environment; **C** on the other-hand provides a consistent sterically encumbering environment.[29]

And so what has been established is that based on the property of bulk we cannot fully explain why one ligand is more sterically encumbering than another; and, even in our reasoning we must employ further explanation as to why one ligand has a higher potential for steric encumbrance than another. This leads us to the second steric factor (if bulk is to

---

[xv]To extrapolate this change in orientation, the energy required for rotation must be determined. This is accomplishable using modern day computational chemistry, though, patience and resources are expended and it is not always efficient to do these calculations during the ligand development stage.

be considered the first factor): **flexibility** and **rigidity**. The more flexible the functional groups which provide a pocket of protection, a cone, or any other conceived term for steric encumbrance, the more chance that the degree of kinetic stabilisation provided can be altered outside of our immediate control. Flexibility in a ligand creates a range of steric encumbrance going from the a fixed value to a spectrum or range value. Taking bulk into consideration with flexibility/rigidity, we can begin to describe kinetically stabilising ligands more precisely. An example is provided in **table 2.1** showing the suggested method of reporting a ligand's steric profile[xvi].

Table 2.1: *An example table for the proposed format and steric data which should be presented when discussing the steric effects of a compound, molecule, or ligand. Within the table, the steric data for examples* **A**, **B**, *and* **C** *are presented. These are computationally derived values.*

Molecule	Bulk	Flexibility	Proximal Bulk	Distal Bulk
A	234.7 Å^2	180° rotation 31.3-47.6%	44.0%	21.6%
B	469.9 Å^2	180° rotation 33.9-73.1%	44.8%	35.1%
C	305.0 Å^2	45° rotation 36.7-40.4%	36.7%	27.7%

Note: Bulk is expressed as a surface area in values of Å^2. All following values are expressed as a bV% value. Flexibility is qualitatively described; the bV% value is that of the approximate least to most sterically encumbering orientation of the molecule in relation to the ECOI. Proximal bulk is measured using a 3.5 Å radius sphere; distal bulk a 6.0 Å radius sphere. The degree of rotation pertains to the 2,6-substituents upon the aryl rings.
Note: The magnitude of degree rotation is based on observed steric clash within the molecular model upon rotation.

The last factor to be proposed is **proximity** or **proximal bulk**. Proximal bulk defines the spatial arrangement/distance of a ligand's bulk in relation to the ECOI: when the bulk afforded by a ligand is spatially close to the donor-atom of the ligand, the ligand is considered to be proximally bulky. The opposite of this is **distality** or **distal bulk**; a ligand with bulk situated away from the ECOI is said to have distal bulk.

Proximal bulk directly influences the reactivity that occurs at the ECOI. Increasing the proximal bulk of a ligand decreases the accesible coordination site on the ECOI, and so decreases reactivity. This can be manipulated to form unique steric pockets which preferentially allow particular reactions to occur at the ECOI. In this way, proximal bulk can be thought of as inhibiting ECOI reactivity (and therefore increasing stability). This qualitative description describes the ligand's impact on the kinetic diamater/face of the ECOI; the

---

[xvi]This data was calculated as stated within the methods section of this chapter, using hypothetical models as determined by the author.

reaction rate at the ECOI is affected, but the description emphasises the type of reactivity allowed for at the ECOI.

Distal bulk influences the reactivity at the ECOI with larger molecules and influences the reaction rate of the entire complex as does total bulk (complex surface area). Distal bulk can create steric pressure on larger molecules preventing contact with the ECOI and disallowing reactivity. Distal bulk and total bulk should correlate with rate of reaction for the complex: by increasing both, the kinetic diameter of the complex increases and reactivity of the whole complex goes up, but reactivity of the ECOI goes down. The reactivity at the ECOI goes down as it represents a smaller percentage of the kinetic sphere relative to the ligand. In flexible ligand systems, distal bulk may reflect the ligand's bulk which is flexed away from the proximal sphere and could potentially orientate towards the ECOI in the solution state.[xvii]

Theoretically, the optimal ligand would have enough proximal bulk to stabilise the ECOI and allow for the desired reactivity whilst having minimal distal bulk as to reduce the total surface area/bulk of the complex and increasing reaction rate at the ECOI[xviii].

If flexibility and proximity are to be taken as a spectral characteristic of bulk, then the idea of proximal branching is a point of detail in our expression of proximity, and will be defined here: **Branching** is when an element has multiple single bonds to non-hydrogen elements; therefore, **proximal branching** is specifying the element/point which branching occurs relative to a donor element. When comparing similar substituents the one which displays proximal branchiation is most likely to impart greater steric encumbrance to a ECOI as it may restrict the flexibility of the proximal bulk and, intrinsically, this group offers more proximal bulk i.e. it occupies more space closer to the ECOI. However, this is not an absolute and more work needs to be done to confirm or deny this concept.

The intention of this qualitative characterisation (approximation) of a steric profile is to enable a qualitative identification of why, how, or what class of steric environment is being afforded to an ECOI. These terms allow for the suggestion of steric parameters and identify the boons and short-fallings of ligands: ligands with too much flexibility may lead to quicker decomposition of unstable low-oxidation state compounds; too many proximally situated ligand-parts may impede ECOI reactivity; the bulk of the ligand, whilst large, may not actually impede decomposition pathways. Evidently, these parameters can be refined with the utilisation of further computational chemistry techniques, though this endeavour can be inefficient (in relation to time) when in the ligand design phase.

[xvii]It also provides a measure of potential proximal bulk for when the L-M bond distance increases.

[xviii]Proximal bulk should lead to greater steric encumbrance of the ECOI but this is not absolute. A counter example would be to imagine a ECOI captured within a buckminsterfullerenes: it is completely sterically encumbered yet has no proximal bulk, just distal bulk.

2.5   Research Proposal

Sterically encumbering monodentate ligands with the potential to stabilise low-oxidation state main-group elements comprise of two factors: sterics and electronics (and unknown factors, refer *vide supra* to **equation 2.1**) . With the end goal of formulating low-oxidation state group 14 elements compounds, we looked to synthesise a range of novel ligands. A two pronged approach was taken where ligand steric factors would be investigated; secondly, the electronic influence of a nitrogen's secondary substituent in bulky amines would be investigated, focusing on boryl amides.

2.5.1   Part 1: Tricyclic Ringed Motifs and Bulky Amines

Within the Jones group, the use of benzhydrol-like amide ligands has led to the synthesis of a range of low-oxidation state main-group element compounds. This success has not been without the occurrence of undesirable phenomena: weak aryl interactions between the phenyl moiety of the benzhydrol-like motifs and the ECOI, decreasing reactivity; ECOI activation of the benzhydrol-like tertiary proton, oxidising itself and reducing reactivity; and the majority of the benzhydrol-like amide ligands' bulk is flexible, hence potentially not always providing the consistent kinetic stabilisation desired. The desirability of the amine/amide ligands is their high functionalisation: the secondary (typically, non-aromatic) substituent on the nitrogen can be modified to tune the steric profile and, or, the electronic profile.

Recently, the Matsuo group have developed saturated indances (*vide supra*). These ligands utilise a fused tricyclic ring motif, forcing a high degree of structural rigidity and have no acidic protons prominent to the bound element centre.[29]

We propose that by combining the concept of rigidity (as seen in saturated indacenes) with the functionalisation of bulky amides we can produce a new class of tricyclic ringed bulky amines/amides capable of stabilising low-oxidation state main-group element compounds.

2.5.2   Part 2: The Electronic and Kinetic Influence of Boryl Subsitutents

Amides are prominent within the field of low-oxidation state main-group element chemistry. Within the Jones group, silyl amides with a large aromatic moiety have allowed for the isolation of a range of compounds. However, it has been suggested that the donor-nitrogen lone-pair may donate into the formally empty non-bonding p orbital of the bound low-oxidation state tetrel element centre and reduce their reactivity.

To investigate this, a range of boryl amides were synthesised in an attempt to create a

nitrogen-donor ligand with reduced nitrogen lone-pair donation towards its bound ECOI. The first of these ligands was {($^{\text{Dipp}}$DAB)B}(TMS)N$^-$, which due to electronic saturation of the boryl moiety displayed no significant back-bonding donation from the donor nitrogen towards the boryl fragment (*vide infra*).[27]

Unpublished work from within the group took advantage of monodentate boryl amide ligands, utilising aryl and alkyl boryl substituents upon the nitrogen donor atom. These substituents reduced electronic over saturation of the boron allowing nitrogen π back-donation; consequently, these ligands may potentially render the tetrel element centre (the ECOI) an an empty p orbital, increasing complex reactivity.[24]

We propose that the development and utilisation of ligands based on these principles may eventuate in the formation of highly reactive monodentate tetrel element complexes.

2.6 Results & Discussion (R&D): Ligand Design and Synthesis

The following sections are broken down into tricyclic ring containing amine and boryl amines ligand precursors (pro-ligands), where each section looks at a particular subclass. Each of these pro-ligands are characterised both experimentally and computationally - the steric characterisation methodology detailed *vide infra* is used to elucidate the potential kinetic stabilisation of these pro-ligands.

2.7 R&D: Tricyclic Ringed Motifs and Bulky Amines

On the presumption that our proposal of bulk, flexibility, and proximity are pertinent factors in relation to the steric profile of ligands, we sought to synthesise ligands which allowed for rigidity and proximity of bulk in relation to a bound main-group element centre. In order to achieve this we looked towards multiple-cyclic groups which would enforce rigidity within the desired aromatic moieties. The ubiquity of tricyclic aromatics within the literature - and recent efforts to synthesise similar aromatics within the group - pushed our efforts in this direction.[34]

In our efforts, we successfully synthesised a range of pro-ligands meeting our rigidity and proximity requirements. However in our shortsightedness, we did not foresee the ease of internal redox activity tricyclic ringed compounds can undergo; that, combined with a multitude of ligand efficacy issues, caused problems in further chemistry with group 14 halides (be discussed in **chapter 3**).

2.7.1 Anthryl Amines

Forays into tricyclic ringed ligand systems eventually led us to anthracenes - chemically the simplest and potentially smallest in bulk of the tricyclic aromatics.

Previous reports had shown the successful utilisation of anthracene as carbon donor ligands in low-oxidation state boron and selenium chemistry. In this work the well-documented redox activity of anthracene was not observed in-spite of harsh reducing conditions.[35–37] Based on that work, anthracene's redox activity was not believed to be an issue and, hence, suitable as moiety for inclusion in secondary amine pro-ligands. (bulky anthryl amines, or 9-(R)aminoanthracenes where R = alkyl/aryl).

Synthesis

Based on the tremendous work of Buchwald and Hartwig, we believed that the simplest course of action in synthesising *N*-R-9-anthramine (anthryl amines) was via Buchwald-Hartwig palladium coupling (amination). Similar synthetic work to synthesise secondary anthryl amines has been carried out by a number of research groups.[38,39] This synthetic route allowed for the successful preparation of a range of anythryl amines with a range of alkyl substituents as shown in **scheme 2.8**. This synthetic route has previously been reported for the synthesis of the *N*-'chiral'-9-anthramines **5** & **6**.[38]

Name	R
An(tBu)NH (**1**)	tBu
An(Cyc)NH (**2**)	Cyc
An(tOct)NH (**3**)	tOct
An(Ad)NH (**4**)	C1
An(C1)NH (**5**)	C2
An(C2)NH (**6**)	Ad
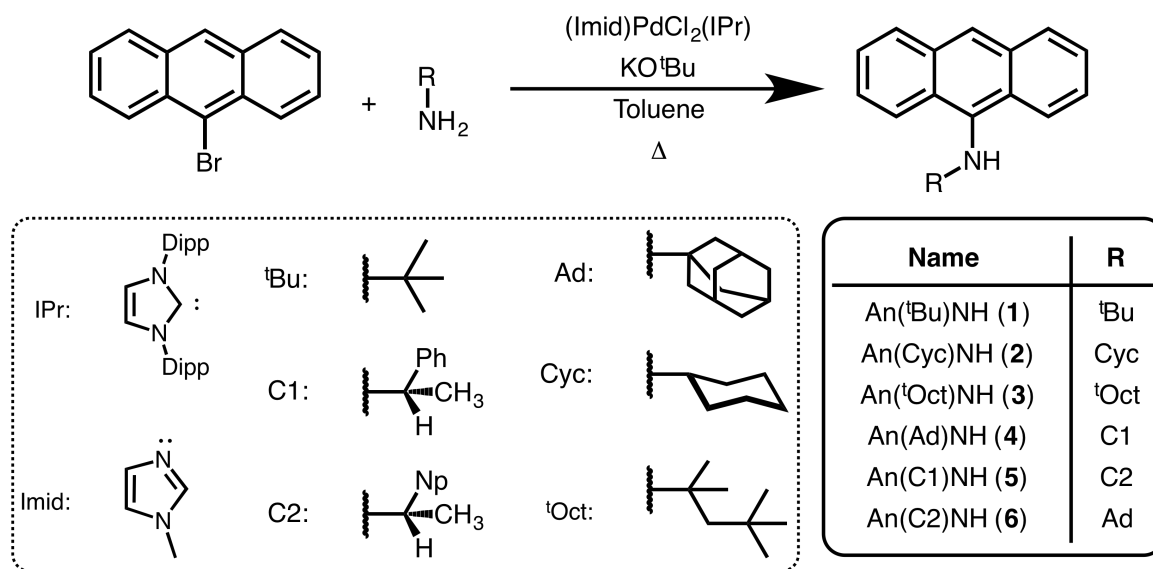
*Scheme 2.8: Preparation of the anthryl alkyl amines **1-6** via Buckwald-Hartwig palladium amination coupling (C1 and C2 are used as enantiopure reagents).*

Overall, the syntheses are straightforward and require little alteration aside from the workup phases of **5** & **6**. The desired reaction temperature is dependent on the amine used, lower boiling amines requiring less heat and more time for completion; though, it

was found that having the reaction temperature too low would drastically lower yields as the reaction struggles to commence. The optimal temperatures for the synthesis of pro-ligands **1**-**6** were approximately 5°C below the respective amines boiling point, and when lower temperatures are required more solvent should be used to avoid too viscous a solution from forming. The reaction can be monitored by ^{1}H NMR spectroscopy to ensure conversion to the desired product; if after 2-3 hours the reaction hasn't finished, extra equivalents of catalyst and amine are required (upon workup these can be filtered away from, or boiled away, respectively). For **5** & **6** enantiopure reagents were used.

The reactions were generally high yielding and crystallisation of the pro-ligand occurred upon concentration of the respective hexane mother liquor. This however was not the case for An(C1)NH (**5**) and An(C2)NH (**6**) which upon removal of volatiles were isolated as oils. Solidification required sonication in iso-propanol, though **6** slowly returns to a viscous oil (which was spectroscopically pure).

Analysis of the ^{1}H NMR spectra for **1**-**6** indicates the presence of an acidic N-H proton: the assigned N-*H* chemical shifts ranging from δ 3.5-4.2 ppm (the greatest outlier being δ 4.21 ppm for **6**). Surprisingly, **3** displayed a N-*H* proton signal at δ 3.62 ppm which does not correlate with our difficulties in lithiating this pro-ligand (discussed in **chapter 3**)[xix]. All other obtained data were in concordance with our ^{1}H NMR spectroscopic analyses: mass-spectroscopy was used to identify the molecular ion and infrared spectroscopy confirmed the presence of an amine functional group.

Exceptions to this synthetic route's success were our attempts to prepare *N*-phenyl-9-anthramine (An(Ph)NH) **7**, *N*-2,6-diisopropylphenyl-9-anthramine (An(Dipp)NH) **8**, and *N*-Ar†-9-anthramine (An(Ar†)NH) **9**. From our attempts to form **9** we isolated the aniline, Ar†NH$_2$, and 9-bromoanthracene, both starting materials (determined by ^{1}H NMR spectroscopy). We believe that steric repulsion between the anthracene and Ar† fragments created too high an energy barrier to allow coupling to occur, or that steric repulsion caused cleavage of the presumptive product (**9**) from this reaction. For **7** and **8** we isolated a crop of red needle-shaped crystals, indicating the formation of an unexpected product[xx]. This anomaly occurred on two other occasions, and single red crystals were isolated away from crystalline **1** and **2**. In each case, preliminary X-ray crystallographic diffraction indicated the formation of the oxidised anthraquinone monoimine derivatives of the expected 9-arylaminoanthracenes (**figure 2.3**). Due to time-constraints and the nature of the compounds, full X-ray crystallographic data were not collected on all these samples, only on N-phenyl p-anthraquinone **10** (*vide infra*).

Oxidation of **7** and **8** was believed to have occurred during the workup phase due to the

---

[xix]The acidities of the N-H proton are a tenuous assignment; due to the presence of the anthryl moiety it is possible that the proton chemical shifts do not correlate directly with acidity.

[xx]All other isolated crystalline material of these species were found to be yellow.

presence of adventitious moisture/water (the most likely oxidant contamination). Due to further developments with these ligands, repeated syntheses of **7** and **8** were not pursued further.
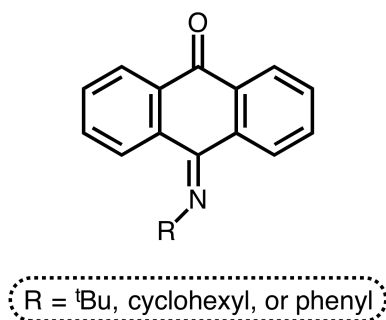

R = ^{t}Bu, cyclohexyl, or phenyl

Figure 2.3: General structure of oxidised product, the N-phenyl p-anthraquinone **10**.

It is difficult to ascertain the exact cause for the formation of the anthraquinone monoimine derivatives during this reaction pathway, but there is some precedent. 9-aminoanthracenes are known to undergo air oxidation, in some cases. Contrary to our findings, it has been suggested by Shaughnessy and co-workers that 9-arylaminoanthracenes are typically more stable (unless sterically hindered) to oxidation due to delocalisation of the amine lone pair into the aryl substituent.[39] The electron density of the ligand is delocalised towards the aryl moiety rather than towards the anthryl moiety. The exceptions to this theory are the sterically hindered 9-arylaminoanthracenes, such as **8**, which display increased air sensitivity (oxidation potential) as there is a decrease in the resonance delocalisation across the nitrogen, aryl, and anthryl moiety, as the nitrogen bound substituents are forced into a perpendicular arrangement[xxi], favouring delocalisation towards the anthryl moiety[xxii].[39] Essentially, Shaughnessy and co-workers relate the oxidation potential of these species to the magnitude of delocalisation from the nitrogen across the bound substituents, which is influenced by the substituent's conformation about the nitrogen relative to one another (where more delocalisation across both substituents decreases the oxidative potential of the anthryl moiety).

This facile explanation ignores the influence of σ withdrawal by the non-anthryl substituent and how this affects delocalisation across the compound. Also, it presumes simultaneous nitrogen lone-pair delocalisation towards both substituents is prevented based on geometric constraints, when rather the scale of delocalisation is skewed to favour the anthracene whilst still being somewhat directed towards the aryl moiety. The perpendicular arrangements of the substituents is not an absolute orientation. Furthermore, it does not

---

[xxi]This perpendicular arrangement does not allow the nitrogen's lone-pair-of-electrons orbital to sit in the orientation which allows for simultaneous delocalisation towards the aryl and anthryl moieties.

[xxii]For 9-arylaminoanthracenes, the anthracene's aromaticity is broken more easily than that of the aryl fragment as it is comparatively weaker than that of single ringed aryl systems.[37]

account for the formation of **7**[xxiii]. Based on their explanation, it would follow that the 9-alkylaminoanthracenes (**1-4**) should have a comparatively increased affinity towards oxidation. This would be due to the alkyl moiety's decreased capacity to accept π electron density from the amine, pushing delocalisation towards the anthryl moiety, which based on our findings they do not.

It is proposed that the the increased oxidative potential of 9-arylaminoanthracenes is due to increased electron withdrawal properties from the amine by the respective aryl moiety (comparative to alkyl substituents), and that steric hindrance plays a secondary role in this phenomenon. The increased electron withdrawal of the aryl moiety has a concerted effect on the nitrogen π donation, i.e. the nitrogen interacts through its lone-pair with the anthryl moiety as to become electronically satisfied. Also, this explains the comparative decreased oxidative potential we observed in the 9-alkylaminoanthracenes: increased electron donation from the alkyl group to the nitrogen through the σ bond reduces the necessity for π donation into the anthryl ring as the nitrogen is electronically satisfied.

Spectroscopic Analysis

A comparative analysis of the ^{1}H NMR spectra of **1** and **7** supports our hypothesis stated above: for **1**, the N-H peak is significantly more shielded (δ 3.43 ppm, collected in C_6D_6) than in **7** (δ 6.01 ppm, collected in $CDCl_3$). These chemical shifts suggest a more electron rich nitrogen centre in **1** than for **7**. Presumably, this is due to the weaker electron withdrawing effect of the tert-butyl subsitutent upon the nitrogen. A similar contrast can be drawn between **7** and compounds **2-6**. Analysis of the ^{1}H NMR spectra of **1-6** suggests decreased nitrogen lone-pair delocalisation and resistantce to oxidation.

Formation of oxidised anthriquinones indicates an increase in the oxidation potential of the anthracene moiety (relative to anthracene) upon the addition of an amine functional group. This is supported by ^{1}H NMR spectroscopic analyses, showing a general shift upfield for the backbone Ar-H, indicating increased electron density - increased electronic resonance - within the anthryl moiety, in comparison to anthracene.[40] The ^{1}H NMR spectra for compounds **1-6** display indicative Ar-H proton signals at $\approx \delta$ 7.84 to 8.08 ppm which is believed to correspond to the backbone Ar-H proton environment (based on the integration).

The possibility of internal redox activity is apparently a definitive characteristic of tricyclic-ringed aromatic containing amines as similar results were noted for the Ar^X ligand system upon complexation to group 14 elements, discussed in **chapter 3**.

[xxiii]**7** is non-hindered and should orientate as to increase delocalisation upon the aryl moiety rather than the anthryl moiety and, based on their rationale, decreasing oxidation of the anthryl moiety

Synthesis of Anthryl Bis-tert-butylamine

The possibility of redox activity within these pro-ligands, albeit not expected, prompted us to synthesise 9-10-(di-tert-butylamine)-anthracene (An(^{t}BuNH)$_2$) **11** (**scheme 2.9**). The synthetic procedure of this pro-ligand is analogous to the synthesis of **1**. By protecting the backbone aromatic position (10) we believed we would forgo the formation of any backbone activated compounds, oxidised or otherwise. Furthermore, this bifunctional monodentate ligand could theoretically allow for the synthesis of bis-tetrel low-oxidation state compounds (discussed in **chapter 3**).
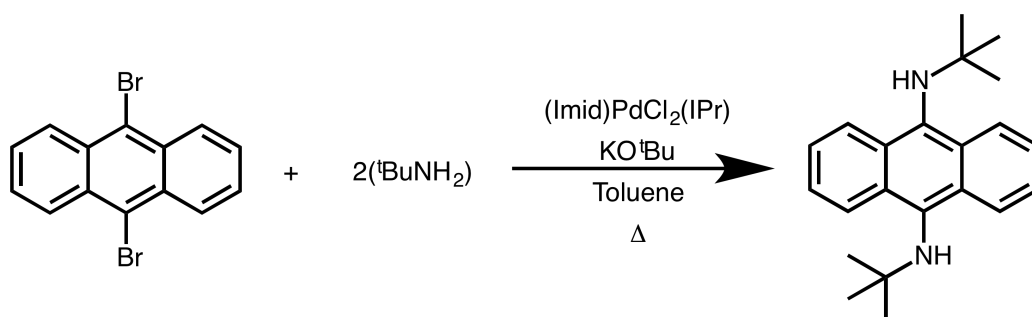
*Scheme 2.9: Synthesis of 9-10-(di-tert-butylamine)-anthracene (An(^{t}BuNH)$_2$) **11**.*

The successful synthesis of **11** was confirmed using ^{1}H, ^{13}C NMR and mass spectroscopic analyses. On a single occasion the synthesis of **11** yielded **1** as a minor product, determined by X-ray diffraction characterisation. Due to the similarities of **1** and **11**'s ^{1}H NMR spectra, it is imperative to note the absence of the Ar-*H* chemical shift which is present in **1** and not in **11**, though this is sometimes difficult due to the complexity of the aromatic region observed in the ^{1}H NMR spectra. The formation of **1** indicated impurity of 9-bromoanthracene within our stock of 9-10-dibromoanthracene.

Chirality and Characterisation of An(C1)NH (5) and An(C2)NH (6)

The presence of the respective chiral moiety in **5** and **6** was determined by optical rotation. There was no evidence to suggest significant racemisation. The enatiomeric excess of the product was slightly lower than the respective precursor amine. Partial racemisation in such reactions has been previously reported.[41]

Analysis of **5**'s and **6**'s spectra showed a doublet splitting pattern[xxiv] of the proton at the chiral C-centre, which is caused by the amine proton - this splitting is reflected for the amine proton, which is observable as a doublet. For both **5** and **6** the N-*H* proton signals are shifted downfield in contrast to **1-4**, indicating an increased acidity of the N-*H* proton

---

[xxiv]Theoretically, it should be observed as a quartet of doublets, coupling to the methyl protons and then the amine protons.

(δ 3.83 (**4**) and δ 4.21 ppm (**5**)). It is suspected that the acidity of the proton at the chiral C-centre in **4** and **5** (δ 4.43-4.50 ppm & δ 5.24-5.31 ppm, respectively) may be preferentially abstracted in the presence of a strong base such as ^{n}BuLi, ^{t}BuLi, or benzyl-pottassium etc., the common reagents used when converting secondary amines into their bulky amide alkali salt congener. Further chemistry done with these systems will be discussed in **chapter 3**.

X-ray Crystallographic Characterisation of An(^{t}Bu)NH (1), An(Cyc)NH (2), An(^{t}Oct)NH (3), and 10-(phenylimino)-9(10H)-anthracenone 10.

Crystals of the secondary anthryl amines were isolated from concentrated hexane solutions, though often conditions meant co-precipitation of the product occurred over time. These crystals were generally suitable for X-ray diffraction and allowed full X-ray crystallographic characterisation of the pro-ligands **1**, **2**, and **3**. Red crystals of **10** were hand-picked from a mixture of 9-bromoanthracene crystals.
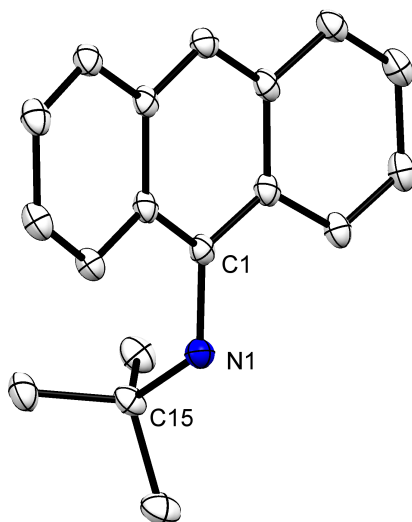
*Figure 2.4: Thermal ellipsoid plot (30% probability surface) of An(^{t}Bu)NH (**1**) (hydrogen atoms omitted). Selected bond lengths (Å) and angles (°): N1-C1 1.421(3), N1-C15 1.492(3); 121.8(2); C2-C1-N1-C15 93.42 (3).*
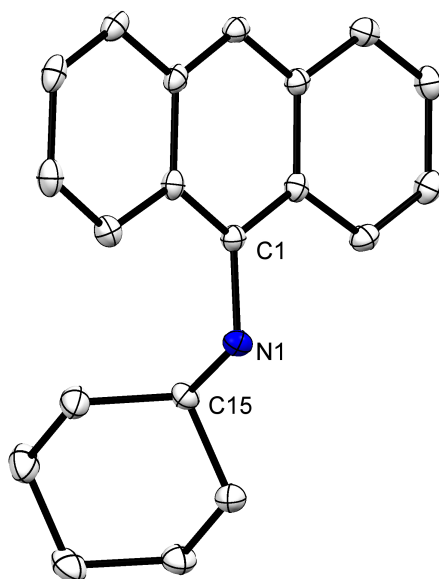
*Figure 2.5: Thermal ellipsoid plot (30% probability surface) of An(Cyc)NH (**2**) (hydrogen atoms omitted). Selected bond lengths (Å) and angles (°): N1-C1 1.424(3), N1-C15 1.473(3); C1-N1-C15 117.5(2); C2-C1-N1-C15 109.68 (2).*

*Figure 2.6: Thermal ellipsoid plot (30% probability surface) of An(^{t}Oct)NH (**3**) (hydrogen atoms omitted). Selected bond lengths (Å) and angles (°): N1-C1 1.430(4), N1-C15 1.510(4); C1-N1-C15 121.3(2); C2-C1-N1-C15 92.97(2).*
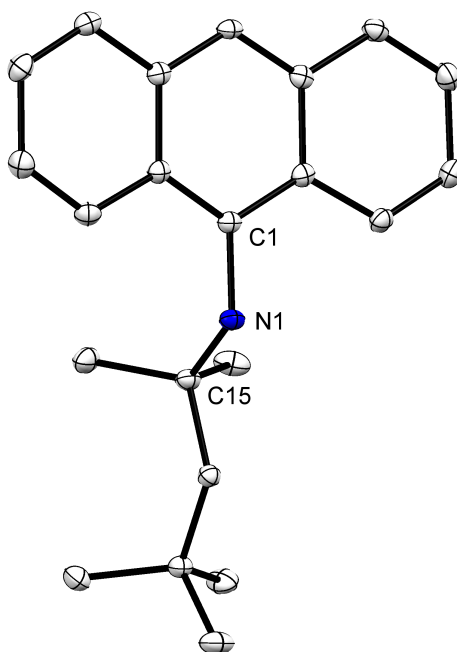
Between the molecular structures of **1** (**figure 2.4**), **2** (**figure 2.5**), and **3** (**figure 2.6**), the N1-C1 (nitrogen to anthryl carbon) bond lengths do not substantially deviate but are

marginally longer than the N-C bond lengths observed in anilines (approximately 1.395 Å). The elongation of the N-C bond is presumably a consequence of steric accommodation, reducing the steric repulsion between the anthryl and alkyl substituents upon the nitrogen. Based upon our tentative assignment of the H1N protons, both **1** and **3** display a nitrogen atom with a planar geometry whilst **2** displays a tetrahedral geometric nitrogen atom; though, no other data can compliment this assignment. Variation of the C2-C1-N1-C15 torsion angle is prominent between **1** (93.42(3)°) and **3** (92.97(2)°) with **2** (109.68(2)°), and is believed to be a consequence of steric repulsion. The cyclohexyl moiety is a smaller alkyl fragment, creating less repulsion between itself and the anthryl moiety; because of this, the cyclohexyl moiety can rotate "underneath" the anthryl aromatic group. For the tert-butyl and tert-octyl moieties this cannot occur as readily due to their increased size. Slight deviation from planarity across the anthryl moiety is observable, the two outer (non-central) aromatics flex away from the direction of the respective alkyl group. This was quantised by calculating the angle between three centroids upon the anthyrl moiety: **1** shows the largest deviation from an ideal plane (180°) at 173.98°; **2** and **3** are 177.36°and 176.05°, respectively. This non-ideal aromatic geometric character may be indicative of the anthryl moiety's potential for redox activation.
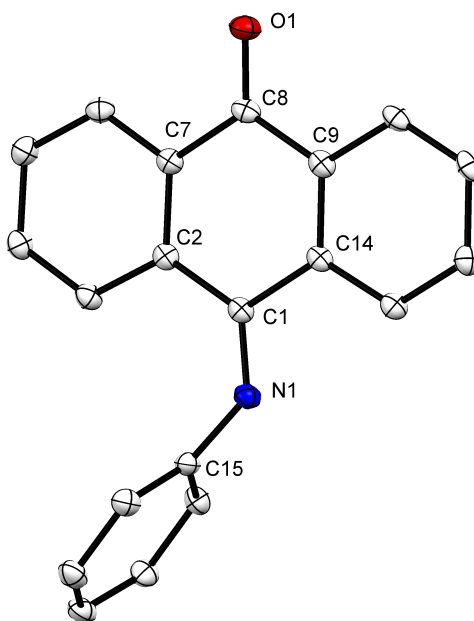
*Figure 2.7: Thermal ellipsoid plot (30% probability surface) of 10-(phenylimino)-9(10H)-anthracenone **10** (hydrogen atoms omitted). Selected bond lengths (Å) and angles (°): N1-C1 1.407(2), N1-C15 1.492(2), O1-C8 1.227(2), C1-C2 1.492(2), C1-C14 1.500(2), C2-C7 1.407(2), C7-C8 1.488(2), C8-C9 1.475(2),C9-C14 1.399(2); C1-N1-C15 128.8(1), C7-C8-O1 120.92 (1); C2-C1-N1-C15 2.99(1).*

The solid-state structure of **10** does not absolutely reflect the bonding expected (**figure 2.7**). N1-C1 bond lengths are similar to those observed in anilines (approximately 1.395 Å),

the bond length between that of a single and double nitrogen-carbon bond. The nitrogen atom adopts a pseudo-trigonal planar geometry as indicated by the C1-N1-C15 bond angle (128.8(1)°), though the proton could not be assigned based on obtained X-ray diffraction data. The central ring of the anthryl moiety displays C-C bond lengths which suggest a loss of aromaticity: the C1-C14 bond length being the longest at 1.500(2) Å.[42] The central anthryl C-C bond lengths (C2-C7 & C9-14) are as expected for aromatic bonds, indicating the flanking aromatic rings maintain aromaticity. The planarity of the anthryl moiety is maintained with no significant deviation from an ideal plane. The O1-C8 bond length of 1.227(2) Å is analogous to carbon-oxygen double-bond lengths observed in carbonyl compounds ($\approx$ 1.23 Å).

Steric Profile

In keeping with the ideals of steric encumbrance factors presented in **section 2.4**, we sought to characterise these pro-ligands in terms of bulk, flexibility, and proximity[xxv]. To maintain consistency, all the obtained values are from the optimised models of **1-6** which we believe adequately reflect the actual structures of these amines. The almost exact replication of buried-volume values between the optimised amine structures and those obtained from X-ray crystallographic diffraction for **1**, **2**, and **3**, indicated the validity in our optimisation calculations (refer to the **methodology** of this chapter). All optimised structures are carried out using density functional calculations (DFT) at the B3YLP/6-31G(d, p) level.

The bulk of **1-6** was established using the software VEGA-ZZ, which calculates the accessible surface area[xxvi].[43–45] To date, and to the best of our knowledge, there is no software to quantise or suggest the flexibility of a molecule in relation to the sterics afforded to an assigned centre. Because of this, the flexibility stated is only suggested based on our chemical intuition. For proximity, the software sambVCA was used to establish the bV% of the proton upon these compounds and the bV% afforded at a dummy distance of $\approx$1.85 Å[xxvii].[46] The proximal bulk bV% value reflects the steric environment these amines - when converted to and used as ligands - may create about a ECOI when in the solid-state.[xxviii]

Outside of qualitative descriptors of proximal bulk, there is no direct measurement of

---

[xxv]As there is no discernible/appropriate way to measure flexibility of a molecule in relation to its steric profile, the presented data is based on intuition and our rationale i.e. on approximate least to most sterically encumbering orientations a molecules conforms to about a ECOI (refer to section 2.4).

[xxvi]The surface area gives a relative measurement of the bulk to the kinetic stability afforded towards an ECOI (refer to **section 2.4**).

[xxvii]Based on average N-Ge bond distances.

[xxviii]For comparative reasons it is important to use the same element in the bV% calculations; hydrogen was used as this best represented the amines/ligands as a stand-alone compound. The bV% of a ligand is only exact when talking in relation to a specific element-centre - all other discussion is based upon extrapolation from these values i.e. pro-ligand bV% are larger than those where a larger element is used as the sphere of reference.

this steric parameter and so the bV% is used.

Table 2.2: Bulk, flexibility, and proximity data for ligands **1**-**6**. Bulk is expressed as a surface area in values of $Å^2$.

Compound (#)	Bulk	Flexibility	Proximal Bulk	Distal Bulk
An(tBu)NH (**1**)	295.6 $Å^2$	n/a	56% (27.7%)	27.3% (21.5%)
An(Cyc)NH (**2**)	325.6 $Å^2$	change of chair conformation	54.8% (28.2%)	29.8% (22.8%)
An(tOct)NH (**3**)	351.3 $Å^2$	R flex[a] and N-R axial rotation[b] 52.1-71.7%	64.1% (33.0%)	34.7% (27.3%)
An(Ad)NH (**4**)	354.1 $Å^2$	n/a	57.5% (28.3%)	34.0% (24.9%)
An(C1)NH (**5**)	332.2 $Å^2$	N-R axial rotation[b] 51.6-57.2%	52.7% (25.3%)	29.8% (20.6%)
An(C2)NH (**6**)	407.6 $Å^2$	N-R axial rotation[b] 51.6-60.7%	53.0% (25.9%)	31.7% (21.0%)

Note: Bulk is expressed as a surface area in values of $Å^2$. All following values are expressed as a bV% value. Flexibility is qualitatively described; the bV% value is that of the approximate least to most sterically encumbering orientation of the molecule in relation to the ECOI. Bracketed bV% values are those measured at a dummy distance of ≈1.8 Å. Proximal bulk is measured using a 3.5 Å radius sphere; distal bulk a 6.0 Å radius sphere.
(a) R flex refers to possible flexibility within the R moiety (not modelled or reflected in the data).
(b) N-R refers to the nitrogen-alkyl bond. The pseudo maximal/minimal sterically encumbering orientations positions the bulky of the R moiety closest or furthest from the ECOI (180° rotation).

Displayed in **table 2.2** are the characteristic steric features of the anthryl amine pro-ligands **1**-**6**. In the initial discussion, **3** will be ignored as it provides a significant and unique example to the benefits of defining ligands based on the shown factors; primarily, highlighting the issues with chemists' using their intuition to design ligands.

4 is the second bulkiest of the anthryl amines listed and displays the second highest potential steric encumbrance at 57.5%, which stands as a good example of why bulk is perceived to create greater steric encumbrance. In contrast to this, the least bulky pro-ligand **1** displays the third highest potential for creating a sterically encumbering environment with a buried volume of 56%. **1** and **4** are essentially rigid and inflexible, and so the steric steric environment provided is consistent.[xxix]

Buried volume values for **2**, the second smallest (least bulky) pro-ligand, are at 54.8%. Again, it is proposed that the cyclohexyl moiety is more rigid than the comparative C1 and

---

[xxix]Flexibility factors for **1** and **4** are deemed non-applicable (n/a) as rotation about the C15-N axis should not create a significantly altered steric environment due to the symmetry of the substituents. Any flex within these moieties is believed to be n/a according to the same rationale.

C2 alkyl substituents. The symmetry of cyclohexyl is greater than that of the C1 and C2 moieties in **5** and **6**, potentially influencing the greater bV% values obtained. Change of chair conformation and or rotation about the N-anthryl bond axis may lead to decreased steric encumbrance but was deemed unlikely. Change in chair conformation showed no meaningful change in bV% values; rotation of the N-anthryl bond axis when a substituent other than hydrogen is bound to the nitrogen atom is non-preferential due to the steric pressure this conformation would cause.

5 and **6** contain chiral alkyl moieties which can rotate in solution leading to a range of potential buried volumes, i.e. they are inconstant in the extent of steric encumbrance they can afford towards an ECOI. Their preferred conformations are skewed towards the lower bV% values, perhaps a consequence of weak aryl-aryl interactions between the phenyl/naphthyl and anthryl moieties. The bV% values obtained for **6** are the lowest despite being the bulkiest/largest pro-ligand in the series.

3 displays the highest potential steric encumbrance, possibly ranging from 52.1-71.7% with a preferred (least-energy) orientation which provides the highest steric encumbrance of the series (64.1%). It was our original contention that tert-octyl could contribute to a semi-proximal and sterically encumbering environment, though due to its apparent flexibility (being a long alkyl chain) it would be significantly lower than what would otherwise be expected. However, due to the proximity of dimethyl brachiation upon the tert-octyl moiety, greater rigidity is afforded to the molecule and consequently a more sterically encumbering enviornment (steric pressure influences it to orientate towards the most sterically encumbering orientation).

3 provides an excellent example of how shallow ligand design is when not properly theorised. There are many factors which can not be articulated without taking a theoretical approach. This small sample of pro-ligands and the theoretical approach to their characterisation illustrates a greater understanding and explanation of these systems even when used as an approximate explanative tool, and is a better approach to ligand design relatable to their kinetic stabilising properties. Whilst future work with these pro-ligands in the area of group 14 chemistry was lacklustre, they may find some use in other fields of chemistry more reliant on steric consistency than greater kinetic stability.

The steric maps of **1**-**6** are displayed in **figure 2.8**, as generated when viewed down the N-H axis with a 3.5 Å radius sphere [xxx]. These pro-ligands do not provide uniform (spherical) steric encumbrance about the 3.5 Å radius sphere, the exception to this is **3**.

[xxx]As is the case when calculating the buried volume, the steric maps are a magnitude higher/denser than would be expected when a non-hydrogen element is placed as the central sphere (as the bond distance is lengthened and the sphere is pulled away from the ligand). The steric maps for distal bulk (6.0 Å radius sphere) , and analogous maps at a set distance of ≈1.8 Å from the donor atom, are provided in the supplementary.
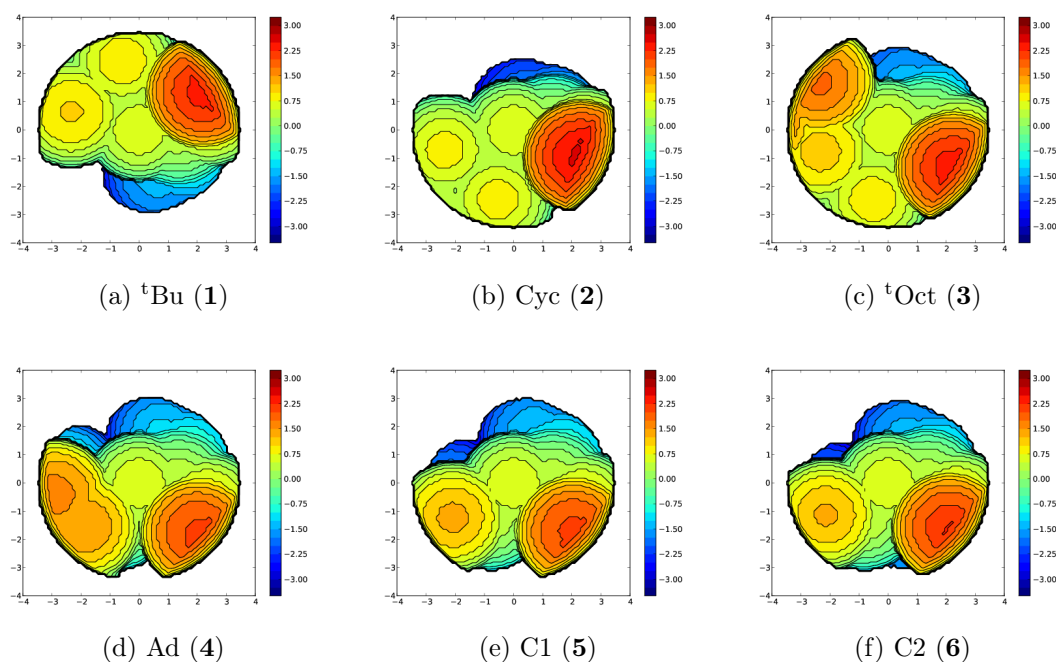
(a) ^{t}Bu (**1**)   (b) Cyc (**2**)   (c) ^{t}Oct (**3**)

(d) Ad (**4**)   (e) C1 (**5**)   (f) C2 (**6**)

*Figure 2.8: Steric maps of L-H **1**-**6**, viewed down the N-H axis with a sphere radius of 3.5 Å.*

Natural Bond Order (NBO) and Second Order Perturbation Theory (SOPT) Analysis

Natural bond order analysis (NBO) indicated minimal nitrogen lone-pair (LP) electron delocalisation within these molecules: the LP orbital occupancy ranging over approximately 1.85-1.9 electrons. The nitrogen LP acts as a donor, with delocalisation towards both the anthryl and alkyl moiety.

Second order perturbation theory (SOPT) analysis indicated some stabilisation ($<$10 kcal/mol) for all donor-acceptor interactions between the nitrogen LP and anti-bonding orbitals (BD*) of the anthryl and alkyl moieties with **3** as the exception. **3** displays a donor-acceptor relationship between the nitrogen LP and BD* orbitals of the neighbouring anthryl moiety (BD* C-C orbitals, 56.85 kcal/mol) and the BD* C-H orbital of the secondary-carbon of tert-octyl (22.14 kcal/mol).

Conclusion

A library of anthryl amine pro-ligands was successfully synthesised with relative ease. The small potential steric encumbrance offered by this pro-ligand class and their potential for internal redox activity were found to cause issues when used in low-oxidation state group 14 element chemistry (**chapter 3**). Despite this, they serve as a good model system for the

discussion of steric factors and profiling.

2.7.2   Ar^X Amines

Utilisation of tricyclic aromatic groups indicated some redox activity, this compounded by issues with further chemistry elicited the employment of larger ligand systems. To this end, we turned our attention to the tricyclic group 1,1,4,4,5,5,6,6,8,8-octamethyl-1,2,3,4,5,6,7,8-octahydroanthryl, dubbed Ar^X.[47] This tricyclic group features a central aromatic flanked by two saturated six-membered carbon rings containing dimethyl groups at the vertically-terminal ends of the flanking ringed motifs. These dimethyl groups offer a proximal steric effect.

The dimethyl functionality of Ar^X could not be substituted with diethyl functional groups, failing under all conditions. Control of the secondary substituent upon the nitrogen also proved challenging. Whilst trimetyl-silyl (TMS) was successfully coupled to the nitrogen, all other reactions with silyl halides led to an intractable mixture of products or reduced yields. The one exception was the synthesis of Ar^X(TIPS)NH (where TIPS = triisopropyl silyl). However, Ar^X(TIPS)NH could not be de-protonated under a range of conditions and, so, was not pursued.[34]

Synthesis
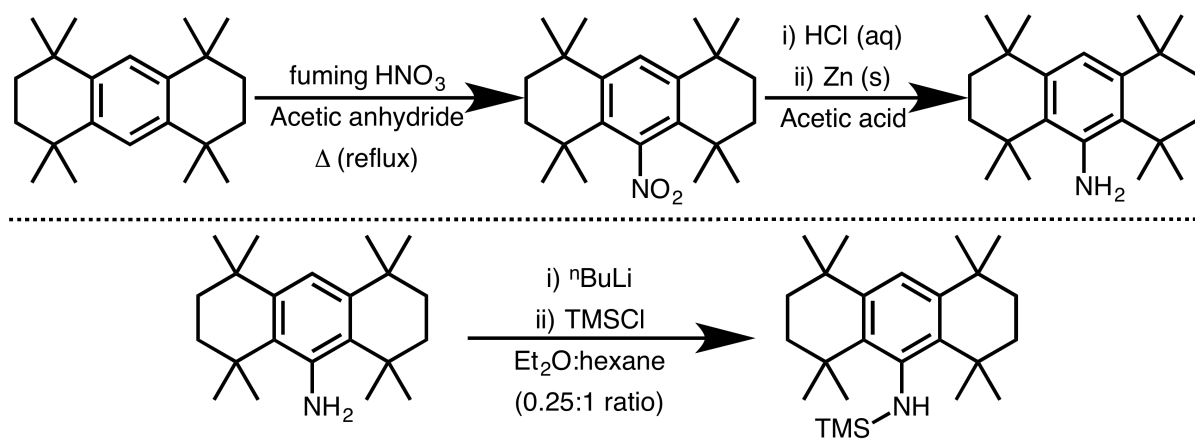
*Scheme 2.10: Synthesis for Ar^{X}NO$_2$ (**12**) & Ar^{X}NH$_2$ (**13**) (top); and the conversion of **13** to Ar^X(TMS)NH (**14**) (bottom).*

The Ar^X aromatic group was synthesised as described by Barclay and Betts.[47] The reported synthesis was slightly modified: performing the initial radical Freidel-Crafts alkylation with excess tert-butyl choride and benzene under dinitrogen was found to improve the yield. Crystallisation of Ar^X was accomplished by placing a hexane solution of the product in a

–30 °C freezer overnight, yielding Ar^X as a fine-needle-like crystaline solid. **Figure 2.9** displays the molecular structure of Ar^X.
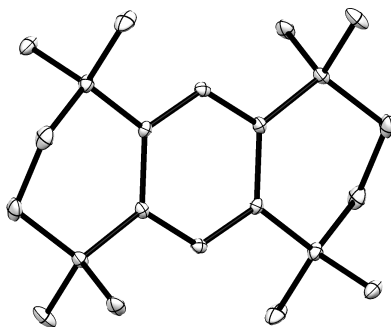

Figure 2.9: Thermal ellipsoid plot (30% probability surface) of Ar^X.

Nitration to form Ar^{X}NO$_2$ (**12**) from Ar^X was accomplished using HNO$_3$ (red fuming acid), added directly to a refluxing acetic anhydride solution of Ar^X (**scheme 2.10**). Unintentionally, it was found that using nickel based needles for the addition of HNO$_3$ led to the adventaceous addition of nickel, turning the final solution green in contrast to the typically observed yellow/orange solution. In the following step, the presence of nickel was found to catalyse the reduction of **12** to Ar^{X}NH$_2$(**13**). Leaving the solution to stand yields **12** as a precipitate. Precipitation can be initiated upon leaving the solution to stand at sub-zero temperatures, though care must be taken to allow frozen acetic anhydride to thaw before isolating **12**. The product is then isolated and washed with methanol before removing volatiles *in vacuo*.

The reduction of **12** to Ar^{X}NH$_2$ (**13**) using HCl(aq) and Zn(s) as the reducing reagents, under a nitrogen atmosphere and in acetic acid, was successful, requiring 4-5 hours for completion (**scheme 2.10**). When performed in the presence of advantageous nickel, the reduction was found to occur approximately five times faster (this is an issue as over-reduction back to the starting material Ar^X can occur). The reaction can be monitored by ^{1}H NMR spectroscopy by taking an aliquot of the reaction mixture, neutralising the solution, and then extracting in CDCl$_3$. Upon completion, the reaction was checked by ^{1}H NMR spectroscopy to ensure the depletion of **12** and whether over-reduction had occurred to form Ar^X. If completed, and there is no trace of Ar^X, **13** can be isolated as off-yellow needles, grown from a hexane solution at –30 °C. If a mixture of Ar^X and Ar^{X}NH$_2$ is obtained acid/base extraction can be used to isolate the desired product.

Converting the primary amine to the secondary amine Ar^X(TMS)NH (**14**) was done via a salt-metathesis coupling. Lithiation of **13** (which forms a yellow solution when dissolved) using ^{n}BuLi gave rise to a red solution. After two hours this was quenched with trimethylsilyl chloride eventuating in the formation of **14**, which was crystallised from a hexane solution

as yellow needle-like crystals.

Spectroscopic Analysis

The ^{1}H NMR spectrum of **12** displays two sets of peaks which correspond to the methyl environments (appearing as a set of single chemical shifts in the ^{1}H NMR spectra of Ar^X) as the compound becomes asymmetrical along its horizontal/x-axis. This loss of horizontal symmetry[xxxi] is also reflected in **13**. The most indicative difference to note when going from **12** to **13** is the appearance of broad chemical shift at δ 3.68 ppm which was assigned to the N-*H* functional group (though chemical shifts corresponding to the N-*H* proton do not appear when deuterated chloroform is used). The backbone Ar-*H* chemical shift at δ 6.94 ppm for **13** appears upfield in comparison to the equivalent peak for **12** (δ 7.40 ppm), and can be used to identify the synthesis of **13**.

As an auxiliary to ^{1}H NMR spectroscopic analysis, we were able to identify the formation of **13** via infrared spectroscopy (IR). Bands corresponding to the presence of a primary amine functional group (NH stretch absorptions) were noted at 3446 cm^{-1} and 3512 cm^{-1} as well as bands at 1592 and 1618 cm^{-1}. The completion of the reaction can be identified quickly using IR spectroscopy by noting the stated peaks and the loss of a strong NO stretch at 1527 cm^{-1}.

For **14**, the ^{1}H NMR spectrum is similar to that of **13**, displaying asymmetric splitting of the methyl moieties. A major point of reference during synthesis is the appearance of a chemical shift at δ 1.30 ppm (assigned to the TMS-CH_3 substituent). An important feature of this pro-ligand, evident in the analysis of its ^{1}H NMR spectra, is the lack of secondary acidic protons accessible and proximal to the ECOI, preventing the possibility of unwanted internal C-H activation (as has been observed in the benzyhydrol-like amide ligands, *vide supra*). Mass spectroscopic analyses of **14** revealed ions of Ar^X (100%), Ar^{X}NH$_2$ (44%) and SiMe$_3$ (25%), which were the predominant species observed.

Steric Profile

Density functional calculations (DFT) at the B3YLP/6-31G(d, p) level were performed to determine the optimised structure of **14**. The steric profile of **14** was found to be less than expected (**table 2.3**), however proximity and rigidity are believed to overcome this shortcoming.

[xxxi]The axis which bisects the Ar^X moiety through each of the three rings.

Table 2.3: *Bulk, flexibility, and proximity steric data for **14**. Ar*(TMS)NH is provided as a complimentary example.*

Compound (#)	Bulk	Flexibility	Proximal Bulk	Distal Bulk
Ar^X(TMS)NH (**14**)	353.0 Å^2	n/a	67.2% (31.6%)	38.0% (28.7%)
Ar*(TMS)NH	531.2 Å^2	2,6 axial rotation$^{(a)}$ 58.6-80.7%	71.4% (49.1%)	48.0% (39.3%)

Note: Ar*(TMS)NH is provided as a complimentary example. Bulk is expressed as a surface area in values of Å^2. All following values are expressed as a bV% value. Flexibility is qualitatively described; the bV% value is that of the approximate least to most sterically encumbering orientation of the molecule in relation to the ECOI. Bracketed bV% values are those measured at a dummy distance of ≈1.8 Å. Proximal bulk is measured using a 3.5 Å radius sphere; distal bulk a 6.0 Å radius sphere.

(a) Rotation is done from a neutral position by which the tertiary protons of the benzhydrol-like fragment are perpendicular to the aryl-nitrogen bond axis. 90° in the upward and downward direction from this position gives the pseudo maximal and minimal encumbering orientations.

The presumed rigid framework of **14** means there is no range of bV% values and when ligated **14** should provide a consistent sterically encumbering environment[xxxii]. Proximal bulk is shown to be greater than the somewhat analogous An(^{t}Bu)NH **1** amine (56%, see **table 2.2**), a consequence of the unsaturated flanking 6-membered carbon rings and dimethyl substituents. This reinforces the suggested requirement of proximal bulk to increase the steric encumbrance profile of a molecule. Possibly, the increased size of the silicon element may also have a positive effect, though the increased bond length of N-Si to N-C should negate this. Distal bulk is significantly greater than observed in **1** and consequently **14** is found to require a longer reaction time to be synthesised, i.e. reactivity at the nitrogen centre is more difficult as observed during its lithiation (**chapter 3**). Comparing **14** to the previously reported amine Ar*(TMS)NH, **14** is smaller and generally yields lower bV% values.

The steric map of **14**, proximal and distal, are displayed in **figure 2.10**. Proximal bulk is shown to be afforded by the flanking methyl substituents (dark orange sections above and below centre), the steric impact of TMS and the aromatic substituent is minimal. Distal bulk is also provided by the methyl substituents with a greater steric impact being made by the TMS and aromatic substituent. Both the proximal and distal steric environments of **14** are uniform[xxxiii].

[xxxii]The rigidity of this compound was confirmed and is detailed in **chapter 3**.

[xxxiii]The steric maps indicate less steric disparity across the analysed sphere: a circular steric map is produced indicating uniform directional steric protection.
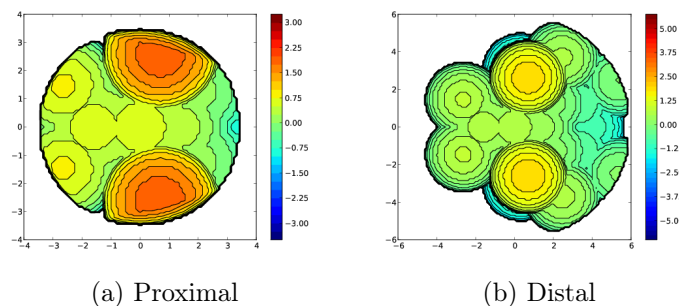
(a) Proximal   (b) Distal

*Figure 2.10: Steric maps of Ar^X(TMS)NH (**14**) as viewed down the N-H axis: proximal bulk (left) measured with a sphere radius of 3.5 Å, and distal bulk (right) measured with a sphere radius of 6.0 Å.*

.

Limitations of Ar^X

The synthesis of Ar^X(TMS)NH was successful, however - as mentioned - all derivatives led to intractable mixtures or difficult to isolate pro-ligands. The steric profile of the pro-ligand was determined to be adequate for further heavy group 14 element chemistry. Further work with this pro-ligand indicated its potential for redox activity; and it is suggested that steric pressure caused by the saturated six-membered carbon rings upon the central aromatic potentiates this activity (discussed in **chapter 3**).

2.7.3   Indacene Amines

The suggested steric pressure of saturated six-membered rings on the central aromatic of tricyclic-ringed aromatics pushed our efforts towards the adoption of indacenes, six-membered aromatics flanked by two five-membered saturated rings (the consistent planarity across the three rings alleviates the steric pressure mentioned for Ar^X). The added boon of this system is the modular nature of their synthesis and (potentially) increased proximal bulk. Inspired by the work of Matsuo and co-workers, who used indacene-based carbon donor ligands for the stabilisation of a range of low-oxidation state main-group chemistry (refer to **section 2.3** & **chapter 3**), we looked to adopt their ligands into the framework of amines/amides.

Synthesis
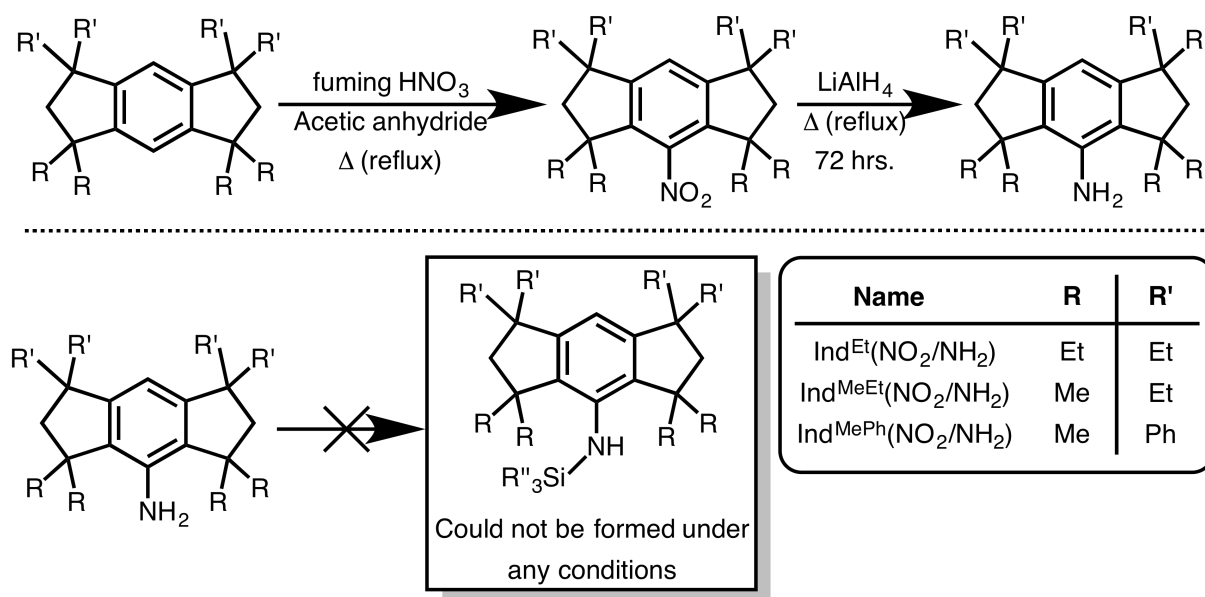
Scheme 2.11: Generic synthesis for the indacene nitrates and amines (top); and the attempted synthesis of the indacene secondary amines (bottom).

The preparation of the indacene aromatic groups, Ind^{Et}, Ind^{MeEt}, and Ind^{MePh}, was done following the reported synthesis by Matsuo and co-workers [xxxiv]. All the following conversion/reaction conditions were the same for Ind^{Et}, Ind^{MeEt}, and Ind^{MePh}. Only the reactions conducted using Ind^{Et} will be discussed as it is deemed the prototypical reaction[xxxv].

Nitration of Ind^{Et} was synthetically analogous to the nitration of $Ar^{X} \rightarrow Ar^{X}NO_2$, to form $Ind^{Et}NO_2$ (**15**). Fuming nitric acid was added to a refluxing acetic anyhydride solution of Ind^{Et} over a period of 4 to 6 hours (**scheme 2.11**). The solution was then allowed to cool to room temperature, at this point precipitation of **15** occurred. This process can be sped up by placing the solution in the fridge, however acetic acid (formed during the synthesis) will freeze at 16.6 °C.

Reduction of **15** to $Ind^{Et}NH_2$ (**16**) proved a challenge. Unlike $Ar^{X}NO_2 \rightarrow Ar^{X}NH_2$, standard zinc/HCl reduction under harsh conditions failed, giving a mixture of products. Unsurprisingly, switching to milder reducing techniques (metal-free reductions[xxxvi]) did not give the desired products.[48–50] Eventually, it was found that refluxing a solution of **15** in THF and adding lithium aluminiumhydride gave the desired compound, but took three days for


[xxxiv] It is noted here that at no stage of this synthesis were the yields reported by Matsuo and co-workers obtained, under no varied conditions or when taking 'extreme care'.

[xxxv] For the following Ind^{MeEt} and Ind^{MePh} derivatives, only ^{1}H NMR spectroscopic data was collected and was generally of a poor resolution. The ^{1}H NMR spectra of these derivatives display decomposition products and are not reported within the experimental.

[xxxvi] Note: we did not perform the micro-wave assisted amination as we did not have the required equipment, but did perform the reductions as stated by Vanier, G.[48]

completion, as determined by ^{1}H NMR spectroscopy (**scheme 2.11**). The yields from this step were low (conversion approximately 30%, isolated yield approximately 25%). Literature suggests that the reduction of bulky nitrates to amines often leads to the formation of azo-compounds (R-N=N-R), but for the conversion of **15**→**16** this was not found to be the case.[51]

With such low yields from the reduction of the nitrate, the practical-efficacy of this ligand was scrutinised and it was believed that we had reached a "dead-end". All attempts to form the secondary trimethyl silyl amine (Ind^R(TMS)NH) failed. Firstly, we attempted lithiation with $^{n/t}$BuLi which by observation looked promising, the solution going from a faded-yellow solution to an orange solution. However ^{1}H NMR spectroscopy indicated only the presence of starting material. Secondly, we attempted to form the potassium salt using a range of pottasiation reagents (benzyl-pottasium, pottasium hydride/hexamethyldisilazane (HMDS), etc.) but all met with the same failure as did our lithiation attempts. Our third and final attempt looked towards a newer procedure outlined in **scheme 2.12**, which was reported by Niggemann and co-workers.[52] The electrophilic amination of **15** directly to the secondary amine was attempted (this would have bypassed the primary amine). However, these attempts also failed; attempts made are detailed within the **experimental** section of this chapter. Further chemistry done with the primary amine **16** is discussed in **chapter 3**.

Name	R	R'
Ind^{Et}(NO$_2$/N(H)Et)	Et	Et
Ind^{MeEt}(NO$_2$/N(H)Et)	Me	Et
Ind^{MePh}(NO$_2$/N(H)Et)	Me	Ph
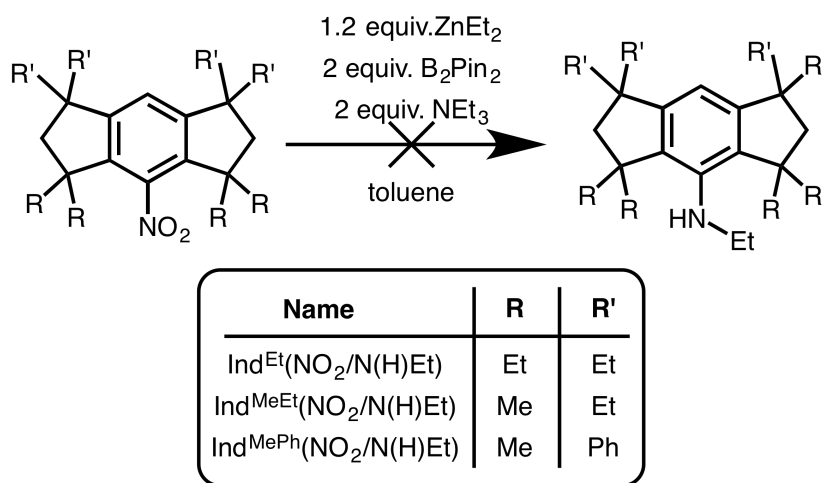
Scheme 2.12: The attempted electrophillic amination of the indacene nitroarenes (Ind^{R}NO$_2$) to their respective secondary amine ethyl derivative (Ind^R(Et)NH).

Spectroscopic Analysis

The synthesis of Ind^{Et}, **15**, and **16**, was predominantly monitored using ^{1}H NMR spectroscopy. **16** is asymmetric across its horizontal axis (x-axis), surprisingly **15** does not show similar ethyl functional group asymmetry. ^{1}H and ^{13}C NMR spectroscopic analyses of **16** indicates a shift upfield for the Ar-*H* backbone (para) proton and the corresponding Ar-*C*, in

contrast to that which is observed in the spectra of **15** (**figure 2.11**). The increased electron density upon the central aromatic of **16** is due to the decreased electron withdrawing effect of the primary amine functional group in comparison to the nitrate of **15**. This suggests a lower potential for redox activity at the central aromatic[xxxvii] moiety and prompted us to explore **16** as a pro-ligand (discussed in **chapter 3**).
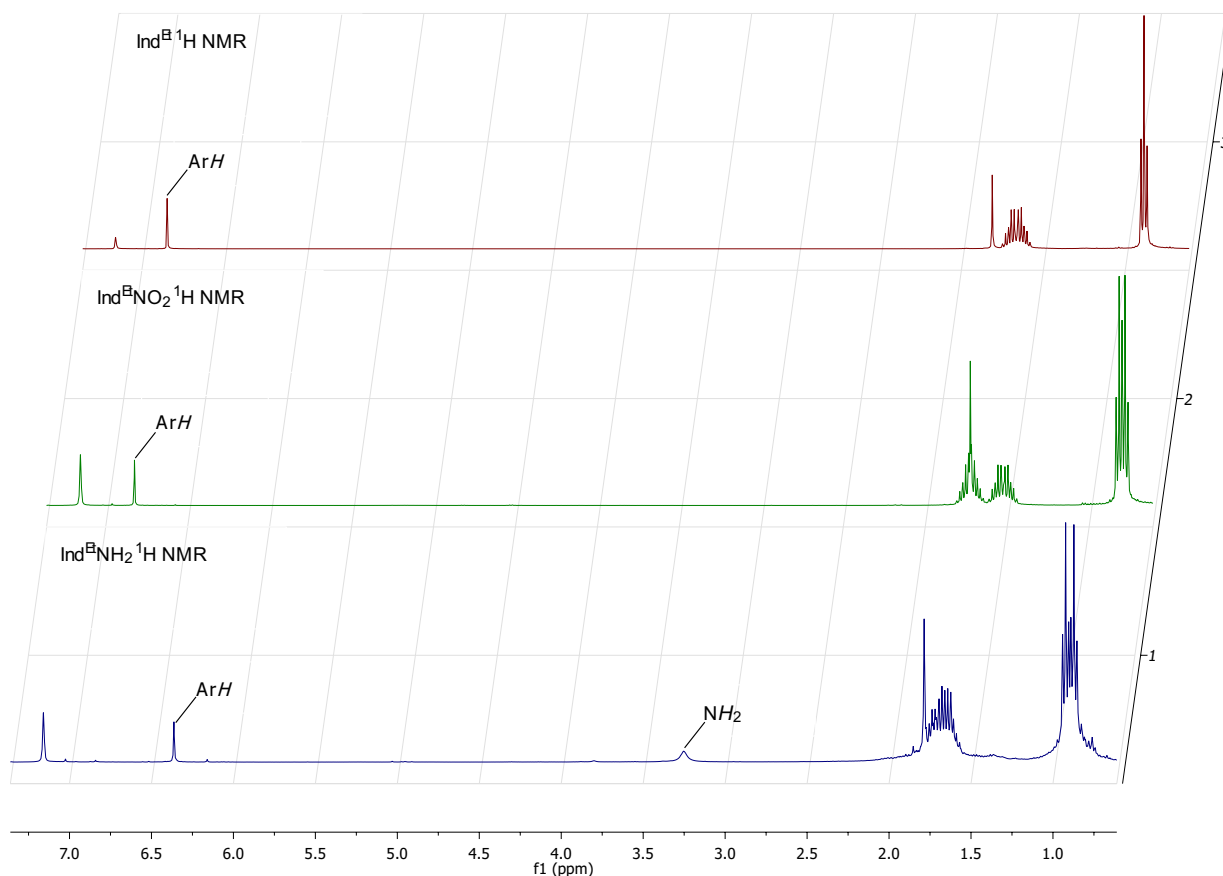

*Figure 2.11: The stacked ^1H NMR spectra of compounds Ind^{Et}, **15**, and **16**.*

Infrared spectroscopic (IR) and mass-spectroscopic (MS) analysis were used to confirm the formation of **15** and **16**, providing a quicker technique to elucidate completion of reduction from **15** to **16**. IR absorption bands at 1610 cm^{-1} in combination with bands at 3486 and 3465 cm^{-1} were assigned to the primary amine functional group within **16**. Accurate MS data analysis indicates the presence of an ion with the molecular mass $\approx$ 398.38 g/mol, believed to be the molecular ion peak of **16**.

[xxxvii]For comparrison, work with the anthryl amides and $Ar^X(TMS)N^-$ amide, discussed in **chapter 3** indicated an increased propensity for backbone Ar-H activation. Hence the importance of decreased aromatic activation.

X-ray Crystallographic Characterisation of Ind^{Et}NH$_2$ (16)

The synthesis of **16** yielded crystals adequate for X-ray diffraction characterisation, and combined with spectroscopic data, confirmed the synthesis of **16** (**figure 2.12**).
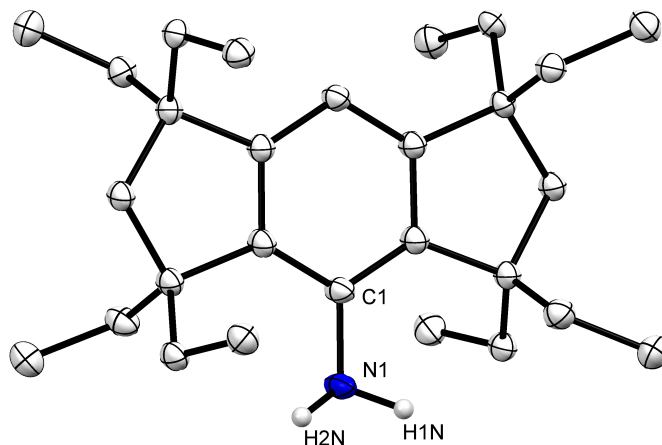

*Figure 2.12: Thermal ellipsoid plot (30% probability surface) of Ind^{Et}NH$_2$ (**16**) (hydrogen atoms, except H1N & H2N, are omitted). Selected bond lengths (Å): N1-C1 1.414(4), N1-H1N 1.00(5), N1-H2N 0.96(5).*

The solid-state structure of **16** displays an N1-C1 distance in accordance with those expected for anilines, albeit marginally longer at 1.414(4) Å (C-N bond length in anilines are ≈ 1.395 Å). The N-H bond distances are to be expected for a typical aniline, though as no neutron diffraction was conducted the N-H bond distances reported are tenuous and should be taken as an approximation. N1-C1 bond length elongation is most probably due to steric accomodation, reducing the steric pressure between then flanking ethyl functional groups and amine moiety. All other bond lengths and angles are as expected.[29]

Why Ind^{Et}N(R)H Could Not be Isolated or Formed

Our failure to produce Ind^{Et}N(R)H was a disappointment. Based on some preliminary computational studies, we deduced that there is enough space about the nitrogen centre of **16** and **17** to allow for lithiation and further reactivity: both the molecular structure of **16** and the optimised model **16-c** gave bV% of approximately 53%. Steric repulsion would, therefore, not seem to be a likely reason for our inability - or instability in - to form Ind^{Et}N(R)H.

2.8 R&D: Boryl Substituents and Bulky Amines

The Jones group's prior success with a range of bulky silyl amide ligands exhibits their efficacy across low-oxidation state main-group chemistry. However, unreported observations from within the group have indicated the heterolytic cleavage of the constituent nitrogen-silicon bond, leading to the decomposition of the low-oxidation state main-group compound.[24] Prior work looked to establish bulky amides with boryl substituents: it was the belief that replacing silicon with boron would create a more robust ligand system as N-B σ bonds are stronger than N-Si σ bonds.[53]

Efforts were made to synthesise a range of boryl secondary amines, the precursors to boryl secondary amides (conversion of the amines to amides is discussed in **chapter 4**).
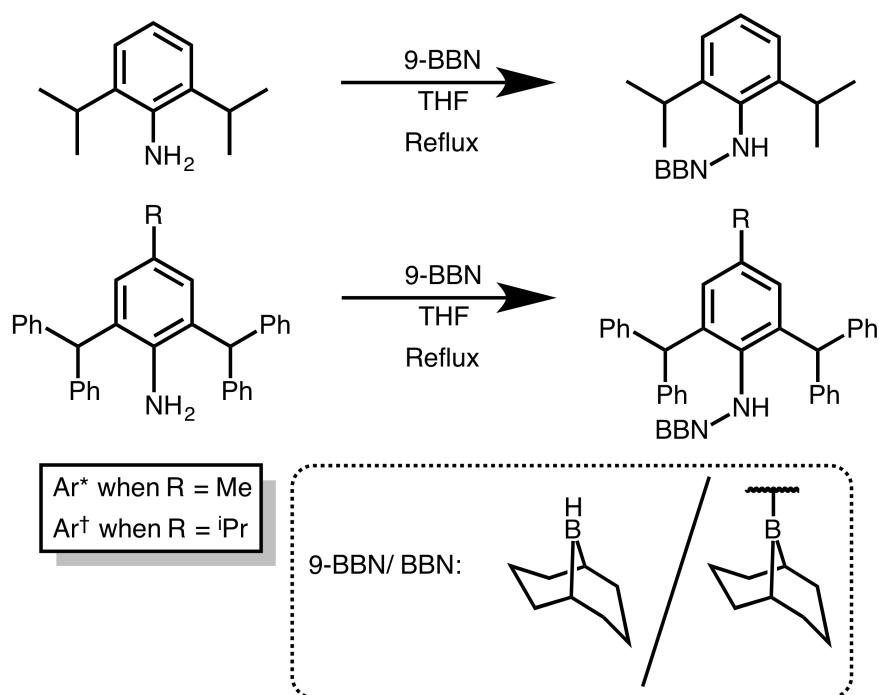
2.8.1 Dipp/Ar$^{*/\dagger}$(BBN)NH

9-Borabicyclo(3.3.1)nonane (9-BBN) is an organoboryl group used throughout chemistry, usually in the study of borylation catalysis. Work published by Bertrand and co-workers indicated a simplistic and straightforward method which allows for the protolysis (dehydro-) coupling of 9-BBN to amines and anilines.[54] With this in mind - and the presumed bulk of 9-BBN - we believed this synthetic route presented a good candidate for our aims towards making bulky boryl amines.

Synthesis

Firstly, we sought to test the ease of the protolysis coupling reaction reported by Bertrand and co-workers, repeating this synthesis to form Dipp(BBN)NH **17**, which was successful.[54] The next stage was to increase the bulk of the aromatic moiety and so we turned to the use of Ar*NH$_2$ and Ar†NH$_2$. These were also successful, albeit these reactions produced higher yields when refluxed as tetrahydrofuran solutions (**scheme 2.13**). Presumably, forcing conditions produce higher yields for Ar*(BBN)NH (**18**) and Ar†(BBN)NH (**19**) as more energy is required to overcome the steric encumbrance about the nitrogen centre of each respective aniline[xxxviii].

[xxxviii]The increased bulk of the Ar* and Ar† moieties decreases the reactivity of the nitrogen element centre. The total surface area of the molecule increases and the nitrogen centre surface area consequently decreases.
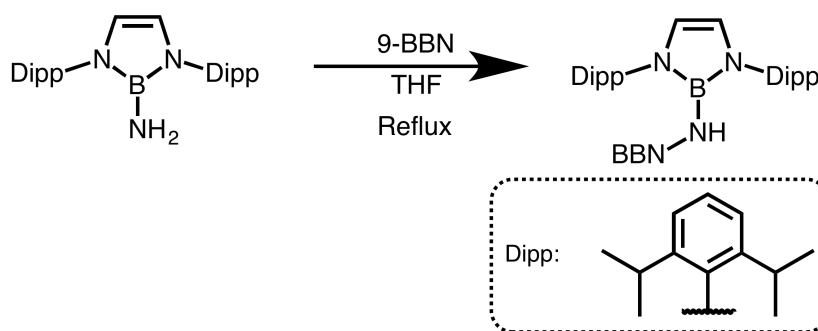
Scheme 2.13: Dehydroboration of Dipp, Ar and Ar† anilines to form the boryl-substituent containing pro-ligands Dipp(BBN)NH (**17**), Ar*(BBN)NH (**18**) and Ar†(BBN)NH (**19**).*

The efficacy of **18** is restricted by its surprisingly low solubility in a range of common hydrocarbon solvents, requiring harsh and long reaction conditions as well as large volumes of solvent in its synthesis. These solubility issues are not reflected in the synthesis of **19**, and are comparatively minor for **17**. The solubility of **18** caused issues in the synthesis of its lithium and potassium salt congeners, detailed in **chapter 4**.

^{1}H and ^{11}B NMR spectroscopy were used to monitor the reactions, the data clearly showing the conversion from the primary amine to the secondary boryl amine; but there is difficulty elucidating the proton environments of the BBN moiety. For the reactions of Ar*/Ar†NH$_2$ with 9-BBN, it is required to add an additional molar equivalent of 9-BBN to ensure completion[xxxix].

The ease of synthesis for these boryl amines prompted pursuit of the bis(boryl) amine {(^{Dipp}DAB)B}(BBN)NH (**20**) using the same dehydrocoupling technique (**scheme 2.14**). A small scale synthesis was attempted and by ^{1}H NMR spectroscopic analyses we believed to have formed **20**. These promising results prompted a scale up of the reaction, at which point problems arose. The upscaled reaction mixture was analysed via ^{1}H NMR spectroscopy and a mixture of compounds was identified. Attempts to isolate **20** were unsuccessful, and at the time of these attempts, developments with the BBN amines/amides influenced the decision to abandon the project.

[xxxix]This may have been due to degradation of 9-BBN reagent used at the time of synthesis.

Scheme 2.14: *Dehydroboration of {(^{Dipp}DAB)B}NH$_2$ to form boryl-subsituent containing pro-ligands {(^{Dipp}DAB)B}(BBN)NH (**20**). This synthesis could not be repeated on large scale.*

Spectroscopic Analysis

Analysis of the ^{1}H NMR spectra of **18** and **19** indicated the presence of de-shielded N-*H* environments, displaying chemical shifts of δ 4.56 ppm and δ 4.59 ppm, respectively, presumably due to decreased electron density present upon the nitrogen centre. This suggests the amine lone-pair is delocalised towards the aryl, boryl, or across both these moieties. In comparison to the N-*H* assigned chemical shifts observed in the ^{1}H NMR spectra of Ar*(TMS)NH at δ 1.75 ppm and Ar†(TMS)NH at δ 3.26 ppm, the amine functional group of **18** and **19** are believed to be more acidic.[18,19]

^{11}B NMR spectra indicated de-shielded boron environments for **18** (δ 57.3 ppm) and **19** (δ 56.8 ppm) in comparison to **17** (δ 50.5 ppm). Comparison to the other BBN-containing species synthesised by Bertrand and co-workers highlights the increased de-shielding observed in **18** and **19** (**figure 2.13**).[54] In-spite of these observations, bond lengths between the nitrogen and boron are shorter than a single bond, as seen in the solid-state structures of **17** and **19** (*vide supra*).
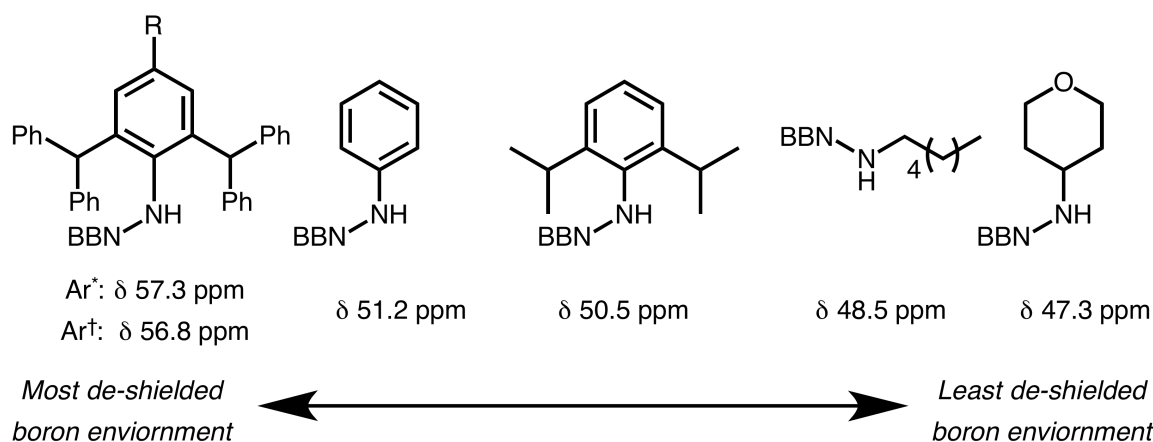

Figure 2.13: *^{11}B NMR chemical shifts for a range of BBN containing secondary amines from least (left) to most (right) de-shielded boron centres.*

The comparatively de-shielded boryl environments of **18** and **19** suggests the amine lone-pair delocalises towards the aryl group more prevalently; but can also be explained by the stronger σ donation from B→N than π back-donation from N→B. Analysis of the ^{13}C NMR spectra suggests increased electron density upon an aromatic carbon, presumably due to the hypothesised nitrogen lone-pair delocalisation across the aryl group; though, the obtained solid-state structure of **19** shows no shortening of the N-C bond but, in fact, a longer than average N-C(aromatic) bond.

The de-shielded boryl and amine environments of **18** and **19** observed by NMR spectroscopy seem to contradict our hypothesis of N→B lone-pair or π electron donation. We hypothesised that this may be a consequence of delocalisation across the whole molecule which would not be noticeably reflected in the respective $_1$H NMR spectrum. To explore this further, we analysed the solid-state structure of **17** and **19**, and computed the optimised structures of each amine to explore their theoretical electronic and steric profile.

X-ray Crystallographic Characterisation of Dipp(BBN)NH (17) and Ar†(BBN)NH (19).

Crystals suitable for X-ray diffraction were obtained for **17** and **19** from concentrated hexane solutions (**figure 2.14** & **figure 2.15**). Both structures are somewhat in accordance with the spectroscopic data detailed above, displaying shorter than single N-B bond lengths and planar nitrogen geometries.
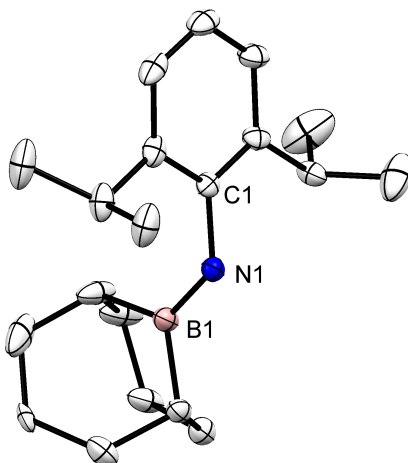
*Figure 2.14: Thermal ellipsoid plot (30% probability surface) of Dipp(BBN)NH (**17**) (hydrogen atoms omitted). Selected bond lengths (Å) and angles (°): N1-B1 1.396(2), N1-C1 1.441(2); B1-N1-C1 127.8(1); B1-N1-C1-C1 -96.6(2).*

For **17**, the short bond between N1 and B1 at 1.396(2) Å indicates some degree of π bonding between the nitrogen lone-pair and the empty p orbital upon the boron element.[55] This partial-double bond between N1-B1 may have an affect on the N1-C1 bond distance

which is slightly longer than N-C(aryl) bond lengths observed in closely related analogues ($\overline{x} = 1.426 \pm 0.011$ Å). N1 exhibits a trigonal planar geometry, further reinforcing our presumption of lone-pair delocalisation across across B1-N1; the nitrogen is sp^2 hybridised. The BBN fragment lies almost perpendicular to the aryl plane as reflected in the B1-N1-C1-C1 torsion angle -96.6(2)°, reducing steric pressure within the compound.
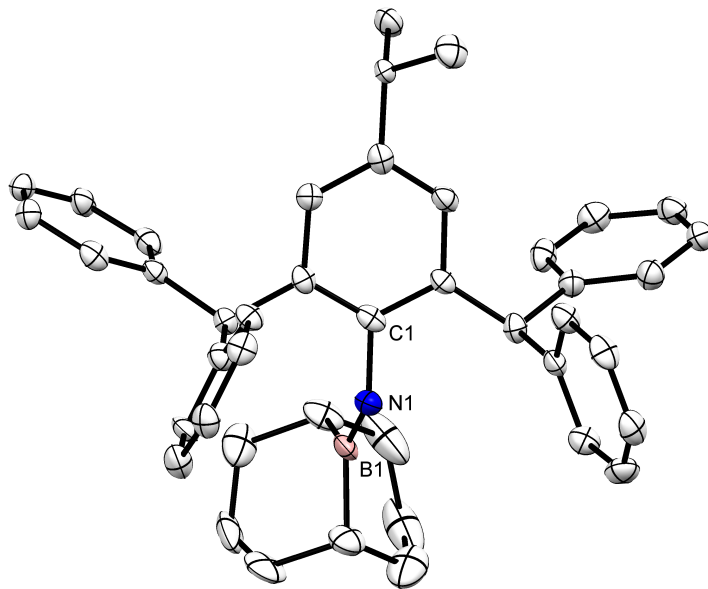

*Figure 2.15: Thermal ellipsoid plot (30% probability surface) of Ar†(BBN)NH (**19**) (hydrogen atoms omitted). Selected bond lengths (Å) and angles (°): N1-B1 1.43(2), N1-C1 1.45(1); B1-N1-C1 128.0(9); B1-N1-C1-C2 -98(1).*

19's N1-B1 bond distance is reflective of a N-B single bond with some π bonding character, as observed for **17**. The geometry of N1 is trigonal planar as expected; nitrogen is sp^2 hybridised. Steric pressure within **19** is reduced as the BBN fragment lies almost perpendicular to the aryl plane as reflected in the B1-N1-C1-C1 torsion angle -98(1)°; this is compounded by the adopted angle of the benzhydrol-like phenyl rings, which point away from the direction of the BBN substutuent.

Steric Profile

Density functional calculations (DFT) at the B3YLP/6-31G(d, p) level were conducted to produce the optimised structures of **17** and **18**; and these structures were used for the calculation of steric parameters. For **19** the obtained molecular structure for **19** (**figure 2.15**) was used[xl].

[xl]The increased computational resources required for iso-propyl vs. methyl (the difference between **18** and **19**) is far greater for the former.

*Table 2.4: Bulky, flexibiliy, proximal and distal bulk data for **17**, **18**, and **19**.*
Ar*(TMS)NH is provided as a complimentary example.

Compound (#)	Bulk	Flexibility	Proximal Bulk	Distal Bulk
Dipp(BBN)NH (**17**)	353.0 Å^2	2,6 axial rotation$^{(a)}$ 52.3-63.6%	43.9% (22.9%)	37.1% (25.7%)
Ar*(BBN)NH (**18**)	562.3 Å^2	2,6 axial rotation$^{(a)}$ 55.5-86.5%	66.1% (35.6%)	51.4% (37.4%)
Ar†(BBN)NH (**19**)	599.1 Å^2	2,6 axial rotation$^{(a)}$ 56.9-87.2%	69.5% (43.0%)	55.3% (42.3%)
Ar*(TMS)NH	531.2 Å^2	rotation 58.6-80.7%	71.4% (49.1%)	48.0% (39.3)

Note: Bulk is expressed as a surface area in values of Å^2. All following values are expressed as a bV% value. Flexibility is qualitatively described; the bV% value is that of the approximate least to most sterically encumbering orientation of the molecule in relation to the ECOI. Bracketed bV% values are those measured at a dummy distance of ≈1.8 Å. Proximal bulk is measured using a 3.5 Å radius sphere; distal bulk a 6.0 Å radius sphere.
(a) Rotation is done from a neutral position by which the tertiary protons of the benzhydrol-like fragment are perpendicular to the aryl-nitrogen bond axis. 90° in the upward and downward direction from this position gives the pseudo maximal and minimal encumbering orientations.

Our contention during the ligand design phase of **18** and **19** was that the BBN moiety would provide a greater degree of steric encumbrance and reduce rotation about the Ar-benzhydrol-like bond axis, but this was not found to be the case. Shown in **table 2.4**, the bV% of **18** and **19** is lower than the comparative bV% values of Ar*(TMS)NH, at least in the solid-state. The range of flexible rotation in **18** and **19** is greater than originally contended: the BBN moiety does not restrict the rotation of the benzhydrol-like substituents. The TMS moiety of Ar*(TMS)NH was observed to restrict rotation due to proximal branchiation at the silicon element[xli]; though, this is based on our computational observations and would need to be explored in more depth for an absolute comment to be made. **18** and **19** could orientate to create a more sterically hindering environment but, equally, it could conform to a less sterically hindering environment. The BBN moiety is believed to create a greater range of steric encumbrance, as flexibility within the molecule increases, when included in these bulky amine pro-ligand frameworks. However, these molecules are found to preferentially conform in a less sterically encumbering geometry than those substituted with TMS.

Their is a discrepancy in the flexibility steric values for **18** and **19**, both should display the same potential bV%. The difference of a methyl vs. iso-propyl functional group at the para (aromatic backbone) position between these compounds was not believed to influence the proximally measured steric parameters.

Steric maps of **17**, **18**, and **19** are displayed in **figure 2.16**. The iso-propyl substituents

---

[xli]This result prompted our discussion on proximal branchiation and how it affects the steric environment *vide supra*.

of **17** are shown to point out of the plane, parallel to the N-H axis, and the steric map illustrates a pseudo-symmetrical steric environment; though, one of the methyl groups of the iso-propyl motif does lie closer to the sphere of reference. The benzhydrol-like subsituents in **18** and **19** do not reflect the same symmetry due to the sterically induced orientation influenced by the BBN substituent. The increased steric uniformity provided by **18** and **19**, in comparison to **17**, is reflected in the circular characteristic of the steric maps. The benzhydrol-like substituents are shown to provide both proximal and distal bulk.

| (a) **17** (proximal) | (b) **18** (proximal) | (c) **19** (proximal) |

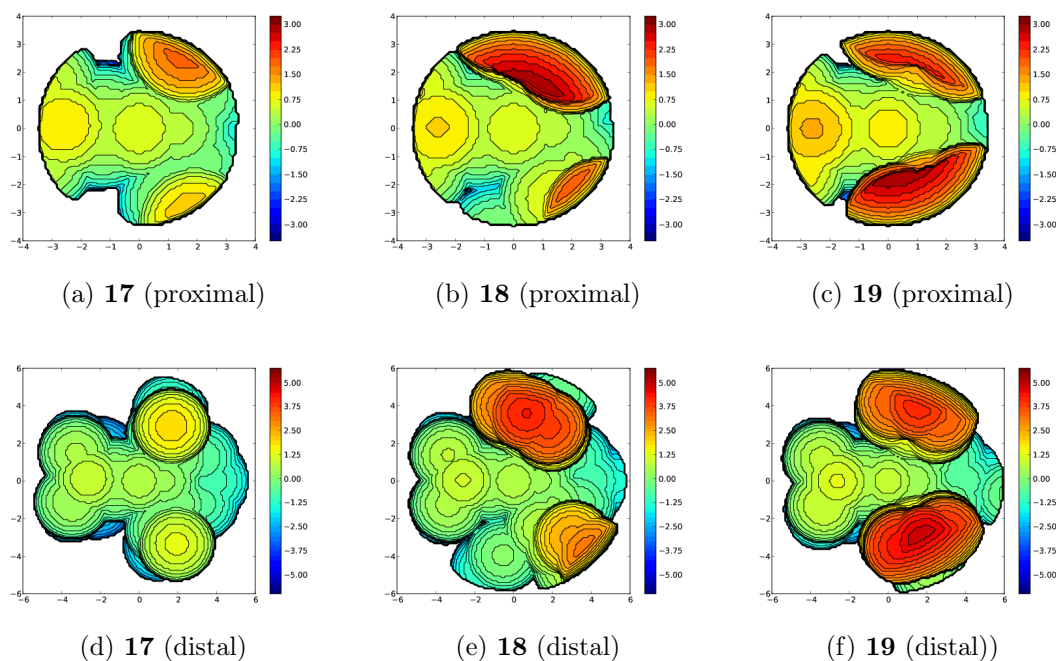| (d) **17** (distal) | (e) **18** (distal) | (f) **19** (distal)) |

*Figure 2.16: Steric maps of **17**, **18**, **19**, as viewed down the N-H axis (maps calculated based on the obtained solid state structures).*

Natural Bond Order (NBO) and Second Order Perturbation Theory (SOPT) Analysis

Our analysis of the NMR spectroscopic data for **17**, **18**, and **19**, suggested the delocalisation of the nitrogen lone-pair (LP). Our initial contention was that this delocalisation should preferentially be directed towards the boryl fragment (BBN). NBO analysis of **18** and **19** suggests decreased electron density in the formally two electron occupied nitrogen LP, for the boryl amines, with an occupancy of approximetely 1.7 electrons. The formally vacant valence p orbital (LP*) of the boron atom was also found to be partially occupied, approximately 0.32 electron occupancy in **17** and 0.35 electron occupancy in **18**, indicative of some donor-acceptor relationship.

SOPT analysis identified the direction of the nitrogen lone-pair delocalisation. For **17**, three relevant donor-acceptor interactions were identified with two going from the nitrogen

LP towards the aromatic moiety, into anti-bonding C-C bond orbitals; the third donation into the LP* orbital of the boron element. The stabilisation energy obtained from the donor-acceptor interactions towards the aromatic moiety are negligible whilst the N(LP)→B(LP*) donor-acceptor stabilisation energy is significant at 74.83 kcal/mol. These values suggest a greater than one bond order between N and B in **17**. The HOMO and LUMO orbitals are characterised by the N(LP) orbital and C-C(BD*) orbitals upon the aromatic moiety, respectively.

18 displays the same donor-acceptor interactions as observed in **17**, albeit granting greater stabilisation: N(LP)→C-C(BD*) stabilisation at 6.83 and 7.09 kcal/mol, and N(LP)→B(LP*) at 79.49 kcal/mol. The predominant character of the HOMO orbital of **18** is the N(LP) delocalisation into the aromatic moiety and BBN moieties. The LUMO is characterised by C-C(BD*) orbitals across the aromatic moiety and the N-H(BD*) orbital. The N(LP) could not be observed.

Though the optimised structure, NBO, nor SOPT analysis was conducted for **19**, we believed that its electronic structure is reflected by the analysis conducted on **18**. The change from a methyl to iso-propyl functional group on the para-position of the aryl moiety within **18** and **19** is not believed to produce a significant change in the electronics of the system. The iso-propyl group should, theoretically, withdraw more electron density from the aromatic than a methyl group, albeit this increased electron withdrawal should be negligible.

2.8.2   Ar$^{*/\dagger}$(BBP)NH

Unpublished work from within the Jones group had indicated the efficacy of utilising boryl-bispyrrolidine (BBP) in the framework of sterically encumbering ligands. Within that work, it was found there is reduced N-B π electron delocalisation and that the nitrogen atoms of the BBP moiety may act as pseudo-donors, i.e. their lone pairs can be directed towards ECOI[xlii]. This observation, this donor activity, is both beneficial and a detriment: it is advantageous as it creates a more electronically favourable and sterically encumbering environment for the ECOI. The detriment is the resultant suppression of reactivity at the ECOI centre.[xliii]. It was our hypothesis that by applying BBP to the ligand framework of benzhydrol-like amines we could synthesise a new class of sterically encumbering ligand. Furthermore, we predicted that the flexibility of the BBP moiety, in comparison to the more rigid BBN moiety, would allow us to more easily couple these ligands to tetrel element centres. The BBP moiety forgoes rigid steric encumbrance but increases the utility of these ligands (discussed in **chapter 4**).

[xlii]The ligand sits somewhere between mono and bidentate ligand.

[xliii]Despite this, a range of low-oxidation state group 14 element compounds were produced (discussed in **chapter 4**).

Synthesis and Spectroscopic Analysis

Ar*(BBP)NH (**21**) and Ar†(BBP)NH (**22**) were prepared via salt-metahthesis of boryl-bispyrrolidine bromide (BBP-Br) and the corresponding lithium amide (**scheme 2.15**).[56] Isolation of the pro-ligands is difficult as they are sparingly soluble in a range of non-donor solvents, though cold extraction of the lithium bromide residue in diethyl ether was found to be the most effective isolation technique[xliv], leaving the pro-ligand behind as a white powder.
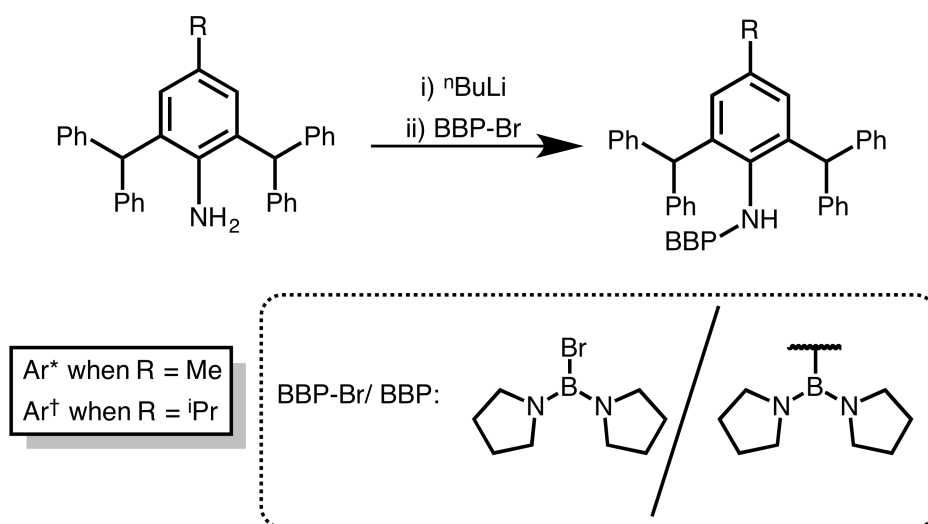
Scheme 2.15: Synthesis of the boryl amides Ar(BBP)NH (**21**) & Ar†(BBP)NH (**22**), via salt-metathesis coupling.*

^{1}H NMR spectra of **21** and **22** display chemical shifts at δ 3.08 ppm for both compounds, assigned to the N-*H* protons, and indicate comparatively shielded N-*H* environments when compared to those observed in **18** (δ 4.56 ppm) and **19** (δ 4.59 ppm) (*vide infra*).

The boron environments of **21** (δ 22.8 ppm) and **2** (δ 27.0 ppm) are comparatively shielded when compared to **18** (δ 57.31 ppm) and **19** (δ 56.8 ppm). The [11]B signals observed for **21** and **22** are closely related to those observed for {([Dipp]DAB)B}(TMS)NH at δ 23.1 ppm which is to be expected; both **21**, **22**, and {([Dipp]DAB)B}(TMS)NH have boron elements saturated by nitrogen bonds.[27] It is difficult to ascertain the delocalisation of the nitrogen lone-pairs using NMR spectroscopy alone. However, we believe the nitrogens of the pyroliodine fragments are the main contributors to the shielded environment of the boron due to the shielded proton environment of N-*H* observed. This is supported by the bond lengths observed in the solid state structures of **21** and **22** (*vide supra*).

Both the ^{1}H and ^{11}B NMR spectra for **21** and **22** suggest that the nitrogen lone-pair is not delocalised towards the boryl substituent and suggests limited nitrogen lone-pair delo-

---

[xliv]Whilst the isolation of the pro-ligands via this method yielded the highest retention of product yield and highest purity it may not have removed the entirety of lithium bromide formed. This lead to issues in further chemistry conducted and will be discussed in **chapter 4**.

calisation comparative to analogues systems.

X-ray Crystallographic Characterisation of Ar*(BBP)NH (21) and Ar†(BBP)NH (22)

Despite isolation difficulties associated with **21** and **22**, crystals with suitable quality were obtained for X-ray crystallography (**figure 2.17**). These crystals were isolated from product mixtures obtained when reacting the lithium amide derivatives with tetrel halides (discussed in **chapter 4**).

Consistent across the solid-state structures is a comparatively longer N-B bond and a shorter N-C bond than those observed in the BBN-based amines **17**, **18**, and **19**.
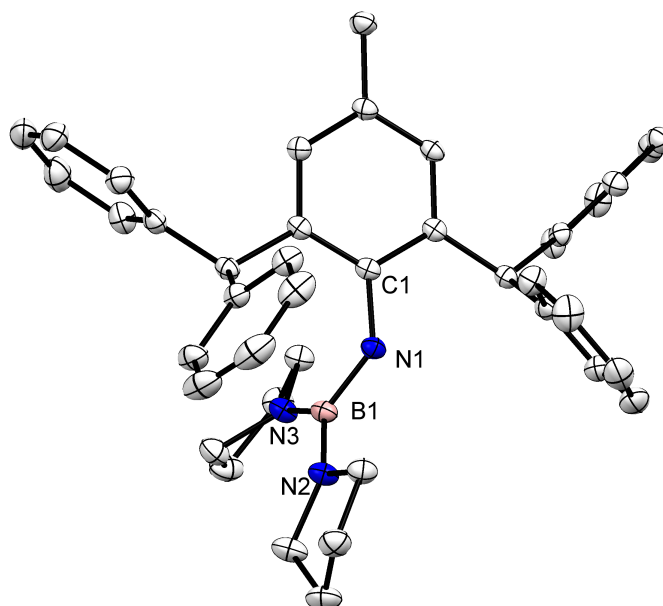
Figure 2.17: Thermal ellipsoid plot (30% probability surface) of Ar(BBP)NH (**21**) (hydrogen atoms omitted). Selected bond lengths (Å) and angles (°): N1-B1 1.445(2), N1-C1 1.409(2), B1-N2 1.422(2), B1-N3 1.424(2); B1-N1-C1 131.7(1), N1-B1-N2 116.0(1), N1-B1-N3 119.3(1), N2-B1-N3 124.6(1); C2-C1-N1-B1 –136.20(1).*

The solid-state structure of **21** (**figure 2.17**) displays a short N1-B1 bond length at 1.445(2) Å, perhaps indicating some degree of electron delocalisation. However, the pyrrolidine B1-N2 and B1-N3 bonds lengths - 1.422(2) & 1.424(2) Å, respectively - are shorter still. We believe that the N2 and N3 lone-pair readily delocalise towards B1 more than those upon N1, which supports our analysis of the NMR spectroscopic data. The dissimilarity between the N-B bond lengths may be a consequence of better orbital overlap between the N2 & N3 lone-pair orbitals with the formally vacant p orbital upon the boron atom. Delocalisation across the boron element is further supported by the total angle of $\approx 360°$ about

the N2 and N3 centres, both conforming to trigonal planar geometries and hence indicating sp^2 hybridisation. N1 is also noted to display a trigonal planar geometry, indicative of sp^2 hybridisation, yet this does not reflect the electronic environment of N1 as determined from the ^{1}H NMR spectra. The disparity between the electronic profile suggested by the NMR data with that suggested by our analysis of the solid-state structure of **21** and **22** is due to reorientation and electronic changes experienced when in solution-state vs. the solid-state.
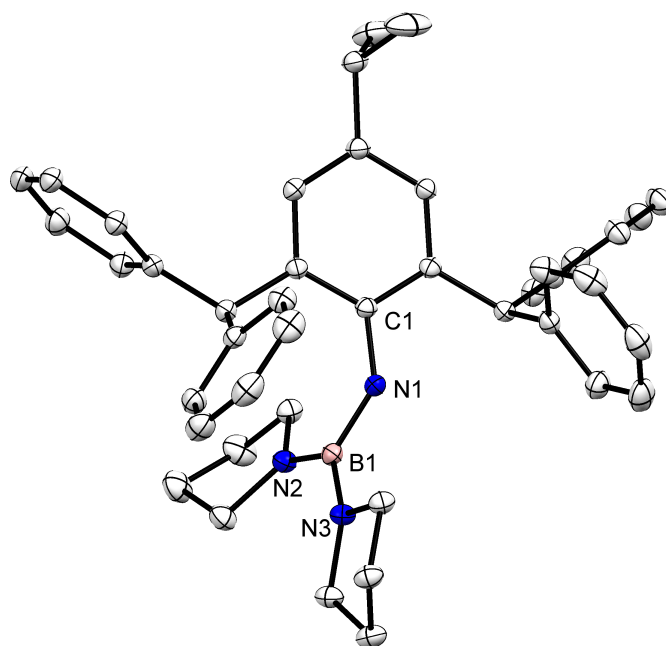

*Figure 2.18: Thermal ellipsoid plot (30% probability surface) of Ar†(BBP)NH (**22**) (hydrogen atoms omitted). Selected bond lengths (Å) and angles (°): N1-C1 1.413(1), N1-B1 1.438(2), B1-N2 1.428(2), B1-N3 1.426(2); B1-N1-C1 134.12(9), N1-B1-N2 121.4(1), N1-B1-N3 115.6(1), N2-B1-N3 123.0(1); C2-C1-N1-B1 –134.13.*

The solid-state structure of **22** (**figure 2.18**) is almost identical to **21**, with small deviations. N1-B1 bond length is slightly shorter at 1.438(2) Å, whilst the pyrolodine nitrogen lengths, N2-B1 and N3-B1, are lengthened. This slight deviation suggests a minor increase in π donation from N1 towards B1 and reduced delocalisation towards the aryl moiety. These small deviations do not reflect a notable difference in the electronic environment when **21** and **22** are in solution. As in **21**, N2 and N3 display trigonal planar geometries which reflect sp^2 hybridisation, supporting our analysis of the ^{11}B NMR spectra.

Steric Profile

Computational issues meant that the optimised structure of **21** was not obtained. The following data for **21** and **22** are based on their respective molecular structures, **figure 2.17 & 2.18**.

Table 2.5: Bulky, flexibiliy, proximal and distal bulk data for **21** and **22**.

Compound (#)	Bulk	Flexibility	Proximal Bulk	Distal Bulk
Ar*(BBP)NH	577.2 (Å)	2,6 axial rotation[a] 66.6-85.6%	82.0% (70.7%)	55.8% (44.0)
ArDag(BBP)NH	611.1 Å^2	2,6 axial rotation[a] 62.4-83.8%	79.5% (66.1%)	56.1% (44.6)

Note: Bulk is expressed as a surface area in values of Å^2. All following values are expressed as a bV% value. Flexibility is qualitatively described; the bV% value is that of the approximate least to most sterically encumbering orientation of the molecule in relation to the ECOI. Bracketed bV% values are those measured at a dummy distance of ≈1.85 Å. Proximal bulk is measured using a 3.5 Å radius sphere; distal bulk a 6.0 Å radius sphere.

(a) Rotation is done from a neutral position by which the tertiary protons of the benzhydrol-like fragment are perpendicular to the aryl-nitrogen bond axis. 90° in the upward and downward direction from this position gives the pseudo maximal and minimal encumbering orientations.

The BBP moiety was found to induce greater rigidity within these pro-ligands by reducing the possible rotation of the benzhydrol-like moieties. This was unexpected, but as the nitrogen adopts/approaches a trigonal planar geometry the magnitude of possible axial-rotation for the BBP substituent diminishes. The pseudo-trigonal planar geometry of the nitrogen forces the BBP substituent into such a position that all orientations lead to steric clash when attempting to model the least sterically encumbering orientation. Again, like for **18** and **19** this would need to explored further for a definitive comment to be made (the comments made thus far are an approximation). Unsurprisingly, the BBP moiety lowers the maximal bulk afforded by the pro-ligands, in comparison to BBN.

The slight deviations between the two pro-ligands in their calculated flexibility bV% values is an artefact of this methodology: as the maximal and minimal bulk orientations are done based on rationale chemical intuition, whilst attempting to minimise the number of corrections/alterations to the orientation, a degree of human error must be acknowledged. Consequently, this result affirms that these values are approximations. The reason behind this disparity is most probably due to the orientation of the phenyl rings of the benzhydrol-like moiety which can axially rotate about the C-Ar bond.
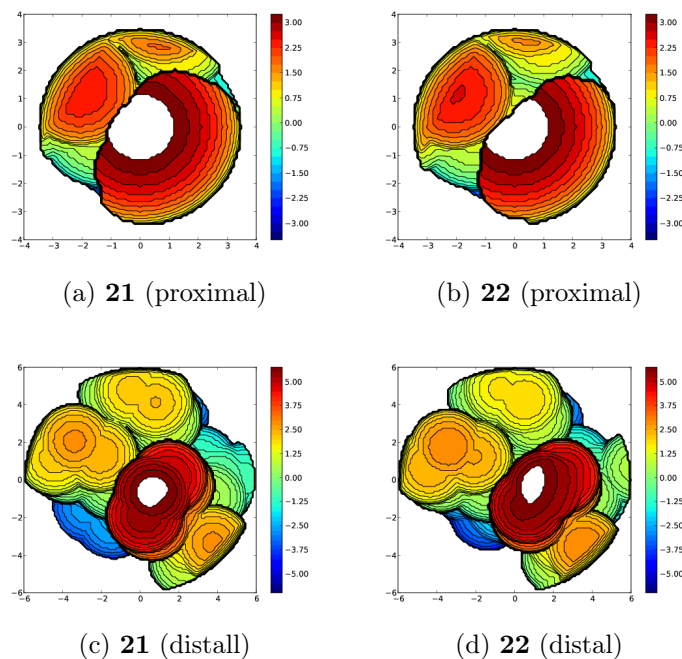
(a) **21** (proximal)   (b) **22** (proximal)

(c) **21** (distall)   (d) **22** (distal)

*Figure 2.19: Steric maps of **21** and **22**, as viewed down the N-H axis (maps calculated based on the obtained solid state structures).*

The steric hole (white area) displayed in these steric maps are due to an interceding atom within the path of the axis. The steric maps maintain a circular chracteristic which is indicative of uniform directional steric protection, though this character is deformed upon observation of distal bulk.

2.9   Final Remarks

With these desired pro-ligands in hand the aim of this project was to apply these systems in the stabilisation and isolation of low-oxidation state group 14 compounds. A primary focus was given towards the synthesis of silicon compounds - where silicon was the element of interest, in the +1 oxidation state. However due to issues which will be discussed, focus shifted away from silicon and towards the heavier tetrel elements.

The novel pro-ligands developed here were not the only utilised ligands, other systems adopted into this work will be discussed where necessary, primarily in **chapters 4** and **5**.

The retrospective analysis of these pro-ligands allowed the further development and understanding of steric and we have developed the ceoncepts of kinetically stabilising ligands, adding proximity, flexibility, and bulk as the primary characteristics required by kinetically stabilising ligands.

2.10   Future Work

Preliminary steric analysis of the tricyclic ring containing amine pro-ligands indicates the likelihood that these systems are rigid, if not as sterically encumbering as previously reported amines. The lack of steric encumbrance afforded by the discussed ligands makes them somewhat inviable for low-oxidation state group 14 chemistry, though adding bulk may overcome these issues; and, or, the scope of tricyclic molecules - employed as the foundation of these ligands - could be increased.

Displayed in **figure 2.20** are some of the suggested tricyclic molecules which may be employed into the ligand framework of amines and amides. The references provided refer to the synthesis of these tricyclic molecules; it is believed that the aforementioned nitration and amination reactions may pose viable pathways to the formation of these proposed compounds[xlv].[57–59]
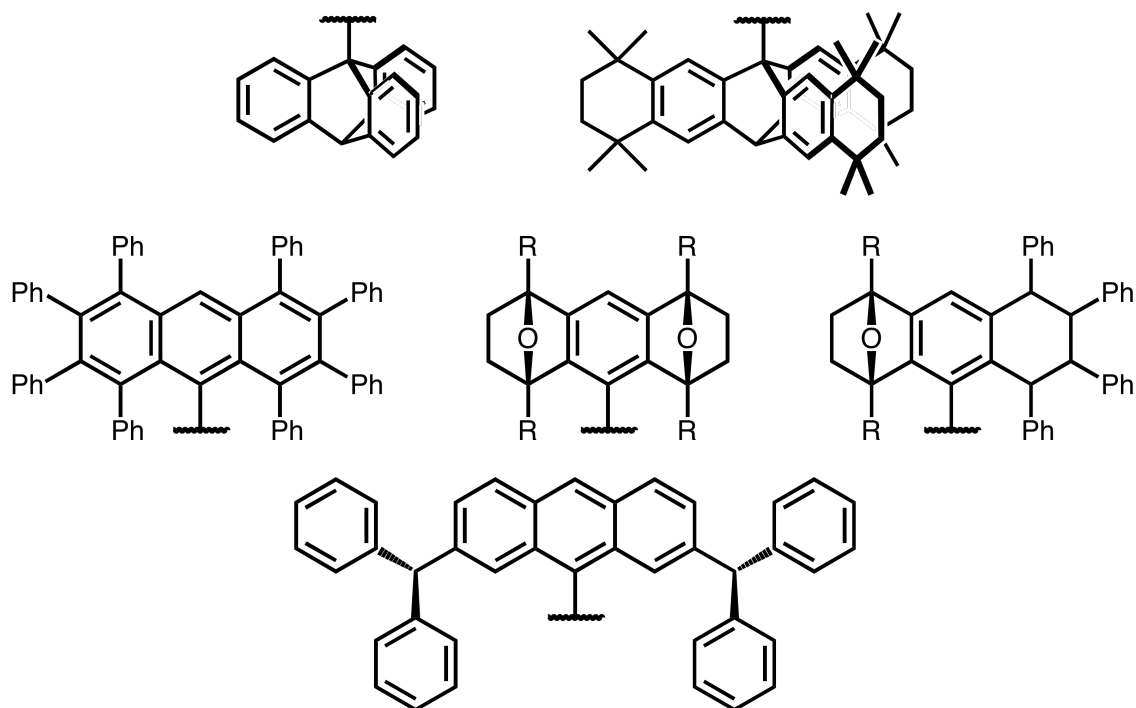
Figure 2.20: Suggested tricyclic motifs for the inclusion in ligand design, primarily for amido type ligands.

[xlv]Discussed in more detail in **chapter 3** and **chapter 4**, the requirement for greater proximal bulk and distal bulk for the tricyclic amide ligand class is mandatory if these ligands are to be viable for low-oxidation state group 14 element chemistry.

2.11   Experimental

Employed Computational Methodology

VEGA-ZZ (version 3.1.2.39)

An appropriate file (extension.xyz or .pdb) is uploaded and opened using VEGA-ZZ.exe. The surface area of the molecule can be calculated using this software. It was found that setting *Mesh* to 0.5 and *Probe Radius* to 1×10^{-7} gave the lowest possible values and hence consistent values.

Approximation of Flexibility bV%

To obtain the range bV%, which highlights the flexibility of a ligand in relation to its provided steric encumbrance, a model of the molecule must be used. This model can be sourced from the molecular structure (the solid-state structure), an optimised model, or, for a more approximate figure, modelled using a molecular modelling program (gaussview or avagadros). The molecular model is then altered based on the desired geometry; for flexibility the least and most sterically encumbering orientations are required. These orientations are based on the rationale of the modeller, introducing an element of **human error** within the obtained values. Once modelled the new structures can be measured. The extent of orientation deformation from the original model, if the model is obtained experimentally or computationally, should be limited to axial rotation as to reduce the introduction of more human error. It is believed that axial rotation is the most likely major movement to effect the sterics of a molecule, and flexibility and bond elongation are too difficult to model correctly without arduous further computation.

For a more in depth analysis the single point energy of the newly formed models can be performed. Another method is to optimise the structure starting from the least or most sterically encumbering models; this gives an indication as to the validity of these structures.

Synthesis

General Methods IPr,[60] (Imid)PdCl$_2$(IPr),[61] Ar*NH$_2$[18] & Ar†NH$_2$,[19] ^{Dipp}DABNH$_2$,[27] and BBP-Br[56] were prepared by literature procedures. All other reagents were used as received.

General procedure for the synthesis of 1-6 (the anthryl alkyl amines): To a solution of KO^{t}Bu (0.524 g, 4.70 mmol), (Imid)PdCl$_2$(IPr) (0.038 g), and the corresponding amine (4.70 mmol) in toluene was added 9-bromoanthracene (1 g, 3.92 mmol). This solution was heated to 90 °C and stirred overnight (unless specified otherwise). Volatiles were removed *in vacuo* and the residue was filtered in hexane through a celite pad. Hexane is removed vacuo to yield the product.

An(^{t}Bu)NH (1). The product was isolated as a yellow crystalline solid. The crystals were fine yellow needles (yield $\approx$ 95%). M.p. = 124.9 °C; ^{1}H NMR (benzene-d$_6$, 400 MHz,

298 K): δ = 1.06 (s, 9H, N-(CH_3)$_3$), 3.43 (s, 1H, NH), 7.26 – 7.28 (m, 4H, Ar-H), 7.81 – 7.83 (m, 2H, Ar-H), 8.04 (s, 1H, Ar-(para-H)), 8.40-8.43 (m, 2H, Ar-H); ^{13}C{^{1}H} NMR (benzene-d$_6$, 75.5MHz, 298K): δ = 31.92 (C-(CH$_3$)$_3$), 56.67 (C-(CH$_3$)$_3$), 124.13, 124.93, 125.85, 126.53, 129.47, 131.08, 133.40 (Ar-C); IR (ATR, Nujol): $\bar{v}$ (cm^{-1}) = 733.4 (s), 798.6 (m), 1351.2 (m), 1166.7(m), 1386.6 (m), 1474.2 (m), 1617.7 (m), 2968.8 (m), 3045.2 (w), 3350.9 (w); EI/MS m/z (%): 250.16 (M$^+$, 100).

An(Cyc)NH (2). The product was isolated as a yellow crystalline solid. The crystals were fine yellow needles (yield $\approx$ 90%). M.p. = 216.1 °C; ^{1}H NMR (benzene-d$_6$, 400 MHz, 298 K): δ = 1.07-1.11 (m, 2H, cyclohexyl-H), 1.25 – 1.29 (m, 2H, cyclohexyl-H, tentative assignment - obscured by hexane), 1.35-1.40 (m, 2H, cyclohexyl-H), 1.45-1.50 (m, 2H, cyclohexyl-H), 1,89-1.93 (m, 2H, cyclohexyl-H), 3.26 – 3.36 (m, 1H, CH-(CH$_2$)$_2$-), 3.68 (d, 1H, NH, coupled to the CH of cyclohexyl), 7.26-7.32 (m, 4H, Ar-H), 7.84-7.86 (m, 2H, Ar-H), 7.98 (s, 1H, Ar-H), 8.23-8.25 (m, 2H, Ar-H); ^{13}C{^{1}H} NMR (benzene-d$_6$, 75.5MHz, 298K): δ = 26.32 (Cycohexyl-CH$_2$), 26.70 (Cycohexyl-CH$_2$), 35.90 (Cycohexyl-CH$_2$), 60.79 (Cycohexyl-CH), 122.05, 1224.65, 125.17, 125.92, 133.49, 142.03 (Ar-C); IR (ATR, Nujol): $\bar{v}$ (cm$_{-1}$) = 731.5 (s), 1105.2 (m), 1452.7(m), 1555.2 (m), 1618.6 (m), 2847.7(m), 2921.0 (m), 2938.1 (m), 3048.0 (w), 3341.1 (w). EI/MS m/z (%): 276.17 (M$^+$, 100).

An(^{t}Oct)NH (3). The product was first isolated as a brown oil which was pure by ^{1}H NMR spectroscopy (yield $\approx$ 92%). Crystallisation of the product occurred from hexane when stored –30 °C, overnight (isolated yield $\approx$ 60-75%). M.p. = 167.9 °C (melted); ^{1}H NMR (benzene-d$_6$, 400 MHz, 298 K): δ = 1.03 (s, 6H, N(H)-C-(CH_3)$_2$-), 1.13 (s, 9H, CH$_2$-^{t}Bu(H_9)), 1.79 (s, 2H, -C(CH$_3$)$_2$-CH_2-), 3.62 (s, 1H, An-NH), 7.25-7.33 (m, 4H,Ar-H), 7.84 (d, J$_{HH}$ = 8.21, 2H, Ar-H), 8.06 (s, 1H, Ar-*(para-H)*), 8.50 (d, J$_{HH}$ = 8.49, 2H, Ar-H); ^{13}C{^{1}H} NMR (benzene-d$_6$, 75.5MHz, 298K): δ = 30.98 (C-(CH$_3$)$_2$), 32.70 (C-(CH$_3$)$_3$), 32.85 (C-(CH$_3$)$_2$), 58.94 (C(CH$_3$)$_2$-CH$_2$), 61.13 (N-C-(CH$_3$)$_2$-), 124.05, 124.90, 125.83, 126.58, 129.51 (Ar-CH), 131.27, 133.44, 140.07 (Ar-C); IR (ATR, Nujol);$\bar{v}$(cm^{-1}) = 732.4 (s), 1135.0 (m), 1341.8 (m), 1459.3 (w), 1619.5 (w), 2949.3 (m), 3029.0 (w); EI/MS m/z (%): 194.10 (AnNH$^+$, 100), 306.22 (M$^+$, 46).

An(Ad)NH (4). The product was isolated as a yellow powder with some yellow needles, which was pure by ^{1}H NMR spectroscopy (yield $\approx$ 95%). Crystallisation of the product occurred from hexane when stored –30 °C, overnight. The crystals were fine yellow needles. M.p. = 201.9 °C; ^{1}H NMR (benzene-d$_6$, 400 MHz, 298 K): δ = 1.30-1.40 (m, 6H, Ad-CH_2, tentatively assigned a roofed doublet), 1.76 (s, 6H, Ad-CH_2), 1.78 (s, 3H, Ad-CH), 3.49 (s, 1H, NH), 7.27-7.34 (m, 4H, Ar-H), 7.84-7.86 (m, 2H, Ar-H), 8.08 (s, 1H, Ar-H), 8.55-8.57 (m, 2H, Ar-H); ^{13}C{^{1}H} NMR (benzene-d$_6$, 75.5MHz, 298K): δ = 31.00, 37.10, 45.61, 57.10 (Ad-C), 123.97, 124.86, 125.90, 126.75, 129.40, 131.32, 133.41, 139.36 (Ar-C); IR (ATR, Nujol): $\bar{v}$ (cm^{-1}) = 736 (s), 797 (s), 842 (s), 889 (m), 1094 (m), 1302 (m), 1351 (m), 1408 (m), 1435 (w), 1449 (w), 1552 (w), 1619 (w), 2847 (s), 2901 (s), 3047 (w), 3346 (w, NH); EI/MS m/z (%): 135.12 (Ad$^+$, 16), 194.10 (AnNH$^+$, 1.25), 328.21 (M$^+$, 100).

An(C1)NH (5). The product was isolated as a brown viscous solid which was pure by ^{1}H NMR spectroscopy (yield $\approx$ 75%). The product could be obtained as a yellow powder through sonication of the brown viscous solid in iso-propanol (isolated yield $\approx$ 30-55%).

Overtime it was found that the named compound returned to a brown viscous solid with the presence of what by eye appeared to be brown needle-like crystals, from the yellow powder. M.p. = 119.4 °C; ^{1}H NMR (benzene-d$_6$, 400 MHz, 298 K): δ = 1.15 (d, J$_{HH}$ = 6.75 Hz, 3H, -C(H)(Ph)-CH_3), 3.83 (d, J$_{HH}$ = 9.79 Hz, 1H, NH, coupling with C(H)-CH$_3$-Ph), 4.43-4.50 (m, 1H, C(H)-CH3-Ph), 6.89 – 7.12 (m, 9H, Ar-H and An-H), 7.68 (d, J$_{HH}$ = 8.89 Hz, 2H, An-H) 7.84 (s, 1H, An-$(para$-$H)$) 7.97 (d, J$_{HH}$ = 8.47 Hz, 2H, An-H); ^{13}C{^{1}H} NMR (benzene-d$_6$, 75.5MHz, 298K): δ = 23.74 (CH), 61.20 (C(CH$_3$), 122.57, 124.57, 125.35, 125.95, 127.10, 127.24, 127.82, 129.27, 129.82, 133.47, 141.67, 145.96 (Ar-C); IR (ATR, Nujol); $\bar{v}$ (cm^{-1}) = 728.7 (s), 1103.3 (s), 1354.9 (s), 1555.2 (m), 1618.5 (m), 2984 (m), 3024.7 (w), 3377.0 (w); EI/MS m/z (%): 194.10 (AnNH$^+$, 26) 298.12 (M$^+$, 100).

An(C2)NH (6). The product was isolated as a brown viscous solid which was pure by ^{1}H NMR spectroscopy (yield $\approx$ 75%). The product could be obtained as a yellow powder through sonication of the brown viscous solid in iso-propanol (isolated yield $\approx$ 30-55%). Overtime it was found that the named compound returned to a brown viscous solid with the presence of what - by eye - appeared to be brown needle-like crystals, from the yellow powder; this occurred at a faster rate then for **5**. M.p. = 100.1 °C; 1H NMR (benzene-d$_6$, 400 MHz, 298 K): δ = 1.305 (d, J$_{HH}$ = 6.64 Hz, 3H, C(H)(Np)-CH_3)), 4.21 (d, J$_{HH}$ = 8.40 Hz, 1H, NH), 5.24-5.31 (m, 1H, C(CH$_3$)(Np)-H, coupling with NH), 7.04-7.19 (m, 6H, Np-H, obscured by residual benzene protons), 7.54-7.62 (m, 3H, Np-H and An-H), 7.77 (d, J$_{HH}$ = 8.47 Hz , 2H, An-H), 7.83 (d, J$_{HH}$ = 7.00 Hz, 1H, Np-H, tentative assignment), 7.94 (s, 1H, An-$(para$-$H)$), 8.11 (d, J$_{HH}$ = 8.76, 2H, An-H); ^{13}C{^{1}H} NMR (benzene-d$_6$, 75.5MHz, 298K): δ = 25.35 (C(H)(Np)-CH$_3$), 57.90 (C(H)(Np)(CH$_3$)), 122.46, 123.75, 124.03, 124.52, 125.49, 126.01, 126.62, 126.60, 126.73, 127.13, 127.97, 131.73, 133.49, 135.05, 142.30, 143.15 (Np-C and An-C); IR (ATR, Nujol); $\bar{v}$ (cm^{-1}) = 732.4 (s), 1135.0 (m), 1341.8 (m), 1459.3 (w), 1619.5 (w), 2949.3 (m), 3029.0 (w, NH); EI/MS m/z (%): 155.09 (C2$^+$, 37.5), 194.10 (AnNH$^+$, 6.25), 348.18 (M$^+$,100).

An(^{t}BuNH)$_2$ (11). To a solution of KO^{t}Bu (0.524 g, 4.70 mmol), Pd catalyst (0.038g), and ^{t}BuNH$_2$ (4.70 mmol) in toluene was added 9,10-dibromoanthracene (0.729g, 2.17 mmol).This solution was then heated to 90 °C and stirred overnight. Volatiles were removed *in vacuo* and the residue was filtered in hexane through a celite pad. Volatiles are removed in vacuo to give the product as a off-yellow/brown solid (yield $\approx$ 85%) .M.p. = 142.3 °C (melted); 1H NMR (benzene-d$_6$, 400 MHz, 298 K): δ = 1.11 (s, 18H, tBu-H), 3.44 (s, 2H, NH), 7.30-7.34 (m, 4H, An-H), 8.49-8.53 (m, 4H, An-H); ^{13}C{^{1}H} NMR (benzene-d$_6$, 75.5MHz, 298K): δ = 31.94 (C-(CH$_3$)$_3$), 56.37 (C-(CH$_3$)$_3$), 124.68, 126.59, 128.12, 129.01, 131.53, 132.03, 136.38 (An-C); IR (ATR, Nujol): $\bar{v}$ (cm^{-1}) = 739 (s), 784 (s), 816 (m), 879 (w), 963 (m), 1021 (m), 1064 (m), 1172 (s), 1194 (m), 1209 (m), 1362 (s), 1377 (s), 1427 (w), 1474 (m), 1617 (w), 2866 (w), 2968 (m), 3078 (w), 3349 (m, NH).

Ar^X (*previously reported*). To a stirred solution of benzene (10 mL, 0.117 mol) in DCM ($\approx$ 50 mL) was added AlCl$_3$ (15.7g, 0.058 mol) at –10 °C. At this temperature was added ^{t}BuCl (87.9 mL, 0.81 mol) dropwise via a dropping funnel over 1 hr. The mixture was then allowed to stir for a further 2 hrs at room temperature (24 °C). After 2 hrs. the mixture was quenched by being added to a beaker of crushed ice and left to stir for an hour. The product was extracted in DCM, washed with water and brine, and dried using sodium

(or magnesium) sulfate. Volatiles were removed on a rotary evaporator. Hexane was then added and the mixture was placed in a –30 °C freezer overnight, until precipitation occurs. The solid was filtered off and collected before being rinsed with cold hexane to give the purified product as a white solid.

Ar^{X}NO$_2$ (12). Over a period of 4 – 6 hrs, 1 molar equivalent portions of fuming red HNO$_3$ (0.465 mL - added in 3 lots for a total of 1.395 mL) were added to a refluxing solution of Ar^X (1g, 3.35 mmol) in acetic anhydride. This mixture was then allowed to stand at room temperature (24 °C) for 24 hrs, over this period precipitation occurs. The precipitate was washed sparingly with cold water and ethanol, leaving fine yellow needles (yield ≈ 60-80%). M.p. = 258.8 °C; 1H NMR (chloroform-d$_1$, 400 MHz, 298 K): δ = 1.28 (s, 12H, C-CH_3), 1.29 (s, 12H, C-CH_3), 1.65 (m, 4H, C(CH$_3$)$_2$-CH_2-), 1.69 (m, C(CH$_3$)$_2$-CH_2-), 7.40 (s, 1H, Ar-H); ^{13}C{^{1}H} NMR (chloroform-d$_1$, 75.5MHz, 298K): IR (ATR, Nujol): $\bar{v}$ (cm^{-1}) = 747 (m), 1143 (m), 1261 (m), 1367 (m), 1460 (m), 1527 (s), 2866 (m), 2924 (m), 2959 (m); EI/MS m/z (%): 344.2570 (M$^+$, 100).

Ar^{X}NH$_2$ (13). Under a stream of nitrogen, to an acetic acid solution of Ar^{X}NO$_2$ (1g, 2.91 mmol) was added HCl (32% i.e. ≈ 10.2 M; 2.86 mL, 29.1 mmol) drop-wise, at reflux. zinc powder (1.9g, 29.1 mmol) was then added in portions to said solution and washed through with minimal HCl. The solution is left to stir at reflux for 1 – 4 hrs. Volatiles were removed on a rotary evaporator to give a sticky solid. The product is extracted in DCM, and washed with dilute HCl (0.1M), K$_2$CO$_3$•H2O, water and then brine. The extract is then dried with magnesium sulfate, filtered and volatiles removed *in vacuo* to give the product as a white powder (yield (yield ≈ 50-70%). M.p. = 214 – 217 °C (decomp.); ^{1}H NMR (benzene-d$_6$, 400 MHz, 298 K): δ = 1.33 (s, 12H, , C-CH_3), 1.39 (s, 12H, , C-CH_3), 1.56 (m, 4H, C(CH$_3$)$_2$-CH_2-), 1.60 (m, 4H, C(CH$_3$)$_2$-CH_2-), 3.68 (s, 2H, NH_2), 6.94 (s, 1H, Ar-H); ^{13}C{^{1}H} NMR (chloroform-d$_1$, 75.5 MHz, 298K): IR(ATR, Nujol): $\bar{v}$ (cm^{-1}) = 1082.8 (m), 1312.0 (m), 1361.4 (s), 1383.8 (s), 1458.3 (s), 1449.9 (s), 1592.5 (m), 1617.7 (m), 2858.9 (s), 2914.8 (s), 2954.8 (s), 3512.1 (w).

Ar^X(TMS)NH (14). To a diethyl ether & hexane (1:4 ratio mix) solution of Ar^{X}NH$_2$ (1g, 3.2 mmol) was added ^{n}BuLi (1.6 M, 2.2 mL, 3.5 mmol) dropwise at –80 °C, the solution was then allowed to stir at room temperature (24 °C) for 2 hrs. TMSCl (0.44 mL, 3.5 mmol) was then added dropwise at 0 °C to the solution, the solution was allowed to stir for a further 12 hrs (overnight). Volatiles were removed *in vacuo* and non-dried toluene was added. The solution was heated and filtered through a celite pad to remove LiCl. Volatiles were removed on a rotary evaporator to give a oily white-yellow solid, this solid was dissolved into hexane and stored at –30 °C resulting in precipitation of the named product as an off-white powder (yield ≈ 70-90%). This named product could be recrystallised from hexane at 0 °C. M.p. 213-215.9 °C; ^{1}H NMR (benzene-d$_6$, 400 MHz, 298 K): δ = 1.30 (s, 9H, Si(CH_3)$_3$), 1.33 (s, 12H, C(CH_3)$_2$), 1.39 (s, 12H, C(CH_3)$_2$), 1.54-1.57 (m, 4H, CH_2), 1.61-1.63 (m, 4H, CH_2), 3.68 (s, 1H, NH), 6.95 (s, 1H, Ar-H); ^{13}C{^{1}H} NMR (benzene-d$_6$, 75.5 MHz, 298 K): δ = 28.2 (Si(CH_3)$_3$), 32.2 (C(CH_3)$_2$), 32.7 (C(CH_3)$_2$), 33.8 (C(CH$_3$)$_2$), 34.2 (C(CH$_3$)$_2$), 35.5 (CH$_2$), 35.7 (CH$_2$, 117.0, 124.4, 142.1, 143.7 (ArC); ^{29}Si {^{1}H} NMR (benzene-d$_6$, 80 MHz, 298 K): δ = –1.3; IR (ATR, Nujol): $\bar{v}$ (cm^{-1}) = 747 (s), 843 (s), 863 (s), 1059 (m), 1261 (m), 1367 (s), 1460 (s), 1529 (s), 1620 (w), 2864 (m), 2961 (m), 2926 (m), 3430 (w); EI/MS

m/z (%): 385.4 (M$^+$, 10), ((M-Me)$^+$, 37), 313.4 (Ar^{X}NH$_2$$^+$, 44), 298.3 (Ar^{X}H$^+$, 100), 73.1 (SiMe$_3$$^+$, 25).

Ind^{Et}NO$_2$ (15). Over the period of 4 – 6 hrs, portions of HNO$_3$ (0.9 mL - added in 2 lots for a total of 1.8 mL) were added at reflux to a solution of EindNO$_2$ (1g, 2.6 mmol) in acetic anhydride. This mixture was then allowed to stand at room temperature (24 hrs) as the product precipitates out. The product was washed sparingly with cold water and ethanol, leaving fine yellow needles (yield ≈ 40-70%; isolated yield ≈ 55%). M.p. = 187.4 °C; ^{1}H NMR (benzene-d$_6$, 400 MHz, 298 K): δ = 0.79 (t, J$_{HH}$ = 7.65 Hz, 12H, -CH$_2$-CH$_3$), 0.82 (t, J$_{HH}$ = 7.29 Hz, 12H, -CH$_2$-CH$_3$), 1.53 (m, 8H, C-CH$_2$), 1.73 (m, 16H, -CH$_2$-CH$_3$), 6.83 (s, 1H, Ar-H). ^{13}C{^{1}H} NMR (chloroform-d1, 75.5MHz, 298K): δ = 9.45, 9.95, 31.98, 33.07, 42.99, 48.36, 52.18 , 121.49, 136.72, 145.74, 152.80 (Ar-H); IR (ATR, Nujol): $\bar{v}$ (cm^{-1}) = 756.6 (s), 955.1 (m), 1275.7 (m), 1380.0 (s, NO), 1465.8 (s), 1518.9 (s, NO), 1551.5 (m), 1637.2 (w), 1718.3 (w), 2286.7 (w), 2875.6 (s), 2934.3 (s), 2962.3 (s); EI/MS m/z (%): 426.34(M$^+$, 100).

Ind^{Et}NH$_2$ (16). To a solution of Ind^{Et}NO$_2$ (1g, 2.34 mmol) in THF was added Li[AlH$_4$] (0.28g, 9.35 mmol) as a THF solution, dropwise at –80 °C. This mixture was then heated to reflux and allowed to stir for 1-2 days, and monitored by ^{1}H NMR spectroscopy until completion (if uncompleted the required Li[AlH$_4$] was added as stated earlier). The solution was then cooled to 0 °C and quenched with NH$_4$Cl in water. The product was then extracted in THF, and washed with water and brine. Volatiles were removed on a rotary evaporator. The product was collected as an off-white powder (yield ≈ 20-40%; isolated yield ≈ 30%).M.p. = 123.4 °C; ^{1}H NMR (chloroform-d$_1$, 400 MHz, 298 K): δ = 0.82 (t, J$_{HH}$ = 7.15 Hz, 24H, C-CH$_2$|-CH$_3$), 1.48 – 1.75 (m, 16H, C-CH$_2$-CH$_3$), 1.78 (s, 4H, C(Et)-CH$_2$-), 3.51 (s, 2H, Ar-NH), 6.16 (s, 1H, Ar-H); ^{13}C{^{1}H} NMR (chloroform-d$_1$, 75.5MHz, 298K): δ = 9.39, 9.53, 31.95, 33.14, 43.65, 48.27, 50.42, 110.35, 130.77, 139.35, 150.44 (Ar-H); IR (ATR, Nujol): $\bar{v}$ (cm^{-1}) = 793.0 (s), 1047.4 (m), 1378.2 (m), 1576.7 (m), 1610.2 (m), 2855.1 (s), 2908.3 (s), 2957.6 (s), 3392.8 (w, NH), 3465.5 (w, NH); EI/MS m/z (%): 398.38 (M$^+$, 100).

Ar*(BBN)NH (18). To a stirred solution Ar*NH$_2$ (1 g, 2.30 mmol) in THF (50 mL) was added 9-BBN (5.52 mL, 2.76 mmol) over 5 min. The resultant solution was then heated to reflux (60 °C) and stirred for 24 hrs. Volatiles were removed in vacuo to afford the titled compound as a white powder (yield 1.22g, 95%). M.p. = 211 – 213 °C (decomp); ^{1}H NMR (toluene-d$_8$, 400 MHz, 298 K): δ 1.48 – 1.56 (m, 4H, BBN-H), 1.87 (s, 3H, Ar-CH_3), 1.90 – 1.96 (m, 8H, BBN-H), 2.07 – 2.09 (m, 2H, BBN-H), 4.56 (s, 1H, Ar-NH(BBN)), 6.02 (s, 2H, Ar-CH(Ph)$_2$), 6.77 (s, 2H, Ar-$(ortho$-$H)$), 7.00 – 7.10 (m, 20H, Ph-H); ^{11}B{^{1}H} NMR (128 MHz, 298 K): δ = 57.31; ^{13}C{^{1}H} NMR (toluene-d$_8$, 75.5 MHz, 298K): δ = 34.83 (BBN-C), 35.03 (BBN-C), 53.86 (CHPh$_2$), 106.33 (CH$_3$), 127.58, 129.63, 130.52, 130.94, 142.98, 144.43(Ar-C); IR (ATR, Nujol): $\bar{v}$ (cm^{-1}) = 697 (s), 762 (s), 1031 (m), 1316 (m), 1380 (m), 1477 (s), 1597 (s), 2832 (w), 2879 (m), 3021 (w), 3366 (w); EI/MS (70eV): m/z (%): 559.4 (M$^+$, 7.5), 429.3 (M$^+$-BBN, 42.5), 167.1 (CHPh$_2$, 65).

Ar†(BBN)NH (19).   This compound was prepared in an analogous fashion to Ar*(BBN)NH, using Ar†NH$_2$ (1.00 g, 2.12 mmol) and 9-BBN (5.2 mL, 2.60 mmol).

Volatiles were removed in vacuo to afford the titled compound as a white powder (yield $\approx$ 1.23g, 99%). M.p. = 214 – 217 °C (decomp.); ^{1}H NMR (toluene-d$_8$, 400 MHz, 298 K): δ = 0.93 (d, J$_{HH}$ = 6.88 Hz, 6H, Ar-CH(CH_3)$_2$), 1.48 – 1.54 (m, 4H, BBN-H), 1.61 – 1.68 (m, 2H, BBN-H), 1.83 – 1.89 (m, 8H, BBN-H), 2.48 (sept., J$_{HH}$ = 6.9 Hz, 1H, Ar-CH(CH$_3$)$_2$), 4.59 (s, 1H, Ar-NH(BBN)), 6.04 (s, 2H, Ar-CH(Ph)$_2$), 6.86 (s, 2H, Ar-(ortho-H)), 6.97 – 7.17 (m, 20H, Ph-H); ^{11}B ^{1}H} NMR (128 MHz, 298 K): δ = 56.77; ^{13}C{^{1}H} NMR (toluene-d$_8$, 75.5MHz, 298K): δ = 24.00 (Ar-CH(CH_3)$_2$), 33.26 (Ar-CH(CH$_3$)$_2$)), 33.80 (BBN-C), 33.86 (BBN-C), 34.05 (BBN-C), 34.08 (BBN-C), 53.05 (CHPh$_2$), 126.60, 126.88, 138.47, 141.90, 145.74 (Ar-C); IR (ATR, Nujol): $\bar{v}$ (cm^{-1}) = 700 (s), 745 (s), 765 (s), 1071 (m), 1283 (w), 1378 (w), 1447 (s), 1480 (s), 1495 (s), 1600 (w), 2849 (m), 2874 (m), 2903 (m), 3024 (w), 3373 (w); EI/MS (70eV): m/z (%): 587.5 (M$^+$, 5.5), 258.1 (M$^+$-^{i}Pr, CHPh$_2$ & BBN, 60.6), 167.1 (CHPh$_2$, 12.1).

{(^{Dipp}DAB)B}(BBN)NH (20) (*presumptive*) . This compound was only fashioned once from a single reaction and could not be successfully re-synthesised at the time of the attempt. This compound was prepared in an analogous fashion as to **18** & **19**. Only ^{1}H & ^{11}B NMR spectroscopic data was collected. 1H NMR (benzene-d$_6$, 400 MHz, 298 K): δ = 1.24 (d, J$_{HH}$ = 7.4 Hz, 12H, Ar-CH(CH_3)$_2$), 1.35 (d, J$_{HH}$ = 7.4 Hz, 12H, Ar-CH(CH_3)$_2$), 1.398-1.45 (m, 4H, BBN-H) 1.839-1.949 (m, 8H, BBN-H), 3.40 (sept. J$_{HH}$ = 7.5 Hz, 4H, Ar-CH(CH$_3$), 4.290 (s, 1H, N-H), 6.108 (s, 2H, N(CH)$_2$N), 7.167-7.196 (Ar-H); ^{11}B{^{1}H} NMR (128 MHz, 298 K): δ = 22.82, 58.63.

Ar*(BBP)NH (21). To a stirred solution of Ar*NH2 (1.00g, 2.28 mmol) in THF was added ^{n}BuLi (1.50 mL, 1.6M) dropwise at –80 °C, the solution was then allowed to stir at room temperature (24 °C) for 2 hrs. To this solution, BBP (0.53g, 2.28 mmol) was added dropwise at 0 °C as a THF solution, and the mixture allowed to stir 12 hours (overnight). Volatiles were removed in vacuo, and the residue extracted in toluene. Toluene was removed in vacuo to give the product as an off-white powder (yield $\approx$ 75%) M.p. = 208.5 °C; 1H NMR (benzene-d$_6$, 400 MHz, 298 K): δ = 1.5 (m, 8H, BBP-H), 1.91 (s, 3H, Ar-CH_3), 2.91 (m, 8H, BBP-H), 3.08 (s, 1H, Ar-NH(BBP)), 6.11 (s, 2H, Ar-CH(Ph)$_2$), 6.83 (s, 2H, Ar-(ortho-H)), 7.02 – 7.16 (m, 20H, Ph-H); ^{11}B{^{1}H} NMR (128 MHz, 298 K): δ = 22.79; ^{13}C{^{1}H} NMR (benzene-d6, 75.5MHz, 298K): δ = 21.28 (Ar-CH$_3$), 27.07 (BBP-C), 47.78 (BBP-C), 53.20 (CHPh$_2$), 126.40, 128.49, 129.41, 130.08, 131.31, 139.49, 140.94, 144.75 (Ar-C); IR (ATR, Nujol): (cm^{-1}) = 697.9 (s), 760.4 (m), 1027.8 (m), 1315.8 (m)., 1420.1 (m), 1444.3 (m), 1490.9 (m), 1597.2 (w), 2886.3 (w), 2952.1 (w), 3021.0 (w), 3395.6 (w); EI/MS m/z (%): 440.24 (Ar*NH$^+$, 100).

Ar†(BBP)NH (22). To a stirred solution of Ar†NH$_2$ (1g, 2.14 mmol) in THF was added ^{n}BuLi (1.40 mL, 1.6M) dropwise at –80 °C, the solution was then allowed to stir at room temperature (24 °C) for 2 hrs. To this solution, BBP (0.494 g, 2.14 mmol) was added dropwise at 0 °C, and the mixture allowed to stir 12 hours (overnight). Volatiles were removed *in vacuo*, and the residue extracted in hexane. Toluene was removed in vacuo to give the product as an off-white powder (yield $\approx$ 75%). M.p. = 184.6 °C; ^{1}H NMR (benzene-d$_6$, 400 MHz, 298 K): δ = 0.97 (d, J$_{HH}$ = 6.71 Hz, 6H, Ar-CH(CH_3)$_2$), 1.49 (m, 8H, BBP-H), 2.52 (sept., J$_{HH}$ = 7.02 Hz, 1H, Ar-CH(CH$_3$)$_2$), 2.90 (m, 8H, BBP-H), 3.08 (s, 1H, Ar-NH(BBP)), 6.11 (s, 2H, Ar-CH(Ph)$_2$), 6.89 (s, 2H, Ar-(ortho-H)), 6.01 – 7.21

(m, 20H, Ph-*H*); ^{11}B{^{1}H} NMR (128 MHz, 298 K): δ = 26.96; ^{13}C{^{1}H} NMR (benzene-d$_6$, 75.5MHz, 298K): δ = 24.22 (Ar-CH(*C*H$_3$)$_2$)), 27.05 (BBP-*C*), 47.75 (Ar-*C*H(CH$_3$)$_2$)), 53.58 (*C*HPh$_2$), 126.39, 126.69, 128.48, 130.06, 139.12, 141.18, 142.11, 144.83 (Ar-*C*); IR (ATR, Nujol): $\bar{v}$ (cm^{-1}) = 697 (s), 741 (m), 762 (m), 1030 (m), 1075 (m), 1233 (w), 1317 (m), 1399 (m), 1446 (m), 1468 (m), 1627 (m), 2864 (w), 2957 (m), 3024 (w), 3058 (w), 2290 (m, NH); EI/MS m/z (%): 468.27 (Ar†NH^{+}, 100).

Bibliography

[1] C. E. Housecroft and A. G. Sharpe, *Inorganic Chemistry.* Pearson Education Limited, 2001.

[2] P. Atkins and T. Overton, *Shriver and Atkins' Inorganic Chemistry.* Oxford University Press, USA, 2010.

[3] F. T. Edelmann, "Lanthanide Amidinates and Guanidinates: From Laboratory Curiosities to Efficient Homogeneous Catalysts and Precursors for Rare-Earth Oxide Thin Films," *Chem. Soc. Rev.*, vol. 38, pp. 2253–2268, 2009.

[4] P. W. van Leeuwen, P. C. Kamer, and J. N. Reek, "The Bite Angle Makes the Catalyst," *Pure and Applied Chemistry*, vol. 71, no. 8, pp. 1443–1452, 1999.

[5] P. Dierkes and P. W. van Leeuwen, "The Bite Angle Makes the Difference: a Practical Ligand Parameter for Diphosphine Ligands," *Journal of the Chemical Society, Dalton Transactions*, no. 10, pp. 1519–1530, 1999.

[6] M.-N. Birkholz, Z. Freixa, and P. W. van Leeuwen, "Bite Angle Effects of Diphosphines in C–C and C–X Bond Forming Cross Coupling Reactions," *Chemical Society Reviews*, vol. 38, no. 4, pp. 1099–1118, 2009.

[7] A. Sanger, "Reactions of Benzonitrile with Lithium Amides," *Inorganic and Nuclear Chemistry Letters*, vol. 9, no. 3, pp. 351 – 354, 1973.

[8] S. P. Green, C. Jones, and A. Stasch, "Stable Magnesium (I) Compounds with Mg-mg Bonds," *Science*, vol. 318, no. 5857, pp. 1754–1757, 2007.

[9] C. Cui, H. W. Roesky, H.-G. Schmidt, M. Noltemeyer, H. Hao, and F. Cimpoesu, "Synthesis and Structure of a Monomeric Aluminum (I) Compound [{HC(CMeNAr)$_2$} Al](Ar = 2, 6–iPr$_2$C$_6$H$_3$): A Stable Aluminum Analogue of a Carbene," *Angewandte Chemie International Edition*, vol. 39, no. 23, pp. 4274–4276, 2000.

[10] P. H. M. Budzelaar, A. B. van Oort, and A. G. Orpen, "β-Diiminato Complexes of VIII and Ti(III) – Formation and Structure of Stable Paramagnetic Dialkylmetal Compounds," *European Journal of Inorganic Chemistry*, vol. 1998, no. 10, pp. 1485–1494, 1998.

[11] L. Bourget-Merle, M. F. Lappert, and J. R. Severn, "The Chemistry of β-Diketiminatometal Complexes," *Chemical reviews*, vol. 102, no. 9, pp. 3031–3066, 2002.

[12] D. C. H. Do, A. Keyser, A. V. Protchenko, B. Maitland, I. Pernik, H. Niu, E. L. Kolychev, A. Rit, D. Vidovic, A. Stasch, *et al.*, "Highly Electron-Rich β-Diketiminato Systems: Synthesis and Coordination Chemistry of Amino-Functionalized "N-nacnac" Ligands," *Chemistry–A European Journal*, vol. 23, no. 24, pp. 5830–5841, 2017.

[13] C. Chen, S. M. Bellows, and P. L. Holland, "Tuning Steric and Electronic Effects in Transition-Metal β-Diketiminate Complexes," *Dalton Transactions*, vol. 44, no. 38, pp. 16654–16670, 2015.

[14] B. Schiemenz and P. P. Power, "Synthesis of Sterically Encumbered Terphenyls and Characterization of their Metal derivatives $Et_2OLiC_6H_3$-2, 6-$Trip_2$ and $Me_2SCuC_6H_3$-2, 6-$Trip_2$ ($Trip$= 2, 4, 6-i-$Pr_3C_6H_2$-)," *Organometallics*, vol. 15, no. 3, pp. 958–964, 1996.

[15] R. J. Wright, J. Steiner, S. Beaini, and P. P. Power, "Synthesis of the Sterically Encumbering Terphenyl Silyl and Alkyl Amines HN (R) $ArMes_2$ (R= Me and $SiMe_3$), their Lithium Derivatives LiN (R) $ArMes_2$, and the Tertiary Amine $Me_2NArMes_2$," *Inorganica chimica acta*, vol. 359, no. 6, pp. 1939–1946, 2006.

[16] R. Wolf, C. Ni, T. Nguyen, M. Brynda, G. J. Long, A. D. Sutton, R. C. Fischer, J. Fettinger, M. Hellman, L. Pu, *et al.*, "Substituent Effects in Formally Quintuple-Bonded ArCrCrAr Compounds (Ar= Terphenyl) and Related Species," *Inorganic chemistry*, vol. 46, no. 26, pp. 11277–11290, 2007.

[17] C. Stanciu, A. F. Richards, J. C. Fettinger, M. Brynda, and P. P. Power, "Synthesis and Characterization of New, Modified Terphenyl Ligands: Increasing the Rotational Barrier for Flanking Rings," *Journal of organometallic chemistry*, vol. 691, no. 11, pp. 2540–2545, 2006.

[18] J. Li, A. Stasch, C. Schenk, and C. Jones, "Extremely Bulky Amido-Group 14 Element Chloride Complexes: Potential Synthons for Low-Oxidation State Main Group Chemistry," *Dalton Transactions*, vol. 40, no. 40, pp. 10448–10456, 2011.

[19] T. J. Hadlington, J. Li, and C. Jones, "Synthesis and Characterization of Extremely Bulky Amido-Germanium (II) Halide Complexes," *Canadian Journal of Chemistry*, vol. 92, no. 6, pp. 427–433, 2013.

[20] A. S. Guram and S. L. Buchwald, "Palladium-Catalyzed Aromatic Aminations with In Situ Generated Aminostannanes," *Journal of the American Chemical Society*, vol. 116, no. 17, pp. 7901–7902, 1994.

[21] F. Paul, J. Patt, and J. F. Hartwig, "Palladium-Catalyzed Formation of Carbon-Nitrogen Bonds. Reaction Intermediates and Catalyst Improvements in the Hetero Cross-Coupling of Aryl Halides and Tin Amides," *Journal of the American Chemical Society*, vol. 116, no. 13, pp. 5969–5970, 1994.

[22] S. L. Buchwald and A. Guram, "Preparation of Arylamines," Nov. 19 1996. US Patent 5,576,460.

[23] B. Maitland, "Novel β-Diketiminates and β-Diketiminate Derivatives for the Synthesis of Main Group Complexes," *PhD. Thesis*, 2015.

[24] J. Kelly, "Synthesis and Reactivity of Novel Low Oxidation State Tetrel Compounds Utilising Bulky Amide Ligands," *PhD. Thesis*, 2017.

[25] T. Hadlington, "Investigations Toward the Catalytic Application of Low-Oxidation State, Low-Coordinate Heavier Group 14 Complexes," *PhD. Thesis*, 2015.

[26] D. Dange, J. Li, C. Schenk, H. Schnöckel, and C. Jones, "Monomeric Group 13 Metal (I) Amides: Enforcing One-Coordination through Extreme Ligand Steric Bulk," *Inorganic chemistry*, vol. 51, no. 23, pp. 13050–13059, 2012.

[27] T. J. Hadlington, J. A. Abdalla, R. Tirfoin, S. Aldridge, and C. Jones, "Stabilization of a Two-Coordinate, Acyclic Diaminosilylene (ADASi): Completion of the Series of Isolable Diaminotetrylenes: E $(NR_2)_2$ (E= Group 14 Element)," *Chemical Communications*, vol. 52, no. 8, pp. 1717–1720, 2016.

[28] Y. Segawa, Y. Suzuki, M. Yamashita, and K. Nozaki, "Chemistry of Boryllithium: Synthesis, Structure, and Reactivity," *Journal of the American Chemical Society*, vol. 130, no. 47, pp. 16069–16079, 2008.

[29] T. Matsuo, K. Suzuki, T. Fukawa, B. Li, M. Ito, Y. Shoji, T. Otani, L. Li, M. Kobayashi, M. Hachiya, *et al.*, "Synthesis and Structures of a Series of Bulky "Rind-Br" Based on a Rigid Fused-Ring s-Hydrindacene Skeleton," *Bulletin of the Chemical Society of Japan*, vol. 84, no. 11, pp. 1178–1191, 2011.

[30] B. Li, T. Matsuo, T. Fukunaga, D. Hashizume, H. Fueno, K. Tanaka, and K. Tamao, "Neutral and Cationic Gold (I) Complexes With π-Conjugated Phosphasilene Ligands," *Organometallics*, vol. 30, no. 13, pp. 3453–3456, 2011.

[31] N. Hayakawa, T. Morimoto, A. Takagi, T. Tanikawa, D. Hashizume, and T. Matsuo, "Synthesis and Structures of Sterically Congested Diarylsilanes Bearing Two Bulky Rind Groups," *Chemistry Letters*, vol. 45, no. 4, pp. 409–411, 2016.

[32] J. M. Smith, N. J. Coville, L. M. Cook, and J. C. Boeyens, "Steric Parameters of Conformationally Flexible Ligands from X-Ray Structural Data. 1. $P(OR)_3$ Ligands in Equivalent Ligand Environments," *Organometallics*, vol. 19, no. 25, pp. 5273–5280, 2000.

[33] I. A. Guzei and M. Wendt, "An Improved Method for the Computation of Ligand Steric Effects Based on Solid Angles," *Dalton Transactions*, no. 33, pp. 3991–3999, 2006.

[34] A. Boutland, "Synthesis and reactivity of Novel Low-oxidation State Magnesium(I) Complexes," *PhD. Thesis*, 2020.

[35] F. Rodríguez, M. D. Blanco, L. F. Adrados, J. Burillo, and J. F. Tijero, "Selective Oxidation of Anthracene to Anthraquinone in Acetic Acid with Air in Presence of Nitric Acid," *Tetrahedron Letters*, vol. 30, no. 18, pp. 2417–2420, 1989.

[36] E. J. Majeski, J. D. Stuart, and W. E. Ohnesorge, "Controlled Potential Oxidation of Anthracene in Acetonitrile. II," *Journal of the American Chemical Society*, vol. 90, no. 3, pp. 633–636, 1968.

[37] G. Hoijtink, "Oxidation Potentials of Conjugated Hydrocarbons," *Recueil des Travaux Chimiques des Pays-Bas*, vol. 77, no. 6, pp. 555–558, 1958.

[38] H. Adams, R. A. Bawa, K. G. McMillan, and S. Jones, "Asymmetric Control in Diels–Alder Cycloadditions of Chiral 9-Aminoanthracenes by Relay of Stereochemical Information," *Tetrahedron: Asymmetry*, vol. 18, no. 8, pp. 1003 – 1012, 2007.

[39] S. M. Raders, J. N. Moore, J. K. Parks, A. D. Miller, T. M. Leißing, S. P. Kelley, R. D. Rogers, and K. H. Shaughnessy, "Trineopentylphosphine: A Conformationally Flexible Ligand for the Coupling of Sterically Demanding Substrates in the Buchwald–Hartwig Amination and Suzuki–Miyaura Reaction," *The Journal of Organic Chemistry*, vol. 78, no. 10, pp. 4649–4664, 2013.

[40] D. An, C. Guo, and Y. Chen, "Analysis of Polycyclic Aromatic Hydrocarbon (PAH) Mixtures Using Diffusion-Ordered NMR Spectroscopy and Adsorption by Powdered Activated Carbon and Biochar," *Materials*, vol. 11, no. 4, p. 460, 2018.

[41] S. Wagaw, R. A. Rennels, and S. L. Buchwald, "Palladium-Catalyzed Coupling of Optically Active Amines with Aryl Bromides," *Journal of the American Chemical Society*, vol. 119, no. 36, pp. 8451–8458, 1997.

[42] C. A. Coulson, R. Daudel, and J. M. Robertson, "Bond Lengths in Naphthalene and Anthracene," *Proceedings of the Royal Society of London. Series A. Mathematical and Physical Sciences*, vol. 207, no. 1090, pp. 306–320, 1921.

[43] A. Pedretti, L. Villa, and G. Vistoli, "VEGA–An Open Platform to Develop Chemo-Bio-Informatics Applications, using Plug-in Architecture and Script Programming," *Journal of computer-aided molecular design*, vol. 18, no. 3, pp. 167–173, 2004.

[44] A. Pedretti, L. Villa, and G. Vistoli, "VEGA: A Versatile Program to Convert, Handle and Visualize Molecular Structure on Windows-based PCs," *Journal of Molecular Graphics and Modelling*, vol. 21, no. 1, pp. 47–49, 2002.

[45] A. Pedretti, L. Villa, and G. Vistoli, "Atom-Type Description Language: A Universal Language to Recognize Atom Types Implemented in the VEGA Program," *Theoretical Chemistry Accounts*, vol. 109, no. 4, pp. 229–232, 2003.

[46] L. Falivene, R. Credendino, A. Poater, A. Petta, L. Serra, R. Oliva, V. Scarano, and L. Cavallo, "SambVca 2. A Web Tool for Analyzing Catalytic Pockets with Topographic Steric Maps," *Organometallics*, vol. 35, no. 13, pp. 2286–2293, 2016.

[47] L. R. C. Barclay and E. E. Betts, "The Tertiarybutylbenzenes: I. Alkylation of 1, 4-Di-t-Butylbenzene with t-Butyl Chloride," *Canadian Journal of Chemistry*, vol. 33, no. 4, pp. 672–678, 1955.

[48] G. S. Vanier, "Simple and Efficient Microwave-Assisted Hydrogenation Reactions at Moderate Temperature and Pressure," *Synlett*, vol. 2007, no. 01, pp. 0131–0135, 2007.

[49] A. Burger, M. L. Stein, and J. B. Clements, "Some Pyridylnitroalkenes, Nitroalkanols, and Alkylamines," *The Journal of Organic Chemistry*, vol. 22, no. 2, pp. 143–144, 1957.

[50] H. Lu, Z. Geng, J. Li, D. Zou, Y. Wu, and Y. Wu, "Metal-Free Reduction of Aromatic Nitro Compounds to Aromatic Amines with B_2Pin_2 in Isopropanol," *Organic letters*, vol. 18, no. 11, pp. 2774–2776, 2016.

[51] R. F. Nystrom and W. G. Brown, "Reduction of Organic Compounds by Lithium Aluminum Hydride. III. Halides, Quinones, Miscellaneous Nitrogen Compounds 1," *Journal of the American Chemical Society*, vol. 70, no. 11, pp. 3738–3740, 1948.

[52] M. Rauser, C. Ascheberg, and M. Niggemann, "Electrophilic Amination with Nitroarenes," *Angewandte Chemie*, vol. 129, no. 38, pp. 11728–11732, 2017.

[53] J. Huheey and T. Cottrell, "The Strengths of Chemical Bonds," 1958.

[54] E. A. Romero, J. L. Peltier, R. Jazzar, and G. Bertrand, "Catalyst-Free Dehydrocoupling of Amines, Alcohols, and Thiols with Pinacol Borane and 9-Borabicyclononane (9-BBN)," *Chemical Communications*, vol. 52, no. 69, pp. 10563–10565, 2016.

[55] S. Berski, Z. Latajka, and A. J. Gordon, "On the Multiple B–N Bonding in Boron Compounds Using the Topological Analysis of Electron Localization Function (ELF)," *New Journal of Chemistry*, vol. 35, no. 1, pp. 89–96, 2011.

[56] H. A. Ali, I. Goldberg, and M. Srebnik, "Tetra (pyrrolidino) diborane (4),$[(c_4h_8n)_2b]_2$, as a New Improved Alternative Synthetic Route to Bis (pinacolato) diborane (4)-Crystal Structures of the Intermediates," *European Journal of Inorganic Chemistry*, vol. 2002, no. 1, pp. 73–78, 2002.

[57] K. Gondo and T. Kitamura, "Improved and Practical Synthesis of [2,4,5-Tris(trimethylsilyl)-phenyl](phenyl)iodonium Triflate and Utilization as a 1,4-Benzdiyne Synthon," *Advanced Synthesis & Catalysis*, vol. 356, no. 9, pp. 2107–2112, 2014.

[58] T. Kitamura, K. Gondo, and J. Oyamada, "Hypervalent Iodine/Triflate Hybrid Benzdiyne Equivalents: Access to Controlled Synthesis of Polycyclic Aromatic Compounds," *Journal of the American Chemical Society*, vol. 139, no. 25, pp. 8416–8419, 2017.

[59] M. Yukimoto and M. Minoura, "The Synthesis of a Novel Bulky Primary Alkyl Group and Its Application toward the Kinetic Stabilization of a Tetraalkyldisilene," *Bulletin of the Chemical Society of Japan*, vol. 91, no. 4, pp. 585–587, 2018.

[60] L. Hintermann, "Expedient Syntheses of the N-heterocyclic Carbene Precursor Imidazolium Salts IPr·HCl, IMes·HCl and IXy·HCl," *Beilstein journal of organic chemistry*, vol. 3, no. 1, p. 22, 2007.

[61] A. Sundararaman and F. Jäkle, "A Comparative Study of Base-Free Arylcopper Reagents for the Transfer of Aryl Groups to Boron Halides," *Journal of organometallic chemistry*, vol. 681, no. 1-2, pp. 134–142, 2003.

Chapter 3

The Utilisation of Monodentate Ligands Containing Tricyclic Substituents for the Stabilisation of Group 14 Element Complexes

The utilisation of kinetically stabilising ligands which provide a rigid and proximal sphere of steric encumbrance is an area of low-oxidation state main-group chemistry which has yielded extremely reactive species. The proposed advantage of such ligands is the consistent kinetic stability they provide: their lack of flexibility in solution ensures the ligand maintains an orientation which is kinetically stabilising about the main-group element centre.

Coupling the ligand and element-centre-of-interest (ECOI) is the first step towards forming low-oxidation state main-group compounds. Multiple synthetic routes can be chosen from to access these compounds: salt-metathesis is the most straightforward and practical option, allowing access to low-oxidation state main-group precursor compounds, viz. main-group element halide species. The reduction of these precursors leads to the formation of their low-oxidation state or element hydride congeners if the ligand is capable of providing the necessary stabilisation.

Firstly, this chapter looks to establish the general synthetic procedures to produce group 14 element halide species (precursor compounds) and the typical pathways to reduce these precursors to their low-oxidation state congener (the principles established here are generally applicable across the group 2, 13, and 15 elements). Secondly, examples of tricyclic ring containing ligands, as well as their utilisation in main-group chemistry are highlighted, before discussing our obtained results using novel tricyclic ring containing ligands in heavy group 14 element chemistry.

3.1 Coupling Ligands to Group 14 Elements

In order to kinetically stabilise the group 14 elements in their low-oxidation states, sterically demanding ligands must be coupled to the group 14 element before reduction[i].[?]This coupling can be accomplished via a number of different coupling-reaction pathways, though the simplest synthetic route is salt-metathesis; because of its simplicity, it is the most common place reaction within the field. The other commonly performed coupling reaction is protolysis. The general reaction scheme of these coupling reactions are presented in **scheme 3.1**.
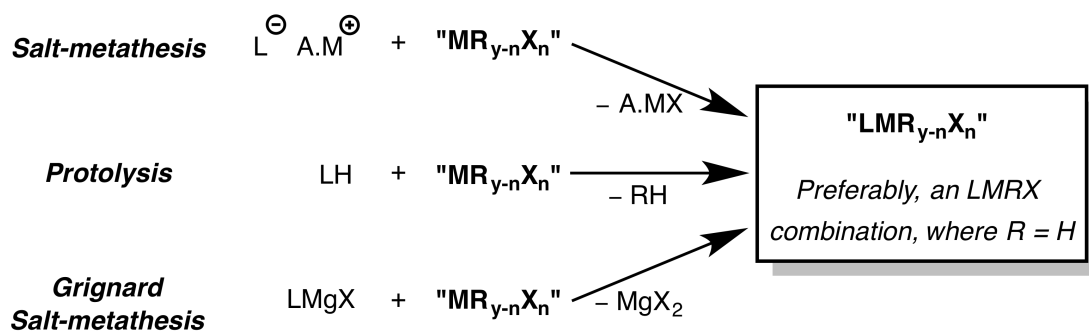
Scheme 3.1: The general coupling reaction of a ligand (L) to a group 14 element (M) halide (X) species (where A.M = alkali metal i.e. such as Li or K).

Salt-metathesis coupling occurs between an alkali metal ligand salt and a element halide molecule (group 14 element halide) with concurrent formation of an ionic salt: the halide of the metal is exchanged for the ligand. The predominant driving force behind this reaction is the formation of the ionic salt: when done in non-polar solutions, the ionic salt precipitates from the solution pushing the equilibrium forward. Also, the ionic salt forms a lattice and hence lattice energy is released, adding a further thermodynamic driving force to the reaction[ii]. An example of salt-metathesis is the reaction between a grignard reagent and a tetrel halide species (**scheme 3.1, bottom**).

Protolysis coupling is the exchange of a proton between two reagents, i.e. a pro-ligand with an acidic hydrogen can undergo hydrogen transfer with a basic R- functional group (such as an alkoxide) upon a group 14 element. This results in the formation of one $LMR_{y-n}X_n$ and a RH molecule. Protolysis can also be used to generate tetrel hydrides, though the exchange is reversed, *vide infra*. The basic requirement of this reaction is to have an acidic proton upon the ligand which is bonded to the desired precursor donor atom, as well as a basic leaving group upon the group 14 element. The reaction of LH with a bis-alkoxide group

---

[i]Generally speaking, this is the most common pathway to synthesising low-oxidation state group 14 element compounds.

[ii]The lattice energy of a crystalline solid is a measure of the energy released when ions are combined to make a compound.[?]

14 (II) element $(M(OR)_2)$, which gives HOR and LMOR as the product, is an example of protolysis.
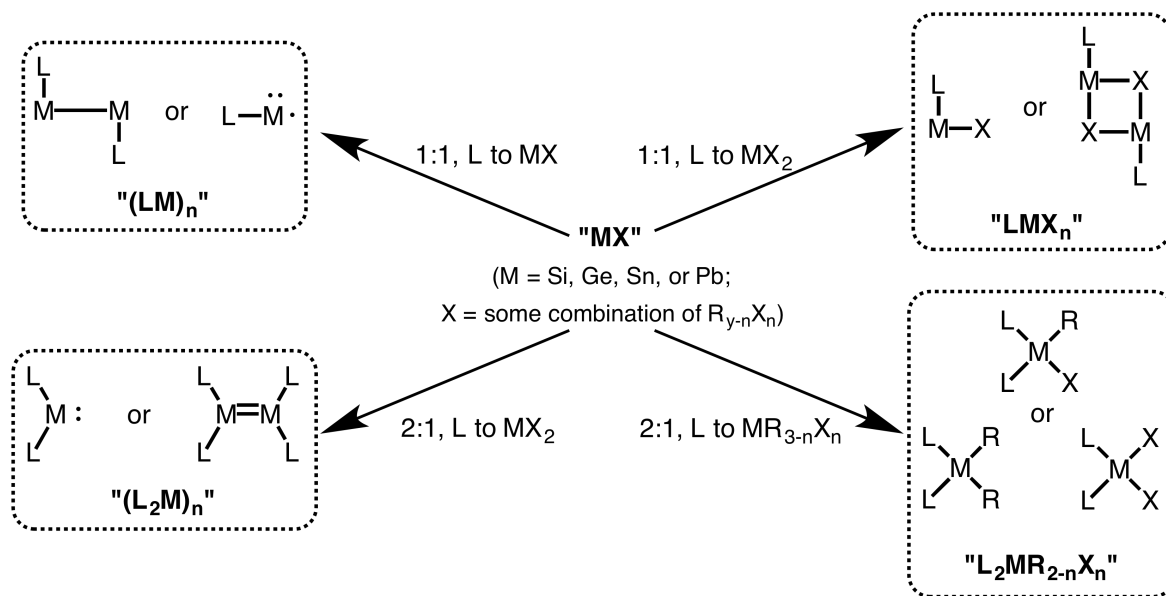
Scheme 3.2: General synthesis of a range of low-oxidation state group 14 element compounds. The reactions of group 14 element halides ("MX") in different ratios to ligands results in the formation of different compounds (where M = Si, Ge, Sn, and or Pb, L = ligand).

Each of these coupling reactions can lead to a number of products depending on the ratio of ligand to group 14 element centre, and the resultant product is dependent upon the group 14 element reagents used in the synthesis (**scheme 3.2**). Assuming a stable low-oxidation state group 14 element compound cannot directly be synthesised from these coupling reactions, the $LMH_{y-n}X_n$ group 14 element halide compound must be reduced.

3.2   Reduction to form Low-Oxidation State Group 14 Element Compounds

The reduction of a halide precursor is the most common way to access low-oxidation state main-group compounds and has been used to synthesise a range of novel compounds. Some of the more common reduction pathways/reactions are halide reductions, dehydrogenation, and dehydrohalogenation. From an organic chemistry perspective, the formation of group 14 element hydride compounds would also be classified as a reduction reaction.

3.2.1 Element Halide Reduction

Element halide reduction involves the abstraction of a halogen from the ECOI with concurrent formation of an ionic salt or a transmetalation species. Typical reagents for these reductions are the alkali metals e.g. sodium (Na), potassium (K), and potassium graphite (KC_8); though, there are more advanced reducing agents such as lithium napthalenide, magnesium anthracene, and the magnesium(I) dimers[iii].[?,?,?]

A tremendous amount of success has been accomplished within the Jones group utilising this reductive pathway: magnesium(I) dimers are synthesised from the reduction of the halide precursor with sodium metal (**scheme 3.3**).
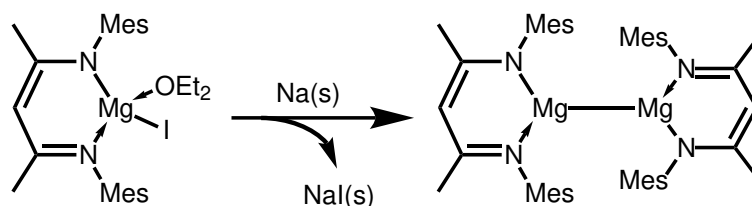
Scheme 3.3: Synthesis of the magnesium(I) dimer [({^{Mes}nacnac}Mg)₂] via halogen abstraction (reduction) of the halide precursor. The ionic salt, NaI, precipitates from solution upon removal of donor-solvents.

These magnesium(I) dimers are themselves used as reducing agents. [({^{Mes}nacnac}Mg)₂] was used as a reductant in the synthesis of the bulky amido digermynes **i-3a**, shown in **scheme 3.4**.[?,?]
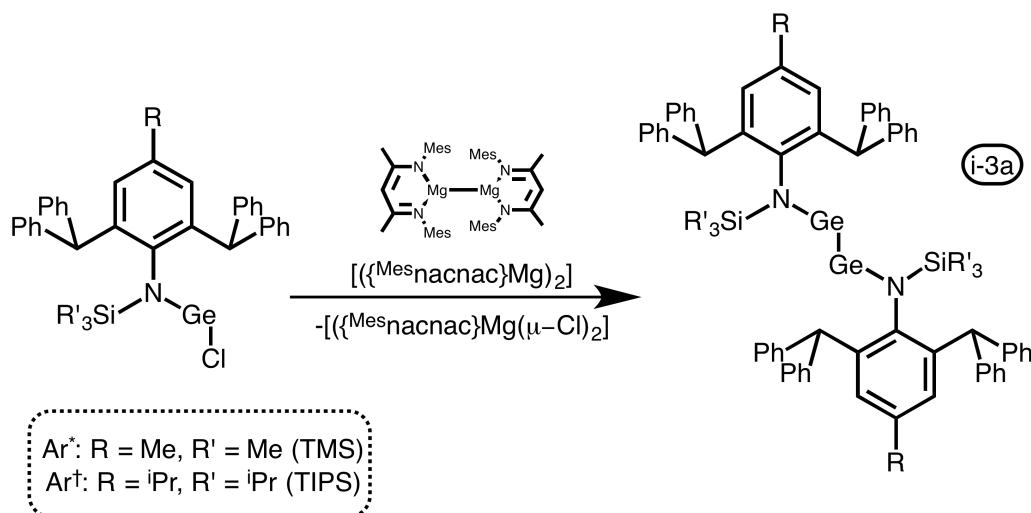
*Scheme 3.4: Synthesis of two bulky amido digermynes **i-3a** with the use of [({^{Mes}nacnac}Mg)₂] as the reducing agent.*

[iii]A major point of disparity between these reducing agents is their safe utility and solubility: modern reducing agents are typically safe to handle, measured stoichiometrically, and hydrocarbon soluble; classic reducing agents are pyrophoric, often used in excess, hydrocarbon insoluble, and can lead to over-reduction and decomposition.[?]

3.2.2   Dehydrohalogenation

A niche reductive pathway, dehydrohalogenation is a reduction which occurs via the elimination (or abstraction) of a hydrohalogen (HX) from the ECOI. It is a typical reaction in the formation of carbenes and has found use in forming heavier carbene analogues. As an example, the 2:1 ratio reaction between the IPr (IPr = 1,3-bis(2,6-diisopropylphenyl)imidazol-2-ylidene], a carbene) with silicochloroform ($HSiCl_3$) is a dehydrohalogenation reduction reaction which leads to the synthesis of IPr→$SiCl_2$ **i-3b**.[?,?]
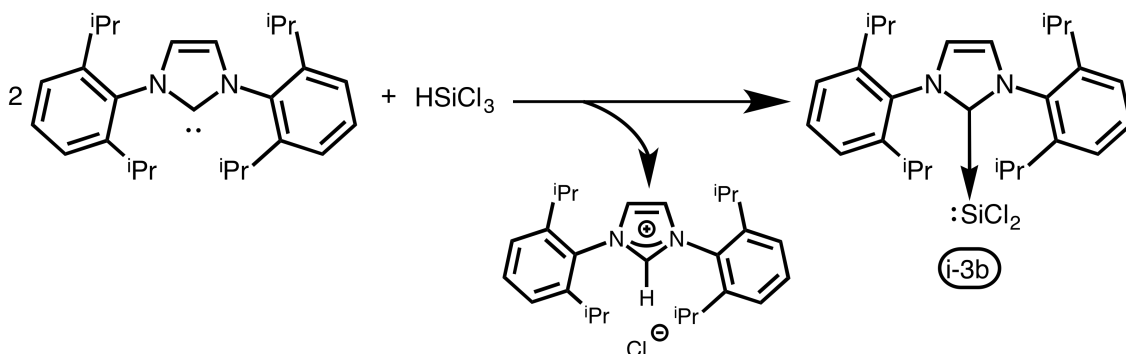
Scheme 3.5: The dehydrohalegenation of silicochloroform ($HSiCl_3$) to form the carbene stabilised dichlorosilylene.

3.2.3   Reduction to Hydrides

The synthesis of main-group hydrides can be accomplished by reduction, albeit they are also accessible via oxidative addition to low-oxidation state main-group compounds[iv]. The general synthetic route to these species is hydride transfer, where the reagents range from diisobutylaluminium hydride (DIBAL) through to lithium borohydride ([$LiBH_4$]) etc.[?] **Scheme 3.6** illustrates the directed synthesis of the digermene hydride **i-3c** via hydride transfer[v].[?]
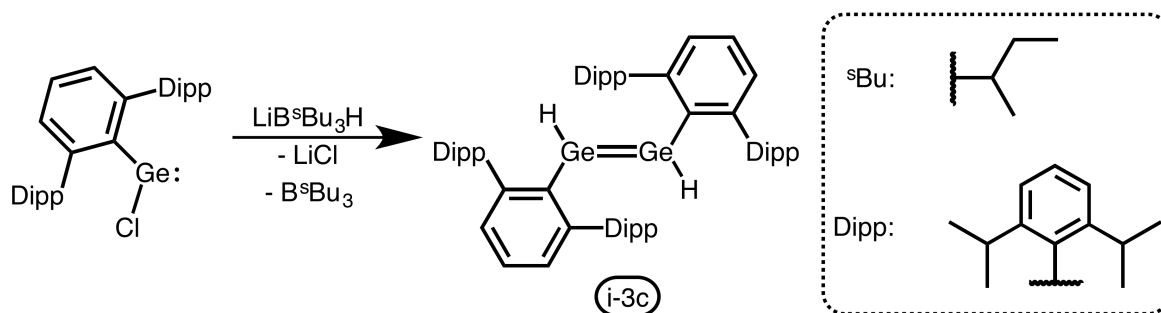

*Scheme 3.6: Synthesis of the digermene **i-3c**.*

[iv]For low-oxidation state heavy group 14 element compounds, oxidative addition of dihydrogen to a +I oxidation state group 14 element centre has been observed (see **chapter 1**).

[v]This germanium hydride is also the product upon dihydrogen activation by the digermyne **i-1d** (refer to **chapter 1**.)

The σ-bond metathesis reaction is another favourable pathway to hydrides, though it does require the synthesis of a main-group element species with an R group sufficiently basic enough to be protonated and act as a leaving group (**scheme 3.7**). In **scheme 3.7** the leaving group upon the ligand is a phosphine. This reaction led to the first isolated example of a lead(II) hydride, **i-3d**.[?]
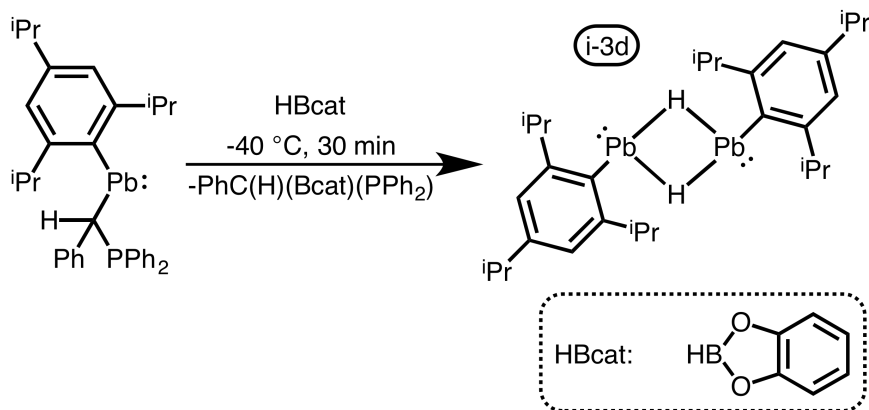
Scheme 3.7: *Synthesis of the first isolated example of a lead hydride complex, the dimeric* $[\{(^{Dipp}Terph)Pb(\mu\text{-}H)_2\}_2]$ (**i-3d**) *(where* $^{Dipp}Terph = 2,4,6\text{-}^iPr\text{-}C_6H_2$*).*

The direct formation/reaction pathway to group 14 element hydrides is typically a harsher synthesis compared to σ-bond metathesis pathways. It has been reported that the latter leads to higher yields of the desired hydride species (low-oxidation state main-group element alkoxide species have been shown to act as pre-catalysts in catalytic systems).[?,?,?]

3.3   Saturated and Un-saturated Rings and Main-Group Chemistry

The chemistry so far illustrated and discussed has primarily focused on some exceptional examples of low-oxidation state group 14 element compound chemistry (**chapter 1**) and, to a smaller degree, the necessary synthetic considerations required to form such compounds. What is presented here is more specific, honing in on the topic of this chapter: the inclusion of tricyclic motifs (saturated and unsaturated molecular rings) in monodentate ligand design, and these ligands use in main-group chemistry (as stated earlier, the major desire to use the tricyclic motif is the steric rigidity they may afford). This area has shown little development in relation to low-oxidation state main-group chemistry, predominantly being explored in the realm of transition metal chemistry. It is therefore a prospective area of development in ligand design relative to main-group chemistry.[vi]

[vi]This section does not include every derivative of tricyclic motif-containing monodentate ligand in the literature, as this would go beyond the scope of this introduction.

3.3.1   Tricycle Substituted Ligands and Group 14 Elements

Anthracene

One of the simplest tricyclic molecules - anthracene - has led to some remarkable group 14 element chemistry. West and co-workers gave one of the first examples of anthracene being used in low-oxidation state silicon chemistry, who reported a thermolysis[vii] reaction which leads to the synthesis of the dimethyldisilyne (Me-Si≡Si-Me) formal anthracene adduct **i-3e** (**figure 3.1**).[?] Noteworthy is the oxidation of the central ring of the anthracene, an event noted within our own chemistry, *vide infra*.

For germanium, tin, and lead, there has been no reported low-oxidation state chemistry performed which utilises anthracene within the framework of the kinetically stabilising ligand.[viii] However, anthracene has been used to synthesise a variety of silicon, germanium, and tin anthryl species with the characteristics of typical halide precursors, i.e. compounds which can be readily reduced to their lower oxidation states[ix].[?,?,?,?,?,?,?] The work with anthracene is admittedly limited[x] and more success has been reported with substituted tricyclic motifs in ligand design towards low-oxidation state main-group chemistry (most probably due to the increase in kinetic stability these larger tricyclic groups afford).
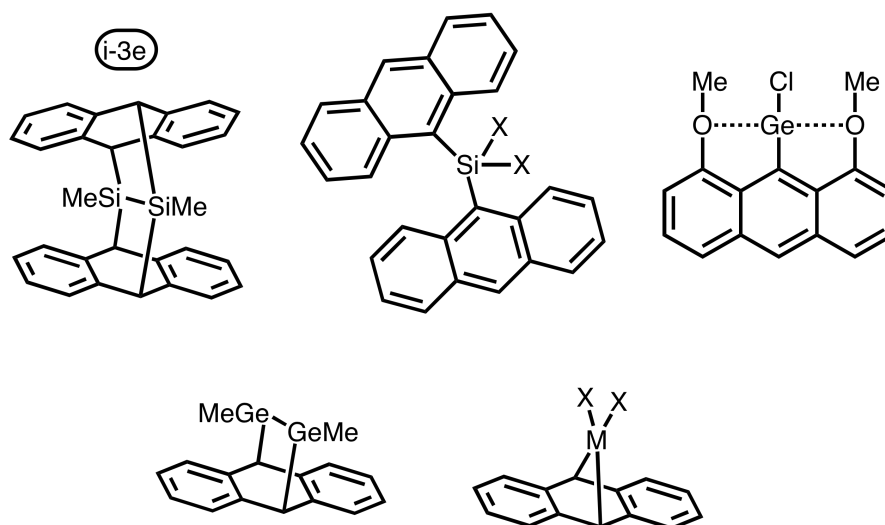

Figure 3.1: Examples of group 14 compounds containing an anthracene (anthryl) moiety (where X = halide).

[vii]By applying heat to the reaction, ligand substitution and reductive elimination was possible.

[viii]Though, it has been utilised in reactivity studies.

[ix]It has been proposed that the anthracene moiety can be removed under mild conditions to access low-oxidation state congeners of the respectively bound element centre. An example of this is reported by Cummins and co-workers, where phosphorous was the ECOI.[?]

[x]It is our contention, based on work to be discussed, that anthracene in itself is not sterically encumbered to the magnitude needed for kinetic stabilisation.

Barrelene

Barrelenes are cyclic groups which contain a central saturated "pinwheel" ring where (typically) each branch ends in a benzene group (tribenzobarrelenes). The conformation of these groups make the whole molecule rotund, hence they offer a non-planar steric profile.[?,?] This is unlike what is typically offered by tricyclic groups which rely on added functionality to increase the their 3D steric profile[xi]. Predominantly, these molecules have been explored in relation to the their static and dynamic stereochemistry and have been particularly explored in the field of molecular machines: e.g. they have allowed for the synthesis of a molecular bevel gear system.[?,?,?,?] Also, it has been reported that the inclusion of this group into ligand design allows for the synthesis of sterically encumbering ligands capable of kinetically stabilising silicon in its low-oxidation states.[?]

In **scheme 3.8**, a tribenzobarrelene (Trp) is modified to include three fused-ring-type substituents in its periphery positions (forming the molecule dubbed Trp*). This ligand and a ligated unsubstituted tribenzobarrelene (Trp) allows for the kinetic stabilisation of the silicon(II) centre and the synthesis of the disilene **i-3f**.[?]
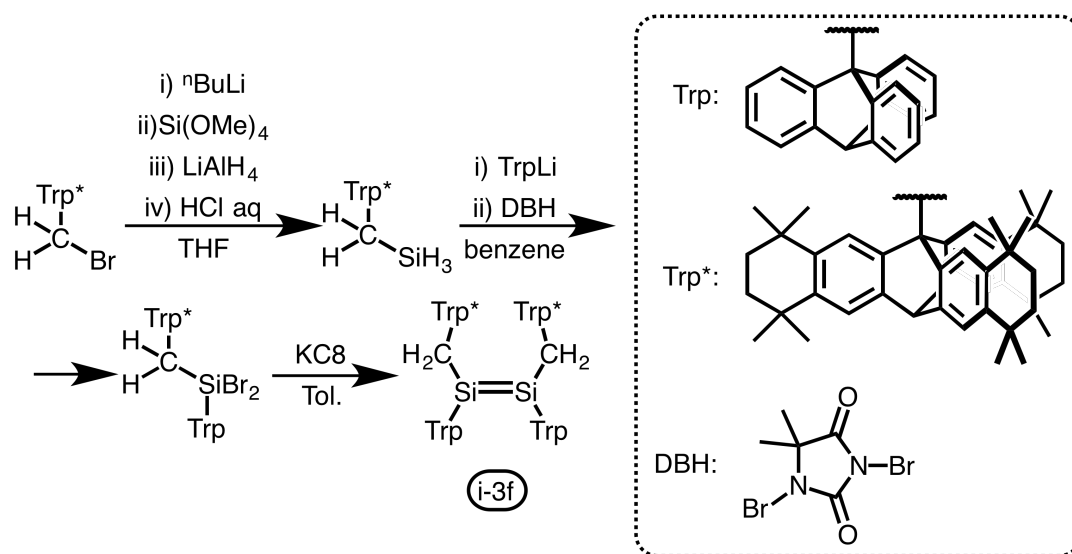
*Scheme 3.8: Synthesis of the disilene **i-3f** using the exgtremly bulky triptycene **Trp***.*

Indacene

The Matsuo group has accomplished the synthesis of a variety of low-oxidation state main-group compounds by adopting a range of saturated monodentate indacene ligands. The rigidity afforded by the indacene framework prevents reorientation of bulk, preventing reduction of the ligand's steric profile. Combined with the directionality afforded by the indacene framework (it pushes the substituent bulk towards the ECOI) this ligand is incredibly

---

[xi]As is the case for Ar^X(TMS)NH and the indacenes whoms tricyclic centre is essentially 2D.

kinetically stabilising (discussed in **chapter 2**).

In 2011, the first facile thermal dissociation of a Si=Si bond was accomplished, establishing the first characterised equilibrium between a silene and silylene, both stabilised by monodentate indacene ligands. The halide precursor **i-3g** is reduced to the silene **i-3h** and can undergo equilibration thermolysis to the corresponding silyene **i-3i** (**scheme 3.9**). This work confirmed the possibility to use silenes as synthetic precursors to silylenes[xii], opening up a new avenue in low-oxidation state silicon chemistry.[?] It also highlights the coupling and reduction reactions discussed *vide supra*; typically, the indacene is lithiated and coupled to the main-group element by salt-metathesis (as shown in **schemes 3.9 & 3.10**).[?,?,?,?,?,?,?]
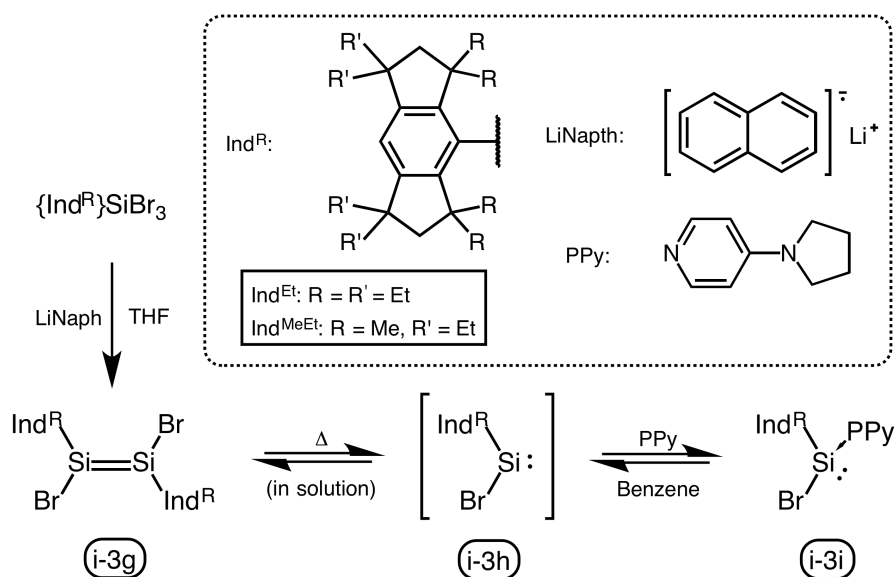
*Scheme 3.9: The general synthesis to form the indacene stabilised silyenes **i-3h**. The reduction of the respective halide precursors **i-3g** gives the silenes **i-3h** which are in equilibrium with the respective **i-3h**.*

Soon after this report, Matsuo and co-workers again broke new frontiers of low-oxidation state germanium chemistry by successfully synthesising the first example of a heavy ketone analogue[xiii], the germanone **i-3j** (L$_2$GeO) (**scheme 3.10**). Until this work, all attempts at similar chemistry had led to the isolation of polymer-like species due to the high tendency for the heavy group 14 element oxides to oligomerise.[?]

[xii]It had long been suggested but never accomplished.

[xiii]C=O vs. M=O, where M = Si, Ge, Sn, or Pb. The polarity of between M and O makes these species highly reactive.
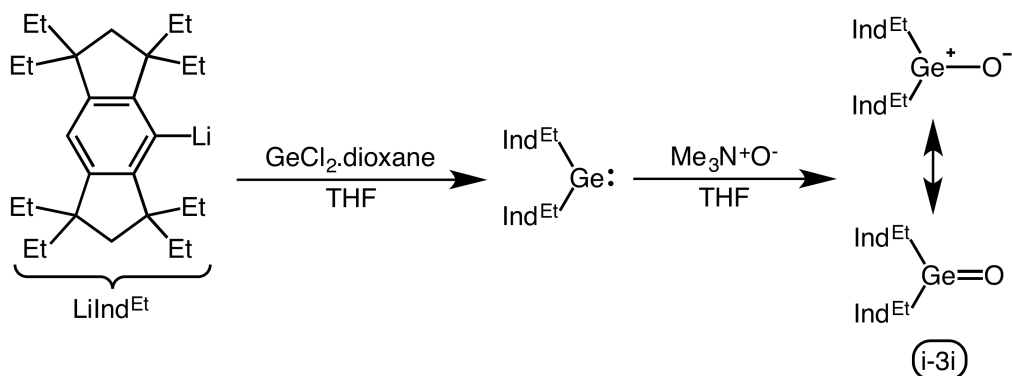
*Scheme 3.10: The synthesis of first isolated heavy ketone analogue - the germanone **i-3j**.*

Work continues using tricyclic ringed motif-containing ligands, though outside of the Matsuo group there has been a relatively low level of reported low-oxidation state tetrel chemistry which utilises such ligands[xiv].

3.3.2 Boron Chemistry: Anthracene in Ligand Design

Work by Braunschweig and co-workers, which inspired our own work, was not focused around group 14 chemistry but instead utilised an anthryl ligand[xv] for the stabilisation of the diborene **i-3k** which was then used in further chemistry (**scheme 3.11**).[?,?]
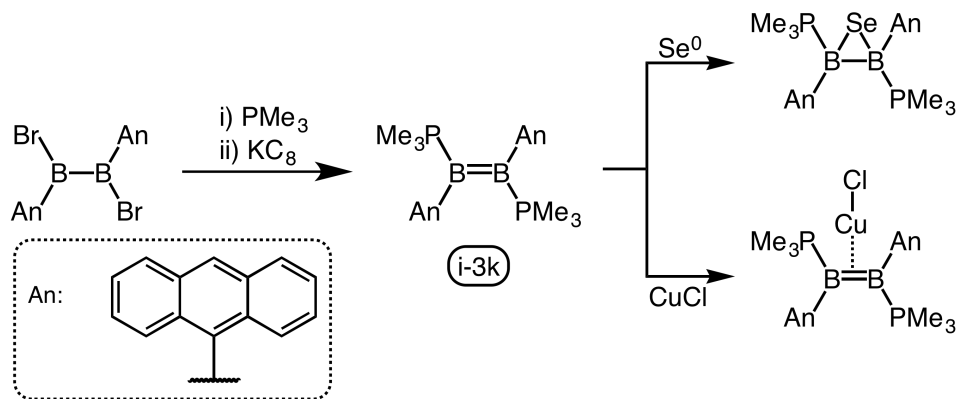
*Scheme 3.11: The diborene **i-3k** is stabilised by a phosphyl and anthryl ligand. Despite harsh reducing conditions the anthryl ligand was not observed to be activated; further chemistry was also noted, but not at the anthryl ligand.*

In this work the expected anthracene ring-activation was not observed despite harsh reducing conditions, nor was any reactivity noted in any further chemistry performed using

---

[xiv]The discussed work of this PhD. candidature was heavily influenced by the successes of the Matsuo group, adopting the indacene moiety into our own ligand designs.

[xv]This influenced our decision to produce the range of anthryl alkyl amines established in **chapter 2**.

the anthryl diborene complex (i.e. anthracene was not noted to be redox active). The low-lying aromatic π^* anti-bonding orbitals of anthracene were therefore not believed to be an issue in our own work.

3.4 Research Proposal

Monodentate ligands can be flexible, causing reorientation about an ECOI; consequently, the kinetic stability afforded to the ECOI becomes compromised. Enforcing a fixed/rigid ligand framework may allow us to avoid this from occurring. Tricyclic motifs (such as indacenes) provide a good foundation for a rigid and proximal ligand framework, as demonstrated by the Matsuo group, and other tricyclic motifs should also provide similiar rigidity.

Tricyclic containing pro-ligands - anthryl alkyl amines, $Ar^X(TMS)NH$, and indacene amines (**chapter 2**) - have been synthesised which may provide the steric qualities required for the kinetic stabilisation of low-oxidation state group 14 element compounds (refer to **chapter 2**). We propose that these ligands should provide a sterically consistent environment, unlike some previously utilised monodentate ligands.

In pursuit of our goals, we attempted ligation of said ligands to a range of group 14 element halides to form tetrel halide precursor compounds (salt-metathesis coupling was the primary synthetic route taken). In the events that this coupling was successful, reduction of these tetrel halides was attempted in the hopes of synthesising the respective low-oxidation state group 14 element compound.

The following section describes the three projects which utilised the tricyclic class of ligands synthesised during the Ph.D. candidature.

3.5 Results & Discussion (R&D): Anthryl Alkyl Amides

The library of anthryl alkyl amine pro-ligands synthesised (as described in **chapter 2**) needed to be deprotonated,to form the respective anthryl alkyl lithium amides. To this end, the alkali metal salt of the respective ligand was synthesised before introduction of a group 14 element halide species ($LSiH_{3-n}Xn$, MX_2, where M = Ge, Sn, or Pb). Our first attempts were aimed at forming the $SiH_{4-n}X_n$ or LMX halide precursors, our final goal being the synthesis and isolation of heavy alkyne analogues (LM≡ML). However, initial results indicated these ligands provide too little steric encumbrance for the isolation of the heavy alkyne analogues, so our focus shifted towards the synthesis of heavy alkene analogues (L_2M:, where M = Si, Ge, Sn, or Pb).

3.5.1   Lithiations and Potassiations

Synthesis and Spectroscopic Characterisation

As shown in **scheme 3.12**, the anthryl alkyl amines can be lithiated in a range of polar and non-polar solvents with no impact on yields[xvi] (**Li-2.3** stands as an partial exception, requiring more time and the presence of a donor-solvent for complete conversion). The most striking observation is the colour contrast upon addition of n-butyl lithium (^{n}BuLi), the yellow coloured solution of the anthryl alkyl amine turning a deep purple colour[xvii]. The anthryl alkyl lithium amides can be isolated as purple powders after extraction. [xviii]
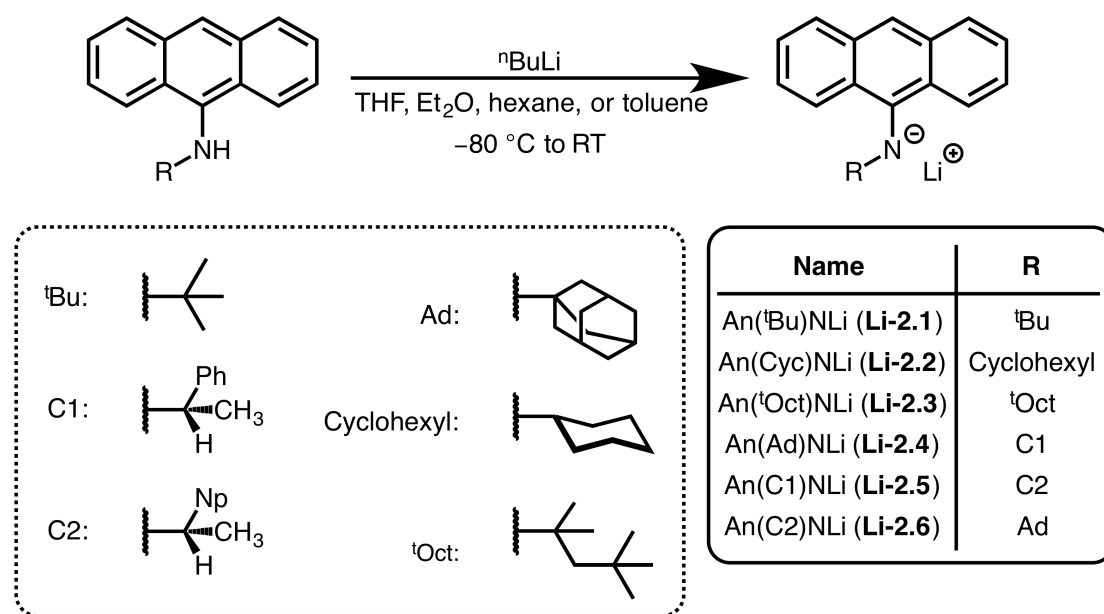
Scheme 3.12: Conversion of the anthryl alkyl amine pro-ligands to their lithium salt congener: the synthesis of lithium anthryl alkyl amides.

Following the same synthesis as described above, the bis-functional amine $An(^{t}BuNH)_2$ (**2.11**) was also converted into its respective lithium amide $An(^{t}BuNLi)_2$ (**Li-2.11**).

^{1}H NMR spectroscopic analysis was the primary technique used to elucidate the conversion of pro-ligands to their lithium salt congener. Our analyses of the ^{1}H NMR spectra focused on the loss of the assigned N-*H* chemical shift for the pro-ligand. Generally, the

---

[xvi]The reaction time increases marginally (one to two hours) when non-polar solvents are utilised, otherwise this reaction is completed within the hour.

[xvii]The vibrant colours observed are due to the anthryl moiety. Anthracene is well known for its dye-colour properties due to its low-lying π^* orbitals.[?,?,?,?,?,?,?,?,?]

[xviii]The compound is extremely moisture and air sensitive and it was observed to become a yellow powder upon exposure to moisture. By ^{1}H NMR spectroscopic analyses this yellow powder was determined to be the pro-ligand, i.e. the respective anthryl alkyl amine. This sensitivity is also noted towards silicone grease; whether this is due to the presence of moisture within the grease or the silcone grease itself is unknown. It is imperative that grease does not contaminate the reaction mixture or isolated powder.

shifts assigned to the alkyl functional groups appeared further downfield upon lithiation in comparison to the pro-ligand, and was also noted for the backbone An-H chemical shifts. This is most likely due to the adopted orientation of these lithium amides in solution, potentially reducing the nitrogen's lone-pair donation towards both of its respective substituents, though this is purely speculation.

^{7}Li NMR spectroscopic analyses indicated the presence of a lithium cation within the compounds, for all except **Li-2.6** (though this was due to very poor NMR resolution, refer to the **experimental**). For **Li-2.4**, when generated in THF, we observed three unique lithium environments with chemical shifts at δ 0.73, 1.128, and 2.00 ppm in the ^{7}Li NMR spectrum. We believe these environments are due to aryl interactions and solvent interactions with the lithium cation. It is possible that their is a mixture of monomeric LiAn(Ad)N and dimeric [An(Ad)N(μ-Li)]$_2$ compounds in solution, although this was not confirmed. When **Li-2.4** is generated in diethyl ether only one lithium resonance is observed at δ 2.19 ppm.

The potassiation of the anthryl alkyl amines by observation looked to have been successful, though all attempts to characterise these compounds were unsuccessful (**scheme 3.13**). Due to the surprisingly low solubility of these species, ^{1}H NMR spectroscopic analysis provided little-to-no information but did indicate the abstraction of the N-H proton. All other observations are analogous to the anthryl alkyl lithium amides.
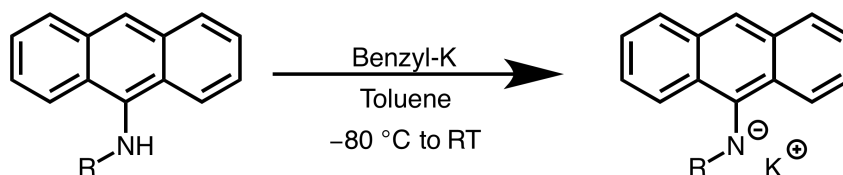
Scheme 3.13: Attempted potassiation of anthryl amides. The ^{1}H NMR spectrum suggests the formation of some new species with a lack of N-H functional group.

X-ray Crystallographic Characterisation of An(^{t}Bu)NLi.2THF (Li(THF)-2.1) and (An(^{t}Oct)Nμ-Li)$_2$ (Li-2.3)

Dark red-purple needle-like crystals[xix] suitable for X-ray diffraction were obtained from a concentrated hexane solution of **Li-2.1** & **Li-2.3**. These crystals were shown to be **Li(THF)-2.1** (the THF adduct of An(^{t}Bu)NLi)[xx] & **Li-2.3**, shown in **figure 3.2** & **figure 3.3**.

[xix]Note: these crystals were found to decompose over time within dried crystalographic oil, as observed by their loss of crystallinity and reversion to a yellow powder.

[xx]It was unexpected that the molecular structure of **Li(THF)-2.1** would contain two THF molecules. Further work with this ligand indicated the difficulty in removing the THF molecules once introduced.
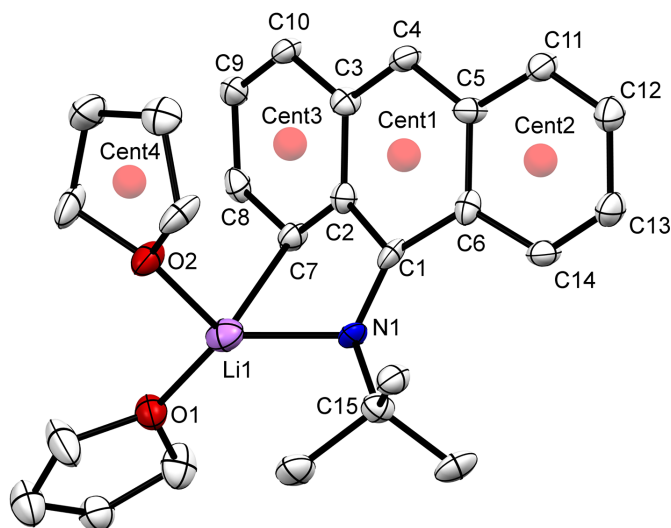
Figure 3.2: Thermal ellipsoid plot (30% probability surface) of An(^tBu)NLi.2THF
*(**Li(THF)-2.1**) (hydrogen atoms omitted). Selected bond lengths (Å) and angles (°):*
N1-C1 1.34(1), N1-C15 1.47(1), N1-Li1 1.95(1), Li1-O1 1.92(2), Li1-O2 1.93(1), Li1-C7
2.43(2), C1-C2 1.49(1), C1-C6 1.46(1), Cent3-Cent4 3.814; Li1-N1-C1 112.6(6),
Li1-N1-C15 114.1(6), C15-N1-C1 128.1(6), C1-C2-C3 119.6(7), C2-C3-C4 120.9(7),
C3-C4-C5 118.8(8), C4-C5-C6 122.4(8), C5-C6-C1 119.0(7), C6-C1-C2 113.3(7),
N1-C1-C2 111.8(6), N1-C1-C6 134.8(7), C1-Cent1-C4 169.76, C7-Cent3-C10 178.6,
C11-Cent2-C14 177.09, Cent2-Cent1-Cent3 168.40.

The most notable characteristic in the molecular structure of **Li(THF)-2.1** is the deformation of the anthryl moiety's geometry: planarity and typical aromatic character has been lost. The loss of planarity is reflected across the structure (*vide infra*), the bond lengths (Ar C-C bonds of 1.49 & 1.46 Å) changing dramatically compared to those which are observable in the pro-ligand, An(^tBu)NH (**2.1**) (**chapter 2, figure 2.4**).

The short N1-C1 bond length of 1.34(1) Å indicates a partial double-bond and delocalisation of the negative charge over the N1-C1 bond and into the anthryl moiety. This is reflected by the long bond lengths for C1-C2 (1.49(1) Å) & C1-C6 (1.46(1) Å). There is a slight lengthening in the N1-C15 bond, contributing to the proposed delocalisation and partial double-bond between nitrogen and the anthryl moiety. The sum of the bond angles at N1 is ≈ 354.8° and each angle is greater than those observed in an ideal sp^3 hybridised nitrogen (109.5°). Therefore, we believe the nitrogen to be closer to sp^2 hybridisation with a pseudo-trigonal planar geometry. The N1-Li1 bond distance are as expected in spite of ligand deformation, presumably due to the ionic nature of the bond. However, the nitrogen is skewed to the side of the lithium, away from the central anthryl axis (axis of C4 to C1).

Looking at the anthryl moiety's central ring, the angle 113.3(7)° (for C6-C1-C2) indicates angular discordance from an ideal six-membered-carbon aromatic (hexagon), reflecting a loss of aromaticity. Loss of planarity is evident by the total angle across the ring, C1-Cent1-C4

169.76°, which bends away from an ideal plane. This loss of planarity can be seen across the anthryl moiety as indicated by the centroid generated angle Cent2-Cent1-Cent3 at 168.40°. Surprisingly, the internal planarity of the flanking aromatics does not deviate significantly from a plane. The geometry of C1 is pseudo-trigonal planar based on the sum of its bond angles.

The Cent3-Cent4 distance at 3.814 Å implies there is some interaction between the anthryl moiety's flanking aromatic and the respective THF molecule, which may explain our difficulty in removing the THF molecules. There is an apparent non-covalent interaction between Li1-C7, with a bond distance of 2.43(2) Å (which was noted in the ^{13}C NMR spectrum of **Li(THF)-2.1** with a Ar-C chemical shift at δ 158.65 ppm).
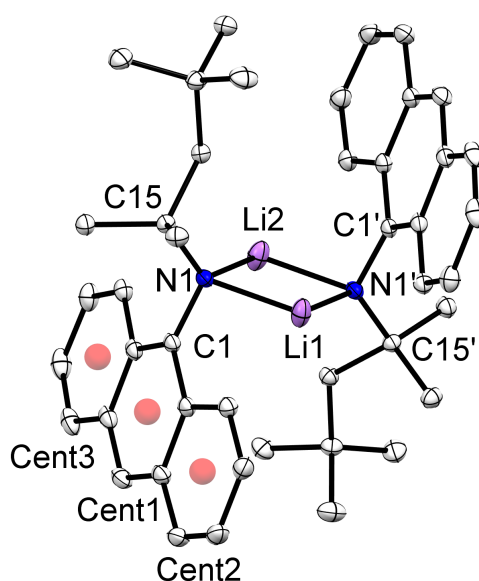
*Figure 3.3: Thermal ellipsoid plot (30% probability surface) of (An(^{t}Oct)Nμ-Li)$_2$ (**Li-2.3**) (hydrogen atoms omitted). Selected bond lengths (Å) and angles (°): N1-Li1 1.951, N1-Li2 1.956, N1-C1 1.409(2), N1-C15 1.493(2); C1-N1-C15 121.2(1), C1-N1-Li1 99.3, C1-N1-Li2 101.5, C15-N1-Li1 126.0, C15-N1-Li2 123.3, Li1-N1-Li2 74.8, Cent2-Cent1-Cent3 176.02.*

The molecular structure of the anthryl tert-octyl lithium amide was found to be the dimeric aggregate **Li-2.3**. N-Li bond distances are consistent between the two lithium centres, as such the lithium atoms are bonded equally to both nitrogen centres. These bond distances are similar to that which are observable in **LiTHF-1**. Aggregation in **Li-2.3** is due to the lack of donor-solvent coordination to the lithium centres.[?]

Unlike **Li(THF)-2.1** the geometric character of of **Li-2.3** is maintained relative to that observed in the molecular structure of An(^{t}Oct)NH (**2.3**). Planarity and aromaticity is maintained within the anthryl moiety: only minor deviations from an ideal plane are observed, e.g. the angle of Cent2-Cent1-Cent3 is 176.02°.

Steric Profiles for An(^{t}Bu)NLi.2THF (Li(THF)-2.1) (Li(THF)-2.1) and (An(^{t}Oct)Nμ-Li)$_2$ (Li-2.3)

The following calculated values of **Li(THF)-2.1** & **Li-2.3** are based on the obtained molecular structures (*vide supra*) whereas the steric values of **2.1/3*/°**are calculated on the optimised structure of **2.1/3** (see **chapter 2**). For **Li(THF)-2.1**, both THF molecules observed in the molecular structure are omitted from these calculated steric values. For **Li-2.3**, the second ligand molecule and lithium atom are omitted, i.e. the steric values are calculated based on the monomer, as this species is presumably monomeric in solution. For **2.1*** & **2.3***[xxi], the proton was replaced by a lithium atom[xxii] as to more closely approximate the theoretical steric values. For **2.1/3*/°**, the proton is replaced by lithium and the angles of substituents about the nitrogen centre are altered to take on a trigonal planar geometry. This change of angle is done to reflect the probable geometry these ligands would adopt when a heavy group 14 element is coupled to the donor nitrogen atom[xxiii]. For consistency and comparison, the proximal and distal bulk is measured at a dummy distance of $\approx$1.8 Å (represented as bracketed bV% values) which is an approximate representation of the steric encumbrance afforded to a germanium centre by these ligand environments.

[xxi]Alterations to a structure are denoted by a the * notation. Alteration to angles are denoted by the °notation.

[xxii]The structure of **2.1/3*** & **2.1/3*°** were not re-optimised as the changes made were for approximate comparison only.

[xxiii]This is often observed when adding larger substituents to an amide and has been commonly observed in the bulky benzhydrol-like amide ligands.[?,?,?,?,?]

Table 3.1: Steric parameters: proximal, distal bulk and flexibility values for
Li(THF)-2.1 *&* ***Li-2.3*** *as well computationally derived comparative examples*
2.1/3$^{*/\circ}$.

Ligand (#)	Bulk	Flexibility	Proximal Bulk	Distal Bulk
An(^{t}Bu)NLi.2THF (**Li(THF)-2.1**)	297.7 Å^2	n/a	43.6% (45.8%)	18.3% (26.1%)
An(^{t}Bu)N(Li*) (**2.1***)	295.6 Å^2	n/a	41.5% (43.5%)	24.9% (25.3%)
An(^{t}Bu)N(Li*)° (**2.1*°**)	295.6 Å^2	n/a	33.8% (36.2%)	25% (25.4%)
An(^{t}Oct)NLi (**Li-2.3**)	355.8 Å^2	Flex & rotation (38.4-63.4%)	39.8% (42.5%)	31.5% (32.1%)
An(^{t}Oct)N(Li*) (**2.3***)	354.3Å^2	Flex & rotation (36.3-63.7%)	48.5% (50.8%)	32.5% (32.9%)
An(^{t}Oct)N(Li*)° (**2.3*°**)	354.3Å^2	Flex & rotation (33.5-56.6%)	46.6% (48.9%)	25% (25.4%)

Note: Bulk is expressed as a surface area in values of Å^2. All following values are expressed as a bV% value. Flexibility is qualitatively described; the bV% value is that of the approximate least to most sterically encumbering orientation of the molecule in relation to the ECOI. Proximal bulk is measured using a 3.5 Å radius sphere; distal bulk a 6.0 Å radius sphere.

As shown from the values in **table 3.1**, the deformation of geometry displayed in **Li(THF)-2.1** has a positive effect on the steric encumbrance afforded by this ligand (presuming that when a group 14 element substitutes the lithium atom the same geometry is maintained). This is represented by the increased buried volume percentage value (bV%) of **Li(THF)-2.1** compared with An(^{t}Bu)N(Li*) (**2.1***) and An(^{t}Bu)N(Li*) (**2.1*°**). If the ligand was to maintain the geometry reflected by **Li(THF)-2.1** - and closely resembled by **2.1*** - the proximal steric encumbrance afforded would be greater than otherwise expected. However, it is believed that upon coupling to the heavier group 14 element - Ge, Sn, and Pb - the geometry adopted would be more closely represented by **2.1*°** as the nitrogen approaches a trigonal planar geometry[xxiv].

The lower than expected steric encumbrance afforded by **Li-2.3** towards the lithium centre is due to the enforced geometry caused by dimserisation, i.e. the bound lithium atom forms an ≈ 90° to the N1-Li2 bond axis and so is shifted away from bulk of the ligand. Compounding this is the rigidity of the dimeric lithium salt which is expressed by its flexibility parameter: the ligand could orientate as to afford greater steric protection but uncontrollable variables[xxv] lead to the preference of a geometrical orientation which provides less steric encumbrance. Comparing **Li-2.3** with the two calculated models **2.3*/°** indicates a flaw within these models or a genuine decrease in steric encumbrance when the

---

[xxiv]The adoption of a trigonal planar geometry at the nitrogen centre upon coupling of a larger element has been ubiquitous throughout the field.

[xxv]Interligand steric effects, crystal packing etc.[?]

dimeric geometry is maintained. As stated *vide supra*, we believe that **2.3*°** provides a closer representation of the steric encumbrance which would be afforded towards a group 14 element centre upon ligation.
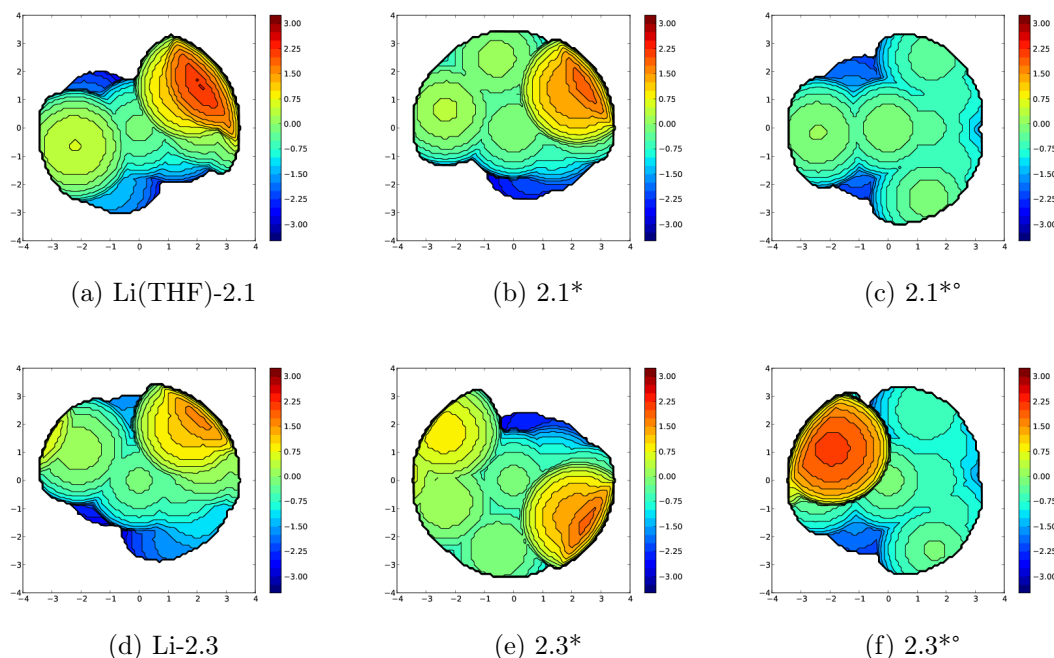

<div align="center">(a) Li(THF)-2.1   (b) 2.1*   (c) 2.1*°</div>

<div align="center">(d) Li-2.3   (e) 2.3*   (f) 2.3*°</div>

Figure 3.4: Proximal steric maps of the experimentally determined and calculated structures of the An(^{t}Bu)NLi and An(^{t}Oct)NLi species, as viewed down the N-Li/H axis, measured at a sphere radius of 3.5Å.

The steric maps displayed in **figure 3.4** attests to the altered steric environments these species afford. Note: when the nitrogen atom adopts a trigonal planar geometry, the steric encumbrance decreases but the steric environment becomes more uniform (as seen by the steric maps becoming more circular in character).

3.5.2   Coupling to Silicon

Synthetic Attempts to Form LSiX$_{3-n}$H$_n$ and L$_2$SiX$_{2-n}$H$_n$

The 1:1 or 2:1[xxvi] stoichiometric salt-metathesis reaction of the lithium anthryl alkyl amides (**2.1**-**2.4**) with a range of silicon halides was partially successful; though, we did not isolate the expected silicon halides. By observation it appears that some reaction takes place between these compounds, producing orange coloured reaction mixtures. These observations did not translate to the expected results (**scheme 3.14**, which also displays the only isolated compounds from these reactions). All reactions gave complicated product mixtures.

[xxvi]Ligand to group 14 element containing species.

No change was noted in the ^{1}H NMR spectrum of these reactions when using the non-THF adduct anthryl alkyl lithium amides, nor when THF was avoided.
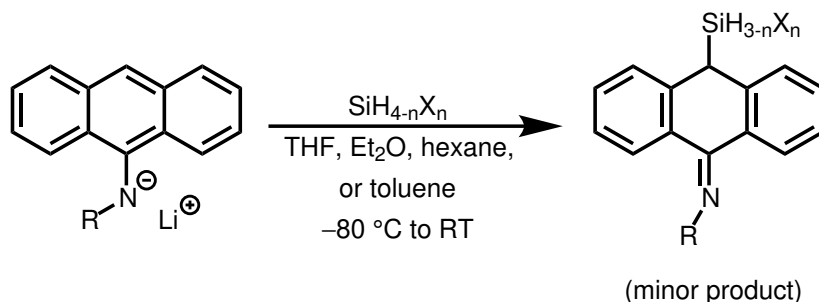
*Scheme 3.14: The attempted reaction to couple anthryl alkyl lithium amides to a range of silicon halides. The only isolated compound from these reactions were the backbone activated silicon compounds **1** & **2**, vide infra (where R = ^{t}butyl, cyclohexyl, adamantyl, or ^{t}octyl; X = Cl, Br, or I).*

Issues with this synthetic strategy influenced our decision to not use all of the anthryl alkyl lithium amides at our disposal. We believed that the overarching issue is the diminished steric encumbrance afforded by these anthryl amides[xxvii]. Therefore, **2.5** and **2.6** were not utilised as they are the least sterically encumbering.

X-ray Crystallographic Characterisation of {*r*-An(^{t}Bu)N}SiBr$_3$ (1) & {*r*-An(Cyc)N}SiCl$_3$ (2)

Fractional crystallisation led to the isolation of single crystals of {*r*-An(^{t}Bu)N}SiBr$_3$ (**1**) & {*r*-An(Cyc)N}SiCl$_3$ (**2**). These crystals were suitable for X-ray diffraction and led to the elucidation of the molecular structures for **1** (**figure 3.5**) and **2** (**figure 3.6**).

[xxvii]The sterics afforded by these ligands could not overcome their destabilising electronic impact.
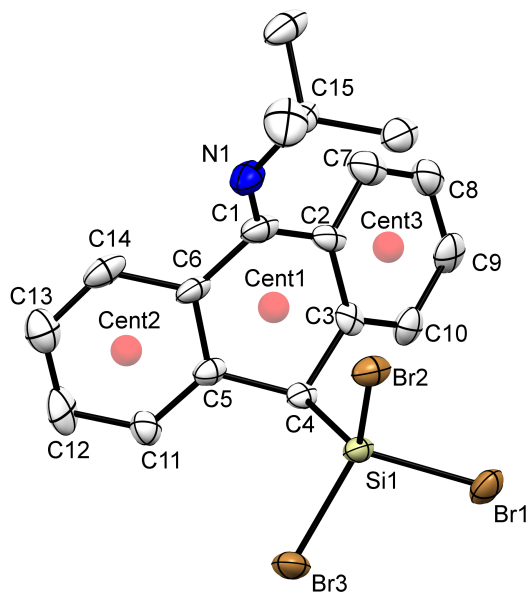
Figure 3.5: *Thermal ellipsoid plot (30% probability surface) of {r-An(^{t}Bu)N}SiBr$_3$ (**1**) (hydrogen atoms omitted). Selected bond lengths (Å) and angles (°): N1-C1 1.32(1), N1-C15 1.46(1), Si1-C4 1.86(1), Si1-Br1 2.214(3), Si1-Br2 2.190(3), Si1-Br3 2.202(3), C1-C2 1.48(2), C3-C4 1.53(1), C4-C5 1.55(1), C6-C1 1.44(1); C3-C4-C5 110.5(7), C6-C1-C2 113.7(9), Si1-C4-Cent1 116.70, N1-C1-Cent1 158.07, C4-Cent1-C1 159.86, C11-Cent2-C14 177.40, C7-Cent3-C10 178.60, Cent2-Cent1-Cent3 153.67; C6-C5-C4-Si1 96.5(9).*
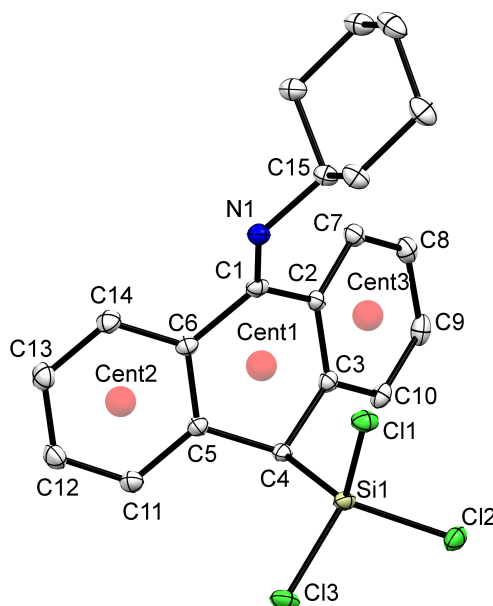
Figure 3.6: *Thermal ellipsoid plot (30% probability surface) of {r-An(Cyc)N}SiCl$_3$ (**2**) (hydrogen atoms omitted). Selected bond lengths (Å) and angles (°): N1-C1 1.280(4), N1-C15 1.452(5), Si1-C4 1.869(2), Si1-Cl1 2.022(1), Si1-Cl2 2.017(1), Si1-Cl3 2.014(1), C1-C2 1.486(3), C3-C4 1.504(4), C4-C5 1.504(3), C6-C1 1.472(5); C1-N1-C15 122.4(2), C2-C1-C6 113.6(2), C5-C4-C3 111.8(2); Cent1-C1-N1 160.25, Cent1-C4-Si1 112.70, C4-Cent1-C1 159.60, Cent2-Cent1-Cent3 155.56; C6-C5-C4-Si1 92.4(3).*

115

The molecular structures of **1** and **2** are essentially the same aside from the change in halide and the nitrogen's alkyl substituents. The N1-C1 bond length is slightly shorter in **2** at 1.280(4)[xxviii] Å, suggesting greater double-bond character between N1-C1. This shorter bond does not give rise to a significant difference - longer bond - for N1-C15. Both structures have lost planarity across the anthryl moiety deviating from an ideal plane by approximately 25°, as determined by the centroids bond angle (Cent1-Cent2-Cent3). The central ring is not planar - presumably the main contributor for the "buckling" of the anthryl moiety - indicating a loss of aromaticity. Bond lengths for the central rings for both structures reflect this deviation from the ideal anthryl geometry[xxix]. The flanking/outer aromatic rings for both complexes remain planar. For **1**, the planarity of these rings is represented by the angle of C7-Cent3-C10 (178.6°) & C11-Cent2-C14 (177.40°) whereas the central ring angle of C1-Cent1-C4 is more acute (159.86°) (these values are essentially the same for **2**). The C6-C5-C4-Si1 torsion angle quantifies how removed the silyl moiety is from the anthryl plane, sitting almost perpendicular to the anthryl group. It is worth noting that the nitrogen and silyl functional groups point in the same direction - despite the possible increase in steric pressure this conformations creates.

Figure 7 illustrates the degree by which these complexes have lost aromaticity in the central ring: the generated planes are based on the ideal planarity expected in the central aromatic of the respective ligands.
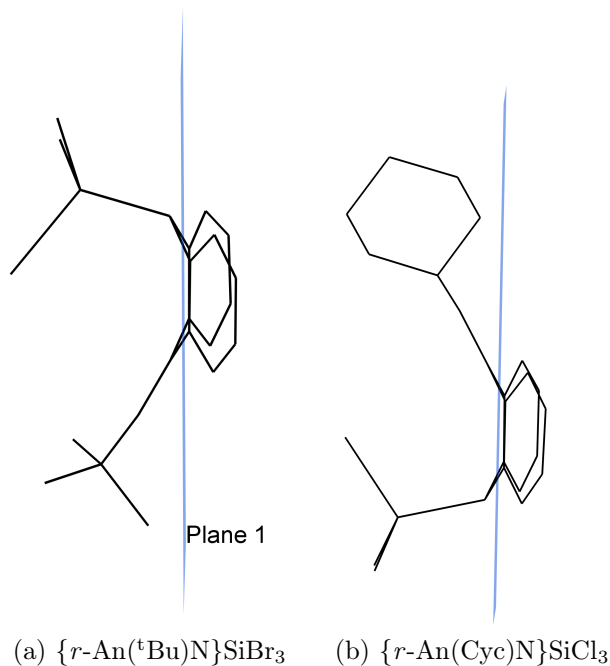

Plane 1

(a) {r-An(^{t}Bu)N}SiBr$_3$ (b) {r-An(Cyc)N}SiCl$_3$

Figure 3.7: Side-profile of the calculated plane in {r-An(^{t}Bu)N}SiBr$_3$ (left) & {r-An(Cyc)N}SiCl$_3$ (right).

[xxviii]Slight statistical overlap based on the standard deviation of error.
[xxix]≈ 1.4 Å with 120° is the expected bonding for a six-remembered-carbon aromatic ring.

Steric Profile

The following calculated values of **1** & **2** are based on the obtained molecular structures (*vide supra*) whereas the steric values of **2.1/2*/°**are calculated on the optimised structure of **2.1/3** (see **chapter 2**). For **2.1*** & **2.2***[xxx], the proton was replaced by a silicon atom[xxxi] as to more closely approximate the theoretical steric values. For **2.1/2*/°**, the proton is replaced by a silicon atom and the angles of substituents about the nitrogen centre are altered to take on a trigonal planar geometry. These changes were made for the sake of comparison between the compounds shown within **table 3.2**. For **1** and **2** the halides have been omitted from all calculations. The nature of the bonding within **1** and **2** and our lack of data would not allow us to make a definitive approximation of orientations these compounds could adopt, consequently flexibility has not be commented on nor reported.

Table 3.2: *Proximal and distal bulk values calculated for **1** and **2** as well as the computationally altered structures of **1** and **2**, i.e. **2.1/2*/°**.*

Compound (#)	Proximal Bulk	Distal Bulk
{r-An(^{t}Bu)N}SiBr$_3$ (**1**)	30.3%	23.3%
An(^{t}Bu)N(Si*) (**2.1***)	42.4%	25.0%
(An(^{t}Bu)N(Si*)° (**2.1*°**)	34.9%	25.3%
{r-An(Cyc)N}SiCl$_3$ (**2**)	30.9%	22.9%
An(Cyc)N(Si*) (**2.2***)	42.3%	26.9%
An(Cyc)N(Si*)° (**2.2*°**)	33.6%	25.5%

Note: Bulk is expressed as a surface area in values of Å^2. All following values are expressed as a bV% value. Flexibility is omitted from the presented data as no discernible impactful flexibility could be rationalised based on our understanding of **1** and **2**. Proximal bulk is measured using a 3.5 Å radius sphere; distal bulk a 6.0 Å radius sphere.

An evaluation of the steric environment provided by the ligand rearrangement seen in **1** and **2** in comparison to the desired {An(R)N}SiX$_3$ compounds (**2.1/2*/°**) is provided in **table 3.2**. Rearrangement of the silicon halide motif to the backbone position of the ligand yields a less sterically congested environment as indicated by the percent buried volume value (bV%). Steric encumbrance, and consequently congestion, would be reduced if the ligand adopted a trigonal-planar nitrogen geometry (**2.1/2*°**) upon silicon coupling than if the pyramidal geometry observed in the pro-ligands (**2.1/2***) was maintained. This indicates that upon silicon-nitrogen centre, the geometry of {An(^{t}Bu)N)}$^-$ and {An(Cyc)N}$^-$

[xxx]Alterations to a structure are denoted by a the * notation. Alteration to angles are denoted by the °notation.

[xxxi]The structure of **2.1/2*** & **2.1/2*°** were not re-optimised as the changes made were for approximate comparison only.

would remain pyramidal leading to greater steric congestion. Therefore, rearrangement of the silicon becomes much more sterically favourable, though this cannot be proven without further work.

The rearrangement observed in compounds **1** and **2** are calculated to offer less distal bulk than the theoretical compounds **2.1/2*/°**, in spite of the predominant bulk of the ligand being situated away from the silicon centre. This highlights that bV% values[xxxii] in general do not consider the directionality of bulk: this can be measured using fixed solid angle Ω as proposed by Guzei and Wendt (ECA), though these calculations go beyond the scope and resources of this project[xxxiii].[?]

(a) {r-An(Cyc)N}SiCl$_3$ (**1**)   (b) 2.1*   (c) 2.1*°

(d) {r-An(^{t}Bu)N}SiBr$_3$ (**2**)   (e) 2.2*   (f) 2.2*°
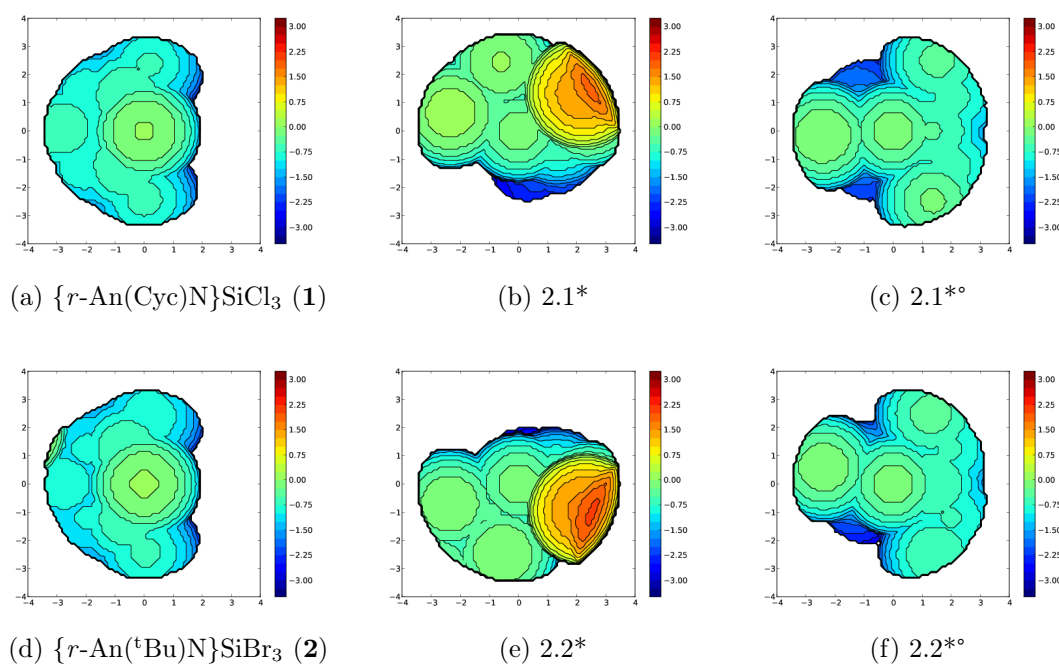
*Figure 3.8: Steric maps of **1**, **2**, and their computational derivatives, as viewed down the N-Si/H axis.*

The steric maps in **figure 3.8** illustrate the increase in circular steric profile these ligands adopt as the nitrogen donor becomes trigonal planar. The more circular (uniform) the steric map is, the greater steric protection these ligands may provide towards the ECOI (in this case, silicon), as it reduces the number of collision pathways from multiple directions.

It is believed that the stability of this rearrangement is primarily electronic: silicon and carbon forming stronger σ bonds than those between silicon and nitrogen. The decreased

---

[xxxii]Whilst this is not the only measurement of distal bulk, for our purposes it was found to be the most practical.

[xxxiii]The time/work required to calculate the fixed solid angle Ω of **1** and **2** was deemed too high considering our interest in these compound. The compounds could not be isolated nor presented any real future oppurtunity for chemistry outside of reduction studies which are *vide infra*.

steric congestion afforded by the rearrangement of the silyl moiety is sterically favourable, though the bulk of the anthryl alkyl amides is believed to be small enough that this wasn't the predominant stabilising factor.

Steric or Electronic Influence: How Did 1 and 2 form?

In retrospect, the isolation of **1** and **2** indicates two possible issues in the design of these ligands. Firstly, they hold the potential for internal redox activation, an issue which was postulated in their synthesis; and secondly, they do not provide adequate steric encumbrance for the stabilisation of low-oxidation state group 14 compounds. We propose that compounds **1** and **2** were formed from the decomposition of the desired $LSiX_3$ compounds. As shown in **scheme 3.15**, heterolytic cleavage of the Si-N bond, due to steric repulsion, leaves a negative charge on the nitrogen atom and a positive charge on the silicon; without the lithium, which has formed LiX and dropped out of solution - the resonance is preserved. Resonance delocalisation allows the negative charge to become situated at the backbone of the anthryl moiety, allowing the silyl fragment to bond at a less sterically congested point. This results in reduced steric pressure and a comparatively stronger Si-C bond rather than the original Si-N bond (**scheme 3.15**). This species is presumably more stable than $LSiX_3$ due to the strength of carbon-silicon bonds. Similar rearrangements have been documented within the literature, albeit the aromaticity of the central ring is maintained and the nitrogen's coordination number is not reduced.[?]
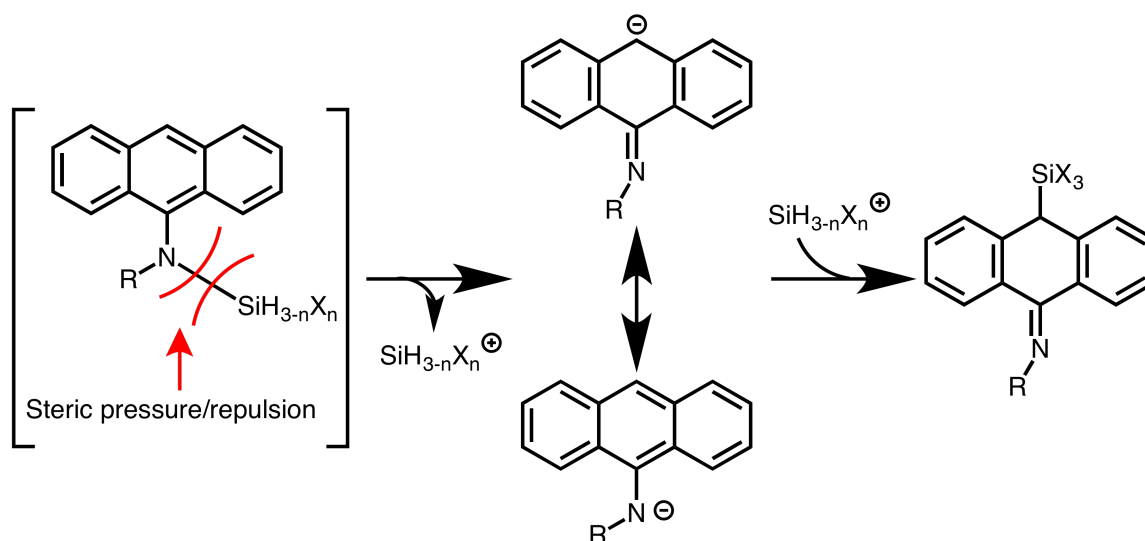

Scheme 3.15: Steric repulsion and weak Si-N bonding leads to heterolytic cleavage of the Si-N bond. Delocalisation of the negative charge allows the cationic silyl fragment to bind at a less sterically congested location as well as forming a stronger Si-C bond.

3.5.3   Coupling to Germanium

Attempts to Form LGeX$_2$ and L$_2$Ge

Germanium is typically more stable in the +II oxidation state than silicon. Because of this, the anthryl alkyl amide ligands (which provide too little steric encumbrance for silicon) were believed to be capable of stabilising low-oxidation state germanium complexes. To these ends, we attempted to synthesise the anthryl alkyl amide germanium chlorides (LGeCl), anthryl alkyl amide supported germyelenes (L$_2$Ge), and to capture germanium in the +1 oxidation state. For all these reactions, the resultant product mixtures were found to be less complex when THF was avoided in preference of diethyl ether.

Reacting **Li-2.1** with GeCl$_2$.dioxane in a 1:1 stoichiometic ratio led to the formation of a major new product, which was initially believed to be {An(^{t}Bu)N}GeCl, and a minor product believed to be the germylene [{An(^{t}Bu)N}$_2$Ge]. Repeating the reaction in a 2:1 stochiometric ratio revealed the major product was in-fact [{An(^{t}Bu)N}$_2$Ge] (**3**) (**scheme 3.16**). The formation of **3** in our 1:1 ratio reaction is likely a product of redistribution.
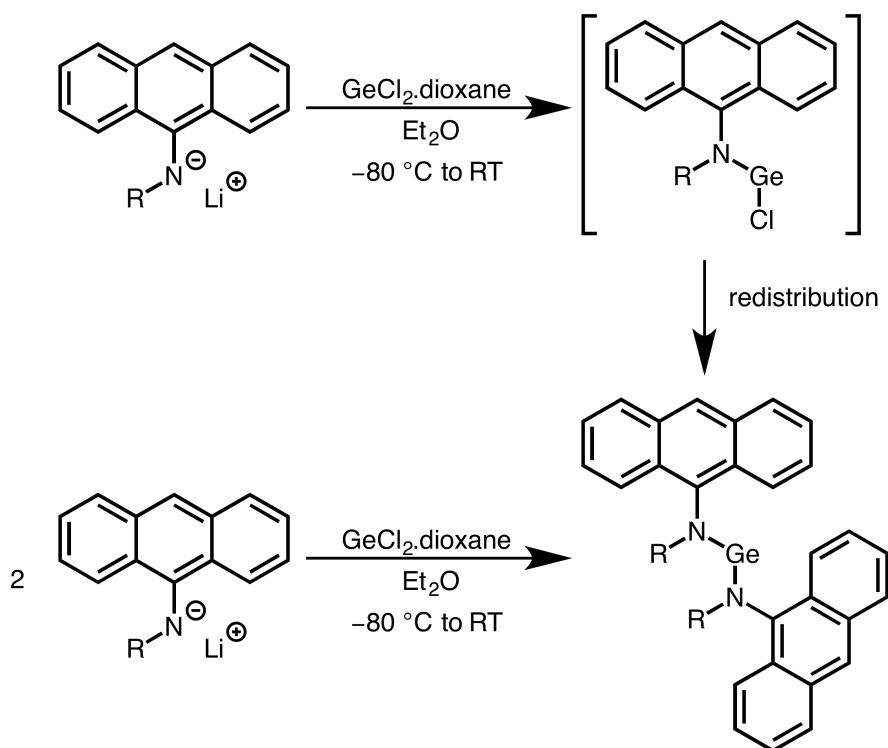
Scheme 3.16: 1:1 (top) and 2:1 (bottom) stoichiometry reactions of anthryl alkyl lithium amides and germanium dichloride dioxane. Minor and major products as determined by ^1H NMR spectroscopic analysis (R is as stated in Scheme 3.12).

All reactions with GeCl$_2$.dioxane and the lithium anthryl alkyl amides rendered similar results as stated above, giving a series of germylenes. When these reactions were performed

with **Li-2.1/3/4** the product mixtures were less complex than in comparison to the reactions where **Li-2.2/5/6** were used. Isolation of these germylenes has proven difficult as they are very soluble in toluene and benzene and are essentially insoluble in all other solvents. Typically, **3** and the other germylenes are obtained as orange/brown moisture-sensitive powders with minor pro-ligand impurities ranging from 10–30%, though **3** was isolated as a crystalline material (*vide infra*). Only **3** has been definitively characterised - the other stated germylenes are presumptive.

Spectroscopic Analysis of [{An(^tBu)N}₂Ge] (3)

Analyses of **3**'s ^{1}H NMR spectrum indicates possible nitrogen lone-pair delocalisation towards the anthryl moiety. The assigned chemical shift for the tert-butyl functional group is shifted downfield (δ 1.31 ppm) and there is a general shift upfield for all the assigned Ar-*H* proton signals[xxxiv]. Decreased electron density upon the alkyl moiety indicates the presence of a nitrogen lone-pair π interaction with the germanium(II) centre[xxxv], also (indicated by the observed N-Ge bond lengths, *vide infra*). The two ligands of the complex are observed to be magnetically equivalent. From the ^{13}C NMR spectrum, the tert-butyl functional group signals are shifted downfield.

It is ongoing work to successfully isolate the presumed germylenes from our reactions with **Li-2.2**-**Li-2.6**. Tentative ^{1}H NMR spectroscopic assignments are presented within the **experimental section** of this chapter for the germylene formed using **Li-2.4**, viz. [{An(Ad)N}₂Ge].

Elemental analysis gave no conclusive evidence or support for the definite formation of **3** as the obtained C/H/N percentages were significantly lower than expected. Repetition of the elemental analyses yielded the same results. Comparing the obtained values with the theoretical value of all rationally derived potential products from this reaction also did not help us untangle these results. We have no suggestion as to the cause behind these observations

Initially, **3** could not be crystallised and was isolated as a semi-pure solid (an orange powder which contains pro-ligand). Crystals of **3** were eventually grown from a concentrated solution of toluene. Unfortunately under all conditions attempted, **3** co-crystallises with An(^tBu)NH (**2.1**) which is unavoidably formed through decomposition of **3** over time in solution. These single crystals of **3** were suitable for X-ray diffraction.

[xxxiv]This trend was noted for the ^{1}H NMR spectrum of **Li(THF)-2.1**, also.

[xxxv]The reduced electron density upon the alkyl moiety is a consequence of an electron-withdrawing inductive effect.

X-ray Crystallographic Characterisation of [{An(^{t}Bu)N}$_2$Ge] (3)

The unit cell of [{An(^{t}Bu)N}$_2$Ge] (**3**) contains three independent molecules with essentially the same geometry: only bond angles for one of the three molecules are focused on (**figure 3.9**) Notable geometric differences between the three molecules are discussed where appropriate.
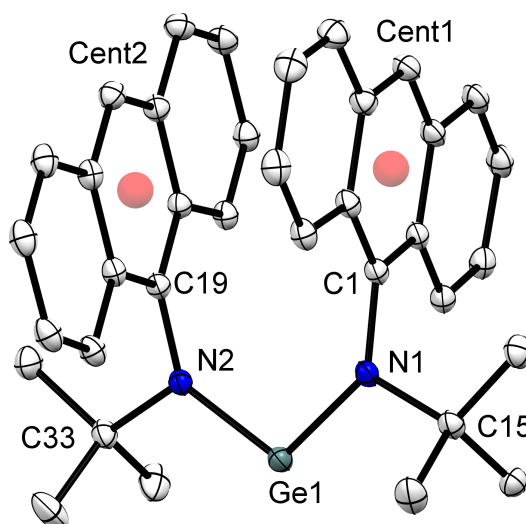

Figure 3.9: Thermal ellipsoid plot (30% probability surface) of [{An(^{t}Bu)N}$_2$Ge] (3) (hydrogen atoms omitted). Selected bond lengths (Å) and angles (°) for molecule one: Ge1-N1 1.860(1), Ge1-N2 1.861(2), N1-C1 1.431(2), N1-C15 1.525(2), N2-C19 1.425(2), N2-C33 1.517(2), Cent1-Cent2 3.523; N1-Ge1-N2 105.74(6), Ge1-N1-C1 127.9(1), C1-N1-C15 116.8(1), C15-N1-Ge1 113.5(1), Ge1-N2-C19 124.6(1), C19-N2-C33 117.5(1), C33-N2-Ge1 116.2(1); C1-N1-N2-C19 –32.3(1).

The molecular structure of **3** displays a germanium(II) centre which is stabilised by two An(^{t}Bu)N$^-$ ligands. There is apparent π-π stacking interactions between the anthryl moieties of the two ligands, observed by the calculated Cent1-Cent2 distance at 3.523 Å. It is believed that this is a true π-π stacking interaction: the measured calculated centroid distances between the anthryl moieties across all three molecules in the unit cell of **3** are within the expected values for such interactions. However, the rings which participate in this π-π stacking interaction vary between the three molecules. For *molecules one* and *two*, the central aromatic of both anthryl moieties, within the same molecule, display the closest interaction at 3.523 Å and 3.494 Å respectively. For *molecule three*, the closest interaction is observed between one of the outer aromatic rings of the anthryl group and the central aromatic ring of the opposing anthryl group at a distance of 3.483 Å. This is reflected in the respective C-N-N-C torsion angle, where C is the aromatic carbon, for each of the three molecules; *molecule one* and *two* display a torsion angle of –32.3(1)° & –31.5(1)°, respectively; *molecule three* displays a torsion angle of -58.2(1)°.

Both Ge-N bond distances are as expected as they are consistent with those observed in analogous germylene ($\overline{x}$ = 1.880 Å).[?,?,?,?,?,?] These bond distances are consistent for each of the contained molecules within the unit cell.

The anthryl moieties of the ligand in all three molecules maintain their ideal geometric structure, i.e. that observed for anthracene and in the pro-ligand **2.1**; though *molecule three* shows slight planar deviation with an average Cent-Cent-Cent angle of 174.75°. The planar deviation experienced in *molecule three* is observed to allow for a closer π-π stacking interaction as both anthryl moieties flex towards each other.

The N-Ge-N bond angle about the germanium(II) centre is 105.74(6)° for *molecule one*, though the angle varies across the three molecules. *Molecule two* displays a bond angle at 106.39(6)° (most obtuse) and *molecule three* displays a bond angle of 104.43(6)° (most acute). All three of these bond angles are congruous to those observed in similar structurally reported germylenes ($\overline{x}$ = 106°).[?,?,?,?,?,?] The slight difference between the germanium(II) bond angles is perhaps related to the degree of π-π stacking interactions - *molecule three* has the most acute bond angle and shortest observed π-π stacking interaction distance. Though, the counter-effect is not observed for *molecule two*. It is more likely is that the N-Ge-N bond angle is related to the degree of steric repulsion between the opposing anthryl moieties of the respective molecules: for *molecule three*, the opposing anthryl moieties are rotated away from one another (display the least overlap) and this could result in a reduction in steric repulsion (though this is just conjecture).

X-ray Crystallographic Characterisation and Discussion of the Formation of [An(^{t}Bu)NH$_2$][GeCl$_3$] (4)

In one instance a single crystal was isolated from the 1:1 stoichiometric reaction of **Li-1** with GeCl$_2$.dioxane. This crystal was revealed by X-ray crystallographic diffraction to be the saltt **[An(^{t}Bu)NH$_2$][GeCl$_3$] (4)** (**figure 3.10**).
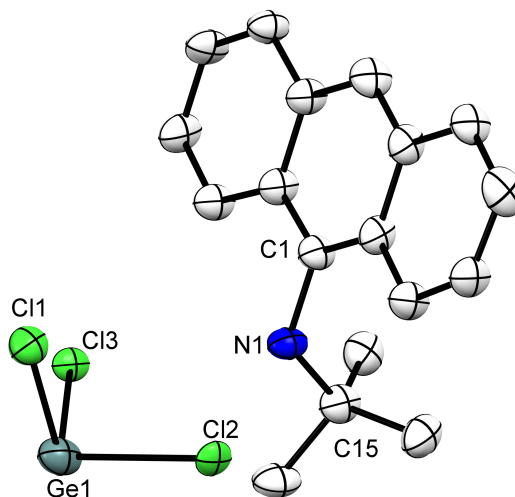
Figure 3.10: Thermal ellipsoid plot (30% probability surface) of [An(^{t}Bu)NH$_2$][GeCl$_3$] (4) (hydrogen atoms omitted). Selected bond lengths (Å) and angles (°): N1-C1 1.47(1), N1-C15 1.58(2), Ge1-Cl1 2.276(4), Ge1-Cl2 2.384(2), Ge1-Cl3 2.381(2), Ge-N1 4.346(8), Cl3-N1 3.307(8), Cl2-N1 3.250(8), Cl1-N1 5.24(1); C1-N1-C15 119.7(8), Cl1-Ge1-Cl2 94.61(9), Cl1-Ge1-Cl3 95.5(1), Cl2-Ge1-Cl3 96.22(8); C2-C1-N1-C15 93(1).

In the structure of **4**, the germanium atom in the [GeCl$_3$]$^-$ anion adopts a pyramidal geometry with an average Cl-Ge-Cl angle of 95.4°. The Ge-Cl bond distances vary with Ge1-Cl2 & Ge1-Cl3 being longer than Ge1-Cl1; the average of the Ge-Cl bond distances (2.347 Å) is slightly longer than those displayed in other structurally characterised [GeCl$_3$]$^-$ anions and to the calculated value (2.309 Å).[?,?,?,?,?] The discrepancy in Ge-Cl bond lengths may be attributed to a weak interaction of the chlorine atoms Cl(2) & Cl(3) with the hydrogen atoms upon the nitrogen.[?] We believe that the orientation of the anion and cation is due to this van de Waals interaction. However, as no neutron diffraction was performed, the presence of the protons cannot be confirmed but only suggested.

It is postulated that the formation of this species is due to the decomposition of some desired LGeCl compound (potentially due to adventitious water) and that the products from this decomposition concertedly react. The pro-ligand, if acidic enough, could undergo an acid-base reaction with GeCl$_2$ forming LGeCl and HCl. The generation of HCl allows another acid-base reaction to occur between itself and the pro-ligand forming the HCl salt HCl.LH. HCl.LH reacts with GeCl$_2$ (another product from decomposition) to form the LH$_2^+$GeCl$_3^-$ species [xxxvi] (**scheme 3.17**).

[xxxvi]The reaction of HCl.LH salts and GeCl$_2$ is the synthetic pathway for the generation of LH$_2^+$GeCl$_3^-$ type species.
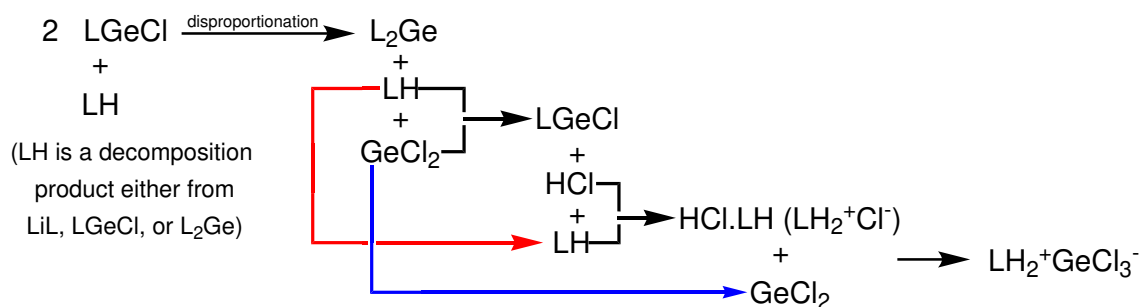
Scheme 3.17: Proposed reaction scheme for the formation of [LH₂][GeCl₃]. The complicated reaction mixture has a mix of decomposition products which concertedly react to finally give LH₂GeCl₃ (where L = An(ᵗBu)N⁻).

3.5.4 Coupling to Tin

Synthetic Attempts to Form LSnX and L₂Sn

Reactions between a range of tin(II) halides and the series of anthryl alkyl lithium amides (**Li-2.1** to **Li-2.6**) led to the synthesis of a range of stannylenes (**scheme 3.18**), of which three have been characterised (*vide infra*). Avoiding THF with the heavier group 14 elements, tin and lead, is difficult: tin/lead(II) halides require a strong donor solvent for full dissolution. For these reasons, minimal THF was used in these mixtures to ensure timely reaction between the ligand and the respective tin halides.
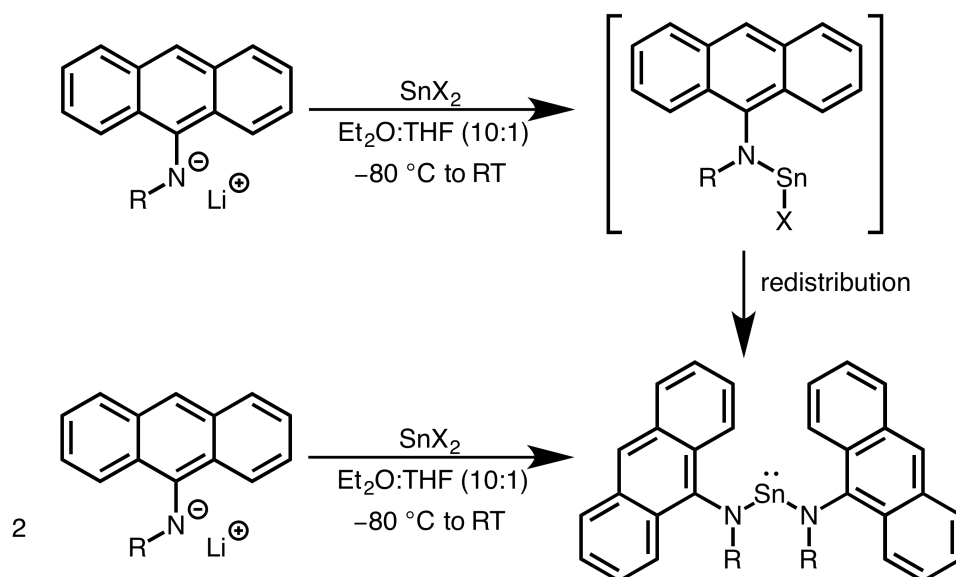
Scheme 3.18: 1:1 (top) and 2:1 (bottom) stoichiometry reactions of the anthryl alkyl lithium amides with tin(II) dihalide (where X = Cl or Br, R = as stated in Scheme 3.12). The LSnX was not observed by ¹H NMR spectroscopic analyses.

In all cases the 1:1 stoichiometric reactions of ligand:tin led to the formation of a new

major and minor compound. As was the case in our reactions with germanium, the major product was believed to be the respective LSnX species, though it was latter found that the major product was in-fact the respective stannylene.

The following discussion is specific to the prototypical 1:1 stoichiometric reaction between **Li-2.1** and SnBr$_2$ (these were attempted before we had identified the stannylene as the major product). Multiple attempts were made to crystallise the major product and on two occasions single crystals of the minor species {An(^{t}Bu)N}SnBr$_2$•Li(THF)$_2$ (**5**) (a tin lithiate species) and [{O-r-An(^{t}Bu)N}$_2$(μ-SnBr)$_2$] (**6**)[xxxvii] resulted (*vide infra*, **figures 11 & 12**, respectively).

X-ray Crystallographic Characterisation of {An(^{t}Bu)N}SnBr$_2$•Li(THF)$_2$ (5) and [{O-r-An(^{t}Bu)N}$_2$(μ-SnBr)$_2$] (6)

Isolation of {An(^{t}Bu)N}SnBr$_2$•Li(THF)$_2$ (**5**) was not expected. Unpublished work from within the Jones group gives precedent for these compounds and these have been found to form when lithium salt congeners of ligands are utilised, and are analogues to aluminium lithiates.[?,?,?,?]
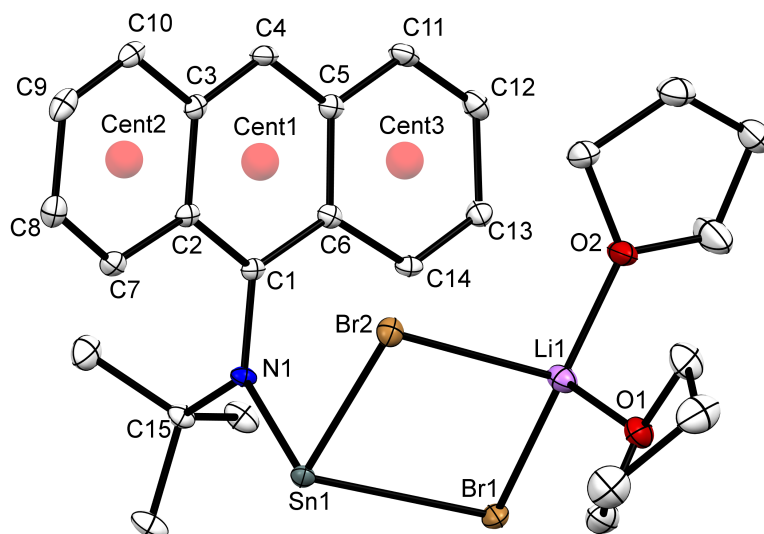
Figure 3.11: Thermal ellipsoid plot (30% probability surface) of {An(^{t}Bu)N}SnBr$_2$•Li(THF)$_2$ (5)(hydrogen atoms omitted). Selected bond lengths (Å) and angles (°): N1-C1 1.423(4), N1-C15 1.503(4), N1-Sn1 2.069(2), Sn1-Br1 2.8239(5), Sn1-Br2 2.6662(4), Br1-Li1 2.523(5), Br2-Li1 2.589(6), Li1-O1 1.906(6), Li1-O2 1.906(5), C7-C8 1.356(5), C9-C10 1.356(4), C11-C12 1.353(5), C13-C14 1.351(4); C1-N1-Sn1 123.1(2), Sn1-N1-C15 119.7(2), C15-N1-C1 117.1(2), N1-Sn1-Br2 94.55(7), N1-Sn1-Br1 100.92(7), Br1-Sn1-Br2 88.15(1), Br1-Li1-Br2 96.7(2), Li1-Br1-Sn1 86.5(1), Sn-Br2-Li1 88.6(1), C1-Cent1-C4 177.69, C7-Cent2-C10 177.49, C11-Cent3-C14 177.52, Cent2-Cent1-Cent3 175.75; C2-C1-N1-C15 95.7(3), C2-C1-N1-Sn1 −80.1(3).

[xxxvii]believed to be a product from adventitious dioxygen oxidation

126

The nitrogen atom of the ligand adopts a trigonal planar geometry, observed by the sum of its bond angles, suggesting π delocalisation of the nitrogen lone-pair, though this is not reflected in any of its bonds lengths. Both N-C bonds are similar to those measured for the respective pro-ligand **2.1**. The tin atom adopts a pseudo-pyramidal geometry, and the N-Sn-Br bond angles vary: the N1-Sn1-Br1 angle (100.92(7)°) is comparatively less acute than the N1-Sn1-Br2 angle (94.55(7))°. Variation between the Sn1-Br1 (2.8239(5)°) and Sn1-Br2 (2.6662(4)°) bonds indicates Br2 is more closely linked with the LSn fragment. This is somewhat reflected in the shorter Br1-Li1 bond length comparative to the Br2-Li1 bond. Unlike in **Li(THF)-2.1**, the lithium atom shows no coordination or interaction to the anthryl moiety. The bond distances and angles of the anthryl moiety are as expected, though some C-C bonds and angles are slightly shorter than expected [xxxviii] . The ring maintains planarity with minor deviations: each aromatic ring displays minute deviations from an ideal plane. Based upon the torsion angles, both of the nitrogen substituents are less-than-perpendicular to the N1-C1 axis and are pointing in opposite directions (this appears to be a common geometric characteristic when the anthryl alkyl amide ligand maintains its aromatic integrity).

The formation of [{O-r-An(^{t}Bu)N}$_2$(μ-SnBr)$_2$] (**6**) indicated the inadvertent addition of oxygen into the reaction mixture, which was not reflected in the ^{1}H NMR spectrum of the product mixture. The poor quality of X-ray diffraction data obtained from the single isolated crystal of **6** only allows us to make a comment on connectivity; all bond lengths and degrees are tenuously assigned.

[xxxviii]As has been stated prior, the ideal anthracene bond distances and angles would reflect that for the ideal geometric properties seen in a six-membered-carbon aromatic viz. benzene, albeit slightly deviated.[?]
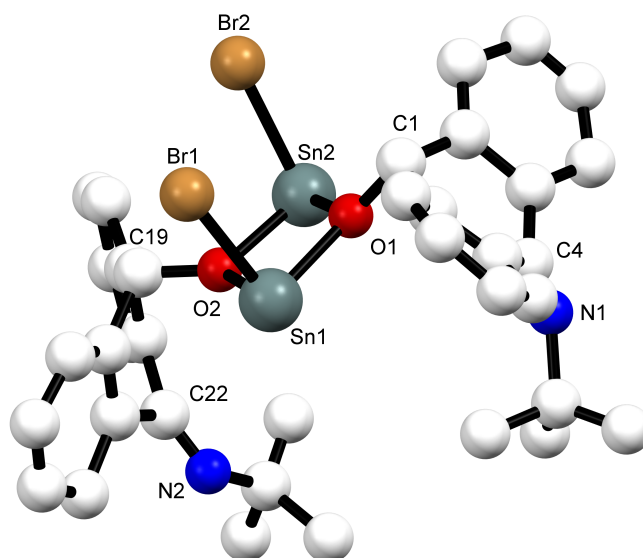
*Figure 3.12: Ball-and-stick representation of $\{r\text{-}An(^tBu)N\}_2(OSnBr)_2$ (**6**) (hydrogen atoms omitted). Selected bond lengths (Å): Sn1-Br1 2.594(3), Sn2-Br2 2.581(3), Sn1-O1 2.20(1), Sn2-O1 2.17(1), Sn1-O2 2.16(1), Sn2-O2 2.18(1), O1-C1 1.44(3), O2-C19 1.40(3), N1-C4 1.21(4), N1-C15 1.55(4), N2-C22 1.21(4), N2-C33 1.43(3), C1-C2 1.49(2), C2-C3 1.38(4), C3-C4 1.39(4), C4-C5 1.52(4), C5-C6 1.47(5), C1-C6 1.49(3), C19-C20 1.47(2), C20-C21 1.43(3), C21-C22 1.55(3), C22-C23 1.57(4), C23-C24 1.32(4), C19-C24 1.50(3).*

The molecular structure of **6** displays the tert-butyl imine reduced anthryl oxo bridged dinuclear tin(II) bromide where the tin(II) centres form a bridging motif. The two tin(II) bromides are captured between the donor oxygen atoms and together the four atoms form a four-membered ring. The Sn-O bond distances (2.16-2.20 Å) are longer than reported single bonds and are consistent between themselves; also, these bond distances are consistent with the Sn-O bond distances observed in reported analogous bis-tin-oxo bridged compounds ($\overline{x}$ = 2.148 Å).[?,?,?] As observed in **1** & **2**, the anthryl moiety of the compound has lost its planarity and aromaticity and the nitrogen atoms form double bonds to their respective former-anthryl moiety (N1-C4 and N2-C21 bond distances are 1.21(4) Å).

Formation and Spectroscopic Analysis of Stannylenes L₂Sn

From our initial 1:1 stoichiometric reactions of **Li-2.1** and SnBr₂, eventually single crystals of the stannylene $[\{An(^tBu)N\}_2Sn]$ (**7**) were isolated. **7** is believed to be the product of redistribution.

The formation of **7** influenced our decision to repeat these reactions as a 2:1 stoichiometric reaction between the rest of the anthryl alkyl lithium amides and SnBr₂, all of which gave similar results and indicated the formation of the respective stannylenes, albeit the yields changed on variation of the anthryl alkyl amide. Of all the reactions in the series: **Li-2.1**, **Li-2.3**, and **Li-2.4** are found to give the best yields of the respective stannylenes -

7, [{An(^{t}Oct)N}$_2$Sn] (**8**), and [{An(Ad)N}$_2$Sn] (**9**) - and the cleanest product mixtures. The reactions performed with **Li-2.2**, **Li-2.5**, and **Li-2.6** gave comparatively complicated product mixtures, as determined by ^{1}H NMR spectroscopic analyses. The isolation of these stannylenes is ongoing work; the data collected thus far display impurities alongside the L$_2$Sn compound.

^{1}H NMR spectroscopic analyses of **7**, **8**, and **9** indicate the two ligands of these complexes and magnetically equivalent with single chemical shifts displayed for all ligand-derived proton chemical environments. A general characteristic displayed in the ^{1}H NMR spectra of these stannylenes is an upfield shift of the Ar-*para-H* (backbone proton of the anthryl moiety) chemical signal, indicating increased electron density within the anthryl moiety. A downfield shift in the chemical shifts of the respective alkyl moieties is also observed. These shifts may indicate increased nitrogen lone-pair delocalisation towards the anthryl moiety which concertedly increases electron withdrawal by the nitrogen element through the N-alkyl σ bond. This delocalisation is in accordance with the observed trigonal planar geometry adopted by the nitrogen (*vide supra*). Also, these observations indicate the likely nitrogen lone-pair π interaction with the formally empty p orbitals upon the tin (II) centre (see N-Sn bond lengths, *vide infra*); however, ^{119}Sn NMR spectroscopic analysis was unsuccessful and no ^{119}Sn signal is observed for any of the stannylenes, and no further comment can be made.

X-ray Crystallographic Characterisation of [{An(^{t}Bu)N}$_2$Sn] (7)

Crystals of **7** suitable for X-ray diffraction were obtained from concentrated solutions of toluene. In each case, the crystals isolated were red and were needle-like. The molecular structure of **7** was elucidated and is shown in **figure 3.13**. For **8** a technical fault in collection renders the structural solution obtained incomplete, though connectivity indicates these crystals correspond to the expected stannylene.
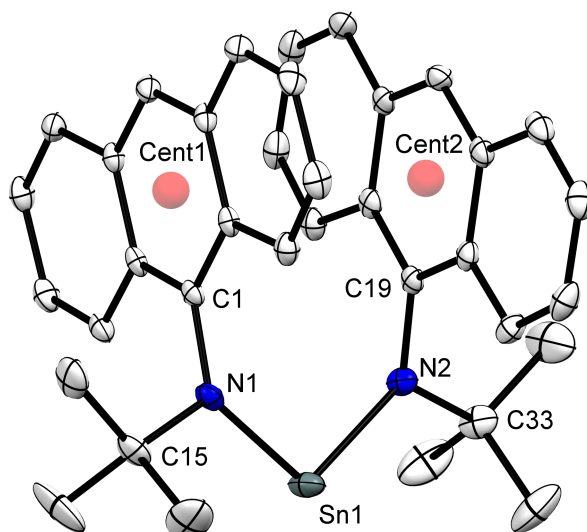
*Figure 3.13: Thermal ellipsoid plot (30% probability surface) of [{An(ᵗBu)N}₂Sn] (**7**) (hydrogen atoms omitted). Selected bond lengths (Å) and angles (°): N1-C1 1.422(5), N1-C15 1.514(5), N2-C19 1.421(5), N2-C33 1.523(5), Sn1-N1 2.064(3), Sn1-N2 2.067(3), Cent1-Cent2 3.507; N1-Sn1-N2 102.9(1), Sn1-N1-C1 125.1(2), Sn1-N1-C15 117.2(2), Sn1-N2-C19 126.0(2), Sn1-N2-C33 116.3(2), C15-N1-C1 116.1(3), C19-N2-C33 117.0(3), C1-Cent1-C4 179.38, C19-Cent2-C22 179.49; C2-C1-N1-Sn1 73.7(4), C6-C1-N1-C15 86.1(4), C20-C19-N2-Sn1 77.3(4), C24-C19-N2-C33 85.3(4), C1-N1-N2-C19 28.9(3).*

The molecular structure of **7** displays a {An(ᵗBu)N}⁻ ligated tin(II) centre with an evident π-π stacking interaction between the anthryl moieties of the opposing ligands at 3.507 Å (measured between the calculated centroids Cent1 and Cent2). It is difficult to ascertain whether this is a true π-π stacking interaction or if it is to accommodate steric strain[xxxix]. However, due to the similarities between **7** and the molecular structure of the analogous germylene **3**, it is suggested that this is likely a true interaction. The two Sn-N bond lengths are essentially the same (2.064 and 2.067 Å) and are in accordance with average Sn-N bond lengths typically observed in analogous stannylenes ($\bar{x}$ = 2.077 Å). The tin(II) centre adopts a bent geometry with a N-Sn-N bond angle of 102.9° which is also consistent with previously reported N-Sn-N angles observed in analogous stannylenes ($\bar{x}$ = 104.7°).[?,?,?,?,?,?,?]

The anthryl moiety of the ligand maintains its planarity and displays bond lengths and angles in agreement with aromaticity. The nitrogen donor atom is pseudo-trigonal planar as can be seen from the sum of angles about its centre ($\sum$ = 358.4° and 359.3°, N1 and N2 respectively). There is no major geometric deviation between the two ligands. The ligands adopt an almost eclipsed/gauche conformation about the tin(II) centre as represented by the C1-N1-N2-C19 torsion angle of 28.9(3)°.

[xxxix]By adopting a pseudo-eclipsed conformation, the ligands reduce steric clash between the tert-butyl and anthryl moieties upon the opposing ligands.

Formation and Spectroscopic Analysis of Bis-stannylenes L$_2$Sn$_2$

The successful formation of the monostannylenes prompted us to synthesise the bis-stannylene {An((^{t}Bu)N)$_2$}$_2$Sn$_2$(**10**) (a dinuclear tin(II) compound). To accomplish this, anthryl bis-tert-butylamine was lithiated in situ and added to a solution of SnBr$_2$ as per **scheme 3.19**.
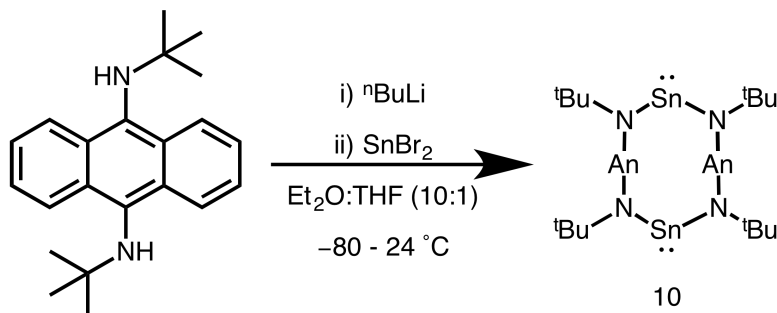
*Scheme 3.19: Salt-metathesis coupling of of the bis-functionalised anthryl amide **Li-2.11** and SnBr$_2$ to form **10**.*

The ^{1}H NMR spectrum of **10** is similar to **7**. Neither mass spectroscopic nor elemental analyses were indicative for the formation of **10**; the same results were observed when said analyses was done on isolated and confirmed crystals of **10**.

Following the isolation procedure which gave **7** & **8**, crystals of **10** were isolated from a concentrated toluene solution and were suitable for X-ray diffraction (**figure 3.14**).

X-ray Crystallographic Characterisation of [{An((^{t}Bu)N)$_2$}$_2$Sn$_2$] (10)
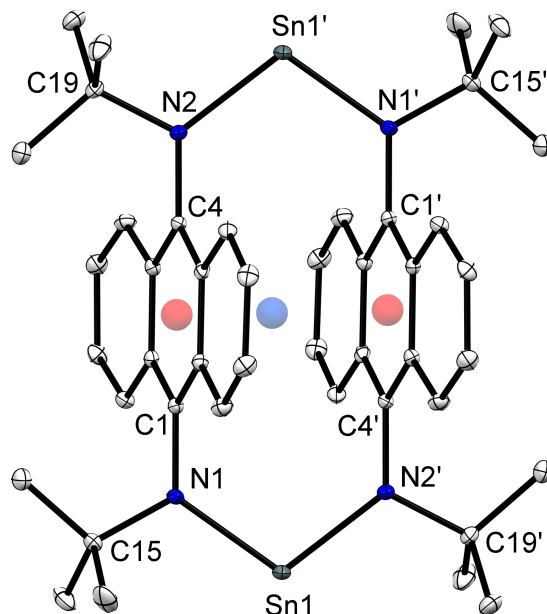
*Figure 3.14: Thermal ellipsoid plot (30% probability surface) of [{An((^{t}Bu)N)$_2$}$_2$Sn$_2$] (**10**) (hydrogen atoms omitted). Selected bond lengths (Å) and angles (°): Sn1-N1 2.069(2), Sn1-N2 2.071(2), N1-C1 1.429(3), N2-C4 1.430(3), N1-C15 1.521(3), N2-C19 1.529(3), Cent1-Cent2 3.334; N1-Sn1-N2 107.04(7); Sn1-N1-C1-C6 –80.6(2); Sn1-N2-C4-C3 105.2(2).*

The molecular structure of **10** displays the dinuclear tin(II) compound. The geometrically enforced distance between the anthryl moieties situates the anthryl groups at a distance which is close enough for a π-π stacking interaction. Sn-N bond distances are marginally longer than observed in the monostannylene **7** but are still consistent with previously observed N-Sn bond lengths in analogous stannylenes ($\bar{x}$ = 2.077 Å).[?,?,?,?,?,?,?] The N-Sn-N bond angle is more obtuse at 107.04(7)° than the N-Sn-N bond angle observed in **7**; this bond angle is considerably more obtuse than the mean average N-Sn-N bond angle ($\bar{x}$ = 104.7°)[xl].

The anthryl moieties maintain their aromaticity and planarity and no significant deviation from the ideal bonding, observed in anthracene, is observable.[?]

3.5.5   Coupling to Lead

Salt-metathesis coupling between **Li-2.1**/**Li-2.4** and PbBr$_2$ looked promising by observation (the solution changed from dark purple to orange/red, the typical colour observed for

---

[xl]For the analogous stannylenes, The most obtuse N-Sn-N angle reported for is 111.05°.[?]

plumbylenes). However, all synthetic attempts led to complicated reaction mixtures as determined by ^{1}H NMR spectroscopy. The lack of immediate success in these coupling reactions to lead(II) halides combined with the experienced difficulties with the lithium anthyl alkyl amide coupling reactions with other heavy group 14 elements influenced our decision to cease this project.

We believe that the size of the anthryl alkyl amide ligands is not appropriate for binding to larger main-group elements as they do no afford great enough kinetic stability to access nor stabilise low-oxidation state tetrel compounds. The electronic destabilisation by removing a halide from these compounds and binding a non-sterically encumbering ligand potentially leads to decomposition. Furthermore, steric repulsion between the ligand and larger metal centres, such as lead, influences decomposition to occur. The exception to this is germanium and tin which are both thermodynamically and kinetically less prone to destabilisation.

3.5.6 Reduction Attempts

The reductions of **1** and **2** were attempted in situ as we could not isolate them successfully. Reductions were attempted using $[(\{^{Mes}nacnac\}Mg)_2]$ or KC_8 and performed in toluene. Drastic solution colour changes were observed on addition of the reductant to the presumed in situ generated **1**/**2** compounds, the reaction mixture going from yellow/orange colour to red/purple for **1** and **2**. Over a period of one hour of stirring at –80 °C, this colour was seen to dissipate and the solution becomes yellow. ^{1}H NMR spectroscopic analyses of the initial reaction mixtures indicated a number of products which could not be identified; the obtained ^{1}H NMR spectrum of the reaction mixture after one hour period indicated the reformation of pro-ligand. No further reduction studies were attempted with **1** or **2**.

For germanium and tin, in situ generation of LMX complexes (the minor products from our 1:1 stoichiometric reactions) was believed to be possible, and so the reduction of these presumed species was attempted. The presumptive species are believed to be thermodynamically unstable; consequently, the respective reaction mixtures were kept at low-temperatures in order to suppress redistribution to the respective germylenes and stannylenes. These attempts were only conducted using the $An(^{t}Bu)N^-$ and $An(Ad)N^-$ ligand LMX derivatives. The reduction attempts followed the same process as stated for **1** and **2**, and met with the same failure. For the presumptive LGeCl and LSnBr, addition of the reductant led to a solution colour change over the period of one to two hours at –50 °C, going from orange/red to dark red/brown. ^{1}H NMR spectroscopic analyses of these reaction mixtures, taken at 1 hour intervals, indicated the conversion of starting materials to some new product. The percent conversion of this new product increased over time (maximum of approximately 40%). However in all cases the prolonged stirring of the solution, regardless of temperature control, led to the generation of pro-ligand as determined by ^{1}H NMR spectroscopy. No further

reduction studies were attempted.

3.5.7 Closing Remarks

Based on the experimental evidence, the anthryl alkyl amides do not posses the ability to sterically encumber nor stabilise +I oxidation state group 14 element compounds. The potential for internal redox activity and the formation of rearrangement compounds, as was noted in our reactions between these ligands and silicon, was unexpected. These ligands provide a kinetically stable environment for germanium and tin, and allowed for the isolation of some germylenes and stannylenes. It is ongoing work to isolate the entire series of these species. Future work looks to examine the reactivity of the germylene and stannylenes presented.

3.6 R&D: Ar^X(TMS)N Amide

As discussed in **chapter 2**, we believed that the greater proximal bulk and forced-rigidity of the pro-ligand **Ar^X(TMS)NH** (**2.14**) would provide a suitable sterically encumbering environment to stabilise low-oxidation state group 14 element compounds. Unlike the anthryl alkyl amines, the facility of the synthetic route to **2.14** did not allow us to synthesise any derivatives, i.e. change the silyl substituent etc. Inspite of this, we had hoped that the steric encumbrance present would be suitable for the stabilisation of low-oxidation state group 14 complexes. Again, salt-metathesis coupling was our preferred ligation pathway in order to synthesise the desired halide compounds.

Our coupling attempts were partially successful, leading to the formation of a novel germanium compound (*vide supra*); however, in the case of Si, Sn, and Pb, we were unsuccessful in isolating the desired halide compounds.

3.6.1 Lithiation

2.14 could only be successfully lithiated in the presence of a donor solvent. We found that diethyl ether leads to the highest conversion rate, whereas using THF led to complex product mixtures. All lithations were performed in a solvent mix of diethyl ether:hexane, as shown in **scheme 3.20**. Ar^X(TMS)NLi (**Li-2.14**) is unstable when isolated as a solid, decomposing to pro-ligand over time. Due to this, **Li-2.14** was generated in situ before being added to a heavy tetrel halide solution, and only ^{1}H NMR spectroscopic data were obtained. The loss of the N-*H* chemical shift (observed for the pro-ligand **2.14**) and the general chemical shifts observed in the ^{1}H NMR spectrum of the in situ generated **Li-2.14** are believed to be adequate indications for the successful conversion of **2.14** into **Li-2.14**.
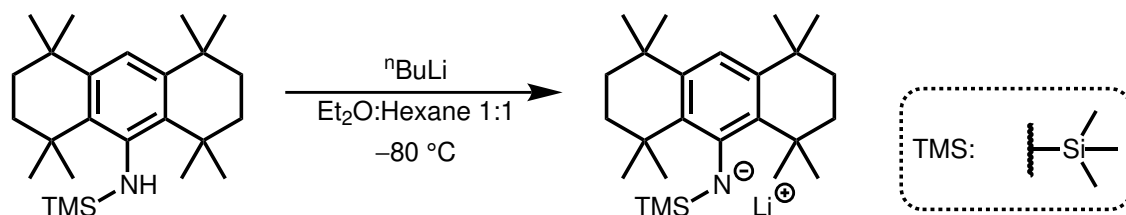
*Scheme 3.20: Conversion of the Ar^X amine pro-ligand to its lithium salt congener Ar^X(TMS)NLi (**Li-2.14**).*

From the tentatively assigned ^{1}H NMR spectrum of **Li-2.14**, the lone-pair of the nitrogen is believed to delocalise across the N-TMS moiety as indicated by the Si-(CH_3)$_3$ chemical shift at δ 1.30 ppm (in comparison to δ 0.57 ppm in **2.14**)[xli]. Consequently, delocalisation of the nitrogen lone-pair of electron is reduced towards the central aromatic of the Ar^X moiety as reflected in the downfield chemical shift of δ 6.76 ppm compared to δ 6.95 ppm in **2.14**.

3.6.2   Coupling to Silicon

Initially, we attempted to form the [{Ar^X(TMS)N}SiH$_{3-n}$X$_n$] species via salt-metathesis, though each attempt was unsuccessful under all reaction conditions. Attempts were then made to form the [{Ar^X(TMS)N}$_2$SiH$_{2-n}$X$_n$] species (carried out based on the same rationale as those proposed for the anthryl alkyl amides (*vide supra*)) which also failed. In all cases these reactions led to complicated reaction mixtures. From these mixtures the major products identified by ^{1}H NMR spectroscopy were Ar^X(TMS)NH, Ar^{X}NH$_2$, and the free-arene Ar^{X}H. We are unsure as to the mechanism of decomposition. It is postulated that weak N-Si bonds formed between the ligand and the silicon-centre-of-interest, if formed cleaved, leading to decomposition[xlii].

3.6.3   Coupling to Germanium

Synthesis and Spectroscopic Analysis

Salt-metathesis coupling of **Li-2.14** to GeCl$_2$.dioxane was successful, giving high yields of [{Ar^X(TMS)N}GeCl] (**11**). *In vacuo* removal of volatiles and extraction of the residue with hexane yields **11** as an orange powder with minor ligand impurities. Crystals were produced by recrystallisation from hexane at –30 °C.

[xli]Without further investigation - which would go beyond the scope and interest of this work - no comment can be made as to which orbitals are involved for the π interaction between the nitrogen lone-pair and the silicon moiety.

[xlii]NBO and SOPT analysis of **2.14** suggests unexpected bonding within the ligand between the nitrogen and silicon atom of the TMS moiety; this bonding appears to be much more polar than would otherwise be expected.
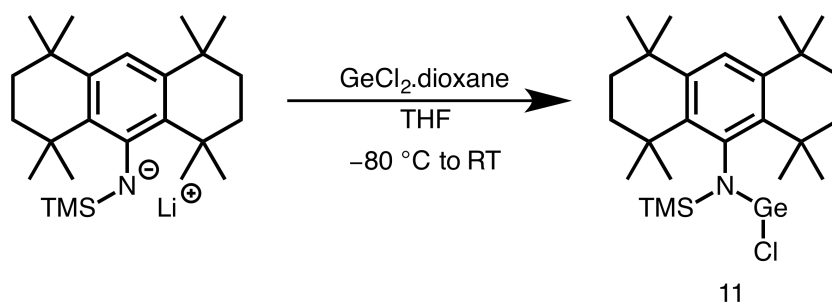
*Scheme 3.21: Synthesis of {Ar^X(TMS)N}GeCl (**11**) from Ar^X(TMS)NLi (**Li-2.14**) and GeCl$_2$.dioxane.*

Surprisingly, analyses of the ^{1}H NMR spectrum obtained for the reaction mixture which yielded **11** indicated no significant by-product formation, nor were any of the unidentifiable products - noted in the ^{1}H NMR spectrum of **Li-2.14** - noticeably present. The four proximal-to-the-germanium-centre methyl groups (the CH$_3$ functional groups which run parallel to the C-N bond axis) are chemically and and magnetically inequivalent, displaying two seperate chemical shifts, whilst the four distal-to-the-germanium-centre methyl groups are equivalent. This chemical shift splitting pattern is reflected in the CH$_2$ functional groups. Of the four CH$_2$ functional groups, two are assigned as proximal and display one set of chemical shifts, the other distal and produce their own set of chemical shifts. The assigned backbone aromatic proton chemical shift at δ 7.33 ppm is significantly more downfield than that which is observed for **Li-2.14** at δ 6.76 ppm and **2.14** at δ 6.95 ppm.

^{29}Si{H} NMR spectroscopic analyses indicates a comparatively deshielded silicon centre in **11** (δ 4.3 ppm) in comparison to **2.14** (δ 1.3 ppm), a consequence of the nitrogen lone-pair delocalisation towards the aromatic moiety of **11**[xliii]. Delocalisation of this nitrogen lone-pair is also directed towards the formally vacant p orbital upon the germanium(II) element as shown by the N-Ge bond lengths (*vide infra*).

X-ray Crystallographic Characterisation of [{Ar^X(TMS)N}GeCl] (11)

{Ar^X(TMS)N}GeCl (**11**) was isolated as yellow-orange coloured crystals from a concentrated solution of hexane; the crystals were adequate for X-ray crystallographic diffraction, allowing us to determine its molecular structure (**figure 3.15**).

[xliii]Through an electron-withdrawing induction effect, the silicon atom becomes deshielded.
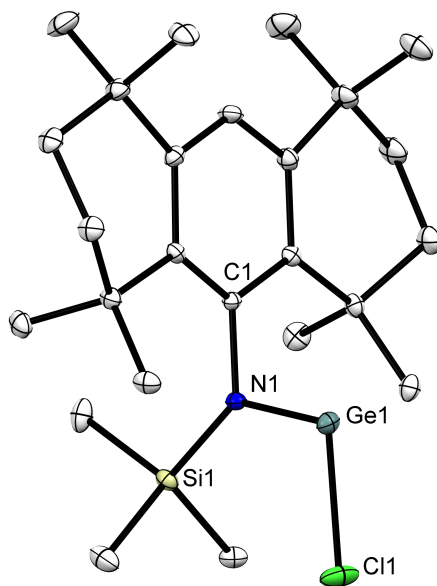
*Figure 3.15: Thermal ellipsoid plot (30% probability surface) of {Ar^X(TMS)N}GeCl (**11**) (hydrogen atoms omitted). Selected bond lengths (Å) and angles (°): N1-Si1 1.771(2), N1-C1 1.466(3), N1-Ge1 1.848(2), Ge1-Cl1 2.2512(7), C1-C2 1.434(3), C11-C4 1.379(3); Ge1-N1-C1 103.9(1), Ge1-N1-Si1 129.2(1), N1-Ge1-Cl1 101.58(6), Si1-N1-C1 126.9(1), C1-C2-C11 116.9(2), C5-C4-C11 125.2(2); Ge1-N1-C1-C2 86.9(2), Si1-N1-C1-C2–93.4(2).*

The molecular structure of **11** is a monomeric chlorogermylene which is ligated by {Ar^X(TMS)N}$^-$ ligand. **11** displays bond lengths akin to those of analogous structurally characterised monodenate LGeCl species. The germanium(II) centre adopts a bent geometry, as expected, with a displayed N1-Ge1-Cl1 bond angle of 101.58(6)°. This value is comparable to the corresponding N-Ge-C1 bond angles observed in analogous germylenes ($\overline{x} = 101$°).[?,?,?,?] Based on the average N-Ge bond distance of previously reported chlorogermylenes ($\overline{x} = 1.871$ Å), the N1-Ge1 bond length in **11** is relatively short (1.848(2) Å).[?,?,?,?] The N1-C1 bond length is marginally longer than typically observed in reported LGeCl species (1.448 Å): this distance is more relatable to N-C bond lengths observed in LGeR compounds (where Cl is replaced by a bulkier substituent (R) such as an alkoxide).[?] The long N-C bond in **11** is most probably due to the proximal steric pressure created by the flanking methyl groups of the aryl moiety, pushing the nitrogen atom and its substituents away from the aryl moiety. The preference for **11** to undergo N1-C1 bond elongation rather than N1-Ge1 bond elongation, as the means by which to accommodate steric strain, may be the result of a weaker nitrogen-(aryl)carbon bonding in this compound in comparison to other reported LGeCl species. The nitrogen atom displays a trigonal planar geometry: the sum of its bond angles equal to 360°. The germanium atom is almost perpendicular from the central C1-N1 bond axis, as reflected by the Ge1-N1-C1 bond angle of 103.9(1)°. Both the germanium and silyl substituents are perpendicular from the central aromatic plane, pointing in opposite directions as shown by the torsion angles Ge1-N1-C1-C2 86.9(2)° and Si1-N1-C1-C2–93.4(2)°. Within the central

ring, C1-C2 (1.434(3) Å) and C4-C11 (1.379(3) Å) bond distances are deviated from the ideal six-carbon-membered aromatic ring bond lengths ($\approx$ 1.40 Å); this deviation is also reflected in the bond angles of the central aromatic ring fragment.

Steric Profile of [{Ar^X(TMS)N}GeCl] (11)

A closer analyses of the steric environment afforded by **{Ar^X(TMS)N}$^-$** towards the germanium centre is presented within **table 3.3**. Here, a comparison is made between the steric encumbrance proposed in **chapter 2** and that observed experimentally. The steric encumbrance observed in **11** is greater than the theoretical steric encumbrance approximated when using the pro-ligand[xliv]. We believed that a closer approximation could be made by altering the optimised structure of the pro-ligand Ar^X(TMS)NH (**2.14**) by substituting the proton with a germanium centre[xlv], Ar^X(TMS)N(Ge*) (**2.14***)[xlvi], though the values obtained from this model do not absolutely reflect the actual steric encumbrance afforded by Ar^X(TMS)N$^-$, i.e. they are still to be taken as only a crude but appropriate approximation.

*Table 3.3: Bulk, flexibility, and proximity steric data for ligand **14** and comparative examples.*

Compound (#)	Bulk	Flexibility	Proximal Bulk	Distal Bulk
{Ar^X(TMS)N}GeCl (**11**)	409.5 Å^2	n/a	45.9%	35.5%
Ar^X(TMS)N(Ge*) (**2.14***)	409.5 Å^2	n/a	50.7%	34.3%
[{Ar*(TMS)N}GeCl]	533.6 Å^2	rotation 58.6-80.7%	62.3%	46.3%

Note: Bulk is expressed as a surface area in values of Å^2. All following values are expressed as a bV% value. Flexibility is qualitatively described; the bV% value is that of the approximate least to most sterically encumbering orientation of the molecule in relation to the ECOI. Proximal bulk is measured using a 3.5 Å radius sphere; distal bulk a 6.0 Å radius sphere.

The discrepancies between the calculated steric parameters, the bV% values, of **11** and **2.14*** are due to the slight changes in bond-angles between the molecular structure of **11** and the optimised structure of **2.14** (from which **2.14*** is derived). Between the two structures, the Ge-N-Si bond-angle observed in **11** is more obtuse and the Ge-N-C bond-angle is more acute than those calculated for **2.14***. Consequently, **2.14*** is a poor structural approximation for the steric encumbrance observed in **11**. However, **2.14*** does indicate that the germanium(II) centre is less sterically impacted by its position relative to the aromatic

---

[xliv]The SambVca algorithm considers the element which is to be considered the centre of the analysed sphere. Having a proton as the centre of consideration makes the sequential analysed spheres smaller and consequently inflates the bV% obtained.

[xlv]The bond length was set to that observed in the molecular structure **11** (1.848 Å) rather then the default distance set by GaussView (1.91967 Å).

[xlvi]For practical reasons, this compound was not optimised. Ligand conformation is therefore the same as that optimised for Ar^X(TMS)NH.

moiety of the {Ar ^{X}(TMS)N}$^-$ ligand than it is by its position to the trimethyl-silyl moiety: the decreased in bV% found for **11** is due to the increased distance the germanium element lies from the silyl moiety.

Comparing **11** to [{Ar*(TMS)N}GeCl], there is a drastic reduction of steric encumbrance afforded in **11**. The believed proximal steric encumbrance provided in **11** does not sufficiently overlap with the sphere of the germanium(II) centre. Only one methyl group from the the two proximal dimethyl functional groups of the Ar^X aryl moiety impart any significant proximal steric encumbrance to the germanium(II) centre. This is exacerbated by the increased N-C bond observed in the molecular structure of **11** (*vide supra*) as the bulk afforded by the Ar^X moiety is shifted away from the germanium(II) centre.

(a) {Ar^X(TMS)N}GeCl (**11**)   (b) Ar^X(TMS)N(Ge*) (**2.14***)

(c) {Ar^X(TMS)N}GeCl (**11**)   (d) Ar^X(TMS)N(Ge*) (**2.14***)
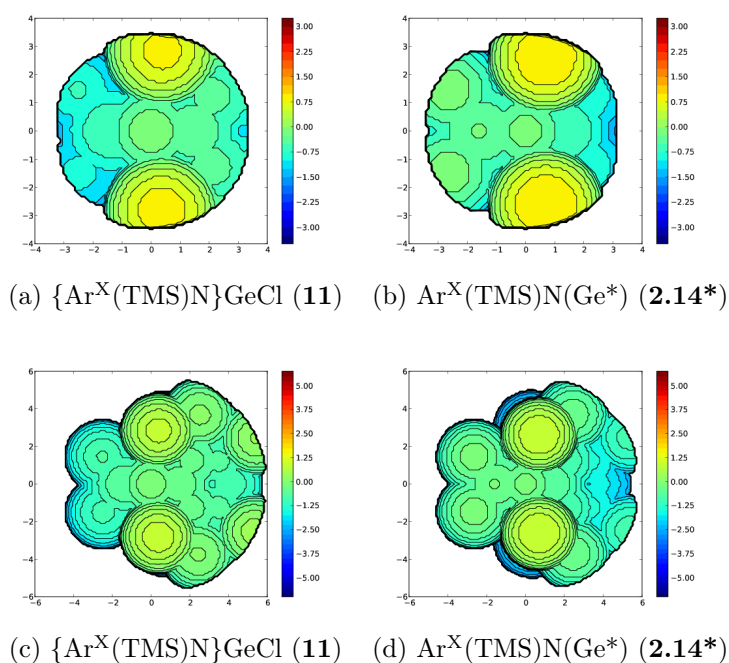
Figure 3.16: Proximal (top) and distal (bottom) steric maps of {Ar^X(TMS)N}GeCl and computational derivatives, as viewed down the N-Ge axis.

The steric maps (**figure 3.17**) give a visual representation of the proximal and distal bulk provided by these ligands to the germanium centre. Unsurprisingly both models produce similar steric maps with minor deviations in the magnitude of steric encumbrance provided. The most notable difference is the positive steric impact of the trimethylsilyl moiety in the proximal steric maps of **2.14*** than in **11**.

3.6.4   Attempted Reduction of [{Ar^X(TMS)N}GeCl] and the Formation of [{Ar^X(TMS)N}$_2$Ge]

Reduction of [{Ar^X(TMS)N}GeCl] (**11**) to form the digermyne [({Ar^X(TMS)N}Ge)$_2$] was ultimately unsuccessful (despite our observations) and we could not isolate the major product from these reactions.

Under all reaction conditions attempted (using either [({^{Mes}nacnac}Mg)$_2$], Na, or KC$_8$ as the reductant) it was observed that a new major product formed from the reaction between **11** and the reductant, as determined by ^{1}H NMR spectroscopy, and that [({^{Mes}nacnac}Mg)$_2$] produced the highest and cleanest conversion of **11** to this new major product. However, all attempts to isolate this major new product failed. Monitoring the reaction mixture over time by ^{1}H NMR spectroscopy indicated the transformation of the major product to mixture of products which could not be identified, i.e. the major product is believed to decompose in solution over time. Attempts to isolate a solid product from these reactions were also unsuccessful. *In vacuo* removal of solvents led to the decomposition of the major product and an oily substance was obtained (the ^{1}H NMR spectrum of this substance displayed a complicated mixture of products which could not be reliably identified). Fractional crystallisation was attempted in order to isolate this major product, but this was unsuccessful. In one instance, a single crystal of the germylene {Ar^X(TMS)N}$_2$Ge (**12**) was obtained and was suitable for X-ray crystallographic diffraction (**figure 3.17**).

Retrospectively, we believe that our failure to isolate [({Ar^X(TMS)N}Ge)$_2$] was due to solvent contamination which only became apparent months later.[xlvii] It is on-going work to repeat these stated reactions and isolate the major product.

X-ray Crystallographic Characterisation of [{Ar^X(TMS)N}$_2$Ge] (12)

The molecular structure of **12** is centrosymmetric and displays a monomeric acyclic germylene where the germaniun(II) centre is stabilised by two {Ar^X(TMS)N}$^-$ ligands. To the best of our knowledge, this compound is the second reported acyclic germyelene stabilised by two aryl silyl amide ligands[xlviii].[?] The unit cells contains two independent molecules of **12** of essentially the same geometry; only bond lengths and angles for one of the two molecules is discussed unless specified otherwise.

[xlvii]The typically sodium distilled solvents used in our reactions were found to be contaminated: non-polar solvents had introduced dried THF and diethyl ether, both known to interact with, and eventuate the decomposition of highly reactive low-oxidation state group 14 element compounds. This was an oversight of the time.

[xlviii]It is the third reported germylene which is stabilised by two silyl amie ligands.[?]
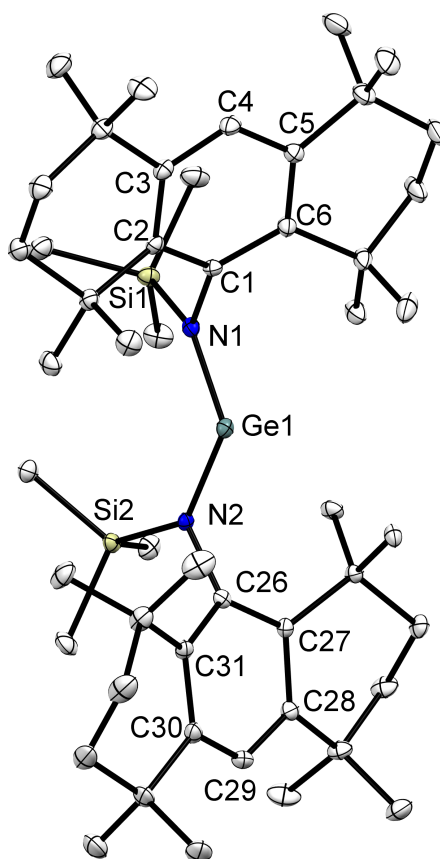
Figure 3.17: Thermal ellipsoid plot (30% probability surface) of [{Ar^X(TMS)N}$_2$Ge] (12) (hydrogen atoms omitted). (12 crystallises with two molecules in the asymmetric unit in the triclinic space group P-1; only one molecule is displayed.) Selected bond lengths (Å) and angles (°): (Molecule one) N1-C1 1.466(3), N1-Si1 1.759(3), Ge1-N1 1.908(3), Ge1-N2 1.917(2), N2-C26 1.473(4), N2-Si2 1.774(2); N1-Ge1-N2 118.1(1), Ge11-N1-Si1 145.1(2), Ge1-N1-C1 107.3(2), Si1-N1-C1 107.5(2), Ge1-N2-Si2 136.0(1), Ge1-N2-C26 118.9(2), Si2-N2-C26 105.1(2), N1-C1-C2 118.6(3), N1-C1-C6 119.4(3), C6-C1-C2 121.4(3), N2-C26-C27 119.1(3), N2-C26-C31 119.2(3), C27-C26-C31 120.6(3); C2-C1-N1-Si1 88.0(3), C2-C1-N1-Ge1 –95.0(3), C1-N1-N2-C26 –38.2(5).

The average N-Ge bond distances observed in the molecular structure of **12** is 1.91 Å and is longer than those reported in analogous aryl silyl amide stabilised germylenes ($\bar{x} = 1.871$ Å). N-Ge-N bond distances vary between *molecule one* and *molecule two* with bond angles of 118.1° and 116.5°, respectively. These angles are significantly more obtuse than the average N-Ge-N bond angle ($\bar{x} = 102.795°$) and to the N-Ge-N bond angle observed in **3** (111.51°).[?,?] This obtuse N-Ge-N bond angle is indicative of heightened reactivity at the germanium(II) centre (as discussed in **chapter 1, section 1.3.2**). The germanium(II) centres assume a pseudo-bent geometries. For all four nitrogen centres, the Si-N-C, Ge-N-C, and Ge-N-Si bond-angles are consistent within themselves, and the silyl substituent lies closer to the Ar^X substituent whilst the germanium(II) centres is angled away from the silyl substituent. It is proposed that the increased angular distance between the germanium(II) centre and silyl

subsistent occurs as to accommodate steric strain within the complexes. The C1-N1-N2-C26 torsion angle of –38.2(5)° shows how the ligands are gauche, presumably to accommodate for steric repulsion between these opposing ligands.

The geometric properties of the ligand are generally as expected. N-Si bond distances are congruous to those reported in structurally characterised bulky aryl silyl amides, and the nitrogen atom adopts a trigonal planar geometry as shown by the sum of its angles (for *molecule one* & *two* the $\overline{x} \sum \approx 360°$). Within the Ar^X aryl moieties of the ligand, for both molecules within the unit cell, there is slight deviation from ideal aromatic geometric character. C-C bonds proximal to the N-C bond are marginally longer ($\overline{x} = 1.42$ Å) than those on the backbone of the aromatic moiety ($\overline{x} = 1.39$ Å), and the central C-C bond distances lie in between these two values ($\overline{x}$ 1.40 Å). Calculated centroids upon the central aromatic of the Ar^X moiety and their average bond angle between the para-positions of the aromatics (C1 and C4, and analogous assignments) ($\overline{x} = 172.875°$) shows a shift from a true plane. This non-ideal plane is perhaps influenced by the steric strain caused by the flanking six-membered carbon rings towards the central aromatic ring.

The chair conformation of the flanking saturated six-membered carbon rings is changed from that which is observed in **12**, adopting the less sterically encumbering conformation for the germanium(II) centre.

Attempted Rational Synthesis of [{Ar^X(TMS)N}$_2$Ge] (12)

Attempts to reproduce **12** were partially successful. The reaction of a 2:1 ratio of **Li-2.14** with GeCl$_2$.dioxane leads to the formation of some new product. This product when isolated is an oily putty-like substance, and by ^{1}H NMR spectroscopic analyses appeared to be **12**. However, the resolution of the obtained spectrum is poor and displays broad shifts making absolute verification difficult without performing temperature-dependent ^{1}H NMR spectroscopic analyses[xlix] . Attempts to crystallise this product were unsuccessful. Due to the disinterest in this compound and the apparent difficulties in its pure isolation of this compound, we did not pursue its synthesis nor characterisation any further.

3.6.5   Coupling to Tin and Lead: An Unexpected Product

Turning our attention to the heavier tetrels, we attempted to form tin and lead halide precursors ({An^X(TMS)N}MX) via salt-metathesis. To accomplish this we used the same method as employed in the synthesis of **11**, as shown in **scheme 3.21**, but what was obtained was not expected.

[xlix]Disinterest in this compound prevented us from exploring it's properties in depth.
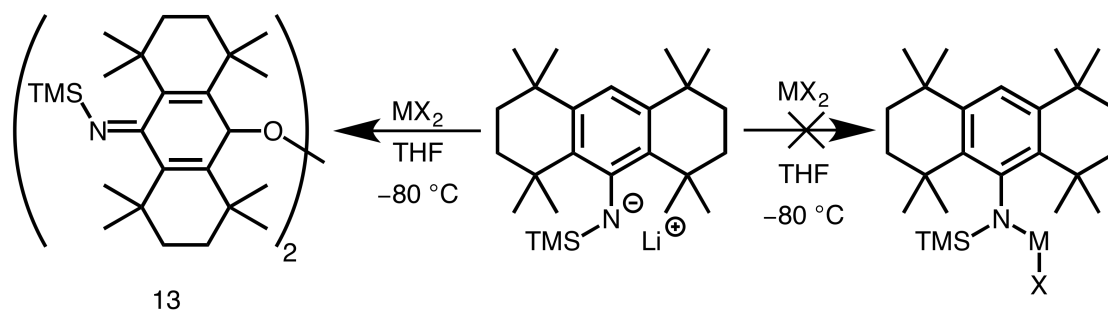
Scheme 3.22: *Attempted synthesis of {Ar^X(TMS)N}MX, the major isolated product from this reactions is [{r-Ar^X(TMS)}O]$_2$ (**13**) (where M = Sn or Pb, X = Cl or Br).*

Upon addition of **Li-2.14** (an orange/red solution) to a THF solution of Sn/PbX$_2$ (colourless), the reaction mixture went from a yellow/orange coloured solution to deep red. Monitoring the reaction by ^{1}H NMR spectroscopic analysis indicated the formation of multiple products which were not identifiable outside of the decomposition products: Ar^X(TMS)NH, Ar^{X}NH$_2$, and the free arene, Ar^X. All attempted reaction conditions led to the formation of complicated reaction mixtures.

In an attempt to elucidate the products of this reaction, fractional crystallisation was employed and eventuated in the isolation of an unexpected redox-product, the dimeric oxygen bridged compound [{r-Ar^X(TMS)}O)$_2$] (**13**) (r-Ar^X(TMS)N peroxide). The crystals obtained were suitable for X-ray diffraction studies (*vide infra*).

The formation of **13** was unexpected and multiple attempts were made to avoid this product, though it was the only isolated product from the reactions. This product was also noted when the reaction was carried out in the absence of donor solvents[1].

---

[1]Diethyl ether was still used during the synthesis of **Li-2.14** but was removed *in vacuo* before addition to the respective tetrel halide.

X-ray Crystallographic Characterisation of [{r-Ar^X(TMS)}O)$_2$] (13)
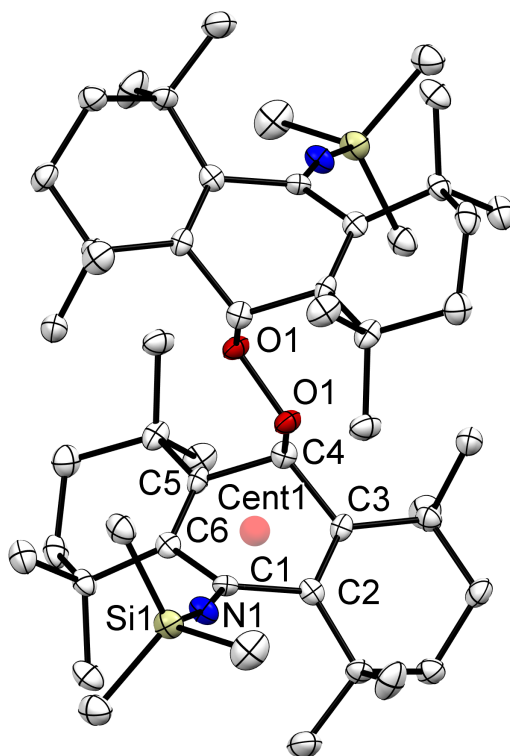
*Figure 3.18: Thermal ellipsoid plot (30% probability surface) of [{r-Ar^X(TMS)}O)$_2$] (**13**) (hydrogen atoms omitted). Selected bond lengths (Å) and angles (°): O1-O1' 1.481(1), O1-C4 1.444(6), N1-C1 1.264(8), N1-Si1 1.679(5), C1-C2 1.501(17), C2-C3 1.315(7), C3-C4 1.528(8), C4-C5 1.517(7), C5-C6 1.327(7), C6-C1 1.525(8); Si1-N1-C1 168.4(4), C4-O1-O1' 104.6(3), Cent1-C4-O1 96.71, C1-Cent1-C4 151.48.*

The molecular structure shown in **figure 3.18** reveals the r-Ar^X(TMS)N peroxide **13** with a centrosymmetric unit cell which contains two halves of the stated molecule. This peroxide appears to be the result of a redox-activated {Ar^X(TMS)N}$^-$ which is then oxidised by adventitious dioxygen (or some other unidentified oxygen source).

Bond angles and distances displayed for the molecular structure of **13** are similar to those observed in characterised imines and peroxides. The N-C bond distance of 1.264(8) Å confirms the presence of the double bond and therefore the presence of the imine functional group.[?] The nitrogen adopts an almost linear geometry between its substituents, with a bond angle of 168.4(4)°. The O1-O1' bond distance of 1.481(1) Å is only marginally longer than observed in hydrogen peroxide (1.474 Å), the bond elongation is due to the steric repulsion between the opposing r-Ar^X(TMS)N imine substituents.[?] The oxygen atoms are essentially perpendicular to the bonded carbon, as shown by the C4-O1-O1' bond angle of 104.6(3)°, more obtuse than the H-O-O bond angle which is observed in hydrogen peroxide (94.8°).

Unsurprisingly, the redox-activated ligand in **13** has an altered geometry compared to that seen in **11** and **12** (*vide supra*). There is an elongation of the terminal C-C bonds of the central ring (C1-C2, C3-C4, C4-C5, and C6-C1), with an average bond length ($\overline{x} = 1.58$ Å) similar to that which is observed between sp^3-sp^2 carbon centres (1.50 Å).[?] The internal/central C-C bonds of the central ring are conversely shortened to lengths similar to a double bond. However, the bond distances expressed for the C-C bonds of the central ring, proximal to the nitrogen centre, do not reflect a sp^3 hybridised carbon centre but a sp^2 hybridised carbon centre.

3.6.6   Closing Remarks

The utilisation of the ligand $\{Ar^X(TMS)N\}^-$ was suitable for germanium(II) chemistry. For the silicon, tin, and lead chemistry performed, no halide or low-oxidation state species could be identified or isolated. It is suggested that the steric strain of the outer saturated six-membered carbon rings influences redox activity of the central aromatic group.

It is proposed that sterically induced redox activity, caused by the steric strain of the outer saturated six-membered carbon rings chair conformation upon the central aromatic ring, occurs within the $\{Ar^X(TMS)N\}^-$ fragment, and is exacerbated during salt-metathesis coupling reactions with silicon, tin, and lead halides. This does not appear to occur with germanium: we speculate that the nitrogen lone-pair preferably donates towards the germanium(II) centre rather then delocalise into the central aromatic, though upon reduction to the respective digermyne, this delocalisation may occur and lead to decomposition.

3.7   R&D: Indacene Amines

Our final forays into tricyclic motif-containing ligands focused on the indacene amines. Discussed in **chapter 2**, the failure to form the indacene silyl amines was a disappointment but it was believed that the amine itself would provide enough steric encumbrance and be useful as a sterically encumbering ligand.

3.7.1   Salt-Metathesis and Protolysis Coupling Attempts

All our attempts to isolate the lithium salt LiInd^{Et}NH failed. Previous work within the group showed the efficacy in the in situ generation of lithium ligand salt congeners and addition of tetrel halides to form halide precursors (general formula: LMX etc.); however, our own analogous attempts failed under various conditions (conditions listed within the **experimental** of this chapter).[?,?]
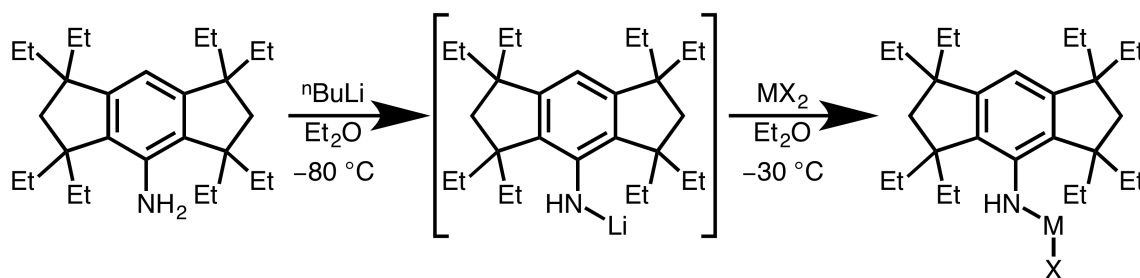
Scheme 3.23: Attempts at in situ generation of LiInd^{Et}NH and salt-metathesis coupling to the heavy group 14 element halides (where M = Ge, Sn, or Pb; X = Cl, Br, or I).

Protolysis coupling between Ind^{Et}NH$_2$ and a range of MR$_2$ species also failed. By ^{1}H NMR spectroscopy it was observed that upon continued heating the reaction mixture decomposed to give a complicated mixture of products.
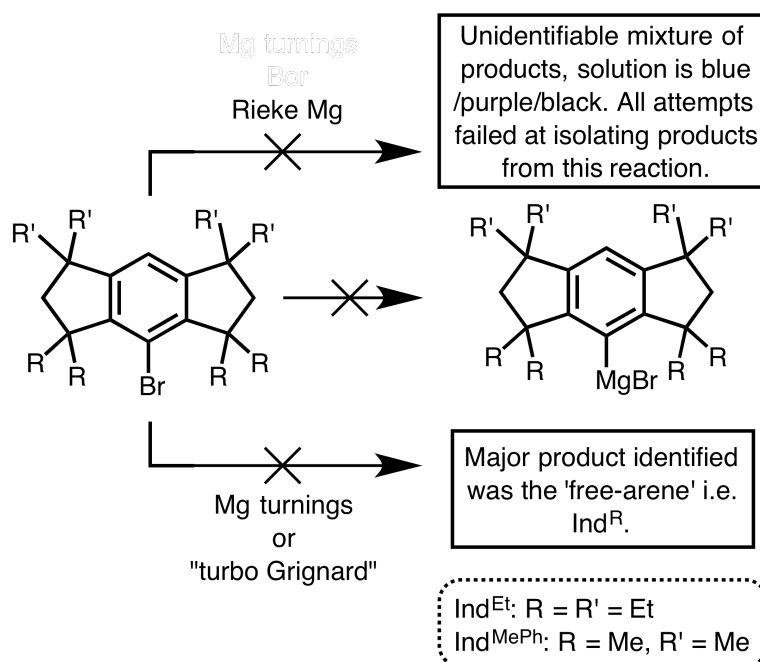
3.7.2 Attempts to Form the Grignard Complexes

Our inability to couple Ind^{Et}NH$_2$ with group 14 element halides via salt-metathesis influenced our decision to attempt the synthesis of the Grignard reagents Ind^{R}MgBr Ind^{Et}N(H)MgBr (where R = Et or MePh). These Grignard reagent were to be used as transmetalation reagents for group 14 chemistry [li].

Multiple synthetic routes were attempted in our pursuit of Ind^{R}MgBr but with no success, as shown in **scheme 3.23**.[?] For routes using magnesium turnings or "turbo Grignards", analysis of the ^{1}H NMR spectrum of the product mixture indicated the reformation of starting material[lii]. When Reike-magnesium was used it was observed that the filtered product mixture was dark blue/purple - akin to the colour of anthryl magnesium in solution. ^{1}H NMR spectroscopic analyses gave no indication for the formation of a major new product and spectra were poorly resolved due to unfiltered magnesium. Multiple filtrations did not improve the ^{1}H NMR spectra resolution. Volatiles were removed *in vacuo* to yield a dark purple/black oil. Attempts to fractionally crystallise and isolate the products from this reaction were unsuccessful and the synthesis was not pursued further. We believe that multiple manipulations may have led to the decomposition of the coloured compound(s), as the blue/purple colour of the solution dissipated over time[liii].

[li]Whilst the direct coupling of sterically encumbering indacenes to a tetrel elements has been described by Matsuo and co-workers, we believed that accessing similar species via the transmetalation pathway would yield the potential to form the heavier tin and lead compounds, finishing the series.

[lii]The "turbo Grignard" utilised was ^{i}PrMgCl.LiCl.[?,?]

[liii]in situ reactions between this product mixture and GeCl$_2$.dioxane, SnBr$_2$, and PbBr$_2$ were conducted. All these reactions gave no discernible results.

Scheme 3.24: Attempted syntheses of the $Ind^R MgBr$ Grignard reagents: all attempts failed or gave inconclusive results.

All attempts to form the Grignard compound were unsuccessful and in each circumstance the only identifiable products determined by ^1H NMR spectrscopic analyses was the starting material $Ind^{Et}NH_2$. The difficulties in synthesising $Ind^{Et}NH_2$ in significant yields led to discontinuation of this synthetic path.

3.7.3   Closing Remarks

The collected data from this series of reactions gives no indication as to why ligation of the amine to a tetrel halide could not be accomplished - or, in the event that a bond did form, remain bonded (stable). We suggest that steric repulsion between the indacene and tetrel element, combined with the relatively weak tetrel-nitrogen bond, prevented ligation. Also, our attempts to form the Grignard indecenes derivatives failed. Any products formed from these reactions are inextricable and probably not worth pursuing using the aforementioned methods.

3.8   Future Work

Tricyclic ligands provide a good framework for sterically rigid ligands. However, based on our preliminary findings, they are still required to provide a degree of "bulk" in order to stabilise low-oxidation state main group centres. Though, generally, the larger tricyclic ligands presented - Ind^R and Ar^X-based ligands - do not allow for the isolation of heavy

group 14 element containing compounds, their smaller counterpart, the anthryl amides, did. These ligands allowed for the isolation of a range of germylenes and stannylenes but did not allow access to the tetrel +I oxidation states.

If the bulk of these tricyclic ligands was to be substantially increased it may be possible to access the +I oxidation states of the group 14 elements. In designing these ligands, we have found that the inclusion of a nitrogen centre may increase the proclivity of internal redox activity at the aryl moiety. It is suggested that elements not bearing a lone-pair be considered as the element donor for future tricylic ligands. By strengthening the ligand-tetrel bond and removing the chance of internal redox activity within the ligand, these ligands should lead to low-oxidation state group 14 element compounds which are more stable than those previously described within the literature.

3.9   Experimental

Synthesis

General Methods [({^{Mes}nacnac}Mg)$_2$],[?] ^{i}PrMgCl.LiCl,[?,?] and Reike-magnesium[?] were prepared by literature procedures. All other reagents were used as received.

For the following reactions, at no point were these reactions performed outside of an inert environment. The presented yields are based on the ^{1}H NMR spectrum for the respective product mixtures. Obtained yields are generally lower by 10 to 30% conversion yield values noted.

An(^{t}Bu)NLi (Li-2.1). To a solution of An^{t}NH (1g, 4.01 mmol) in diethyl ether (Et$_2$O) was added ^{n}BuLi (1.6 M, 2.6 mL, 4.21 mmol) dropwise at –80 °C. The solution was then allowed to stir at room temperature (24 °C for 2 hrs. This solution was used as is for further chemistry or volatiles were removed *in vacuo* to yield a purple/black solid which remained stable at room temperature in an inert atmosphere (yield $\approx$ 95%). ^{1}H NMR (benzene-d$_6$, 400 MHz, 298 K): δ = 0.90 (s, 9H, ^{t}Bu-H), 0.97 (t, JJ^{HH} = 6.87 Hz, 9H, Et$_2$O), 3.17 (q, JJ^{HH} = 7.18 Hz, 6H, Et$_2$O), 7.29 (m, 4H, An-H), 7.88 (s, 1H, *para*-An-H), 7.92 (d, JJ^{HH} = 7.20 Hz, 2H, An-H), 8.46 (d, JJ^{HH} = 7.20 Hz, 2H, An-H); ^{7}Li NMR (benzene-d$_6$, 155 MHz, 298 K): δ = 1.85; ^{13}C{^{1}H} NMR (benzene-d$_6$, 75.5MHz, 298K): δ = 15.63 (Et$_2$O), 34.78 (C(CH$_3$)$_3$), not observed (C(CH$_3$)$_3$), 66.13 (Et$_2$O), 124.88, 125.31, 125.58 131.15, 134.88 (An-C); EI/MS m/z (%): 193.1 (AnNH$^+$, 100), 250.16 (An(^{t}Bu)N$^+$, 67.52).

An(^{t}Bu)NLi(THF) (Li(THF)-2.1). To a solution of An^{t}NH (1g, 4.01 mmol) in THF/hexane was added ^{n}BuLi (1.6 M, 2.6 mL, 4.21 mmol) dropwise at –80 °C. The solution was then allowed to stir at room temperature (24 °C) for 2 hrs: a precipitate forms at this point. The solution was concentrated in vacuo initiating further precipitation, and remaining volatiles were filtered away. The remaining solid was washed with cold hexane, and dried *in vacuo* to give the product as a dark purple solid (yield $\approx$ 75-85%). ^{1}H NMR (benzene-d$_6$, 400 MHz, 298 K): δ = 1.10-1.16 (m, 8H, THF-H), 1.52 (s, 9H, ^{t}Bu-H), 3.12-3.21 (m, 8H, THF-H), 7.04 (t, J$_{HH}$ = 7.71 Hz, 2H, An-H), 7.27-7.31 (m, 2H, An-H), 7.35 (s, 1H, An-*(para-H)*), 7.83 (d, J$_{HH}$ = 8.31 Hz, 2H, An-H), 8.545 (d, J$_{HH}$ = 8.23 Hz, 2H, An-H); ^{7}Li NMR (benzene-d$_6$, 155 MHz, 298 K): δ = 0.56; ^{13}C{^{1}H} NMR (benzene-d$_6$, 75.5MHz, 298K): δ = 25.84 (THF-C), 34.95 (C(CH$_3$)$_3$), 56.13 (C(CH$_3$)$_3$), 68.75 (THF-C), 119.37, 124.14, 125.73, 127.73, 128.70, 135.90, 136.96, 158.65 (An-C, obscured by residual benzene); IR (ATR, Nujol): $\bar{v}$ (cm^{-1} = 764.1 (s), 898.3 (m), 1038.1 (s), 1151.7 (s), 1200.2 (m), 1337.2 (s), 1416.4 (m), 1435.0 (m), 1536.6 (m), 1589.7 (m), 1901.9 (w), 2113.4 (w), 2953.9 (m), 3025.7 (w); EI/MS m/z (%): 193.1 (AnNH$^+$, 100), 248.2 (An(^{t}Bu)N$^+$, 75.56).

An(Cyc)NLi (Li-2.2). To a solution of An(Cyclohexyl)NH (1g, 3.6 mmol) in hexane was added ^{n}BuLi (1.6 M, 2.38 mL, 3.8 mmol) dropwise at –80 °C. The solution was then allowed to stir at room temperature (24 °C) for 2 hrs: a precipitate forms at this point. The solution was concentrated *in vacuo* initiating further precipitation and remaining volatiles

were filtered away. The remaining solid was washed with cold hexane, and dried in *in vacuo* to give the product as a dark purple solid (yield $\approx$ 90%). ^{1}H NMR (benzene-d^6, 400 Hz, 298 K): δ = 1.16-1.19 (m, 10H, THF-*H*), 1.39-1.54 (m, 6H, cyclohexyl-*H*), 1.72-1.75 (m, 1H, cyclcohexyl-*H*), 1.81-1.84 (m, 2H, cyclcohexyl-*H*), 2.11-2.14 (m, 2H, cyclcohexyl-*H*), 3.19 (s (unresolved multiplet), 10H, THF-*H*), 6.86-6.89 (m, 3H, Ar-*H*), 7.25 (t, JJ^{HH} = 7.38 Hz, 2H, Ar-*H*), 7.73 (d, JJ^{HH} = 8.25 Hz, 2H, Ar-*H*), 8.20 (d, JJ^{HH} = 8.10 Hz, 2H, Ar-*H*); ^{7}Li NMR (benzene-d$_6$, 155 MHz, 298 K): δ = 1.79; ^{13}C{^{1}H} NMR (benzene-d$_6$, 75.5MHz, 298K): δ = 25.92 (Cycohexyl-*C*H$_2$), 26.63 (Cycohexyl-*C*H$_2$), 27.94 (Cycohexyl-*C*H$_2$), 38.53 (Cycohexyl-*C*H$_2$), 68.68 (Cycohexyl-*C*H$_2$), 116.68, 124.66, 125.18, 126.17, 126.40, 127.17, 129.82 (Ar-*C*); IR (ATR, Nujol): $\bar{v}$ (cm^{-1} = 760 (s), 890 (m), 1020 (m), 1050 (m), 1150 (m), 1225 (m), 1350 (m), 1410 (m), 1445 (m), 1475 (m), 1500 (w), 1550 (m), 1590 (m), 2925 (m), 2950 (m); EI/MS m/z (%): 193.1 (AnNH$^+$, 100), 276.17 (An(Cyc)NH$^+$, 78.25).

An(^{t}Oct)NLi (Li-2.3). To a solution of An(^{t}Oct)NH (1g, 3.3 mmol) in diethyl ether was added ^{n}BuLi (1.6 M, 2.16 mL, 3.5 mmol) dropwise at –80 °C. The solution was then allowed to stir at room temperature (24 °C) for 5 hrs: a precipitate forms at this point. The solution was concentrated *in vacuo* initiating further precipitation and remaining volatiles were filtered away. The remaining solid was washed with cold hexane, and dried in *in vacuo* to give the product as a red/purple solid (yield $\approx$ 80%). ^{1}H NMR (benzene-d^6, 400 Hz, 298 K): δ = 1.14-1.17 (m, 10H, THF-*H*), 1.21 (br. s, 9H, ^{t}Bu-*H*), 1.55 (br. s, 6H, N-C-(C*H*$_3$)$_2$), 2.14 (s, 2H, C(CH$_3$)$_2$-C*H*$_2$), 3.10-3.13 (m, 10H, THF*H*), 6.97 (br. s, 3H, Ar-*H*), 7.26 (t, JJ^{HH} = 7.20 Hz, 3H, Ar-*H*), 7.77 (d, JJ^{HH} = 8.09 Hz, Ar-*H*), 8.43-8.45 (br. m, 2H, Ar-*H*), (integration indicates an un-identifiable proton within the aromatic region); ^{7}Li (benzene-d$_6$ 155 MHz, 298 K): δ = 0.01 (solvent separated ion due to the presence of THF); ^{13}C {^{1}H} NMR (75.5 MHz, 298K): δ = 32.27 (*C*-(CH$_3$)$_2$), 33.03 (*C*-(CH$_3$)$_2$), 34.68 (C-(*C*H$_3$)$_2$), 57.98 (C(CH$_3$)$_2$-*C*H$_2$), 60.27 (N-*C*-(CH$_3$)$_2$-), 124.93, 125.94, 126.56, 127.58, 128.95, 129.49 (Ar-*C*); EI/MS m/z (%): 194.10 (AnNH$^+$, 100), 306.22 (An(^{t}Oct)NH$^+$, 35.9).

An(Ad)NLi (Li-2.4). To a solution of An(Ad)NH (1g, 3.05 mmol) in hexane was added ^{n}BuLi (1.6 M, 2.0 mL, 3.21 mmol) dropwise at –80 °C. The solution was then allowed to stir at room temperature (24 °C) for 1-2 hrs. The solution was concentrated *in vacuo* initiating further precipitation and remaining volatiles were filtered away. The remaining solid was washed with cold hexane, and dried in *in vacuo* to give the product as a dark purple solid (yield $\approx$ 90%). ^{1}H NMR (benzene-d^6, 400 Hz, 298 K): δ = 1.38-1.43 (m, 6H, AdC*H*$_2$), 1.47-1.50 (m, 6H, AdC*H*$_2$), 1.67 (br. s, 3H, AdC*H*$_2$), 7.29 (br. s, 4H, Ar-*H*), 7.86-7.90 (m, 2H, Ar-*H*), 8.50 (br. s, 1H, Ar-*H*); ^{7}Li (benzene-d$_6$ 155 MHz, 298 K): δ = 2.19 (when generated in diethyl ether), 0.73, 1.128, 2.00 (when generated in THF, multiple signals due to solvation and aryl interactions); ^{13}C {^{1}H} NMR (75.5 MHz, 298K): *Under all conditions the respective NMR spectrum could not be obtained. The spectrums obtained were of a too low resolution for interpretation.*; EI/MS m/z (%): 135.12 (Ad$^+$, 50.3), 328.21 (An(Ad)NH$_+$, 78.3), 194.10 (AnNH$^+$, 100).˙

An(C1)NLi (Li-2.5). To a solution of An(C1)NH (1g, 3.36 mmol) in THF was added ^{n}BuLi (1.6 M, 2.21 mL, 3.53 mmol) dropwise at –80 °C. The solution was then allowed to stir at room temperature (24 °C) for 1 hr. Volatiles were removed *in vacuo* to leave a viscous purple solid. A small volume of hexane was added to this solid and the mixture

was heated with a hairdryer for 2 minutes. Volatiles were removed *in vacuo*, again, to ensure all THF was removed. The product was then washed with cold hexane. A solid may form at this stage; if it does not, the reaction vessel was dipped into liquid nitrogen until the viscous solid hardened. Carefully, using a spatula, the solid is crushed as much as possible before vacuum is reapplied. This is repeated until the product forms a powder which can be easily removed from the vessel (yield $\approx$ 60-75%). ^{1}H NMR (benzene-d$_6$, 400 MHz, 298 K): δ = 1.855 (d, J_{HH} = 6.52 Hz, 3H, C(H)(Ph)-CH_3), (q, J_{HH} = 6.33 Hz, 1H, C(Ph)(CH$_3$)-H), 7.06 (t, J_{HH} = 8.33 Hz, 2H, Ar-H), 7.38-7.41 (m, 1H, Ar-H), 7.47-7.56 (m, 4H, Ar-H), 7.94-8.00 (m, 4H, Ar-H), 8.50 (d, J_{HH} = 8.10 Hz, 2H, An-H); ^{7}Li NMR (155 MHz, 298 K): δ =–0.11; ^{13}C $\{^1$H$\}$ NMR (75.5 MHz, 298K): δ = 28.33 (CH), 59.11 (C(CH$_3$), 98.64, 116.59, 120.15, 126.23, 126.34, 126.95, 127.06, 127.52, 129.39, 138.52, 151.36, 159.42; EI/MS m/z (%): 135.12 (Ad$^+$, 16), 194.10 (AnNH$^+$, 1.25), 328.21 (M$^+$, 100).

An(C2)NLi (Li-2.6).. To a solution of An(C2)NH (1g, 2.88 mmol) in THF was added ^{n}BuLi (1.6M, 1.89 mL, 3.02 mmol) dropwise at –80 °C. The solution was then allowed to stir at room temperature (24 °C) for 1 hrs. Volatiles were removed *in vacuo* to leave a viscous purple solid. A small volume of hexane was added to this solid and the mixture was heated with a hairdryer for 2 minutes. Volatiles were removed *in vacuo*, again, to ensure all THF was removed. The product was then washed with cold hexane. A solid may form at this stage. If it does not, the reaction vessel was dipped into liquid nitrogen until the viscous solid hardened. Carefully, using a spatula, the solid is crushed as much as possible before vacuum is reapplied. This is repeated until the product forms a powder which can be easily removed from the vessel (yield $\approx$ 50-75). *Note: all obtained spectra were of too poor a resolution to make definite assignments. Though, for the ^{1}H NMR spectrum it was observed that no chemical shifts were present in the expected NH chemical shift region.*

An(^{t}BuNLi)$_2$ (Li-2.11). To a solution of An(^{t}BuNH)$_2$ (1g, 3.12 mmol) in hexane was added ^{n}BuLi (1.6M, 2.05 mL, 3.28 mmol) dropwise at –80 °C. The solution was then allowed to stir at room temperature (24 °C) for 2-3 hrs. The solution was concentrated *in vacuo* initiating further precipitation and remaining volatiles were filtered away. The remaining solid was washed with cold hexane, and dried *in vacuo* to give the product as a black/purple solid (yield $\approx$ 85%). ^{1}H NMR (benzene-d$_6$, 400 MHz, 298 K): δ = 1.30-1.33(m, 32H, THF-H), 1.46 (s, 18H, ^{t}Bu-H), 3.46-3.49 (m, 32H, THF-H), 6.98-7.01 (m, 4H, An-H), 7.31 (t, J_{HH} = 7.36 Hz, 4H, An-H), 7.90 (d, J_{HH} = 8.24 Hz, 4H, An-H), 8.47-8.49 (m, 4H, An-H)(Note: Unidentifiable shift at 8.61 ppm, broad singlet, which intergrates to 4H.); 7Li NMR (155 MHz, 298 K): δ = 0.94, .198; ^{13}C$\{^1$H$\}$ NMR (benzene-d$_6$, 75.5MHz, 298K): δ = 25.99 (THF-C), 35.64 (C-(CH$_3$)$_3$), 58.14 (C-(CH$_3$)$_3$), 68.86 (THF-C), 124.55, 125.33, 127.18, 135.87 (An-C); IR (ATR, Nujol): $\bar{v}$ (cm^{-1}) = 678 (s), 736 (s), 780 (s), 879 (m), 907 (m), 952 (m), 1067 (s), 1209 (m), 1360 (m), 1388 (m), 1449 (m), 1595 (m), 1627 (m), 1671 (w), 2864 (m), 2931 (m), 2967 (m), 3062 (w).

{r-An(^{t}Bu)N}SiBr$_3$ (1). To a THF solution of SiBr$_4$ (3.92mmol) was added a THF solution of An(^{t}Bu)NLi (1g, 3.92 mmol) dropwise at –80 °C. The solution was then allowed to stir at room temperature (24 °C) for 12 hrs (overnight). Volatiles were removed *in vacuo* and the residue extracted in toluene. The solution was concentrated and placed in a –30 °C freezer overnight. Fractional crystallisation led to the isolation of a number of crystals,

picked yellow/orange crystals were found to be the title compound. (*All assignments are tentative and based on the extracted reaction mixture.*) ^{1}H NMR (benzene-d$_6$, 400 MHz, 298K): δ = 0.89 (s, 9H, N-(CH_3)$_3$), 3.67 (s, 1H, NH), 7.82-7.85 (m, 4H, Ar-H), 8.24-8.62 (m, 2H, Ar-H), 8.85-8.88 (m, 2H, Ar-H).

{r-An(Cyc)N}SiCl$_3$ (2). To a THF solution of SiCl$_4$ (3.55 mmol) was added a THF solution of An(Cyc)NLi (1g, 3.55 mmol) dropwise at –80 °C. The solution was then allowed to stir at room temperature (24 °C) for 12 hrs (overnight). Volatiles were removed *in vacuo* and the residue extracted in hexane. The solution was concentrated and placed in a –30 °C freezer overnight. Fractional crystallisation led to the isolation of a number of crystals. A single yellow/orange crystal was found to be the title compound.

[An(^{t}Bu)N}$_2$Ge] (3). To a diethyl ether solution of GeCl$_2$.dioxane (0.56g, 3.92mmol) was added a diethyl ether solution of An(^{t}Bu)NLi (1g, 3.92 mmol), dropwise at –80 °C. This solution was allowed to stir and warm to room temperature over 2 hours (stirring overnight was found to decrease yields due to decomposition). Volatiles were removed *in vacuo* and the remaining residue extracted in hexane. The hexane solution was concentrated and placed in a –30 °C freezer overnight to stimulate crystallisation and precipitation of the compound (and trace minor products). The compound was isolated as an orange powder which contained orange/yellow needle like crystals (yield $\approx$ 75%). M.p.: 135.6-137.4 °C; ^{1}H NMR (benzene-d$_6$, 75.5 MHz, 298 K): δ = 1.31 (s, 9H, ^{t}Bu-H), 6.77 (t, J$_{HH}$ = 7.66 Hz, 2H, Ar-H), 7.04 (t, J$_{HH}$ = 8.15 Hz, 2H, Ar-H), 7.11 (s, 1H, Ar-H), 7.30 (d, J$_{HH}$ = 8.63 Hz, 2H, Ar-H), 7.81 (d, J$_{HH}$ = 8.85 Hz, 2H, Ar-H); ^{13}C {^{1}H} NMR (75.5 MHz, 298K): δ = 35.75 (C(-CH$_3$)$_3$), 61.50 (C-CH$_3$)$_3$), 123.47, 124.35, 124.70, 126.15, 129.04, 130.33, 131.84, 146.34 (Ar-C); EI/MS m/z (%): 249.2 (LH, 50%), 193.2 (AnNH$_2$, 100%), 57.2 (^{t}Bu$^-$, 10%).

[An(Ad)N}$_2$Ge]. To a diethyl ether solution of GeCl$_2$.dioxane (0.33g, 1.50 mmol) was added a diethyl ether solution of An(Ad)NLi (1.00g, 3.00 mmol), dropwise at –80 °C. This solution was allowed to stir and warm to room temperature over 2 hours (stirring overnight was found to decrease yields due to decomposition). Volatiles were removed *in vacuo* and the remaining residue extracted in hexane. Volatiles were removed from the extract to yield a yellow/red solid which was found to be a mixture of the aforementioned product and pro-ligand. (yield $\approx$ 70%). *Note: the following analyses are tenuously assigned.* °C; ^{1}H NMR (benzene-d$_6$, 400 MHz, 298 K): δ = 1.32(m, 6H, Ad-CH_2), 1.74 (s, 6H, Ad-CH_2), 1.78 (s, 3H, Ad-CH), 6.86 (t, J$_{HH}$ = 7.63, 2H, Ar-H), 7.22-2.35 (m, 2H, Ar-H), 7.77 (s, 2H, Ar-H), 7.99 (d, J$_{HH}$ = 8.27, 2H, Ar-H), 8.13 (s, 1H, Ar-H); ^{13}C{^{1}H} NMR (benzene-d$_6$, 75.5MHz, 298K): δ = 31.81, 36.86, 45.55, 58.54 (Ad-C), 123.33, 124.20, 124.69, 126.07, 130.08, 131.79 (Ar-C).

[An(^{t}Bu)NH$_2$][GeCl$_3$] (4). The title compound was isolated as a single crystal from a product mixture (from the 1:1 stoichiometry reaction of **Li-2.1** and GeCl$_2$.dioxane) which had been allowed to stand over the period of approximately two weeks. No attempts were made to target this compound.

{An(^{t}Bu)N}SnBr$_2$●Li(THF)$_2$ (5). To a THF solution of SnBr$_2$ (1.1g, 3.92mmol) was added An(^{t}Bu)NLi (1g, 3.92 mmol) as a THF solution, dropwise at –80 °C. The solution

was then allowed to stir at room temperature (24 °C) for 12 hrs (overnight). Volatiles were removed *in vacuo* and the residue extracted in toluene. Volatiles were removed *in vacuo* and hexane was added. The solution was stirred at –30 °C to afford a mixture of crystalline material and a powdery solid. The title compound was handpicked away from the mixture as red crystals. ^{1}H NMR (benzene-d_6, 400 MHz, 298 K): δ = 1.45-1.48 (m, 8H, THF-*H*), 1.77 (s, 9H, [t]Bu-*H*), 3.61-3.64 (m, 8H, THF-*H*),7.93 (d, J_{HH} = 8.62 Hz, 2H, An-*H*), 7.34-7.46 (m, 4H, An-*H*), 8.15 (s, 1H, An-*(para-H)*), 9.36 (d, J_{HH} = 8.86 Hz, 2H, An-*H*), (Note: four un-identified shifts: 1.16 (s,1H),1.24 (s,4H), 6.82 (t, J_{HH} = 7.22 Hz, 1H), 7.875 (d, J_{HH} = 8.85 Hz, 1H.) Too little of the title complex was isolated for further characterisation; all attempts at repeating the synthesis led to the formation of {An([t]Bu)N}$_2$Sn.

[{O-*r*-An([t]Bu)N}$_2$(μ-SnBr)$_2$] (6). The title compound was isolated as a single crystal from the repeated synthesis of **5**. The yield of the title complex was too low for further characterisation.

{An([t]Bu)N}$_2$Sn (7). To a solution of SnBr$_2$ (0.55g, 1.96 mmol) in diethyl ether was added An([t]Bu)NLi (1g, 3.92 mmol) as a diethyl ether solution, dropwise at –80 °C. The solution was then allowed to stir at room temperature (24 °C) for 12 hrs (overnight). Volatiles were removed *in vacuo* and the residue extracted in toluene. Volatiles were removed *in vacuo* and hexane was added. The solution was stored at –30 °C to afford the title compound as a red/orange powder. Red crystals were obtained from a concentrated solution of toluene (yield $\approx$ 70-80%). °C; ^{1}H NMR (benzene-d_6, 400 MHz, 298 K): δ1.19 (s, 9H, [t]Bu-*H*), 6.75-6.79 (m, 4H, An-*H*), 7.06-7.08 (m, 4H, An-*H*), 7.11 (s, 2H, An-*(para-H)*), 7.34 (d, J_{HH} = 8.46 Hz, 4H, An-*H*), 7.82 (d, J_{HH} = 8.79 Hz, 4H, An-*H*); [13]C {[1]H} (benzene-d_6, 75.5MHz, 298K): δ = 36.84 (C-(*CH_3*)$_3$), 62.08 (*C*-(CH$_3$)$_3$), 123.46, 124.43, 124.51, 125.69, 129.42, 130.90, 131.75, 148.35 (An-*C*); ^{119}Sn{^{1}H} NMR (benzene-d[6], 149 MHz, 273 K): δ = not observed IR (ATR, Nujol): $\bar{v}$ (cm^{-1}) = 799, 1020, 1261, 1379, 1577, 1615, 1694, 1732, 2352, 2854, 2924, 2958, 3744, 3832; EI/MS m/z (%): 614.3 (An([t]Bu)N}$_2$Sn$^+$, <1%), 367.1 (An([t]Bu)N}Sn$^\bullet$, 1%) 248.2 (An([t]Bu)N$^-$, 80%); 193.2 (AnNH$_2$$^+$, 100%), 57.2 ([t]Bu$^-$, 10%).

{An(Ad)N}$_2$Sn (8). To a solution of SnBr$_2$ (0.84g, 3.00 mmol) in diethyl ether was added An(Ad)NLi (1.00 g, 3.00 mmol) as a diethyl ether solution, drop-wise at –80 °C. The solution was then allowed to stir at room temperature (24 °C) for 2 hrs. (Longer periods were believed to increase decomposition, leading to higher yields of pro-ligand.) Volatiles were removed *in vacuo* and the residue extracted in toluene. Volatiles were removed *in vacuo* and hexane was added. The solution was stored at –30 °C to afford the title compound as a red/orange powder. Red crystals were obtained from a concentrated solution of toluene (yield $\approx$ 70%). ^{1}H NMR (benzene-d_6, 400 MHz, 298 K): δ = 1.32 (s, 12H, Ad-C*H_2*), 1.73 (br. s, 6H, Ad-C*H*), 2.14 (s, 12H, Ad-C*H_2*), 6.85 (t, J_{HH} = 7.79 Hz, 4H, Ar-*H*), 7.06-7.09 (m, 4H, Ar-*H*), 7.13 (s, 2H, Ar-*H*), 7.34 (d, J_{HH} = 8.81 Hz, 4H, Ar-*H*), 7.95 (d, J_{HH} = 8.94 Hz, 4H, Ar-*H*); ^{13}C{^{1}H} NMR (benzene-d_6, 75.5 MHz, 298 K): δ = 31.84, 36.88, 48.58 (Ad*C*), 123.37, 124.24, 126.48, 129.01, 130.86, 131.85 (Ar-*C*); ^{119}Sn{^{1}H} NMR (benzene-d[6], 149 MHz, 273 K): δ = not observed Anal. Calc. (%) for C$_{48}$H$_{48}$N$_2$Sn: C, 74.72; H, 6.27; N, 3.63; found (%): C, 74.59; H, 6.36; N, 3.78.

{An([t]Oct)N}$_2$Sn (9). To a solution of SnBr$_2$ (0.94g, 3.36 mmol) in diethyl ether was

added An(^{t}Oct)NLi (1.00 g, 3.36mmol) as a diethyl ether solution, dropwise at –80 °C. The solution was then allowed to stir at room temperature (24 °C) for 2-3 hrs. Longer periods are believed to increase decomposition, leading to higher yields of pro-ligand. Volatiles were removed *in vacuo* and the residue extracted in toluene. Volatiles were removed *in vacuo* and hexane was added. The solution was stored at –30 °C to afford the title compound as a red/orange powder. Red crystals were obtained from a concentrated solution of toluene (yield ≈ 60-75%). ^{1}H NMR (benzene-d$_6$, 400 MHz, 298 K): δ = 0.90 (s, 12H, N(H)-C-(CH_3), 1.12 (s, 18H, CH$_2$-^{t}Bu(H_9)), 2.52 (s, 2H, -C(CH$_3$)$_2$-CH_2-), 6.81-6.85 (m, 4H, Ar-H), 7.08-7.12 (m, 4H, Ar-H), 7.36 (d, J$_{HH}$ = 8.24 Hz, 4H, Ar-H), 7.88 (d, J$_{HH}$ = 8.59 Hz, 4H, Ar-H) (Could not observe the Ar-(*para-H* proton); ^{13}C{^{1}H} NMR (benzene-d$_6$, 75.5 MHz, 298 K): δ = = 30.99 (C-(CH$_3$)$_2$), 33.29 (C-(CH$_3$)$_2$), 33.99 (C-(CH$_3$)$_2$), 58.94 (C(CH$_3$)$_2$-CH$_2$), 66.94 (N-C-(CH$_3$)$_2$-), 123.58, 124.06, 124.92, 125.88, 126.59, 129.58, 131.63, 131.99, 227.63 (Ar-C).

Reaction of An(^{t}Bu)NLi and PbBr$_2$. To a solution of PbBr$_2$ in diethyl ether was An(^{t}Bu)NLi, as a diethyl ether solution, dropwise at –80 °C. The solution was then allowed to stir at room temperature (24 °C) for 12 hrs (overnight). Volatiles were removed *in vacuo* and the residue extracted in toluene. Volatiles were removed *in vavcuo* and hexane was added. analyses of the ^{1}H NMR spectrum indicates the formation of some backbone anthracene activated compounds: it is proposed that a lead compound, analogous to {r-An(cyclohexyl)N}SiCl$_3$, is the major product of this reaction. All attempts at isolation were futile.

[{An((^{t}Bu)N)$_2$}$_2$Sn$_2$] (10). To a THF solution of SnBr$_2$ (0.84g, 3.01 mmol) was added a THF solution of An(^{t}BuNLi)$_2$ (1g, 3.01 mmol) at –80 °C. This solution was allowed to stir to room temperature over a period of two hrs. Volatiles were removed *in vacuo* and the residue extracted with hexane and minimal toluene. The extracted solution was concentrated *in vacuo* before being placed in a –30 °C freezer. Over the period of one to four days, precipitation occurs with the concurrent formation of crystals, which are predominantly the title compounds (yield ≈ 70%). °C; ^{1}H NMR (benzene-d$_6$, 400 MHz, 298 K): δ1.55 (s, 36H, ^{t}Bu-H), 7.26-7.39 (m, 8H, An-H), 7.81 (s, 4H, An-H), 9.12 (s, 4H, An-H); ^{13}C {^{1}H} (benzene-d$_6$, 75.5MHz, 298K): δ = 25.82 (C-(CH$_3$)$_3$), 68.87 (C-(CH$_3$)$_3$), 124.47, 125.51, 125.52, 133.49 (An-C); EI/MS m/z (%): 369.2 (LSnH - (^{t}BuNH), 12%), 249.1 (LH - (^{t}BuNH), 8%), 193.1 (AnNH$_2$, 100%), 179.2 (AnH, 90%), 57.1 (^{t}Bu$^-$, 5%); Anal. Calc. (%) for C$_{44}$H$_{52}$Sn$_2$N$_2$: C, 60.44; H, 5.99; N, 6.41; found (%): C, 60.69; H, 5.80; N, 3.24.

Ar^X(TMS)NLi (Li-2.14). To a diethyl ether and hexane solution (25:75) of Ar^X(TMS)NH (1.00g, 2.6 mmol) was added ^{n}BuLi (1.6M, 1.78 mL, 2.85 mmol) dropwise at –80 °C. The solution was then allowed to stir at room temperature (24 °C) for 1-3 hrs. Ar^X(TMS)NLi was typically not isolated as a crystalline solid or otherwise due to its instability. It was primarily used in situ for further chemistry (yield by ^{1}H NMR spectroscopic analysis ≈ 75-80%). (^{1}H NMR is tentatively assigned: obtained spectrum had poor resolutions and contained some pro-ligand i.e. Ar$_X$(TMS)NH.) ^{1}H NMR (benzene-d$_6$, 400 MHz, 298 K): δ = 0.57 (s, 9H, Si(CH_3)$_3$), 1.28 (br. s, 6H, Et$_2$O-(CH_3)$_2$), 1.32 (s, 4H, CH_2), 1.34 (s, 6H, CH_3), 1.48 (s, 6H, CH_3), 1.52 (s, 4H, CH_2), 1.81 (s, 6H, CH_3), 1.85 (s, 6H, CH_3), 3.16 (br. s, 4H, Et$_2$O-(CH_2), 6.76 (s, 1H, Ar-H).

{Ar^X(TMS)N}GeCl (11). To a THF solution of GeCl$_2$.dioxane (0.373g, 2.6 mmol) was added a THF solution of Ar^X(TMS)NLi (2.6 mmol) at –80 °C. This solution was allowed to stir to room temperature over a period of two hrs and then left to stir for a further 12 hours (overnight). Volatiles were removed *in vacuo* and the residue extracted with hexane. The extracted solution was concentrated *in vacuo* before being placed in a –30 °C freezer. From this solution crystals of the title compound grew with the concurrent formation of some precipitate, which also corresponded to the title compound (yield ≈ 75%). ^{1}H NMR (benzene-d$_6$, 400 MHz, 298 K): δ = 0.63 (s, 9H, Si(CH_3)$_3$), 1.10-1.15 (m, 2H, CH_2), 1.19 (s, 6H, CH_3), 1.29 (s, 12H, C(CH_3)$_2$), 1.31 (m, 2H (obscured), CH_2), 1.62 (s, 6H, CH_3), 1.70-1.83 (m, 4H, CH_2), 7.33 (s, 1H, Ar-H);^{13}C{^{1}H} NMR (benzene-d$_6$, 75.5 MHz, 298 K): δ = 6.39 (Si(CH$_3$)$_3$), 31.06 (CH$_3$), 34.23 (CH$_3$), 34.35 (C(CH$_3$)$_2$), 35.05 (C(CH$_3$)$_2$), 36.63 (CH$_2$), 42.55 (CH$_2$), 128.51, 128.75, 143.27, 144.52, 145.59 (Ar-C); ^{29}Si {^{1}H} NMR (benzene-d$_6$, 80 MHz, 298 K): δ = 4.31; IR (ATR, Nujol): $\bar{v}$ (cm^{-1}) = 845 (s), 990 (m), 1235 (w), 1250 (w), 1350 (w), 1590 (w), 2850 (m), 2900 (m), 2950 (m); EI/MS m/z (%): 493.3 (M$^+$, 4.4%), 458.3 (M$^+$–Cl, 2.2%), 385.7 (Ar^X(TMS)NH, 15%, 314.1 (Ar^{X}NH$_2$, 48.4%), 298.3 (Ar^X, 100%).

[{Ar^X(TMS)N}$_2$Ge] (12). Single crystals of the title compound were isolated from our attempted reduction of {Ar^X(TMS)N}GeCl using the reductant [({^{Mes}nacnac}Mg)$_2$]. The crystals appeared as red/yellow blocks. Too little of the title compound was isolated for further characterisation. All attempts to target this compound have been as-of-yet unsuccessful.

[{r-Ar^X(TMS)}O]$_2$ (13). Obtained from the reaction of Ar^X(TMS)NLi with SnX$_2$ and PbX$_2$ halides. This reaction was conducted under an atmosphere of dried nitrogen gas and repeated under dried argon gas with doubly distilled THF. The crystals obtained of the compound were red and needle-like in shape.

Attempted synthesis of Ar^{X}Br. The following are the routes attempted to synthesise the title compound. All attempts showed no indication for the formation of Ar^{X}Br.

1. To a dichloromethane solution of Ar^X was added bromine, dropwise at 0 °)C over five minutes. After 30 minutes the solution was analysed by ^{1}H NMR spectroscopy: no reaction was noted. This solution as then allowed to warm to room temperature an stir overnight; again, no change was noted when analysed. Attaching a reflux-condener to the reaction vessel and heating the solution for 2 hours did not initiate a reaction. More bromine was added but did not lead to any change.

2. To triethyl phosphate solution of Ar^X was added 8 equivalents of bromine. The mixture was placed in a some-what pressure stable vessel, which was then foiled over. This solution was heated at 100 °C for one to three days. There was no evidence for the formation of the title compound nor for any reaction to have taken place.

Attempted synthesis of Ind^{Et}N(H)MX (where M = Ge, Sn, or Pb; and X = Cl or Br). The following is the general reaction routes attempted to synthesise the title compound. All attempts showed no indication for the formation of X, unless otherwise stated.

1. Ind^{Et}NH$_2$ was dissolved in a solution of THF and hexane and ^{n}BuLi was added dropwise at –80 °C (*solution 1*). This solution was allowed to stir for approximately 30

minutes and warm to –30 °C before being transferred to a THF solution of MX_2 (*solution 2*). *Solution 1* was monitored by ^{1}H NMR spectroscopy immediately after the addition of ^{n}BuLi, though no discernible information was forthcoming other than some reaction had occurred. *Solution 2* was monitored twice by ^{1}H NMR spectroscopy, once immediately after the addition of *solution 1* and again after 30 minutes of stirring at 0 °C. At all stages ^{1}H NMR spectroscopic analyses indicated the formation of convoluted product mixtures. Volatiles were removed *in vacuo* from *solution 2* after 1-2 hours of stirring at 0 to 24 °C, yielding an off-white solid. This solid was analysed by ^{1}H NMR spectroscopy but gave no discernible results.

2. As above, with the substitution of ^{n}BuLi with ^{t}BuLi.

Attempted synthesis of Ind^{R}MgBr The following is the general reaction routes attempted to synthesise the title compound. All attempts showed no indication for the title compound, unless otherwise stated.

1. The following was carried out in a Schlenk reflux apparatus. To magnesium turning in ether, which had been activated iodine, was added an ether solution of Ind^{R}Br dropwise. This solution was warmed until reflux begun. Over a period of 2 hours heat was applied to instigate self-sufficient refluxing conditions. After approximately 6 hours the mixture was analysed by ^{1}H NMR spectroscopy and found to contain primarily unreacted start materials (other species were intractable and could not be identified). Allowing the reaction to proceed overnight, being kept at approximetly 35-50 °C, did not make any significant difference.

2. The following was done in a schlenck reflux apparatus. In situ generated "turbo Grignard" (^{i}PrMgCl.LiCl), in diethyl ether, was reacted with a diethyl ether solution of Ind^{R}Br. The procedure was as stated above.

3. Reike-magnesium was generated in situ before a toluene solution of the title compound was added dropwise. Addition was conducted at –80 °C and allowed to stir up to room temperature. Monitoring the reaction by ^{1}H NMR spectroscopy indicated multiple species had been formed from this reaction, though the resolution was low due to unfiltered colloidal magnesium. The solution was extracted away from the colloidal magnesium and was a dark black/blue/purple solution. analyses of this solution did not give anymore information than the prior analyses. Removing the solvent *in vacuo* gives an oily substance and displays the same ^{1}H NMR spectrum. All attempts to crystallise any products from these reactions was unsuccessful. This reaction was re-attempted under heating conditions which led to the same results.

Attempted synthesis of Ind^{Et}N(H)MgBr The following is the general reaction routes attempted to synthesise the title compound. All attempts showed no indication for the formation of the title compound, unless otherwise stated.

1. As stated above for **Ind^{R}MgBr**.

Bibliography

[1] C. Jones and G. A. Koutsantonis, "Modern Main Group Chemistry: From Renaissance to Revolution," *Australian Journal of Chemistry*, vol. 66, no. 10, pp. 1115–1117, 2013.

[2] P. Atkins and T. Overton, *Shriver and Atkins' Inorganic Chemistry*. Oxford University Press, USA, 2010.

[3] S. J. Bonyhady, D. Collis, G. Frenking, N. Holzmann, C. Jones, and A. Stasch, "Synthesis of a Stable Adduct of Dialane $(4)(Al_2H_4)$ via Hydrogenation of a Magnesium (I) Dimer," *Nature Chemistry*, vol. 2, no. 10, p. 865, 2010.

[4] H. E. Ramsden, "Magnesium and Tin Derivatives of Fusedring Hydrocarbons and the Preparation Thereof," Nov. 21 1967. US Patent 3,354,190.

[5] B. Bogdanovic, "Magnesium Anthracene Systems and their Application in Synthesis and Catalysis," *Accounts of Chemical Research*, vol. 21, no. 7, pp. 261–267, 1988.

[6] S. P. Green, C. Jones, and A. Stasch, "Stable Magnesium (I) Compounds with Mg-Mg Bonds," *Science*, vol. 318, no. 5857, pp. 1754–1757, 2007.

[7] J. Li, C. Schenk, C. Goedecke, G. Frenking, and C. Jones, "A Digermyne with a Ge–Ge Single Bond that Activates Dihydrogen in the Solid state," *Journal of the American Chemical Society*, vol. 133, no. 46, pp. 18622–18625, 2011.

[8] T. J. Hadlington, M. Hermann, J. Li, G. Frenking, and C. Jones, "Activation of H_2 by a Multiply Bonded Amido–Digermyne: Evidence for the Formation of a Hydrido–Germylene," *Angewandte Chemie International Edition*, vol. 52, no. 39, pp. 10199–10203, 2013.

[9] J. Li, S. Merkel, J. Henn, K. Meindl, A. Döring, H. W. Roesky, R. S. Ghadwal, and D. Stalke, "Lewis-Base-Stabilized Dichlorosilylene: a Two-Electron σ-Donor Ligand," *Inorganic Chemistry*, vol. 49, no. 3, pp. 775–777, 2009.

[10] R. S. Ghadwal, H. W. Roesky, S. Merkel, and D. Stalke, "Ambiphilicity of Dichlorosilylene in a Single Molecule," *Chemistry–A European Journal*, vol. 16, no. 1, pp. 85–88, 2010.

[11] T. J. Hadlington, M. Driess, and C. Jones, "Low-Valent Group 14 Element Hydride Chemistry: Towards Catalysis," *Chemical Society Reviews*, vol. 47, no. 11, pp. 4176–4197, 2018.

[12] A. F. Richards, A. D. Phillips, M. M. Olmstead, and P. P. Power, "Isomeric Forms of Divalent Heavier Group 14 Element Hydrides: Characterization of Ar'(H)GeGe(H)Ar 'and Ar '(H) 2GeGeAr '•PMe$_3$ (Ar '= C_6H_3-2,6-Dipp$_2$; Dipp= C_6H_3-2,6-Pr$^i_2$)," *Journal of the American Chemical Society*, vol. 125, no. 11, pp. 3204–3205, 2003.

[13] J. Schneider, C. P. Sindlinger, K. Eichele, H. Schubert, and L. Wesemann, "Low-Valent Lead Hydride and Its Extreme Low-Field ^{1}H NMR Chemical Shift," *Journal of the American Chemical Society*, vol. 139, no. 19, pp. 6542–6545, 2017.

[14] T. Hadlington, "Investigations Toward the Catalytic Application of Low-Oxidation State, Low-Coordinate Heavier Group 14 Complexes," *PhD. Thesis*.

[15] J. Kelly, "Synthesis and Reactivity of Novel Low Oxidation State Tetrel Compounds Utilising Bulky Amide Ligands," *PhD. Thesis*.

[16] A. Sekiguchi, S. S. Zigler, R. West, and J. Michl, "A Synthon for the Silicon-Silicon Triple Bond," *Journal of the American Chemical Society*, vol. 108, no. 14, pp. 4241–4242, 1986.

[17] A. Velian and C. C. Cummins, "Facile Synthesis of Dibenzo-7λ3-Phosphanorbornadiene Derivatives using Magnesium Anthracene," *Journal of the American Chemical Society*, vol. 134, no. 34, pp. 13978–13981, 2012.

[18] H. Appler, L. W. Gross, B. Mayer, and W. P. Neumann, "Die Chemie der Schweren Carben-Analogen $R_2M|$, M= Si, Ge, Sn: IX. Eigenschaften und Thermolyse Von neuen 7-Silabicyclo [2.2.1] Heptadienen," *Journal of Organometallic Chemistry*, vol. 291, no. 1, pp. 9–23, 1985.

[19] M. Yamashita, H. Murakami, T. Unrin-in, A. Kawachi, K.-y. Akiba, and Y. Yamamoto, "Synthesis and Structure of a Germylene Bearing a 1,8-Dimethoxyanthracene Ligand," *Chemistry Letters*, vol. 34, no. 5, pp. 690–691, 2005.

[20] J. Binder, R. C. Fischer, M. Flock, A. Torvisco, and F. Uhlig, "Novel Aryl Substituted Silanes Part I: Synthesis and Characterization of Diaryl Silicon Dichlorides," *Phosphorus, Sulfur, and Silicon and the Related Elements*, vol. 190, no. 11, pp. 1980–1993, 2015.

[21] A. Velian, W. J. Transue, and C. C. Cummins, "Synthesis, Characterization, and Thermolysis of Dibenzo-7-dimethylgermanorbornadiene," *Organometallics*, vol. 34, no. 19, pp. 4644–4646, 2015.

[22] J. Binder, R. C. Fischer, M. Flock, H.-G. Stammler, A. Torvisco, and F. Uhlig, "Novel Aryl-Substituted Silanes Part II: Synthesis and Characterization of Diaryl Silicon Dihydrides," *Phosphorus, Sulfur, and Silicon and the Related Elements*, vol. 191, no. 3, pp. 478–487, 2016.

[23] N. Nakamura, "A Stable Sulfenic Acid, 9-triptycenesulfenic Acid: Its Isolation and Characterization," *Journal of the American Chemical Society*, vol. 105, no. 24, pp. 7172–7173, 1983.

[24] A. Ishii, S. Matsubayashi, T. Takahashi, and J. Nakayama, "Preparation of a Selenenic Acid and Isolation of Selenoseleninates," *The Journal of Organic Chemistry*, vol. 64, no. 4, pp. 1084–1085, 1999.

[25] J. M. Chance, J. H. Geiger, Y. Okamoto, R. Aburatani, and K. Mislow, "Stereochemical Consequences of a Parity Restriction on Dynamic Gearing in Tris (9-triptycyl) Germanium Chloride and tris (9-triptycyl) Cyclopropenium Perchlorate," *Journal of the American Chemical Society*, vol. 112, no. 9, pp. 3540–3547, 1990.

[26] G. Yamamoto, S. Ohta, M. Kaneko, K. Mouri, M. Ohkuma, R. Mikami, Y. Uchiyama, and M. Minoura, "Static and Dynamic StereoChemistry of Tris (9-triptycyl) Stannane Derivatives," *Bulletin of the Chemical Society of Japan*, vol. 78, no. 3, pp. 487–497, 2005.

[27] W. Setaka, T. Nirengi, C. Kabuto, and M. Kira, "Introduction of Clutch Function into a Molecular Gear System by Silane-Silicate Interconversion," *Journal of the American Chemical Society*, vol. 130, no. 47, pp. 15762–15763, 2008.

[28] J.-H. Lamm, Y. V. Vishnevskiy, E. Ziemann, B. Neumann, H.-G. Stammler, and N. W. Mitzel, "Regiochemical Control in Triptycene Formation—An Exercise in Subtle Balancing Multiple Factors," *ChemistryOpen*, vol. 7, no. 1, pp. 111–114, 2018.

[29] M. Yukimoto and M. Minoura, "The Synthesis of a Novel Bulky Primary Alkyl Group and Its Application toward the Kinetic Stabilization of a Tetraalkyldisilene," *Bulletin of the Chemical Society of Japan*, vol. 91, no. 4, pp. 585–587, 2018.

[30] K. Suzuki, T. Matsuo, D. Hashizume, and K. Tamao, "Room-Temperature Dissociation of 1,2-Dibromodisilenes to Bromosilylenes," *Journal of the American Chemical Society*, vol. 133, no. 49, pp. 19710–19713, 2011.

[31] T. Matsuo, K. Suzuki, T. Fukawa, B. Li, M. Ito, Y. Shoji, T. Otani, L. Li, M. Kobayashi, M. Hachiya, *et al.*, "Synthesis and Structures of a Series of Bulky "Rind-Br" Based on a Rigid Fused-Ring s-Hydrindacene Skeleton," *Bulletin of the Chemical Society of Japan*, vol. 84, no. 11, pp. 1178–1191, 2011.

[32] B. Li, T. Matsuo, T. Fukunaga, D. Hashizume, H. Fueno, K. Tanaka, and K. Tamao, "Neutral and Cationic Gold(i) Complexes with π-Conjugated Phosphasilene Ligands," *Organometallics*, vol. 30, no. 13, pp. 3453–3456, 2011.

[33] N. Hayakawa, T. Morimoto, A. Takagi, T. Tanikawa, D. Hashizume, and T. Matsuo, "Synthesis and Structures of Sterically Congested Diarylsilanes Bearing Two Bulky Rind Groups," *Chemistry Letters*, vol. 45, no. 4, pp. 409–411, 2016.

[34] L. Li, T. Fukawa, T. Matsuo, D. Hashizume, H. Fueno, K. Tanaka, and K. Tamao, "A Stable Germanone as the First Ssolated Heavy Ketone with a Terminal Oxygen Atom," *Nature Chemistry*, vol. 4, no. 5, p. 361, 2012.

[35] K. Suzuki, Y. Numata, N. Fujita, N. Hayakawa, T. Tanikawa, D. Hashizume, K. Tamao, H. Fueno, K. Tanaka, and T. Matsuo, "A Stable Free Tetragermacyclobutadiene Incorporating Fused-Ring Bulky EMind Groups," *Chemical Communications*, vol. 54, no. 18, pp. 2200–2203, 2018.

[36] N. Hayakawa, T. Sugahara, Y. Numata, H. Kawaai, K. Yamatani, S. Nishimura, S. Goda, Y. Suzuki, T. Tanikawa, H. Nakai, *et al.*, "1, 2-Dihalodigermenes Bearing Bulky Eind groups: Synthesis, Characterization, and Conversion to Halogermylenoids," *Dalton Transactions*, vol. 47, no. 3, pp. 814–822, 2018.

[37] S. R. Wang, M. Arrowsmith, J. Böhnke, H. Braunschweig, T. Dellermann, R. D. Dewhurst, H. Kelch, I. Krummenacher, J. D. Mattock, J. H. Müssig, *et al.*, "Engineering a Small HOMO–LUMO Gap and Intramolecular C-H Borylation by Diborene/Anthracene Orbital Intercalation," *Angewandte Chemie International Edition*, vol. 56, no. 27, pp. 8009–8013, 2017.

[38] S. R. Wang, M. Arrowsmith, H. Braunschweig, R. D. Dewhurst, V. Paprocki, and L. Winner, "CuOTf-Mediated Intramolecular Diborene Hydroarylation," *Chemical Communications*, vol. 53, no. 87, pp. 11945–11947, 2017.

[39] P. Thomaschewski, "Anthracene Compound.," Nov. 2 1909. US Patent 938,617.

[40] H. Wolff, "Green anthracene Dyes and Process of Making the Same.," June 20 1911. US Patent 995,936.

[41] M. M. Champenois, "Copolymers of Dyes and Acrylamide," Jan. 2 1979. US Patent 4,132,841.

[42] L. A. Bunes, "Products Including Edibles Colored with Polymeric Red Colors," Feb. 23 1982. US Patent 4,316,918.

[43] J. B. Melpolder, "Polymerizable Dye," Oct. 8 1991. US Patent 5,055,602.

[44] C. Hoffend, F. Schödel, M. Bolte, H.-W. Lerner, and M. Wagner, "Boron-Doped Tri (9,10-Anthrylene) s: Synthesis, Structural Characterization, and Optoelectronic Properties," *Chemistry–A European Journal*, vol. 18, no. 48, pp. 15394–15405, 2012.

[45] N. M. Obeid, L. Klemmer, D. Maus, M. Zimmer, J. Jeck, I. Bejan, A. J. White, V. Huch, G. Jung, and D. Scheschkewitz, "(oligo) aromatic species with one or two conjugated si [double bond, length as m-dash] si bonds: near-ir emission of anthracenyl-bridged tetrasiladiene," *Dalton Transactions*, vol. 46, no. 27, pp. 8839–8848, 2017.

[46] A. C. Hoepker and D. B. Collum, "Computational Studies of Lithium Diisopropylamide Deaggregation," *The Journal of Organic Chemistry*, vol. 76, no. 19, pp. 7985–7993, 2011.

[47] J. Li, A. Stasch, C. Schenk, and C. Jones, "Extremely Bulky Amido-group 14 Element Chloride Complexes: Potential Synthons for Low Oxidation State Main Group Chemistry," *Dalton Transactions*, vol. 40, no. 40, pp. 10448–10456, 2011.

[48] J. Li, C. Schenk, F. Winter, H. Scherer, N. Trapp, A. Higelin, S. Keller, R. Pöttgen, I. Krossing, and C. Jones, "Weak Arene Stabilization of Bulky Amido-Germanium(II) and Tin(II) Monocations," *Angewandte Chemie International Edition*, vol. 51, no. 38, pp. 9557–9561, 2012.

[49] D. Dange, J. Li, C. Schenk, H. Schnöckel, and C. Jones, "Monomeric Group 13 Metal (I) Amides: Enforcing One-Coordination Through Extreme Ligand Steric Bulk," *Inorganic Chemistry*, vol. 51, no. 23, pp. 13050–13059, 2012.

[50] I. A. Guzei and M. Wendt, "An Improved Method for the Computation of Ligand Steric Effects Based on Solid Angles," *Dalton Transactions*, no. 33, pp. 3991–3999, 2006.

[51] M. F. Lappert, M. J. Slade, J. L. Atwood, and M. J. Zaworotko, "Monomeric, Coloured Germanium(II) and Tin(II) Di-t-butylamides, and the Crystal and Molecular Structure of Ge(NCMe$_2$[CH$_2$]$_3$CMe$_2$)$_2$," *Journal of the Chemical Society, Chemical Communications*, no. 13, pp. 621–622, 1980.

[52] M. Huang, M. M. Kireenko, K. V. Zaitsev, Y. F. Oprunenko, A. V. Churakov, J. A. Howard, E. K. Lermontova, D. Sorokin, T. Linder, J. Sundermeyer, *et al.*, "Stabilized Germylenes Based on Diethylenetriamines and Related Diamines: Synthesis, Structures, and Chemical Properties," *European Journal of Inorganic Chemistry*, vol. 2012, no. 23, pp. 3712–3724, 2012.

[53] E. W. Wong, T. J. Hadlington, and C. Jones, "Synthesis and Crystal structures of Two Bulky Bis (Amido) Germylenes," *Main Group Metal Chemistry*, vol. 36, no. 3-4, pp. 133–136, 2013.

[54] J. Oetzel, N. Weyer, C. Bruhn, M. Leibold, B. Gerke, R. Poettgen, M. Maier, R. F. Winter, M. C. Holthausen, and U. Siemeling, "Redox-Active N-Heterocyclic Germylenes and Stannylenes with a Ferrocene-1, 1'-diyl Backbone," *Chemistry–A European Journal*, vol. 23, no. 5, pp. 1187–1199, 2017.

[55] F. Walz, E. Moos, D. Garnier, R. Köppe, C. E. Anson, and F. Breher, "A Redox-Switchable Germylene and its Ligating Properties in Selected Transition Metal Complexes," *Chemistry–A European Journal*, vol. 23, no. 5, pp. 1173–1186, 2017.

[56] L. Du, S. Du, and Y. Ding, "A Potential Method Using Ge {iPrNC [N (SiMe3) 2] NiPr} 2,(Et3Si) 2Te and Anhydrous Hydrazine for Germanium Tellurides," *Zeitschrift für Anorganische und Allgemeine Chemie*, vol. 643, no. 24, pp. 2168–2171, 2017.

[57] A. Steiner and D. Stalke, "Poly (Pyrazolyl) Germanium (II) and-Tin (II) Derivatives-Tuneable Monoanionic Ligands and Dinuclear Cationic Cages," *Inorganic Chemistry*, vol. 34, no. 19, pp. 4846–4853, 1995.

[58] N. S. Hosmane, J. Yang, K.-J. Lu, H. Zhang, U. Siriwardane, M. S. Islam, J. L. Thomas, and J. A. Maguire, "Chemistry of C-Trimethylsilyl-Substituted Heterocarboranes. 25. Syntheses, Structures, and Reactivities of $GeCl_3$-Substituted Half-Sandwich Germacarboranes, closo-1-Ge-2-$(SiMe_3)$-3-(R)-5-$(GeCl_3)$-2,3-$C_2B_4H_3$ (R= $SiMe_3$, Me, and H)," *Organometallics*, vol. 17, no. 13, pp. 2784–2796, 1998.

[59] S. Kolesnikov, S. Maksimov, and E. Smolenskii, "Proton-Donor Properties of $HCCl_3$, $HSiCl_3$, and $HGeCl_3$ Molecules: a Quantum-Chemical Study," *Russian Chemical Bulletin*, vol. 50, no. 4, pp. 740–742, 2001.

[60] K. Yamada, K. Mikawa, T. Okuda, and K. S. Knight, "Static and Dynamic Structures of $CD_3ND_3GeCl_3$ Studied by TOF High Resolution Neutron Powder Diffraction and Solid State NMR," *Journal of the Chemical Society, Dalton Transactions*, no. 10, pp. 2112–2118, 2002.

[61] I. L. Fedushkin, N. M. Khvoinova, A. Y. Baurin, G. K. Fukin, V. K. Cherkasov, and M. P. Bubnov, "Divalent Germanium Compound with a Radical-Anionic Ligand: Molecular Structures of (dpp-BIAN)$^{\bullet-}$GeCl and Its Hydrochloration Products [(dpp-BIAN)$(H)_2$]$^{\bullet+}$[$GeCl_3$]$^-$ and [{(dpp-BIAN)$(H)_2$$^{\bullet+}$}$_2$(Cl$^-$)]$^+$[$GeCl_3$]-(dpp-BIAN = 1,2-Bis {(2,6-diisopropylphenyl)imino} acenaphthene)," *Inorganic Chemistry*, vol. 43, no. 24, pp. 7807–7815, 2004.

[62] Y. V. Zefirov and P. M. Zorky, "New Applications of Van der Waals Radii in Chemistry," *Russian Chemical Reviews*, vol. 64, no. 5, p. 415, 1995.

[63] J. Atkinson-Bodourian, "The Utilization of Bulky Monodentate Amido and Cyclic(Alkyl)(Amino)Carbene Ligands for the Kinetic Stabilization of low Oxidation State Group 13 Complexes," *Honours Thesis*.

[64] C. A. Coulson, R. Daudel, and J. M. Robertson, "Bond Lengths in Naphthalene and Anthracene," *Proceedings of the Royal Society of London. Series A. Mathematical and Physical Sciences*, vol. 207, no. 1090, pp. 306–320, 1921.

[65] M. Beswick, M. G. Mosquera, J. Palmer, D. Wright, *et al.*, "Synthesis and Structure of the Heterobimetallic Oxo Complex [(thf)(Me$_2$NH)$_2$Cl$_2$Cr(III)]$_2$ {ClSn(II) (Á-O)}$_2$," *Chemical Communications*, no. 13, pp. 1341–1342, 1998.

[66] T. Chlupatỳ, Z. Padělková, A. Lyčka, J. Brus, and A. Růžička, "Reactivity of Lithium n-Butyl Amidinates Towards Group 14 Metal(II) Chlorides Providing Steries of Hetero-and Homoleptic Tetrylenes," *Dalton Transactions*, vol. 41, no. 16, pp. 5010–5019, 2012.

[67] L. Wang, C. E. Kefalidis, T. Roisnel, S. Sinbandhit, L. Maron, J.-F. Carpentier, and Y. Sarazin, "Structure vs ^{119}Sn NMR Chemical Shift in Three-Coordinated Tin(II) Complexes: Experimental Data and Predictive DFT Computations," *Organometallics*, vol. 34, no. 11, pp. 2139–2150, 2014.

[68] H. Braunschweig, P. B. Hitchcock, M. F. Lappert, and L. J.-M. Pierssens, "Synthesis, Structures, and Reactions of Two Bis (diaminostannylene) s and a Bis (diaminogermylene) Containing a Central C$_6$ Ring," *Angewandte Chemie International Edition in English*, vol. 33, no. 11, pp. 1156–1158, 1994.

[69] H. Braunschweig, C. Drost, P. B. Hitchcock, M. F. Lappert, and L. J.-M. Pierssens, "A Dinuclear Tin(II) Amide, a meta-Stannylaminocyclophane and Its Orthostannylated Derivative, a Dimeric Trinuclear Tin(II) Cluster," *Angewandte Chemie International Edition in English*, vol. 36, no. 3, pp. 261–263, 1997.

[70] P. B. Hitchcock, J. Hu, M. F. Lappert, M. Layh, and J. Severn, "Variation of Bonding Modes in Homoleptic Tin(II) 1-Azaallyls," *Chemical Communications*, no. 13, pp. 1189–1190, 1997.

[71] J. R. Babcock, L. Liable-Sands, A. L. Rheingold, and L. R. Sita, "Syntheses, structural characterizations, and heterocumulene metathesis studies of new monomeric bis (triorganosilylamido) tin(ii) derivatives," *Organometallics*, vol. 18, no. 21, pp. 4437–4441, 1999.

[72] Y. Tang, A. M. Felix, L. N. Zakharov, A. L. Rheingold, and R. A. Kemp, "Syntheses and Structural Characterization of a Monomeric Tin(II) Diamide and a Novel Chlorotin(II) Amide Trimer," *Inorganic Chemistry*, vol. 43, no. 22, pp. 7239–7242, 2004.

[73] C. Förster, P. M. Becker, and K. Heinze, "A Ferrocenyl Amino Substituted Stannylene as an Intramolecular Fe→Sn Lewis Adduct," *Zeitschrift für Anorganische und Allgemeine Chemie*, vol. 644, no. 17, pp. 1057–1063, 2018.

[74] T. J. Hadlington, J. Li, and C. Jones, "Synthesis and Characterization of Extremely Bulky Amido-Germanium(II) Halide Complexes," *Canadian Journal of Chemistry*, vol. 92, no. 6, pp. 427–433, 2013.

[75] A. Hinz and J. M. Goicoechea, "Limitations of Steric Bulk: Towards Phospha-germynes and Phospha-stannynes," *Chemistry–A European Journal*, vol. 24, no. 29, pp. 7358–7363, 2018.

[76] T. J. Hadlington, M. Hermann, G. Frenking, and C. Jones, "Two-Coordinate group 14 Element(II) Hydrides as Reagents for the Facile, and Sometimes Reversible, Hydrogermylation/Hydrostannylation of Unactivated Alkenes and Alkynes," *Chemical Science*, vol. 6, no. 12, pp. 7249–7257, 2015.

[77] H. Arii, T. Amari, J. Kobayashi, K. Mochida, and T. Kawashima, "Low-Coordinate Germanium(II) Centers Within Distorted Axially Chiral Seven-Membered Chelates: Stereo- and Enantioselective Cycloadditions," *Angewandte Chemie*, vol. 124, no. 27, pp. 6842–6845, 2012.

[78] A. Meller, G. Ossig, W. Maringgele, M. Noltemeyer, D. Stalke, R. Herbst-Irmer, S. Freitag, and G. M. Sheldrick, "Reaktionen von Germylenen mit Säureaziden/Reactions of Germylenes with Acid Azides," *Zeitschrift für Naturforschung B*, vol. 47, no. 2, pp. 162–170, 1992.

[79] L. E. Sutton, *Tables of Interatomic Distances and Configuration in Molecules and Ions: Supplement 1956-59*. No. 18, Chemical Society, 1965.

[80] S. Abrahams, R. Collin, and W. Lipscomb, "The Crystal Structure of Hydrogen Peroxide," *Acta Crystallographica*, vol. 4, no. 1, pp. 15–20, 1951.

[81] M. A. Fox and J. K. Whitesell, *Organische Chemie: Grundlagen, Mechanismen, Bioorganische Anwendungen*. Spektrum Akad. Verlag, 1995.

[82] B. Haag, M. Mosrin, H. Ila, V. Malakhov, and P. Knochel, "Regio-and Chemoselective Metalation of Arenes and Heteroarenes using Hindered Metal Amide Bases," *Angewandte Chemie International Edition*, vol. 50, no. 42, pp. 9794–9824, 2011.

[83] S. Sakamoto, T. Imamoto, and K. Yamaguchi, "Constitution of Grignard Reagent RMgCl in Tetrahydrofuran," *Organic Letters*, vol. 3, no. 12, pp. 1793–1795, 2001.

[84] R. L.-Y. Bao, R. Zhao, and L. Shi, "Progress and Developments in the Turbo Grignard Reagent i-PrMgCl· LiCl: A Ten-Year Journey," *Chemical Communications*, vol. 51, no. 32, pp. 6884–6900, 2015.

[85] A. Lorbach, C. Reus, M. Bolte, H.-W. Lerner, and M. Wagner, "Improved synthesis of 1, 2-bis(trimethylsilyl) benzenes using rieke-magnesium or the entrainment method," *Advanced Synthesis & Catalysis*, vol. 352, no. 18, pp. 3443–3449, 2010.

Chapter 4

The Utilisation of Boryl Amides, Amidinates, and Nacnacs for the Stabilisation of Low-Oxidation Group 14 Complexes

Altering the ligands attached to a element-centre-of-interest (ECOI) has a direct impact on the reactivity of the resulting complex. This is due to the concerted affects of the ligand's electronic and steric character on the ECOI.

Electronically, a ligand's donor atom's electronic configuration affects the electronics of the main-group element centre. This electronic effect can be manipulated by altering the substituents about the donor atom. For amide-type ligands: aryl, boryl, silyl, and alkyl substituents can be used to alter the electronic profile of the nitrogen-donor atom (this is true for multidentate ligands).

Kinetically, the size and shape of the ligand influences the stability and reactivity of the final compound. Typically bidentate ligands, such as amidinates and β-diketiminates, provide greater kinetic stabilisation towards an ECOI.

This chapter seeks to detail some of the low-oxidation state tetrel element chemistry performed which utilise monodentate aryl amides, and bidentate amidinates and nacnacs. The results and discussion of this chapter focuses on the use of said ligands [i] in low-oxidation state group 14 element chemistry.

---

[i]The coupling of a ligand to a main-group element centre and their subsequent reduction is discussed in **chapter 3**, and so is not repeated within this chapter.

4.1 Aryl Amides in Low-Oxidation State Tetrel Chemistry

Monodentate aryl amides have been utilised extensively within the field of low-oxidation state main-group chemistry[ii]. The desire to use such ligands is the magnitude of steric encumbrance they provide through their aryl moiety. Also, the bulk/size of the aryl substituent influences the type of compounds formed during synthesis: smaller aryl groups tend towards the formation of poly/multinuclear compounds; and larger aryl groups towards monomeric or dimeric compounds.

Aryl amides can have differing secondary substituents upon the nitrogen atom: alkyl, aryl, boryl, and silyl substituents are ubiquitous throughout the field. These substituents can have a unique affect upon the donor nitrogen's electronic profile, concertedly affecting the electronic profile of the ECOI. The bonding strength between the substituent and the nitrogen also varies, affecting the stability of these ligands and their related compounds[iii].

4.1.1 Aryl Silyl Amides

Aryl silyl amides have allowed for the synthesis of a multitude of compounds, ranging from transition metal complexes to low-oxidation state main-group compounds. In some cases, these ligands have been utilised in the presence of a different ligand, though these are not discussed here[iv].[2,3] The advantages of these ligands is discussed in **chapter 2, section 2.3.2**. The greatest disadvantage of these ligands is the comparatively weak N-Si bond which has been sometimes found to undergo fission and lead to unwanted by-product formation. Whilst this is not always observed or found to cause issues, in the event that it does occur the following chemistry done with these compounds can become overly complex.

Dipp Silyl Amides

Of the Dipp silyl amides (where Dipp = 2,6-diisopropylphenyl), when these ligands are used for low-oxidation state group 14 chemistry they typically lead to the formation of multinuclear/polymeric compounds. For silicon, when this ligand is adopted, it is often found that further reactivity leads to the formation of cluster[v] compounds (see **figure 4.1**

[ii]Examples presented in **chapter 1** and their synthesis is discussed in **chapter 2**.

[iii]B-N bonds are stronger than Si-N bonds, for example.[1]

[iv]See **chapter 1, scheme 1.4**.

[v]The term metalloid cluster was coined by Schnöckel and co-workers in the context of their aluminium work. The term has since been extended to the predominant main-group elements explored in low-oxidation state main-group chemistry.[4]

(left), **i-4a** & **i-4b**)[vi]. Tin-based cluster compounds have also been reported when utilising the ligand {Dipp(TMS)N}⁻ & {Dipp(SiMe₂Ph)N}⁻ (see **figure 4.1**, **i-4c**)[vii].[4] The formation of such cluster compounds indicates the inability of this ligand type to sterically prevent the formation of multinuclear compounds, dimeric, cluster, or otherwise.
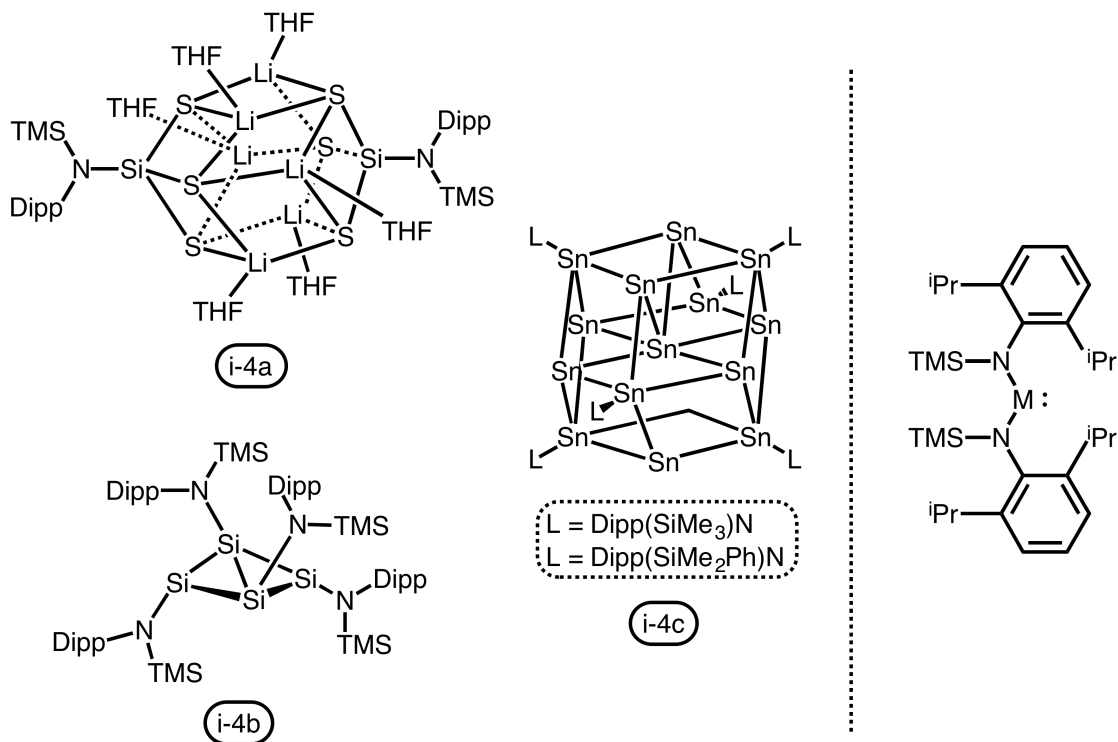

Figure 4.1: Examples of the cluster-type compounds formed when utilising the {Dipp(TMS)N}⁻ ligand (left); Generic structure of the heavy carbene analogues stabilised by two {Dipp(TMS)N}⁻ ligands (where M = Ge, Sn, or Pb) (right).

For the heavier tetrel elements (germanium, tin, and lead) this ligand does not provide the necessary kinetic stabilisation to isolate the heavy alkyne analogues but does allow for the synthesis of heavy carbene and alkene analogues (**figure 4.1, (right)**). Further reactivity of these germylene and stannylene species often lead to cluster compounds.[3, 10–12]

Benzhydrol-like Silyl Amides

In recent years, the development and inclusion of larger and bulkier aryl groups has increased the steric encumbrance afforded by this ligand class. An example of this is from within our own group. Success has been achieved utilising the ligands {Ar*/†(SiR₃)N}⁻ (where Ar* = C₆H₂{C(H)Ph₂}₂Me-2,6,4; and Ar† = C₆H₂{C(H)Ph₂}₂ⁱPr-2,6,4) which have

---

[vi]For more silicon-based cluster compounds see the referenced work by Roesky and co-workers.[5–9] Though, these clusters are not the product of low-oxidation state silicon compounds, and are merely mentioned as to highlight the inability of the {Dipp(TMS)N}⁻ ligand to prevent cluster compounds from forming.

[vii]The tin clusters **i-4c** display the highest-nuclearity observed for a group 14 metalloid cluster.

led to the isolation of a range of reactive low-oxidation state main-group element containing compounds.[13–20] These ligands have also allowed the synthesis of chloropnictogen ions, as reported by Schulz and co-workers.[21] These compounds include the low-oxidation state heavy group 14 element alkyne analogues **i-4d**[viii] & **i-4e**, which display small-molecule activation such as the activation of dihydrogen, as shown in **scheme 4.1**.[18,19]
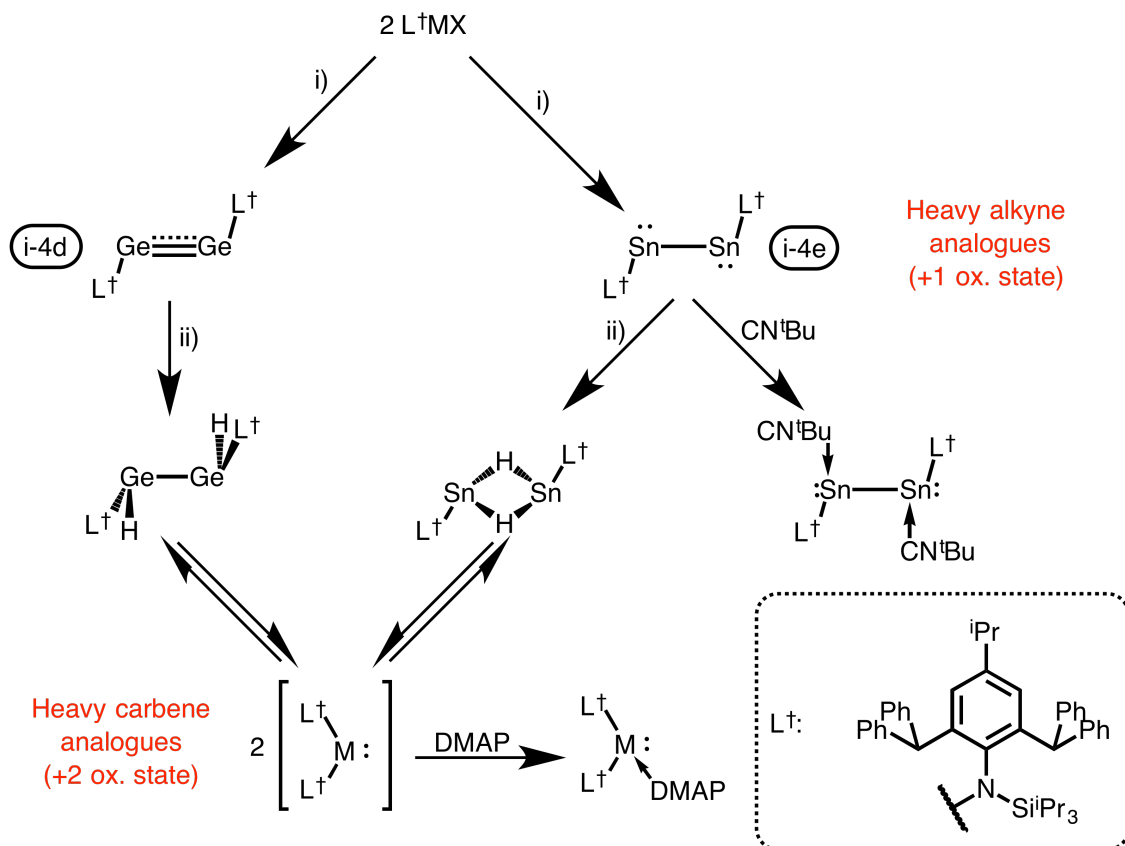
*Scheme 4.1: Synthesis of the heavy alkyne analogues (**i-4d**[i] & **i-4e**) and their reactivity to form the hydrido complexes, and the isocyanide coordination by the tin derivative. The hydrido complexes are in equilibrium with the heavy carbene analogues (where M = Ge or Sn, X = Cl or Br). Reagents and conditions: (i) [({^{Mes}nacnac}Mg)$_2$] and (ii) H$_2$ or Li[HB^{i}Bu$_3$].*

4.1.2 Aryl Boryl Amides

Unlike the aryl silyl amides, the analogous aryl boryl amides have not seen the same level of adoption in main-group chemistry.

It is has been suggested that the inclusion of boryl substituents upon a nitrogen donor atom allows for π donation of the nitrogen lone-pair into the empty p orbital(s) of the boron atom(s), increasing the ECOI's reactivity.[22] N-B bonds are also stronger than N-Si bonds and hence less likely to undergo fission.

[viii]**i-4d** is discussed in **chapter 3**.

{($^{\text{Dipp}}$DAB)B} Silyl Amides

The aryl moieties (Dipp) within {($^{\text{Dipp}}$DAB)B}(TMS)N}⁻ are constituents of the boryl moiety, and the secondary substituent is trimethyl silyl (TMS). Neither the issues of N-Si bond fission nor of B-N π back-donation are addressed in the design of this ligand (discussed in **chapter 2**).

The larger than typical boryl moiety provides enough steric encumbrance to stabilise low-oxidation state group 14 compounds (and group 15 compounds, discussed in **chapter 5**). This ligand allowed for the isolation of the acyclic amido silylene **i-4f**, which was found to activate ammonia, an important step in some catalysis, forming the compound **i-4g** (**scheme 4.2**).[23]
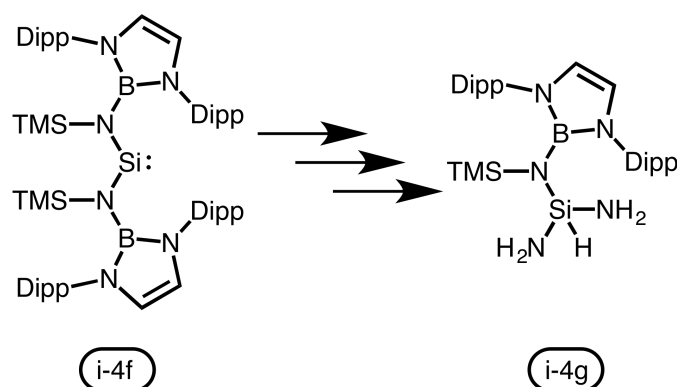
*Scheme 4.2: NH₃ activation by the silylene **i-4f** to form the compound **i-4g**.*

4.2   Amidinates and Nacnacs in Low-Oxidation State Tetrel Chemistry

Amidinates and nacnacs are typically more sterically inhibiting than their monodentate equivalents. The increased stability afforded by the bulk of bidentates is compounded by the chelate stabilising effect (discussed in **chapter 2**).

Amidinate and nacnac supported low-oxidation state tetrel compounds are typically less reactive but more stable. These ligands increase the electronic saturation of the tetrel element by increasing the energy of the LUMO orbital (usually the π* orbital). For this reason, when these ligands support germanium, tin, or lead in the +II oxidation state, the resultant compounds are less reactive than their monodentate counterparts. This is less true for low-oxidation state silicon centres as they have a narrower HOMO-LUMO gap.

4.2.1   Amidinates

Amidinates have been shown to stabilise silicon in the +II and +I oxidation states, allowing for the synthesis and isolation of a number of reactive silylenes. **Scheme 4.3** illustrates the ability of the amidinato silylene **i-4h** to react with white phosphorous (P_4) forming the unique P_4 chain containing compound **i-4i**[ix].[24] The analogous chlorosilylene **i4j** reacts with adamantyl phosphaalkyne to produce **i-4k**, representing the first example of triple bond cleavage at a main-group centre. The related reaction of **i-4j** with diphenylacetylene results in only partial cleavage of the C-C bonds producing **i-4l**.
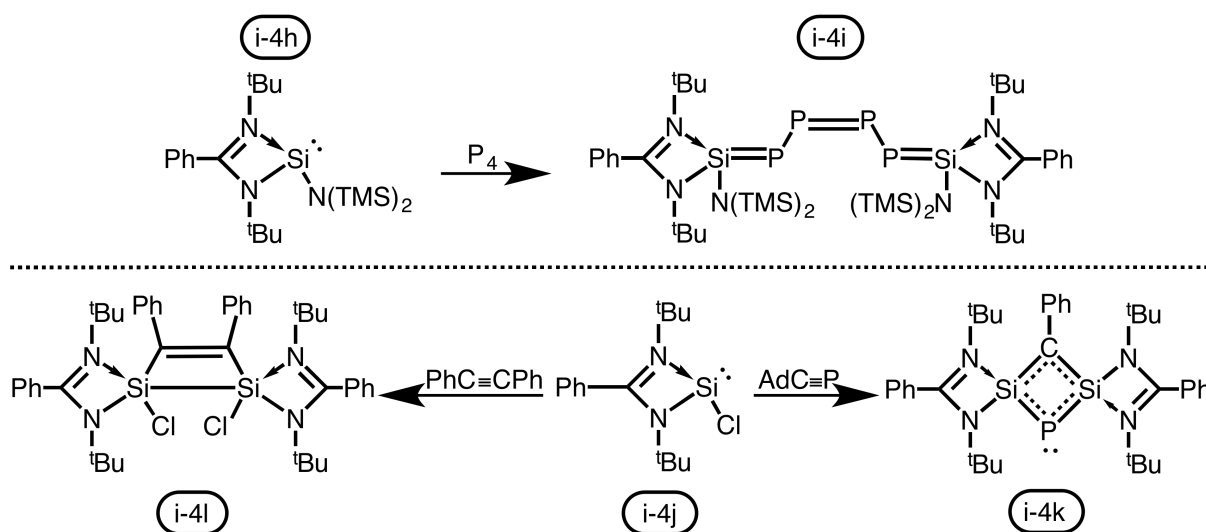
*Scheme 4.3: Top: the reaction of the amidinate stabilised silylene **i-4h** with P_4 to form **i-4i**; Bottom: **i-4j** reacted with adamantyl phosphaalkyne, constituting the first example of triple-bond cleave at a main-group centre. Also, **i-4J** can partially cleaves alkyne bonds.*

Typically the comparative Ge, Sn, and Pb analogous species (examples provided in **figure 4.2**) are considerably less reactive[x].[25–29] Similar amidinate germylenes and stannylenes display oxidative addition of elemental chalcogens, which has also been observed for the analogues silylene species.[30–33]

[ix]Many amidinate supported silicon(II) compounds have displayed reactivity with white phosphorous (P_4).
[x]Another example of amindinate supported tetrel compound reactivity is presented in **chapter 1, scheme 1.8**.
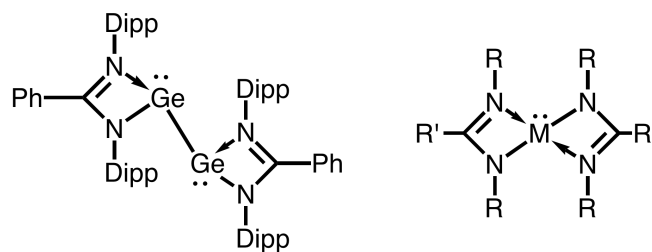
Figure 4.2: Examples of amidinate suported germylenes, stannylenes, and plumbylenes (where M = Sn, R = ^{t}Bu, and R' = Ph; M = Pb, R = Dipp, and R' = H).

4.2.2   β-diketiminates, the Nacnacs

Like amidinates, low-oxidation state tetrel compounds which utilise nacnacs are generally less reactive. The most reactive of these compounds is the silicon heterocycle **i-4m**, though the nacnac motif has lost aromaticity and itself becomes dianionic upon formation of the silylene.[34,35] The analogous germylene complex **i-4o** has also been synthesised but is less reactive (*vide infra*).[36] Macrocylic nacnac supporterd germylenes and stannylenes have been reported and are reactive towards elemental chalcogens.[37,38]

i-4m's reactivity has allowed for the activation of a range of bond types[xi]. As an example **scheme 4.4** illustrates exemplary products from the reaction of **i-4m** with a range of differing substrates, including the Lewis-base stabilised silanone **i-4m**.[31,46,47]
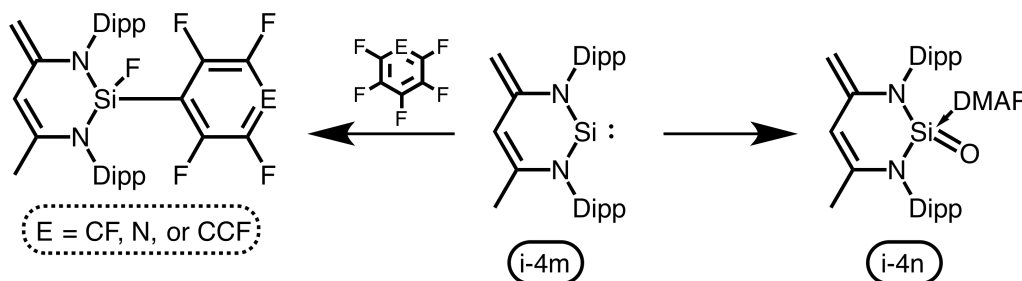
*Scheme 4.4: C-F activation and formation of the silanone (**i-4n**) from the heterocyclic "nacnac" supported silylene (**i-4m**).*

In comparison, only C-H,[48,49] N-H,[50] P-H,[51] and O-H[52] bond activation by **i-4o** has been disclosed: the products of these reactions display the re-aromatisation of the heterocyclic moiety and reformation of the monoanionic nacnac fragment (C-H activation is given as an example in **scheme 4.5**).

[xi]Al-H,[39] C-H,[31,40] N-H,[41] S-H,[42] O-H,[43] C-X,[40,44] and P$_4$[45] bond activation have been reported using **i-4m**.
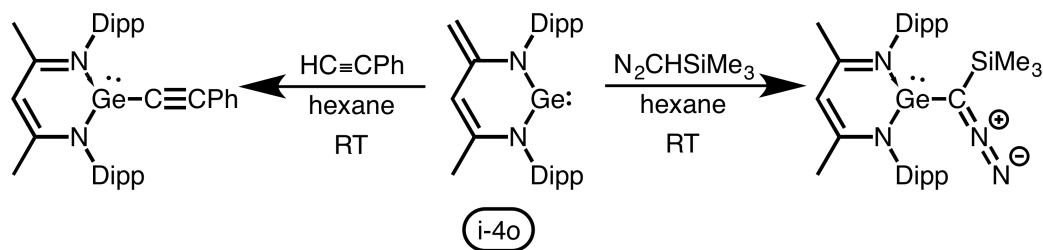
*Scheme 4.5: C-H activation by the heterocyclic "nacnac" supported germyelene (**i-4o**).*
Note: the reformation of the nacnac fragment upon reaction.

4.3   Research Proposal

The reactivity of previously reported monodentate and bidentate stabilised low-oxidation state group 14 element containing compounds is of primary interest to us. These compounds have illustrated the ability of main-group centres to perform chemistry like that observed for transition metals.

The synthesis of a range of aryl boryl amines gives us the precursors for the synthesis of a new series of monodentate ligands. The electronic profile of these ligands may impart some unique reactivity towards group 14 element centres when ligated. Firstly, the concerted σ donation from the boron to the nitrogen should have some impact on the energetics of the group 14 element lone-pair of electrons (present in the n-orbital). Secondly, the formally vacant p orbital upon the boron is capable of accepting electron density and it is believed that the nitrogen lone-pair may preferentially delocalise towards the boron rather than towards the group 14 element centre. These two affects should culminate in a reduced HOMO-LUMO gap for the resulting compounds.

The utilisation of bulkier multi-dentate ligands has allowed access to unique low-oxidation state group 2 alkali metal compounds previously un-isolable.[53] Despite the vast work done using this ligand type for group 14 element chemistry, it is our proposal that utilising even larger derivatives of these ligands may allow for the isolation of monomeric low-oxidation state group 14 element containing compounds which have eluded synthesis. By adopting Ar* and, or, Ar† into a amidinate framework there is potential to isolate monomeric or cationic group 14 element compounds.

The aforementioned amidinates have recently been modulated to include chiral moieties;[54] and, from within the Jones group, a range of chiral moiety containing amidinates and β-diketiminates (nacnacs) have been prepared, showing promising results in the realm of low-oxidation state group 1 and 2 chemistry. The utilisation of these chiral ligands may eventuate in the synthesis of low-oxidation state group 14 element compounds which show enantioselectivity

4.4 Results & Discussion (R&D): Monodentate Boryl Amides

The range of boryl amine pro-ligands synthesised, containing either 9-borabicyclo[3.3.1]nonane-like (BBN) or boron bis(pyrrolidene) (BBP), were converted into their respective lithium amides. These lithium amides were reacted with a series of group 14 halide species in attempts to form compounds of the general formula $LSiH_{3-n}X_n$ or LMX (where M = Ge, Sn, or Pb). The terminal goal was to synthesise a range of heavy alkyne, heavy alkene analogues, and, or species of a similar type. Generally speaking, this project was ultimately unsuccessful and mainly undesired by-products were isolated from our attempts.

4.4.1 Lithiations and Potassiations

Synthesis

Scheme 4.6 displays the lithiation of the aryl BBN/BBP amines, accomplished using n-butyl lithium (^{n}BuLi) in polar solvents. For Ar*$^{/\dagger}$(BBN)NH (**2.18**/**2.19**) and Ar*$^{/\dagger}$(BBP)NH (**2.21**/**2.22**), lithiation proved troublesome and full conversion to the lithium amides, without the formation undesired by-products[xii], was not achieved. Ar*(BBN)NLi (**Li-2.18**) could not be isolated cleanly due to solubility issues and was not used for further chemistry.

For the syntheses of both lithium aryl BBN & BBP amides, observations were similar with a distinct solution colour change on addition of lithiating reagent ($^{n/t}$BuLi) to the aryl boryl amine solution: the solutions going from colourless to orange/red as the reaction mixture was allowed to slowly warm to room temperature. Upon *in vacuo* removal of volatiles and extraction of the product residue, the lithium amides were isolated as orange/red solid powders. For the Ar* derivatives, this workup procedure did not work due to the low-solubility of the respective lithium amides.

[xii]The only by-products identified were the respective anilines (Ar*NH_2 & Ar$^\dagger NH_2$), and occasionally the protonated boryl fragment. Determined by ^{1}H NMR spectroscopy).
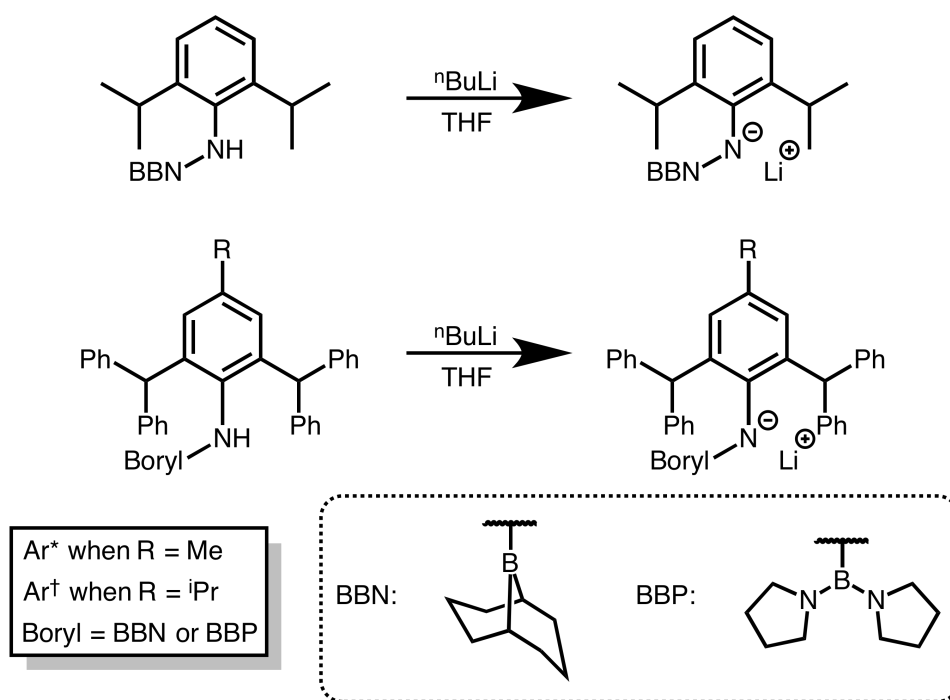
Scheme 4.6: Lithiation of $^{Dipp}Ar(BBN)NH$ (**2.17**) and the $Ar^{*/\dagger}(Boryl)NH$
(**2.18/19/21/22**) amines to form their respective lithium amides
(**Li-2.17/18/19/21/22**) (where Boryl = BBN or BBP).

For the aryl BBN amines, almost complete conversion of Dipp(BBN)NH (**2.17**) to
Dipp(BBN)NLi (**Li-2.17**) is observed, with an approximate yield of 90% as determined
by ^{1}H NMR spectroscopic analyses. For **2.18** & **2.19**, conversion to the respective lithium
amides $Ar^{*/\dagger}(BBN)NLi$ (**Li-2.18** & **Li-2.19**) was consistently low[xiii]. Lithiation was not
improved under any attempted reaction conditions: forcing conditions (heating the reac-
tion) led to increased by-product formation and presumptive decomposition, and the use of
tert-butyl lithium (^{t}BuLi) gave similar results[xiv].

For the aryl BBP amines (**2.21** & **2.22**) conversion to the lithium amides $Ar^{*/\dagger}(BBP)NLi$
(**Li-2.21** & **Li-2.22**) was accomplished, though as was the case for converting **2.18/19** to
Li-2.18/19, yields were generally low (approximately 60% for **Li-2.21** and 70% for **Li-2.22**,
scheme 4.7). The aforementioned rationale for the low conversion of the larger aryl BBN
amines to the respective lithium amides also applies here. Under forcing conditions, these
lithiation reactions produced significantly more by-products.

[xiii]The highest yields obtained were approximately 50% (for **Li-2.18**) and 75% (for **Li-2.19**) (**scheme 4.7**)
[xiv]It is believed that the low conversion of **2.18/19**→**Li-2.18/19** is due to the magnitude of steric en-
cumbrance about the nitrogen centre in these compounds. The low-solubility of the **2.18** in polar and
non-polar hydrocarbon solvents compounds the difficulty of said lithiation (refer to **chapter 2, section
2.81**).

4.4.2 Coupling to Group 14 Elements

For all the lithium amides and subsequent salt-metathesis reactions, it was observed that the respective lithium amide was reactive towards group 14 element halides. However, ^{1}H NMR spectroscopic analyses of the resulting product mixtures were complex.

Unless otherwise stated, the following reactions were first conducted in a 1:1 ligand:tetrel element stoichiometric ratio. Later attempts were made using a 2:1 stoichiometry, which were all unsuccessful.
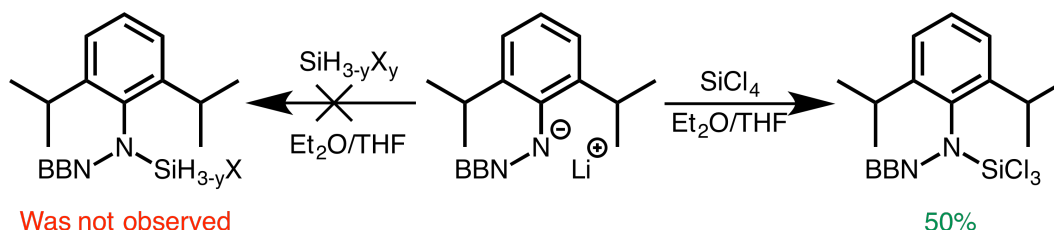
Silicon

Coupling **Li-2.17/19/22** to a silicon centre, to form species of the formula $LSiH_{3-y}X_y$, was generally unsuccessful (**scheme 4.7** and **4.8**). Preliminary ^{1}H & ^{29}Si NMR spectroscopic analyses indicated the trace formation of some new silicon species from these reactions. Upon standing in solution over 1-2 hours, the product mixtures were found to become increasingly more complex, indicative of product decomposition/further reaction.
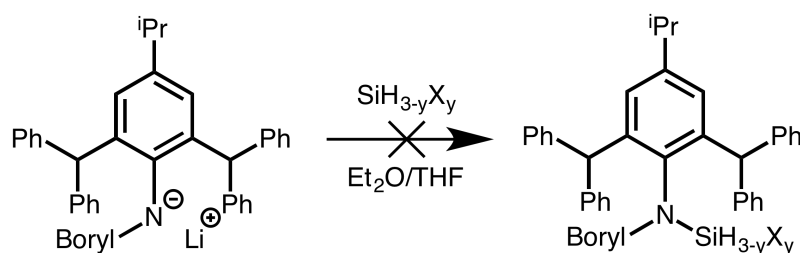
*Scheme 4.7: General scheme for the reaction of $Ar^{\dagger}(BBN/BBP)NLi$ (**Li-2.19/22**) and silicon species of the type $SiH_{3-y}X_y$ (where Boryl = BBN or BBP; X = Cl, Br, or I).*

In a single case, the reaction between **Li-2.17** and $SiCl_4$ yielded a product mixture which by ^{1}H NMR spectroscopic analyses was determined to be a 50:50 mixture of the pro-ligand **2.17** and some new compound. This new compound is presumed to be the desired $LSiCl_3$ compound (**scheme 4.8**).

*Scheme 4.8: General scheme for the reaction of $Dipp(BBN)NLi$ (**Li-2.17**) and silicon species of the type $SiH_{3-y}X_y$ (where X = Cl, Br, or I). Reactivity between the aforementioned compounds may have led to the formation of $[\{Dipp(BBN)N\}SiCl_3]$, based on ^{1}H NMR spectroscopic analyses.*

Attempts to isolate this new compound were not successful: upon standing in solution for 3-6 hours, the concentration of **2.17** increased with a decrease in concentration of the new compound. This decomposition could not be arrested using temperature control and isolating the crude-product mixture as a powder was shown to lead to decomposition[xv].

It is proposed that the increase N→B π bonding and subsequent weakening of the N-Si bond is the cause for instability in these compounds.

Germanium, Tin, and Lead

Dipp(BBN)NLi and MX₂: All reactions between **Li-2.17** and the heavier tetrel elements were fruitless and none of the desired LMX species were isolated (**scheme 4.9**). Preliminary ¹H NMR spectroscopic analyses of these reactions indicated the formation of complicated product mixtures[xvi].
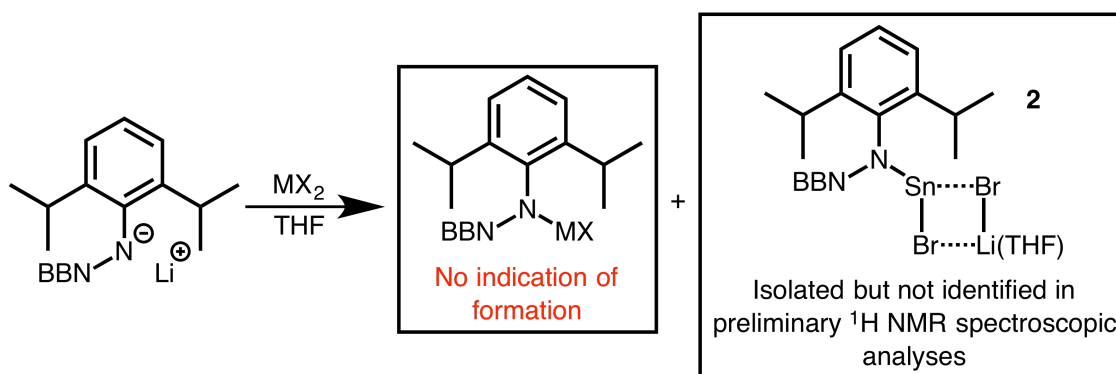
*Scheme 4.9: General scheme for the reaction of Dipp(BBN)NLi (**Li-2.17**) and MX₂ species and the formation of **3** (where X = Cl, Br, or I, and M = Ge, Sn, or Pb). All analyses indicated failure to form the desired species and, or, decomposition of some LMX compounds.*

From these reactions, fractional crystallisation allowed us to extricate some of the products. On three seperate occasions single crystals were isolated away from the bulk product mixture. These were found to be the compounds (DippNH₂)GeCl₂ (**1**), and [{Dipp(BBN)N}SnBr₂•Li(THF)₂] (**2**) (*vide infra*).

The inability of {Dipp(BBN)N}⁻ to form stable bonds with germanium, tin[xvii], or lead halides may be due to weaker nitrogen-tetrel bonding (as based on the stated rationale for our reactions with silicon, *vide supra*).

[xv]The ¹H NMR spectrum of the isolated powder did not resemble the product mixture in solution.

[xvi]The ¹H NMR spectra for these reaction mixtures indicated the reformation of starting materials, i.e. Dipp(BBN)NH (**2.17**), DippNH₂, and BBN, and therefore the occurrence of some decomposition.

[xvii]The exception to this is **4**, though the tin centre is more electronically saturated in comparison to the desired LMX species reffered to.

Ar†(BBN)NLi and MX$_2$: Under all attempted reaction conditions, the reaction of **Li-2.19** with germanium, tin, and lead halides eventuated in the formation of complicated product mixtures, as determined by ^{1}H NMR spectroscopic analyses (**scheme 4.10**.
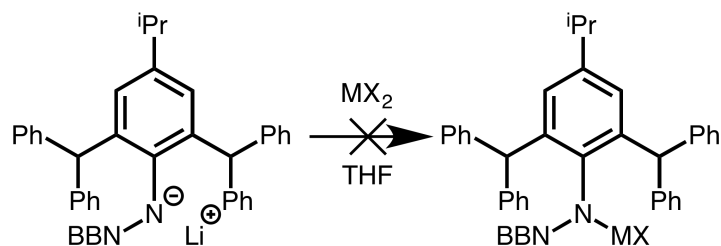
*Scheme 4.10: General scheme for reactions of Ar†(BBN)NLi (**Li-2.19**) with MX$_2$ (where X = Cl or Br and M = Ge, Sn, or Pb).*

For germanium and tin halides, upon addition of **Li-2.19**, the reaction solution went from a yellow/orange colour to deep red[xviii]. As the solution approached room temperature from –80 °C, at approximately –50 °C the red solution blackened due to the production of colloidal metal. The formation of colloidal metal occurs almost instantaneously (at approximately –70 °C) in the reactions with lead halides. This decomposition was confirmed by preliminary ^{1}H NMR spectroscopic analyses of the respective reaction mixtures.

Ar†(BBP)NLi and MX$_2$: Aside from lead halides, the reactions of tetrel halides with **Li-2.22** were somewhat successful, though the resultant compounds from these reactions were found to be unstable (**scheme 4.11**).
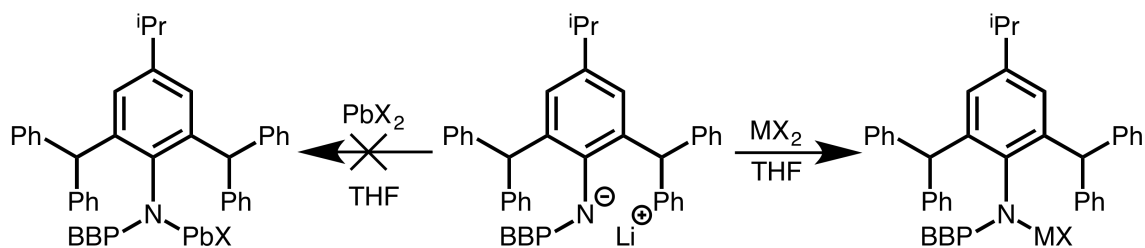
*Scheme 4.11: General scheme for the reaction of Ar†(BBP)NLi (**Li-2.22**) with MX$_2$ species (where M = Ge, X = Cl; For Pb and when M = Sn, X = Cl or Br).*

Addition of **Li-2.21** or **Li-2.22** to GeX$_2$ or SnX$_2$ at –80 °C eventuates in a red solution at –30 °C. The red colour is maintained if the solution is kept at below 0 °C[xix]. ^{1}H NMR spectroscopic analyses indicate the formation of a new compound, believed to be the respective LMX compounds. As the reaction proceeds, the concentration of this compound increases

---

[xviii]A typical observation for the formation of germylenes and stannylenes.

[xix]When the solution is allowed to reach room temperature the red colour of the solution dissipates to yellow/orange.

until approximately 0 °C. Temperatures past this point lead to increasingly complex product mixtures. Under optimal reaction conditions, the yield of these new products was found to be approximately 60% (for LGeCl) and 75% (For LSnBr).

Attempts to isolate the respective LMX compounds have proven difficult due to their instability in solution. It is on-going work to isolate these species, though their inherent instability does not bode well for future chemistry. Fractional crystallisation has led to the isolation of a number of compounds (*vide infra*).

For the reactions involving GeCl$_2$.dioxane, the compound [{Ar†(BBP)N}GeCl}] (**3**) was crystallised as a single crytsal (**figure 4.3**). Work is ongoing to characterise this compound.
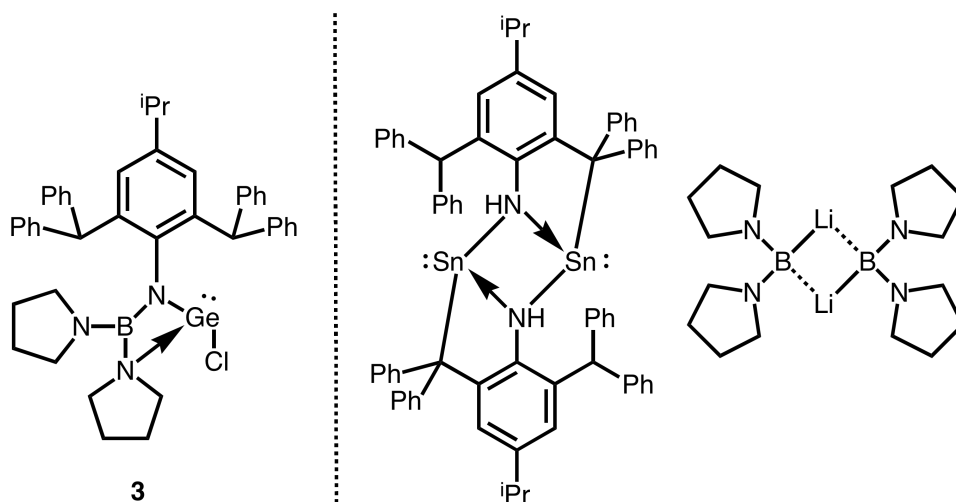
*Figure 4.3: Illustrations of the compounds obtained from the reactions of **Li-2.21/22** with GeCl$_2$.dioxane, viz. [{Ar†(BBP)N}GeCl}] (3), (left) and SnBr$_2$ (right).*

For the reactions involving SnBr$_2$, the co-crystalised compounds found do not correspond to the desired LSnBr compound but to decomposition products[xx] shown in **figure 4.3** (above). These products do not reflect the chemical shifts observed in the ^{1}H NMR spectrum of the mother liquor.

X-ray Crystallographic Characterisation of (DippNH$_2$)GeCl$_2$ (1) and [{Dipp(BBN)N}SnBr$_2$•Li(THF)$_2$] (2)

Single crystals of **1** and **2** were isolated from concentrated toluene solutions, hand-picked from unidentified co-microcrystaline and precipitous material.

[xx]Due to the low quality of the crystals and our dis-interest in these compounds, X-ray crystallographic characterisation was not fully conducted on these crystals.
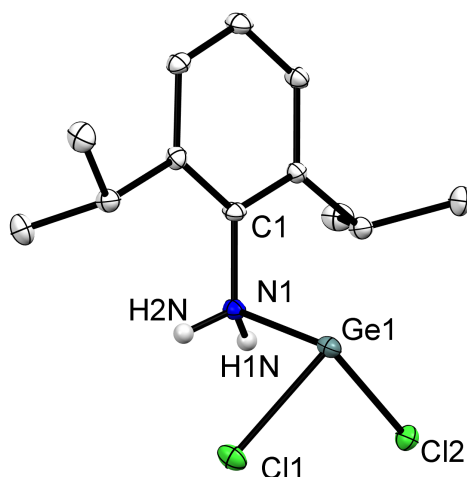
*Figure 4.4: Thermal ellipsoid plot (30% probability surface) of (DippNH₂)GeCl₂ (**1**) (hydrogen atoms omitted). Selected bond lengths (Å) and angles (°): Ge1-N1 2.171(3), Ge1-Cl1 2.279(1), Ge1-Cl2 2.274(1), N1-C1 1.448(5), N1-H1N 0.82(4), N1-H2N 0.88(5); C1-N1-Ge1 110.4(2), N1-Ge1-Cl1 90.80(8), N1-Ge-Cl2 90.59(8); C2-C1-N1-Ge1 88.7(3).*

The molecular structure of **1** reveals the Lewis-base adduct (DippNH$_2$)GeCl$_2$. The formally empty p orbital of the germanium atom accepts the nitrogen lone-pair of electrons forming a donor-acceptor interaction. The long Ge1-N1 bond length of 2.171(3) Å discounts the possibility of an electron sharing covalent bond between these two centres. This bond is longer than the average observed Ge-N bond length in loosely related and previously structurally characterised nitrogen-germanium-type Lewis-base adducts ($\overline{x}$ = 2.116 Å).[55–57] All other bond lengths and geometries are as expected.

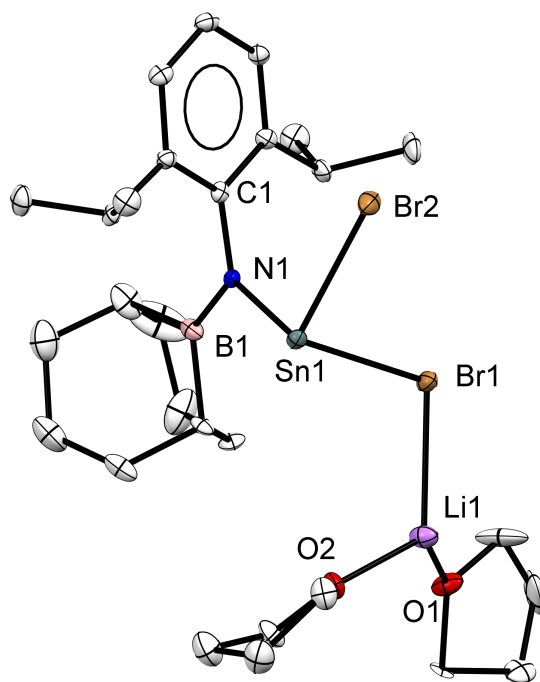*Figure 4.5: Thermal ellipsoid plot (30% probability surface) of [{Dipp(BBN)N}SnBr₂•Li(THF)₂] (**2**) (hydrogen atoms omitted). Selected bond lengths (Å) and angles (°): Sn1-N1 2.123(5), Sn1-Br1 2.681(7), Sn1-Br2 2.665(8), Br1-Li1 2.56(1), N1-C1 1.428(7), N1-B1 1.413(7); C6-C1-N1-Sn1 104.7(5), C6-C1-N1-B1 -85.9(7).*

2 is similar to the tin lithiate species {An(ᵗBu)N}SnBr₂•Li(THF)₂ (**3.5**), discussed in **chapter 3**. The nitrogen atom adopts a trigonal planar geometry and the ligand conformity is as expected, with bond distances and angles similar to that observed in the proligand Dipp(BBN)NH (**2.17**) (discussed in **chapter 2**). The tin atoms adopts a pseudo-pyramidal geometry and the Sn-Br bond distances vary slightly; the shorter Sn1-Br2 bond being 2.665(8) Å indicates its relation to the LSn fragment in comparison to Br1 which is more related to the Li(THF)₂ fragment.

4.4.3 Final Remarks

The weaker silicon-nitrogen bond, due to the presence of the BBN moiety, is a major contributor to the instability of the presumed transient $LSiH_{3-y}X_y$ & heavier tetrel LMX species. In the case of the BBP ligands we are unsure as to the reasons for decomposition, though based on our steric analysis of these ligands, instability and decomposition may be due to steric repulsion between the ligand and larger group 14 elements (presented in **chapter 2**). Work is on-going to isolate some of the aforementioned LMX species.

4.5 R&D: Bulky Amidinates

The predominant interest in the utilisation of bulky amidinates of the type $^{Dipp}Am^{*/\dagger}(^tBu/Ad)NH$ (**4** & **5**) was to access monomeric low-oxidation state group 14 complexes (of the formula $[LM]^+$) and, failing this, the related dimeric compounds (LMML).

4.5.1 Lithiations and Potassiations

The potassium amidinate salts $^{Dipp}Ar^{\dagger}(^tBu/Ad)NK$ (**K-4** & **K-5**) were synthesised as reported by Jones and co-workers (**scheme 4.12**).[53] The insolubility of $^{Dipp}Am^{*}(^tBu/Ad)NH$ in typical organic solvents precluded its further chemistry and lithiation and potassiation was unsuccessful[xxi]. Attempts to form the lithium salt for the $Ar^{\dagger}$ derivatives were also unsuccessful.
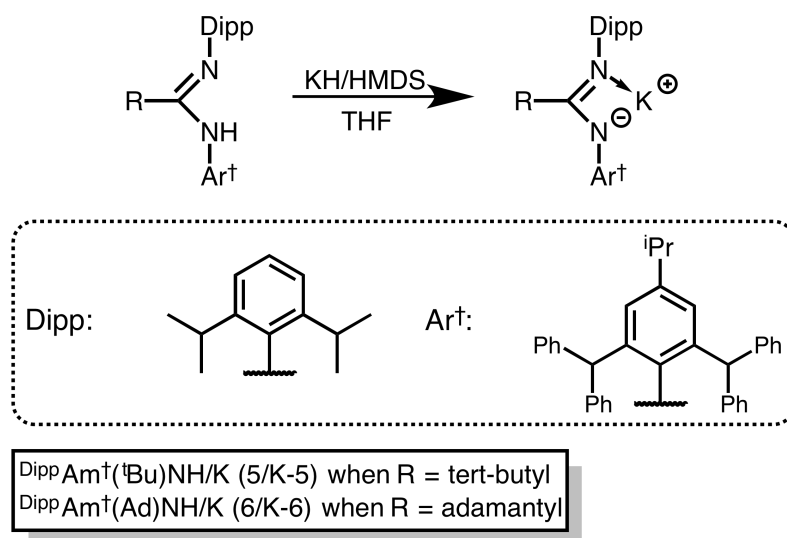
Scheme 4.12: Potassiation of $^{Dipp}Am^{\dagger}(^tBu/Ad)NH$ (**5** & **6**) to form $^{Dipp}Am^{\dagger}(^tBu/Ad)NK$ (**K-4** & **K-5**).

4.5.2 Coupling to Group 14 Elements

Isolation of the potassium salts $^{Dipp}Ar^{\dagger}(^tBu/Ad)NK$ (**K-4** & **K-5**) allowed us to explore their potential to bond to a range of group 14 element halides. As stated, **K-4** was utilised in our preliminary studies and will be the focus of discussion hereon in.

Generally, observations made for the 1:1 stoichiometric reactions of **K-5** against a tetrel halide species ("MX", where M = group 14 element and X = halide) was promising. Upon

---

[xxi]The insolubility of $^{Dipp}Ar^{*}(^tBu/Ad)NH$ meant conversion rates to the lithium or potassium salt congener were slow, and over time it was observed by ^1H NMR spectroscopic analyses that the potassium and lithium salts decompose, producing complicated reaction mixtures. The efficacy of this ligand is not appropriate for this chemistry.

reaction it was found that the dark/brown solution of **K-5** and "MX", at –80 °C, became
an off-yellow/orange colour with the concurrent formation of a white precipitate (believed
to be the respective KX species) at –30 °C. Preliminary ^{1}H NMR spectroscopic analyses of
the reaction mixture indicated the formation of multiple products where the primary/main
compound identified was the pro-ligand **5**. Minor products identified indicated some decom-
position[xxii]. Potentially, the presumptive $LSiH_{3-y}X_y$ and LMX species are formed during this
reaction but are too unstable due to steric congestion.

For the reactions between **K-4** and $HSiCl_3$, $GeCl_2.dioxane$, or $SnBr_2$, closer analyses of
the ^{1}H NMR spectra indicated the formation of a distinct new minor product (approximately
30-35% yield) (**scheme 4.13**).
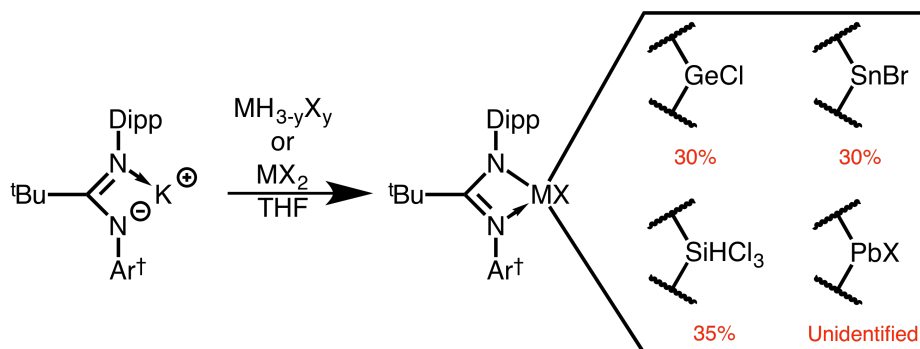
*Scheme 4.13: General synthesis of the presumptive $LSiH_{3-y}X_x$ and LMX species (where L =
$\{^{Dipp}Am^\dagger(^tBu)N\}^-$ and M = Ge, Sn, or Pb).*

Under no circumstances were these minor products isolated away from the bulk prod-
uct mixture[xxiii]. Fractional crystallisation continuously led to the co-crystalisation of **5**
and an unidentified micro-crystalline material. In a single instance crystals of the salt
$[^{Dipp}Am^\dagger(^tBu)NH_2][GeCl_3]$ (**6**) were isolated and garnered the molecular structure (*vide in-
fra*).

Attempts were made to form the desired LGeX and LSnX compounds via a protolysis
pathway, though under no conditions was this achieved using either **5** or **6**. For both ger-
manium(II) and tin(II) halides, the halides were substituted with an alkoxide, methoxide
($\{MeO\}^-$) or tert-butoxide ($\{^tBuO\}^-$), or the bis(silyl) amide ($\{(TMS)_2N\}^-$, before being
reacted with the pro-ligand. The major products from these reactions are the respective
pro-ligand and fragments of said ligand.

K-5 gave similar results: the final product mixtures were more complex from these
reactions. The altered bite angle - between **K-4** and **K-5** - is the most likely cause for this

---

[xxii]Fragments of the ligand being identified within the product mixture ($Ar^\dagger NH_2(10\%)$, $DippNH_2$ (5%), etc.
[xxiii]The similar solubility between these products and the pro-ligand has not allowed for separation of these
    species. *In vacuo* removal of solvents caused some decomposition of the identified minor product; allowing
    the product mixture solution to stand also leads to decomposition.

increase in decomposition.

X-ray Crystallographic Characterisation of [^{Dipp}Am†(^{t}Bu)NH$_2$][GeCl$_3$] (6)

The molecular structure of the Lewis acid-base adduct **6** displays the doubly protonated cationic amidinate [^{Dipp}Ar†(^{t}Bu)NH$_2$]$^+$ and the anionic germanium halide [GeCl$_3$] (**figure 4.6**). The unit cell of this crystal contains two independent molecules of **6** with essentially the same geometry; only bond angles for one of the two molecules are focused on. Notable geometric differences between the three molecules are discussed where appropriate.
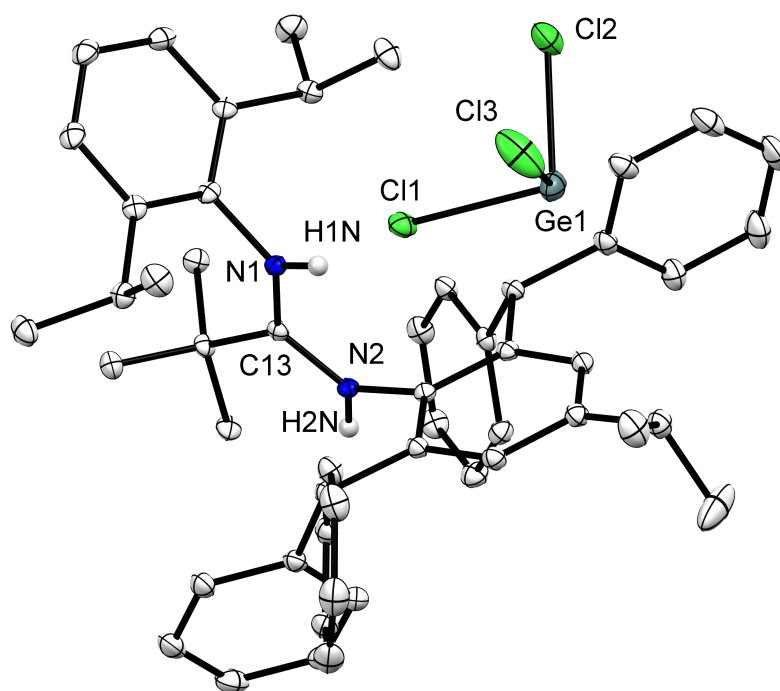

*Figure 4.6: Thermal ellipsoid plot (30% probability surface) of [^{Dipp}Am†(^{t}Bu)NH$_2$][GeCl$_3$] (**6**) (hydrogen atoms and extraneous molecules of **6** are omitted for clarity). Selected bond lengths (Å) and angles (°): Molecule One: N1-C1 1.455(3), N1-C13 1.326(3), N2-C13 1.329(3), N2-C18 1.488(3), C13-C14 1.546(4), N1-H1N 0.82(3), N1-H2N 0.82(4), Cl1-H1N 2.48(4), Ge1-Cl1 2.329(1), Ge1-Cl2, 2.286(1), Ge1-Cl3 2.277(2); Cl1-Ge1-Cl3 93.66(4), Cl3-Ge1-Cl2 96.19(4), Cl2-Ge1-Cl1 96.99(3), C1-N1-C13 128.8(2), H1N-N1-C1 115.0(3), H1N-N1-C13 116.0(3), C13-N2-C18 129.2(2), H2N-N2-C13 117.0(2), H2N-N2-C18 114.0(2).*

The germanium atom in the [GeCl$_3$]$^-$ anion adopts a pyramidal geometry with an average Cl-Ge-Cl bond angle of 95.61 °. The Ge-Cl bond distances vary with Ge1-Cl2 & Ge1-Cl3 being shorter than the Ge1-Cl1 bond; the average Ge-Cl bond length of this compound ($\bar{x}$ = 2.297 Å) is similar to those of other structurally charcaterised [GeCl$_3$]$^-$ anions and to the calculated to the calculated Ge-Cl bond length value (2.309 Å).[58–61] The slight discrepancy between the Ge-Cl bond distances within this molecular structure may be attributed

to a weak interaction between Cl1 with the H1N[xxiv] proton upon the N1 centre, with a bond distance of 2.48 Å.[62] The cation-to-anion orientation is believed to be caused by this interaction.

6 is believed to have formed in the same way as described for [An(^{t}Bu)NH$_2$][GeCl$_3$](**3.4**), discussed in **chapter 3**.

4.5.3 Conclusion

The inability to form compounds of the general formula LSiH$_{3-y}$X$_y$ or LMX, using **K-4** or **K-5** prompted us to abandon the project. Whilst there is no evidence to suggest why these compounds could not be formed and stabilised, it is apparent that some reaction occurs between the tetrel halides and **K-4/5**, as the potassium salt is not retained in the final product mixture. It is proposed that steric congestion in the presumptive LSiH$_{3-y}$X$_y$ or LMX species, which form during this reaction, leads to decomposition and bond fission within the compound. Such decomposition explains the observed ligand fragmentation.

4.6 R&D: Chiral Amidinates

Unpublished work from the Jones group indicated the potential to form low-oxidation state group 2 alkaline earth compounds which contain a chiral moiety.[63] These compounds were stabilised using the amidinate ^{C1}Am*(^{t}Bu)NH (**7**) as the ligand ({^{C1}Am*(^{t}Bu)N}$^-$; where C1 = -C(H)(Me)(Ph)). Preliminary reactivity studies with these chiral-amidinate stabilised group 2 compounds indicate their potential enantioselectivity. The promise shown from these initial results prompted us to investigate complexes where the ECOI is a group 14 element centre. However, it was found that these ligands do not provide the necessary kinetic stabilisation nor the innocence[xxv] required for low-oxidation state group 14 chemistry.

### 4.6.1 Lithiations and Potassiations

Synthesis

7 was synthesised via unpublished methods and lithiated in situ to form ^{C1}Am*(^{t}Bu)NLi (**Li-7**), as shown in **scheme 4.14** (C1 was used as an enantiopure reagent). Conversion to the lithium amidinate salt **Li-7** was successful. Isolation of **Li-7** was not accomplished: removing solvents *in vacuo* leads to the partial decomposition of **Li-7** and regeneration of

---

[xxiv]However, as no neutron diffraction were performed, the presence of these protons cannot be confirmed but only suggested.

[xxv]They are reactive at sites not expected, i.e. the tertiary proton of the benzhydrol-like moieties of Ar*.

7.
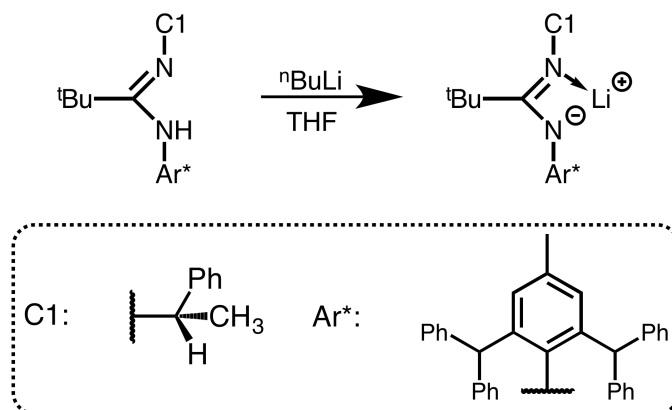
*Scheme 4.14: Lithiation of $^{C1}Am^*(^tBu)NH$ (**7**) to form $^{C1}Am^*(^tBu)NLi$ (**Li-7**).*

4.6.2   Coupling to Group 14 Elements

Synthesis

The addition of **Li-7**, generated in situ, to a range of tetrel halide species was conducted in THF and gave varying results (**scheme 4.15**). The following reactions were all conducted in a 1:1 stoichiometric ratio unless otherwise stated.
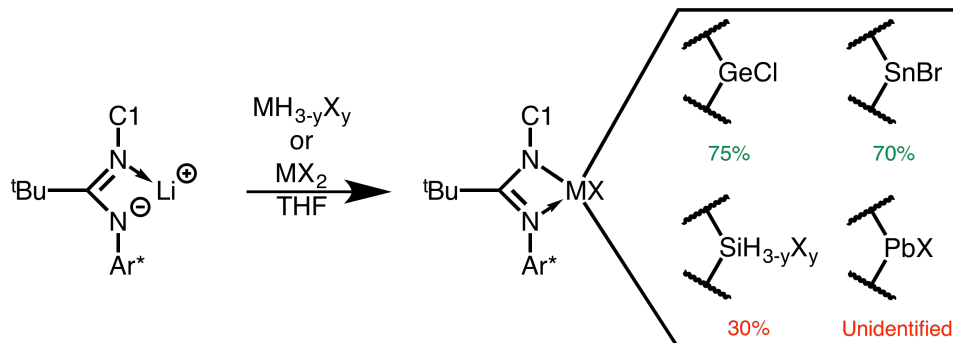
Scheme 4.15: General synthesis for the presumptive $LSiH_{3-y}X_x$ species and the isolated LGeCl and LSnBr compounds (where $L = \{^{C1}Am^*(^tBu)N\}^-$).

The least promising results came from our reactions with silicon ($SiH_{3-y}X_y$) and lead (PbX_2) species. These reactions resulted in the formation of complicated product mixtures where the major product identified was **7** (ca. 50% as determined by ^1H NMR spectroscopy). Generally, the reactions conducted with $SiH_{3-y}X_y$ species, a minor new product was identified by ^1H NMR spectroscopic analyses at $<0°$ C, though over time the concentration of this species decreases regardless of the reaction temperature. This compound is somewhat unstable and all attempts to isolate it have been unsuccessful.

For germanium and tin halides, the reactions with **Li-7** led to the successful formation of [{^{C1}Am*(^{t}Bu)N}GeCl] (**8**) and [{^{C1}Am*(^{t}Bu)N}GeCl] (**9**). Both compounds can be isolated as powders by the *in vacuo* removal of solvents and subsequent extraction, though there is always contamination with by-products[xxvi]. Crystallisation efforts for these compounds are ongoing.

4.6.3   Attempted Reduction and Hydride Formation

All attempts to reduce **8** & **9** have been unsuccessful, always leading to the reformation of starting materials and other by-products. These reductions have been attempted using KC$_8$, activated sodium metal, and [{(^{Mes}nacnac}Mg)$_2$]. Metal deposition occurs within these reactions, which suggests some reaction takes place, though the resulting products decompose.

The formation of the germanium and tin hydrides ([{^{C1}Am*(^{t}Bu)N}GeH] & [{^{C1}Am*(^{t}Bu)N}SnH]) is on-going work. Direct synthesis of these compounds using di-isobutylaluminium hydride (DIBAL), lithium borohydride ([LiBH$_4$]), and lithium aluminium hydride ([LiBH$_4$]), has not yet been successful. Current work focuses on σ-bond metathesis reactions to form the hydride complexes.

Synthesis of LMOR Species

Hydride precursor species of the type LMOR should allow access to the desired hydride germanium and tin species[xxvii]. **Scheme 4.16** illustrates the general synthetic routes to such LMOR compounds and the yields of each respective compound. The most promising of these reactions utilised KOMe, presumably due to a reduction in steric congestion in comparison to KO^{t}Bu.

[xxvi]This has made analysis difficult thus far.
[xxvii]See **chapter 3, section 3.2**
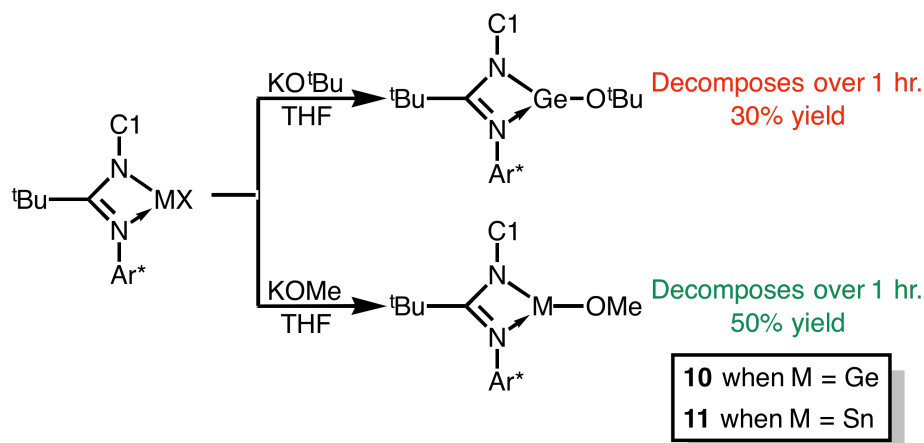
Scheme 4.16: General synthesis of LMOR compounds (where L = {^{C1}Am(^{t}Bu)N}$^-$; M = Ge or Sn; R = Me or ^{t}Bu). Only [{^{C1}Am*(^{t}Bu)N}GeOMe] (**10**) and [{^{C1}Am*(^{t}Bu)N}SnOMe] (**11**) have been isolated.*

Reactions using both KO^{t}Bu and KOMe with **8** and **9** produced the respective LMOR compounds when allowed to reach room temperature. However, prolonged stirring at room temperature results in decomposition. This is accelerated for those compounds containing -O^{t}Bu. The compounds [{^{C1}Am*(^{t}Bu)N}GeOMe] (**10**) and [{^{C1}Am*(^{t}Bu)N}SnOMe] (**11**) are believed to have been formed, though all analyses indicates their rapid decomposition. This was noted as metal deposition occurred over the period of one hour. The spectra of these reaction mixtures indicate 50% yield of the target compounds, at best. Ongoing work is to isolate these compounds and, or, generate them in situ for further chemistry (*vide infra*).

Attempts to convert **10** and **11** to the respective hydride compounds is our current focus, though preliminary results are not promising. For both compounds, pinacolborane (HBPin[xxviii]) was used as the hydride source of choice, being added to a toluene solution of **10** or **11** at –80 °C. Allowing these reactions to stir above 0 °C leads to the production of colloidal metal. This occurs at a faster rate for tin than germanium. Preliminary ^{1}H NMR spectroscopic analyses indicates that some new minor compound is formed in both these reactions.

4.6.4   Conclusion

The utilisation of **Li-7** did not yield the desired silicon or lead halide complexes, though did allow for the synthesis of the germanium and tin halide complexes, **8** & **9**. Our attempts to reduce **8** & **9** have not been successful as of yet. Current work is focused on producing the related germanium and tin hydride compounds. Initial results seem promising and we have formed the alkoxide precursors **10** & **11**. The greatest issues this project faces is the

---

[xxviii]Also known as 4,4,5,5-Tetramethyl-1,3,2-dioxaborolane

reduced kinetic stability these ligands provide to the ECOI.

4.7 R&D: Chiral Nacnacs

Lee and co-workers published the synthesis of a chiral nacnac ^{Dipp}nacnac^{C1} (**12**); and, within our own group, this work has allowed access to chiral nacnac magnesium hydrides species.[54] The successful utilisation of **12** in the stabilisation of magnesium hydrides indicated its suitability for use as a kinetically stabilising ligand. Our interest in catalysis drove us to adopt similar nacnacs and incorporate them for low-oxidation state group 14 element chemistry. To these ends, salt-metathesis coupling of this ligand to a range of group 14 element centres were attempted, albeit to little success.

4.7.1 In Situ Lithiation and Group 14 Element Coupling

Attempted Synthesis

12 was synthesised as per previously reported methods, and lithiated in situ to generate **Li-12**.[63] The ^{1}H NMR spectrum of the reaction mixture displays chemical shifts which are generally shifted downfield, in comparison to those of the pro-ligand **12**, and the loss of the chemical shift assigned to the N-H proton.
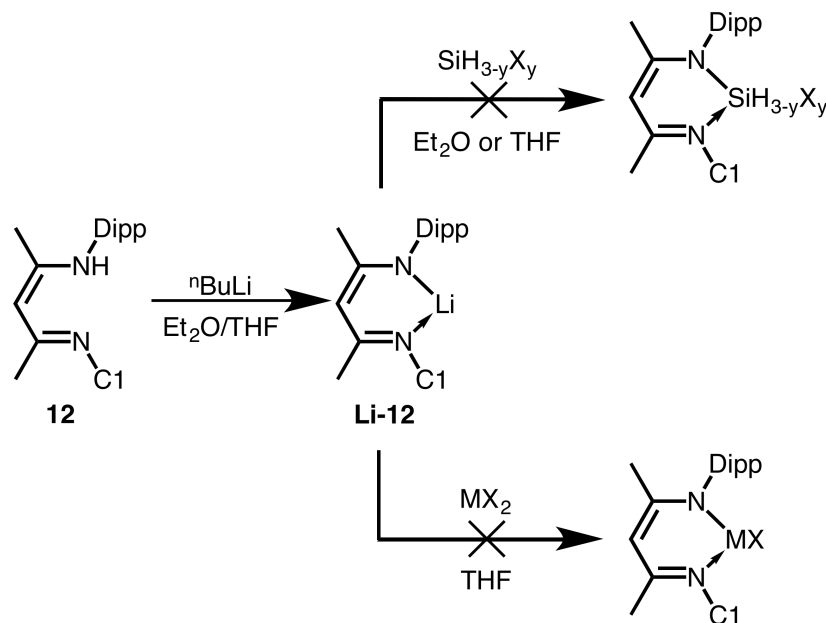
Scheme 4.17: *General synthesis of the presumptive LSiH$_{3-y}$X$_x$ and LMX species (where L = {$^{C1/Dipp}$nacnac}$^-$ and M = Ge or Pb). Work is ongoing with SnX$_2$.*

In situ generated **Li-12** was reacted with a series of tetrel halides in an attempt to form

$LSiH_{3-y}X_y$ and LMX compounds. In all cases, a reaction appeared to take place. The starting orange coloured reaction mixture, at –80 °C, produced a white precipitate as the solution was allowed to approach room temperature with the concurrent change to a yellow/orange solution. Preliminary ^{1}H NMR spectroscopic analyses of the crude product mixtures from these reactions generally indicated the formation of a minor new product, aside from those reactions conducted with lead halides.

Reactions with lead halides were - by observation - believed to form some new product but decomposed at –70 °C as indicated by lead deposition, which remained suspended in solution. ^{1}H NMR spectroscopic analyses of this mixture indicated a complicated mixture of products.

Reactions with silicon and germanium halides gave some new minor product in approximate yield of 10-30%. However, upon leaving the respective reaction mixtures to stand in solution, at any temperature, the new minor products were observed to decompose (or further react) and were no longer observable by ^{1}H NMR spectroscopy. The product mixture from all these reactions gave complicated mixtures of products. Reactions with tin(II) dibromide are ongoing, though early results look promising. A new product has been formed in approximately 80% yield as determined by ^{1}H NMR spectroscopic analyses.

4.7.2   Conclusion

The utilisation of **Li-12** as a kinetically stabilising ligand for silicon, germanium, and lead centres was partially successful. For silicon and germanium, the formation of complicated product mixtures and the fast rate of decomposition of an identified minor new product (for each tetrel element noted) indicate the inability of this ligand to stabilise the product. This was also observed in our reactions of **Li-12** with lead halides, though decomposition occurs almost instantaneously. Lead deposition was the indicative sign of said decomposition. Work is on-going with this ligand in relation to low-oxidation state germanium and tin chemistry, which gave the most promising results.

4.8   Future Work

The inclusion of boryl substituents within the framework of bulk amide ligands may to lead to weaker N-M bonds due to reduced π interaction. This in combination with increased steric repulsion makes the resulting LMX and $LSiH_{3-y}X_x$ compounds unstable. It is suggested that work shift towards the use of smaller amide ligands or the inclusion of boryl motifs in carbon donor based ligands.

Our work with super bulky amidinates indicates there is a steric limit for ligands, which

when reached may disallow coupling to group 14 element centres[xxix]. Similar work incorporating chiral moieties into the ligand design have proved promising and may provide a route to forming chiral low-oxidation state tetrel compounds. However, early work indicates issues with the kinetic stability of these compounds. Focus should be shifted towards ligands which provide a chiral auxiliary whilst maintaining sufficient steric encumbrance.

[xxix]Coupling is possible, though from our work it is found to lead to ionic complexes.

4.9 Experimental

Ar$^{\text{Dipp}}$(BBN)NLi (Li-2.17). To a stirred solution of Ar$^{\text{Dipp}}$(BBN)NH (1.00g, 3.3 mmol) in THF (or diethyl ether) was added $^{\text{n}}$BuLi (1.6 M, 3.5 mmol) dropwise at –80 °C, the solution was then allowed to stir at room temperature (24 °C) for 2 hrs. This solution was used in situ for further chemistry. ^{1}H NMR (benzene-d$_6$, 400 MHz, 298 K): δ = 0.825 (d, J$_{\text{HH}}$ = 7.21 Hz, 6H, CH-(CH_3)$_2$), 1.17 (d, J$_{\text{HH}}$ = 7.32 Hz, 6H, CH-(CH_3)$_2$), 1.51, 1.77, 2.03, 2.07 (overlapping multiplets, 11H, BBN-H), 3.41 (sept., J$_{\text{HH}}$ = 6.80 Hz, 2H, CH-(CH$_3$)$_2$), 6.90-7.16 (3H, Ar-H); ^{7}Li NMR (155 MHz, 298 K): δ = 0.37; ^{11}B{^{1}H} NMR (128 MHz, 298 K): δ = 17.44; ^{13}C{^{1}H} NMR (benzene-d$_6$, 75.5 MHz, 298K): δ = 22.03 (Dipp-CH(CH_3)$_2$), 25.52, 35.12, 36.19 (BBN-C), 52.73 (Dipp-CH(CH$_3$)$_2$), 126.26, 126.41, 129.52, 130.78, 136.24 (Ar-C).

(DippNH$_2$)GeCl$_2$ (1). The named compound was isolated from the reaction of **Li-2.17** and GeCl$_2$.dioxane. Adding both reagents together as THF mixtures, at –80 °C, and allowing to stir to room temperature overnight gave an orange/yellow solution. Extracting the products from this reaction gives a mixture of compounds including **1**. No other new products were identified from this reaction.

{Dipp(BBN)N}SnBr.LiBr(THF)$_2$ (2). To a THF solution of SnBr$_2$ (1.00g, 3.6 mmol) was added a THF solution of **Li-2.17** (1.143g, 3.8 mmol), dropwise, at –80 °C. The solution was then allowed to stir to room temperature for 8 hrs. Volatiles were removed *in vacuo* and the remaining residue extracted in hexane. This extract was concentrated *in vacuo* until precipitation was noted and the solution filtered away. The filtrate was placed in a 5 °C fridge, over two-weeks a few red-blocked crystals were isolated, which were suitable for X-ray diffraction at the Australian Synchrotron. The yield of **2** was too low for the collection of spectroscopic data.

Ar*(BBN)NLi (Li-2.18). To a stirred solution of Ar*(BBN)NH (1.00g, 1.8 mmol) in THF (or diethyl ether) was added $^{\text{n}}$BuLi (1.6 M, 1.9 mmol), dropwise, at –80 °C. This solution was then allowed to stir at room temperature (24 °C) for 2 hrs. This solution was used in situ for further chemistry. ^{1}H NMR (benzene-d$_6$, 400 MHz, 298 K): δ = 1.85 (br. s, 3H, BBN-H, *tenuous assignment*), 2.05 (s, 3H, Ar-CH_3), 2.13, 2.23, 2.42 (overlapping multiplets, 9H, BBN-H), 6.39 (s, 2H, -CH-(CH$_3$)$_2$), 6.67 (s, 2H, CHPh$_2$), 7.01-7.34 (Ar-H); ^{11}B{^{1}H} NMR (128 MHz, 298 K): δ = 54.95.

Ar†(BBN)Li (Li-2.19). To a stirred solution of Ar†(BBN)NH (1.00g, 1.7 mmol) in THF (or diethyl ether) was added $^{\text{n}}$BuLi (1.6 M, 1.9 mmol) dropwise at –80 °C. The solution was then allowed to stir at room temperature (24 °C) for 2 hrs. This solution was used in situ for further chemistry. ^{1}H NMR (benzene-d$_6$, 400 MHz, 298 K): δ = 1.095 (d, J$_{\text{HH}}$ = 7.30 Hz, 6H, -CH(CH_3)$_2$), 1.76, 2.97, 2.20 (multiple overlapping multiplets, 11H, BBN-H), 2.65 (sept., J$_{\text{HH}}$ = 6.83 Hz, 1H, -CH(CH$_3$)$_2$), 6.53 (s, 2H, CHPh$_2$), 6.93-7.40 (Ar-H), ^{7}Li NMR (155 MHz, 298 K): δ = -0.72; ^{13}C{^{1}H} NMR (benzene-d$_6$, 75.5 MHz, 298K): δ = 25.40 (Ar-CH(CH_3)$_2$), 34.54 (Ar-CH(CH$_3$)$_2$), 35.14, 36.20 (BBN-C), 52.88 (CPh$_2$), 126.29,

126.00, 128.75, 128.96, 130.72, 130.83, 135.94, 136.94, 147.38, 147.83, 157.56 (Ar-C).

Ar*(BBP)NLi (Li-2.21). To a stirred solution of Ar*(BBP)NH (1.00g, 1.70 mmol) in THF (or diethyl ether) was added ^{n}BuLi (1.12 mL, 1.6M) dropwise at –80 °C, the solution was then allowed to stir at room temperature (24 °C) for 2 hrs. This solution was used in situ for further chemistry. ^{1}H NMR (benzene-d_6, 400 MHz, 298 K): δ = 1.56 (m, 8H, BBP-H), 2.14 (s, 3H, Ar-CH_3), 3.14 (m, 8H, BBP-H), 6.55 (s, 2H, Ar-CH(Ph)$_2$), 7.00 (s, 2H, Ar-*(ortho-H)*), 7.01 – 7.43 (m, 20H, Ph-H); ^{7}Li NMR (155 MHz, 298 K): δ = 0.40; ^{11}B1H NMR (128 MHz, 298 K): δ = 22.93; ^{13}C{^{1}H} NMR (benzene-d_6, 75.5 MHz, 298 K): δ = 22.08 (Ar-CH_3), 27.35 (BBP-C), 27.64 (BBP-C), 48.36 (BBP-C), 49.41 (BBP-C), 53.70 (CHPh$_2$), 122.35, 126.01, 128.86, 129.07, 130.66, 131.05, 134.87, 145.34, 148.44, 156.30 (Ar-C).

{Ar†(BBP)N}Li (Li-2.22). To a stirred solution of Ar†(BBP)NH (1.00g, 1.62 mmol) in THF (or diethyl ether) was added ^{n}BuLi (1.06 mL, 1.6M) dropwise at –80 °C, the solution was then allowed to stir at room temperature (24 °C) for 2 hrs. This solution was used in situ for further chemistry. ^{1}H NMR (benzene-d_6, 400 MHz, 298 K): δ = 1.17 (d, J_{HH} = 7.07 Hz, 6H, Ar-CH(CH_3)$_2$), 1.58 (m, 8H, BBP-H), 2.74 (sept. J_{HH} = 6.86 Hz, 1H, Ar-CH(CH$_3$)$_2$), 3.14 (m, 8H, BBP-H), 6.45 (s, 2H, Ar-CH(Ph)$_2$), 7.07 (s, 2H, Ar-*(ortho-H)*), 7.16 – 7.47 (m, 20H, Ph-H); ^{7}Li NMR (155 MHz, 298 K): δ = -0.14; ^{11}B{^{1}H} NMR (128 MHz, 298 K): δ = 21.52, 31.33, 45.22; ^{13}C{^{1}H} NMR (benzene-d_6, 75.5 MHz, 298K): δ = 25.41 (Ar-CH(CH_3)$_2$), 26.12 (BBP-C), 27.43 (BBP-C), 34.44 (BBP-C), 49.25 (Ar-CH(CH$_3$)$_2$), 53.81 (CHPH$_2$), 68.61(BBP-C), 126.38, 130.90, 134.86, 148.12 (Ar-C).

{Ar†(BBP)N}GeCl (3). The named compound was isolated as a single crystal from the reaction of **Li-2.22** and GeCl$_2$.dioxane in THF. Both reagents were added together at –80 °C and allowed to stir to room temperature. The residue from the reaction were extracted in hexane and this solution was concentrated. The solution was placed in a –30 ° freezer were precipitation and crystallisation occurred. ^{1}H NMR (benzene-d_6, 400 MHz, 298 K): δ = 1.005 (d, J_{HH} = 6.98 Hz, 6H, Ar-CH(CH_3)$_2$), 1.43 (m, 4H, BBP-H), 2.26 (m, 4H, BBP-H), 2.56 (sept. J_{HH} = 6.81 Hz, 1H, Ar-CH(CH$_3$)$_2$), 3.56 (m, 4H, BBP-H), 6.73 (s, 2H, Ar-CH(Ph)$_2$), 6.89 – 7.47 (Ar-H).

[^{Dipp}Am†(^{t}Bu)NH$_2$]$^+$[GeCl$_3$]$^-$ (6). To a THF solution of GeCl$_2$.dioxane was added a THF solution of ^{Cl}Am*NLi at –80 °C, dropwise over five minutes. The solution was then allowed to warm to room temperature (24 °C) and stir overnight (12 hrs). Volatiles were removed *in vacuo* and the residue extracted in hexane. This hexane solution was concentrated *in vacuo* before being placed in a –30 °C. Single colourless needle-like crystals formed under these conditions in the presence of unidentified precipitate and with concurrent co-crystalisation of the pro-ligand ^{Dipp}Ar†(^{t}Bu)NH

Note: the following compounds have only been tenuously assigned. Due to instability and our current inability to isolate the single compounds the obtained NMR spectra are convoluted and difficult to definitively assign.

{^{Cl}Am*(^{t}Bu)N}GeCl (8). To a diethyl ether solution of GeCl$_2$.dioxane (0.366g, 1.58

mmol) was added a diethyl ether solution of ^{C1}Am*NLi (1.00g, 1.58 mmol) at –80 °C, the solution was then allowed to warm to room temperature (24 °C) and stir overnight (12 hrs). Volatiles were removed *in vacuo* and the residue extracted with hexane. This solution was pumped dry to yield the product as an off-white/orange powder (yield ≈75%). ^{1}H NMR (benzene-d$_6$, 400 MHz, 298 K): δ = 0.86 (s, 9H, -^{t}Bu-H), 1.695 (d, J$_{HH}$ = 7.20 Hz, 3H, C(H)(Ph)-CH_3), 1.82 (s, 3H, Ar-CH_3), 5.015 (sept. J$_{HH}$ = 6.78 Hz, C(CH$_3$)(Ph)H), 5.70 (s, 1H, CHPh$_2$), 6.70 (s, 1H, CHPh$_2$), 6.80-7.75 (Ar-H); ^{13}C{^{1}H} NMR (benzene-d$_6$, 75.5 MHz, 298K): δ = 14.93, 21.75, 23.61, 24.56, 29.33, 30.61, 32.51, 40.47, 51.46, 53.15, 53.74, 57.40, 126.65, 127.57, 129.76, 130.29, 135.22, 140.95, 141.11, 142.52, 142.95, 143.92, 144.36, 145.13, 147.20, 180.53; IR (ATR, Nujol): $\bar{v}$ (cm^{-1}) = 801, 1020, 1095, 1261, 1378, 1463, 1557, 1600, 1360, 2856, 2956, 3564, 3915; EI/MS m/z (%): 734.4 (M$^+$, >1%), 699.5 (M$^+$ − Cl, >1%), 626.5 (LH$_+$, 20%), 459.4 (M − (GeCl & CHPh$_2$), 80%), 422.2 (Ar*NH$_2$$^+$, 5%), 253.2 (M$^+$ − (^{t}Bu & Ar*), 2%), 206.1 (N(C^{t}Bu)NHGeCl$^+$, 5%), 167.1 (CPh$_2$$^+$, 75%), 105.1 (C1$^-$, 100%), 57.2 (^{t}Bu$^-$, 10%); Anal. Calc. (%) for C$_{50}$H$_{53}$ClGeN$_2$: C, 75.28; H, 6.18; N, 3.82; found (%): C, 76.55; H, 6.91; N, 3.28.

{^{C1}Am*(^{t}Bu)N}SnBr (9). To a dietyl ether solution of SnBr$_2$ (0.44g, 1.58 mmol) was added a diethyl ether solution of ^{C1}Am*NLi (1.00g, 1.58 mmol) at —80 °C, the solution was then allowed to warm to room temperature (24 °C) and stir overnight (12 hrs). Volatiles were removed *in vacuo* and the residue extracted with hexane. This solution was pumped dry to yield the product as an off-white/orange powder (yield ≈70%). ^{1}H NMR (benzene-d$_6$, 400 MHz, 298 K): δ = 0.95 (s, 9H, -^{t}Bu-H), 1.70 (br. s (should be doublet), 3H, C(H)(Ph)-CH_3), 1.865 (s, 3H, Ar-CH_3), 5.20-5.25 (m, 1H, C(CH$_3$)(Ph)H), 6.42 (s, 1H, CHPh$_2$), 6.71 (s, 1H, CHPh$_2$), 6.78-7.77 (Ar-H); ^{13}C{^{1}H} NMR (benzene-d$_6$, 75.5 MHz, 298K): δ = 12.81, 19.58, 21.51, 27.44, 28.01, 28.50, 30.43, 40.64, 55.03, 125.18, 127.26, 127.29, 127.31, 127.88, 128.56, 132.14, 132.57, 133.13, 137.22, 136.66, 139.08, 140.11, 141.65, 142.14, 143.76, 144.02, 178.21; ^{119}Sn{^{1}H} NMR (benzene-d^6, 149 MHz, 273 K): δ = 204.09; IR (ATR, Nujol): $\bar{v}$ (cm^{-1}) = 700, 801, 1020, 1093, 1261, 1463, 1494, 1600, 2424, 2730, 2854, 2024, 3058, 3650; EI/MS m/z (%): 824.4 (M$^+$, >1%), 745.5 (LSn$^+$, >1%), 626.6 (L$^+$, 22.5%), 521.4 (L$^+$H (-C1 & SnBr), 32%), 429.3 (Ar*NH$_2$, 10%), 294.1 (N(C^{t}Bu)NSnBr, 10%), 167.1 (CPh$_2$$^+$, 50%), 105.1 (C1$^-$, 100%), 57.2 (^{t}Bu$^-$, 5%); Anal. Calc. (%) for C$_{50}$H$_{53}$BrSnN$_2$: C, 67.01; H, 5.50; N, 3.40; found (%): C, 68.64; H, 6.16; N, 3.20.

Bibliography

[1] J. Huheey and T. Cottrell, "The Strengths of Chemical Bonds," 1958.

[2] A. V. Protchenko, K. H. Birjkumar, D. Dange, A. D. Schwarz, D. Vidovic, C. Jones, N. Kaltsoyannis, P. Mountford, and S. Aldridge, "A Stable Two-Coordinate Acyclic Silylene," *Journal of the American Chemical Society*, vol. 134, no. 15, pp. 6500–6503, 2012.

[3] A. V. Protchenko, M. P. Blake, A. D. Schwarz, C. Jones, P. Mountford, and S. Aldridge, "Reactivity of Boryl-and Silyl-Substituted Carbenoids toward Alkynes: Insertion and Cycloaddition Chemistry," *Organometallics*, vol. 34, no. 11, pp. 2126–2129, 2015.

[4] M. Brynda, R. Herber, P. B. Hitchcock, M. F. Lappert, I. Nowik, P. P. Power, A. V. Protchenko, A. Růžička, and J. Steiner, "Higher-Nuclearity Group 14 Metalloid Clusters: $[Sn_9\{Sn(NRR')\}_6]$," *Angewandte Chemie International Edition*, vol. 45, no. 26, pp. 4333–4337, 2006.

[5] M. L. Montero, A. Voigt, M. Teichert, I. Usón, and H. W. Roesky, "Soluble Aluminosilicates with Frameworks of Minerals," *Angewandte Chemie International Edition in English*, vol. 34, no. 22, pp. 2504–2506, 1995.

[6] A. Voigt, M. G. Walawalkar, R. Murugavel, H. W. Roesky, E. Parisini, and P. Lubini, "Organic-Soluble Neutral and Ionic Indium Siloxane Cages: Potential Precursors for Indium-Containing Silicates," *Angewandte Chemie International Edition in English*, vol. 36, no. 20, pp. 2203–2205, 1997.

[7] A. Klemp, H. W. Roesky, H.-G. Schmidt, H. S. Park, and M. Noltemeyer, "A Polyhedral Magnesium Silicate with a $Mg_5Si_4O_{10}$ Framework: X-ray Crystal Structure of $[\{(2,6-i\text{-}Pr_2C_6H_3)N(SiMe3)SiO3\}2\text{-}\{(2, \quad 6\text{-}i\text{-}Pr_2C_6H_3)N(SiMe_3)SiO_2(OH)\}_2(Mg\bullet C_4H_8O)_5]$," *Organometallics*, vol. 17, no. 24, pp. 5225–5227, 1998.

[8] P. Böttcher, H. W. Roesky, M. G. Walawalkar, and H.-G. Schmidt, "Synthesis and Structure of the First Soluble Ternary Metal Amide-Imide Compounds with an $M_2Al_2Si_2N_6$ Core (M= Li, Na)," *Organometallics*, vol. 20, no. 4, pp. 790–793, 2001.

[9] U. N. Nehete, V. Chandrasekhar, H. W. Roesky, and J. Magull, "The Formal Conversion of SiOH Protons into Hydrides by Germanium(II) Species Leads to the Formation of the Germanium(IV) Hydride Cluster $[(RSiO_3GeH)_4]$," *Angewandte Chemie*, vol. 117, no. 2, pp. 285–288, 2005.

[10] A. Meller, G. Ossig, W. Maringgele, D. Stalke, R. Herbst-Irmer, S. Freitag, and G. M. Sheldrick, "Synthesis and X-ray Crystal Structure of Germaimines," *Journal of the Chemical Society, Chemical Communications*, no. 16, pp. 1123–1124, 1991.

[11] J. Bareš, V. Šourek, Z. Padělková, P. Meunier, N. Pirio, I. Cìsařová, A. Røužička, and J. Holeček, "Structure, Properties and Comparison of C, N-Chelated and Amido-Stabilized Plumbylenes," *Collection of Czechoslovak Chemical Communications*, vol. 75, no. 1, pp. 121–131, 2010.

[12] M. Zhong, Z. Yang, Y. Yi, D. Zhang, K. Sun, H. W. Roesky, and Y. Yang, "Tin Sulfide and Selenide Clusters Soluble in Organic Solvents with the Core Structures of Sn_4S_6 and Sn_4Se_6," *Journal of the Chemical Society, Dalton Transactions*, vol. 44, no. 46, pp. 19800–19804, 2015.

[13] J. Li, A. Stasch, C. Schenk, and C. Jones, "Extremely Bulky Amido-Group 14 Element Chloride Complexes: Potential Synthons for Low Oxidation State Main Group Chemistry," *Journal of the Chemical Society, Dalton Transactions*, vol. 40, no. 40, pp. 10448–10456, 2011.

[14] J. Li, C. Schenk, C. Goedecke, G. Frenking, and C. Jones, "A Digermyne with a Ge–Ge Single Bond that Activates Dihydrogen in the Solid state," *Journal of the American Chemical Society*, vol. 133, no. 46, pp. 18622–18625, 2011.

[15] D. Dange, J. Li, C. Schenk, H. Schnöckel, and C. Jones, "Monomeric Group 13 Metal(I) Amides: Enforcing One-Coordination Through Extreme Ligand Steric Bulk," *Inorganic Chemistry*, vol. 51, no. 23, pp. 13050–13059, 2012.

[16] E. W. Wong, D. Dange, L. Fohlmeister, T. J. Hadlington, and C. Jones, "Extremely Bulky Amido and Amidinato Complexes of Boron and Aluminium Halides: Synthesis and Reduction Studies," *Australian Journal of Chemistry*, vol. 66, no. 10, pp. 1144–1154, 2013.

[17] T. J. Hadlington, J. Li, and C. Jones, "Synthesis and Characterization of Extremely Bulky Amido-Germanium(II) Halide Complexes," *Canadian Journal of Chemistry*, vol. 92, no. 6, pp. 427–433, 2013.

[18] T. J. Hadlington, M. Hermann, J. Li, G. Frenking, and C. Jones, "Activation of H_2 by a Multiply Bonded Amido–Digermyne: Evidence for the Formation of a Hydrido–Germylene," *Angewandte Chemie International Edition*, vol. 52, no. 39, pp. 10199–10203, 2013.

[19] T. J. Hadlington and C. Jones, "A Singly Bonded Amido-Distannyne: H_2 Activation and Isocyanide Coordination," *Chemical Communications*, vol. 50, no. 18, pp. 2321–2323, 2014.

[20] A. J. Boutland, D. Dange, A. Stasch, L. Maron, and C. Jones, "Two-Coordinate Magnesium(I) Dimers Stabilized by Super Bulky Amido Ligands," *Angewandte Chemie International Edition*, vol. 55, no. 32, pp. 9239–9243, 2016.

[21] C. Hering-Junghans, M. Thomas, A. Villinger, and A. Schulz, "Synthesis of Elusive Chloropnictenium Ions," *Chemistry–A European Journal*, vol. 21, no. 18, pp. 6713–6717, 2015.

[22] T. J. Hadlington, J. A. Abdalla, R. Tirfoin, S. Aldridge, and C. Jones, "Stabilization of a Two-Coordinate, Acyclic Diaminosilylene (ADASi): Completion of the Series of Isolable Diaminotetrylenes: $E(NR_2)_2$ (E= Group 14 Element)," *Chemical Communications*, vol. 52, no. 8, pp. 1717–1720, 2016.

[23] J. Haggin, "Chemists Seek Greater Recognition for Catalysis," *Chemical and Engineering News;(United States)*, vol. 71, no. 22, 1993.

[24] S. Khan, R. Michel, S. S. Sen, H. W. Roesky, and D. Stalke, "A P_4 Chain and Cage from Silylene-Activated White Phosphorus," *Angewandte Chemie International Edition*, vol. 50, no. 49, pp. 11786–11789, 2011.

[25] A. Stasch, C. M. Forsyth, C. Jones, and P. C. Junk, "Thermally Stable Lead(II) Amidinates and Guanidinates," *New Journal of Chemistry*, vol. 32, no. 5, pp. 829–834, 2008.

[26] S. Nagendran, S. S. Sen, H. W. Roesky, D. Koley, H. Grubmüller, A. Pal, and R. Herbst-Irmer, "RGe(I) Ge(I) R Compound (R= PhC (N^{t}Bu)$_2$) with a Ge-Ge Single Bond and a Comparison with the Gauche Conformation of Hydrazine," *Organometallics*, vol. 27, no. 21, pp. 5459–5463, 2008.

[27] S. S. Sen, M. P. Kritzler-Kosch, S. Nagendran, H. W. Roesky, T. Beck, A. Pal, and R. Herbst-Irmer, "Synthesis of Monomeric Divalent Tin(II) Compounds with Terminal Chloride, Amide, and Triflate Substituents," *European Journal of Inorganic Chemistry*, vol. 2010, no. 33, pp. 5304–5311, 2010.

[28] C. Jones, S. J. Bonyhady, N. Holzmann, G. Frenking, and A. Stasch, "Preparation, Characterization, and Theoretical Analysis of Group 14 Element (I) Dimers: a Case Study of Magnesium (I) Compounds as Reducing Agents in Inorganic Synthesis," *Inorganic Chemistry*, vol. 50, no. 24, pp. 12315–12325, 2011.

[29] M. K. Barman and S. Nembenna, "Mixed Guanidinato-Amido Ge(IV) and Sn(IV) Complexes with Ge [Double Bond, Length as m-dash] E (E=S, Se) Double Bond and SnS$_4$, Sn$_2$Se$_2$ Rings," *RSC Advances*, vol. 6, no. 1, pp. 338–345, 2016.

[30] S. R. Foley, G. P. Yap, and D. S. Richeson, "Oxidative addition to M(II)(M= Ge, Sn) Amidinate Complexes: Routes to Group 14 Chalcogenolates with Hypervalent Coordination Environments," *Journal of the Chemical Society, Dalton Transactions*, no. 10, pp. 1663–1668, 2000.

[31] S. Yao, C. van Wüllen, X.-Y. Sun, and M. Driess, "Dichotomic Reactivity of a Stable Silylene toward Terminal Alkynes: Facile C-H Bond Insertion versus Autocatalytic Formation of Silacycloprop-3-ene," *Angewandte Chemie International Edition*, vol. 47, no. 17, pp. 3250–3253, 2008.

[32] K. Junold, J. A. Baus, C. Burschka, D. Auerhammer, and R. Tacke, "Stable Five-Coordinate Silicon(IV) Complexes with SiN4X Skeletons (X= S, Se, Te) and Si=X Double Bonds," *Chemistry–A European Journal*, vol. 18, no. 51, pp. 16288–16291, 2012.

[33] N. Parvin, S. Pal, S. Khan, S. Das, S. K. Pati, and H. W. Roesky, "Unique Approach to Copper (I) Silylene Chalcogenone Complexes," *Inorganic Chemistry*, vol. 56, no. 3, pp. 1706–1712, 2017.

[34] M. Driess, S. Yao, M. Brym, C. van Wüllen, and D. Lentz, "A New Type of N-Heterocyclic Silylene with Ambivalent Reactivity," *Journal of the American Chemical Society*, vol. 128, no. 30, pp. 9628–9629, 2006.

[35] M. Driess, S. Yao, M. Brym, and C. van Wüllen, "Low-Valent Silicon Cations with Two-Coordinate Silicon and Aromatic Character," *Angewandte Chemie International Edition*, vol. 45, no. 40, pp. 6730–6733, 2006.

[36] M. Driess, S. Yao, M. Brym, and C. van Wüllen, "A Heterofulvene-Like Germylene with a Betain Reactivity," *Angewandte Chemie International Edition*, vol. 45, no. 26, pp. 4349–4352, 2006.

[37] M. C. Kuchta and G. Parkin, "Multiple Bonding Between Germanium and the Chalcogens: the Syntheses and Structures of the Terminal Chalogenido Complexes (η 4-Me$_8$taa) GeE (E= S, Se, Te)," *Journal of the Chemical Society, Chemical Communications*, no. 11, pp. 1351–1352, 1994.

[38] M. C. Kuchta and G. Parkin, "Terminal Sulfido and Selenido Complexes of Tin: Syntheses and Structures of [η^4-Me$_8$taa] SnE (E= S, Se)," *Journal of the American Chemical Society*, vol. 116, no. 18, pp. 8372–8373, 1994.

[39] Y. Xiong, S. Yao, and M. Driess, "Versatile Conversion of N-Heterocyclic Silylene to Silyl Metal Compounds by Insertion of Divalent Silicon into Metal–Carbon and Metal–Hydrogen Bonds," *Chemistry–A European Journal*, vol. 18, no. 11, pp. 3316–3320, 2012.

[40] A. Jana, P. P. Samuel, G. Tavčar, H. W. Roesky, and C. Schulzke, "Selective Aromatic C- F and C- H bond Activation with Silylenes of Different Coordinate Silicon," *Journal of the American Chemical Society*, vol. 132, no. 29, pp. 10164–10170, 2010.

[41] A. Jana, C. Schulzke, and H. W. Roesky, "Oxidative Addition of Ammonia at a Silicon(II) Center and an Unprecedented Hydrogenation Reaction of Compounds with Low-Valent Group 14 Elements Using Ammonia Borane," *Journal of the American Chemical Society*, vol. 131, no. 13, pp. 4600–4601, 2009.

[42] A. Meltzer, S. Inoue, C. Präsang, and M. Driess, "Steering S-H and N-H Bond Activation by a Stable N-Heterocyclic Silylene: Different Addition of H$_2$S, NH$_3$, and Organoamines on a Silicon(II) Ligand versus Its Si(II)→Ni (CO)$_3$ Complex," *Journal of the American Chemical Society*, vol. 132, no. 9, pp. 3038–3046, 2010.

[43] S. Yao, M. Brym, C. van Wüllen, and M. Driess, "From a Stable Silylene to a Mixed-Valent Disiloxane and an Isolable Silaformamide–Borane Complex with Considerable Silicon–Oxygen Double-Bond Character," *Angewandte Chemie International Edition*, vol. 46, no. 22, pp. 4159–4162, 2007.

[44] Y. Xiong, S. Yao, and M. Driess, "Reactivity of a Zwitterionic Stable Silylene Toward Halosilanes and Haloalkanes," *Organometallics*, vol. 28, no. 6, pp. 1927–1933, 2009.

[45] Y. Xiong, S. Yao, M. Brym, and M. Driess, "Consecutive Insertion of a Silylene into the P$_4$ Tetrahedron: Facile Access to Strained SiP$_4$ and Si$_2$P$_4$ Cage Compounds," *Angewandte Chemie International Edition*, vol. 46, no. 24, pp. 4511–4513, 2007.

[46] Y. Xiong, S. Yao, and M. Driess, "An Isolable NHC-Supported Silanone," *Journal of the American Chemical Society*, vol. 131, no. 22, pp. 7562–7563, 2009.

[47] Y. Xiong, S. Yao, R. Müller, M. Kaupp, and M. Driess, "From Silicon(II)-Based Dioxygen Activation to Adducts of Elusive Dioxasiliranes and Sila-Ureas Stable at Room Temperature," *Nature Chemistry*, vol. 2, no. 7, p. 577, 2010.

[48] S. Yao, C. van Wüllen, and M. Driess, "Striking reactivity of ylide-like germylene toward terminal alkynes:[4+ 2] cycloaddition versus C–H bond activation," *Chemical Communications*, no. 42, pp. 5393–5395, 2008.

[49] A. Jana, I. Objartel, H. W. Roesky, and D. Stalke, "Dehydrogenation of LGeH by a Lewis N-Heterocyclic Carbene Borane Pair Under the Formation of L'Ge and its Reactions with $B(C_6F_5)_3$ and Trimethylsilyl Diazomethane: An Unprecedented Rearrangement of a Diazocompound to an Isonitrile," *Inorganic Chemistry*, vol. 48, no. 16, pp. 7645–7649, 2009.

[50] A. Jana, I. Objartel, H. W. Roesky, and D. Stalke, "Cleavage of a N-H Bond of Ammonia at Room Temperature by a Germylene," *Inorganic Chemistry*, vol. 48, no. 3, pp. 798–800, 2008.

[51] Y. Wu, L. Liu, J. Su, K. Yan, T. Wang, J. Zhu, X. Gao, Y. Gao, and Y. Zhao, "Reactivity of Germylene Toward Phosphorus-Containing Compounds: Nucleophilic Addition and Tautomerism," *Inorganic Chemistry*, vol. 54, no. 9, pp. 4423–4430, 2015.

[52] A. Jana, B. Nekoueishahraki, H. W. Roesky, and C. Schulzke, "Stable Compounds of Composition LGe(II)R (R= OH, PhO, C_6F_5O, $PhCO_2$) Prepared by Nucleophilic Addition Reactions," *Organometallics*, vol. 28, no. 13, pp. 3763–3766, 2009.

[53] C. N. de Bruin-Dickason, T. Sutcliffe, C. A. Lamsfus, G. B. Deacon, L. Maron, and C. Jones, "Kinetic Stabilisation of a Molecular Strontium Hydride Complex using an Extremely Bulky Amidinate Ligand," *Chemical Communications*, vol. 54, no. 7, pp. 786–789, 2018.

[54] E. A. Weerawardhana, A. Pena, M. Zeller, and W.-T. Lee, "Synthesis and Characterization of Iron and Cobalt Complexes with an Asymmetric N-alkyl, N'-aryl-β-Diketiminate Ligand," *Inorganica Chimica Acta*, vol. 460, pp. 29–34, 2017.

[55] M. Vornefeld, F. Huber, H. Preut, and H. Brunner, "Synthesis and Spectroscopic Characterization of Dimethylgermanium Derivatives of Dipeptides, Crystal Structure of Dimethylgermanium Glycylglycinate and in Vivo Effects of Dimethylgermanium Glycylglycinate Against Murine Leukemia P388," *Applied Organometallic Chemistry*, vol. 3, no. 2, pp. 177–182, 1989.

[56] S. Suh and D. M. Hoffman, "Synthesis of Tin Oxide Precursors and Related Germanium and Lead Compounds," *Inorganic Chemistry*, vol. 35, no. 21, pp. 6164–6169, 1996.

[57] L. Fang, L. Liu, Y. Yun, A. K. Inge, W. Wan, X. Zou, and F. Gao, "SU-77: An Open-Framework Germanate Containing 12× 10× 10-Ring Channels Solved by Combining Rotation Electron Diffraction and Powder X-ray Diffraction," *Crystal Growth & Design*, vol. 14, no. 10, pp. 5072–5078, 2014.

[58] A. Steiner and D. Stalke, "Poly (Pyrazolyl) Germanium (II) and-Tin (II) Derivatives-Tuneable Monoanionic Ligands and Dinuclear Cationic Cages," *Inorganic Chemistry*, vol. 34, no. 19, pp. 4846–4853, 1995.

[59] N. S. Hosmane, J. Yang, K.-J. Lu, H. Zhang, U. Siriwardane, M. S. Islam, J. L. Thomas, and J. A. Maguire, "Chemistry of C-Trimethylsilyl-Substituted Heterocarboranes. 25. Syntheses, Structures, and Reactivities of GeCl$_3$-Substituted Half-Sandwich Germacarboranes, closo-1-Ge-2-(SiMe$_3$)-3-(R)-5-(GeCl$_3$)-2,3-C$_2$B$_4$H$_3$ (R= SiMe$_3$, Me, and H)," *Organometallics*, vol. 17, no. 13, pp. 2784–2796, 1998.

[60] S. Kolesnikov, S. Maksimov, and E. Smolenskii, "Proton-Donor Properties of HCCl$_3$, HSiCl$_3$, and HGeCl$_3$ Molecules: a Quantum-Chemical Study," *Russian Chemical Bulletin*, vol. 50, no. 4, pp. 740–742, 2001.

[61] K. Yamada, K. Mikawa, T. Okuda, and K. S. Knight, "Static and Dynamic Structures of CD$_3$ND$_3$GeCl$_3$ Studied by TOF High Resolution Neutron Powder Diffraction and Solid State NMR," *Journal of the Chemical Society, Dalton Transactions*, no. 10, pp. 2112–2118, 2002.

[62] Y. V. Zefirov and P. M. Zorky, "New Applications of Van der Waals Radii in Chemistry," *Russian Chemical Reviews*, vol. 64, no. 5, p. 415, 1995.

[63] C. N. de Bruin-Dickason, "Alkaline Earth and Lanthanoid Complexes of Sterically Demanding Amide and Amidinate Ligands," *Honours Thesis*, 2015.

Chapter 5

The Utilisation of Boryl Amides as Monodentate Ligands for Low-Oxidation State Group 15 Chemistry

Low-oxidation state group 15[i] compounds are reactive due to the presence of accessible electrons and orbitals at the pnictogen centre. Unlike low-oxidation state tetrel compounds[ii], the electronic profile for low-oxidation state pnictogen compounds does not contain a formally empty valence orbital but has full or partially filled valence orbitals. This radical electronic profile may lead to reactivity not often observed at a main group centre.

Accessing these compounds can be typically accomplished by similar methods as those mentioned throughout this thesis (see **chapter 1 & 3**); requrinig kinetically stabilising ligands for their isolation. Because of this, ligands used for other low-oxidation state main-group compound synthetic pursuits are often suitable for similar pnictogen chemistry. However, due to the higher number of accessible oxidation states and bonding modes observed for pnictogen compounds their chemistry is often unpredictable.

This chapter provides a brief introduction into the fundamentals of said chemistry, exemplified with previously reported low-oxidation state pnictogen compounds. The latter half focuses on the use of the boryl silyl amide ligand, $\{(^{\text{Dipp}}\text{DAB})\text{B}\}(\text{TMS})\text{N}^-$, in low-oxidation state pnictogen chemistry.

---

[i]The pnictogens: nitrogen (N), phosphorus (P), arsenic (As), antimony (Sb), and bismuth (Bi).

[ii]This compound class typically has an empty p orbital and a lone-pair of electrons, e.g. $\text{LGe:}^{\cdot+}$, where L = ligand.

5.1 Low-Oxidation State Chemistry of the Heavy Group 15 Elements

The fundamentals of low-oxidation state heavy group 15 (pnictogen) element chemistry is the same as that for group 14: these compounds are reactive as they contain energetic electron filled orbitals sometimes, as well as partially filled orbitals capable of donating and accepting electron density, i.e. reactive and accessible HOMO, LUMO, and SOMO orbitals. Albeit, their is evident differences between the chemistry of low-oxidation state group 14 element compounds and the respective group 15 element compounds.

Low-oxidation state pnictogen compounds are often characterised by the absence of a formally vacant valence p orbital, reducing their proclivity to accept electrons. The pnictogen centre of these compounds typically has a lone-pair of electron and a differing number of unpaired radical electrons (which is dependent on the singlet-triplet gap ($\Delta_{\mathrm{s}\rightarrow\mathrm{t}}$), discussed in **chapter 1**)). The +II oxidation state has an electronic configuration which leaves a radical electron upon the pnictogen centre; and the +I oxidation state electronic configuration leaves two unpaired radical electrons at the pnictogen centre (triplet state) or an extra lone-pair[iii] (singlet).

The lack of a formally vacant p orbital upon the pnictogen centre contributes to the lack of reported reactivity by these compounds, though there are other factors (*vide infra*). **Figure 5.1** displays the electronic configuration of the pnictogen centre (Pn) in the +I, +II, & +III oxidation states[iv].[1–3] Whilst this is a basic view of low-oxidation state pnictogen compound's electronic profiles it does give some basis as to the observed bonding seen in these compounds (*vide infra*).
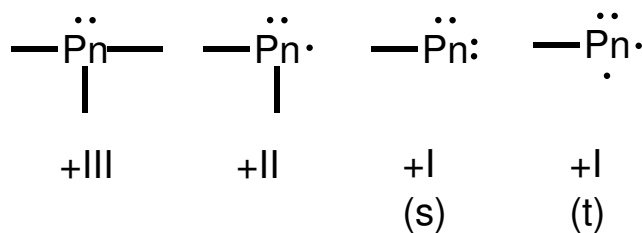

Figure 5.1: The low-oxidation states of pnictogens. The bonds suggest a typical number of covalent bonds that may be made to a pnictogen in each oxidation state.

[iii]For comparison, refer to **chapter 1** for the electronic configuration of the low-oxidation state group 14 element compounds.

[iv]This model is based on the definition of oxidation state which relates the number of non-bonding electrons associated with the pnictogen centre. The assumptions of such a model are outlined in the review *"Stable Compounds Containing Heavier Group 15 Elements in the +1 Oxidation State"* by Ellis & Macdonald.[1]

5.1.1 Bonding in Low-Oxidation State Pnictogen Compounds (RPn=PnR)

The pnicotgens, unlike the majority of the p-block elements, have a higher number of accessible oxidation states[v], which can complicate their chemistry. Adding to this is the multitude of bonding modes/motifs to which these compounds may exhibit, depending on the oxidation state of the pnictogen centre (some examples are provided in **figure 5.2**).[1]
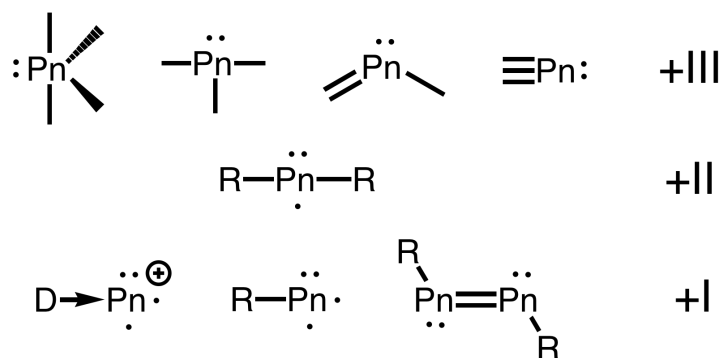
Figure 5.2: Some general structural drawings of pnictogens in the +I, +II, and +III oxidation states (D = lewis base, R = ligand).

Bonding modes which contain Pn=E double bonds (where E = some element) are the direct result of the π bonding character exhibited by the group 15 elements. As is discussed in **chapter 1**, typically an increase in atomic number causes a decrease in hybridisation and π bonding strength/prevalence in these compounds; however the extent to which this occurs for the pnictogens is lesser than for the group 13 & 14 elements.

Though π bonding is weakened with increasing atomic number, as is the case for antimony and bismuth, it remains "quite appreciable" in strength as stated by Power's and co-workers.[4] This is evidenced by the the observed planar bonding array and short Pn=Pn bond lengths[vi] observed in RPn=PnR compounds (pnictenes, where R = some ligand, Pn = pnictogen). In stating this, both antimony and bismuth have predominantly *s* orbital character lone-pairs whilst the σ and π bonds comprising Sb=Sb and Bi=Bi bonds are primarily composed of *p* obitals. This is in contrast to the group 14 elements which show a considerable decrease in π bonding character with an increase in atomic number (refer to **chapter 1**).[4,5] The increased π character observed in these compounds reduces their reactivity when compared to low-oxidation state group 13 and 14 element compounds.

---

[v] +IV through to -III have all been reported, albeit not for all of the pnictogens.[1]

[vi] *Ca.* 6-7% shorter than single bonds *cf. ca.* 7-10% shorterning in diphosphenes and diarsenes, discussed *vide infra.*

5.2   Low-Oxidation State Group 15 Element Compounds

The first isolated +1 oxidation state pnictogen containing compound was the diphosphene **i-5a**, synthesised by Yoshifuji and co-workers (**scheme 5.1**).[6] As is common in low-oxidation state main-group chemistry, this compound was stabilised and isolated by employing a sterically demanding ligand which is capable of kinetically stabilising the phosphorus(I) centre (see **chapter 1**).
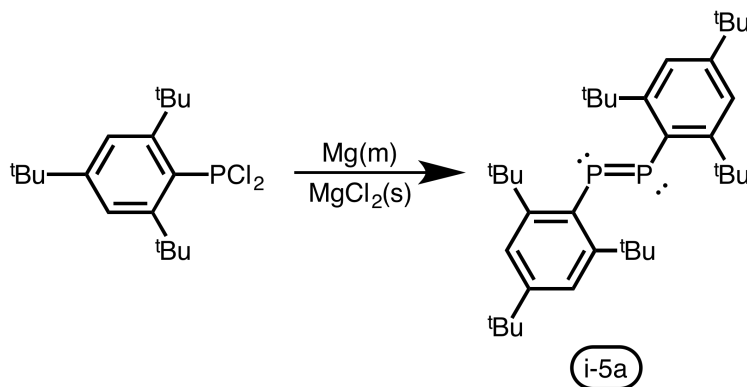
*Scheme 5.1: Synthesis of the first kinetically stabilised and isolated diphosphene **i-5a**.*

The synthesis of **i-5a** exemplifies the halide precursor compounds commonly targeted, which enable access to these low-oxidation state compounds. Furthermore, it highlights a typical reduction pathway (alkali earth metal reduction) to form the low-oxidation state group 15 compounds (see **chapter 3**).

Since the synthesis of **i-5a** there has been ample research done towards stabilising the heavier group 15 low-oxidation state derivatives; and much has focused on furthering low-oxidation state phosphorus chemistry.[4,7] Less work has focused on the heavier pnictogens (arsenic, antimony, and bismuth) due to the difficulty in kinetically stabilising these compounds in their low-oxidation states.[8] Compounding this is the lack of reactivity which has been observed by these pnictogen in compairson to phosphorus (and to some degree arsenic). The rest of this section will discuss the few examples of reactive low-oxidation state dipnictenes and present some examples of unique cluster-type pnictogen compounds.

5.2.1   Monodentate Ligand Stabilised Dipnictenes

The requirement for more sterically demanding ligands for the stabilisation of low-oxidation state arsenic, antimony, and bismuth compounds has limited the scope of this chemistry. Because of this, the heavier group 15 homologues of diphosphenes (RE=ER, E = As, Sb, or Bi), the dipnictenes, have only more recently been isolated alongside the use of larger and more sterically demanding ligands.

Tokitoh and co-workers reported the first antomony and bismuth dipnictenes (**figure 5.3**. In both cases the pnicotgen is stabilised by the large monodentate ligand **i-5b**, allowing for the isolation of these doubly-bonded compounds.[9,10]
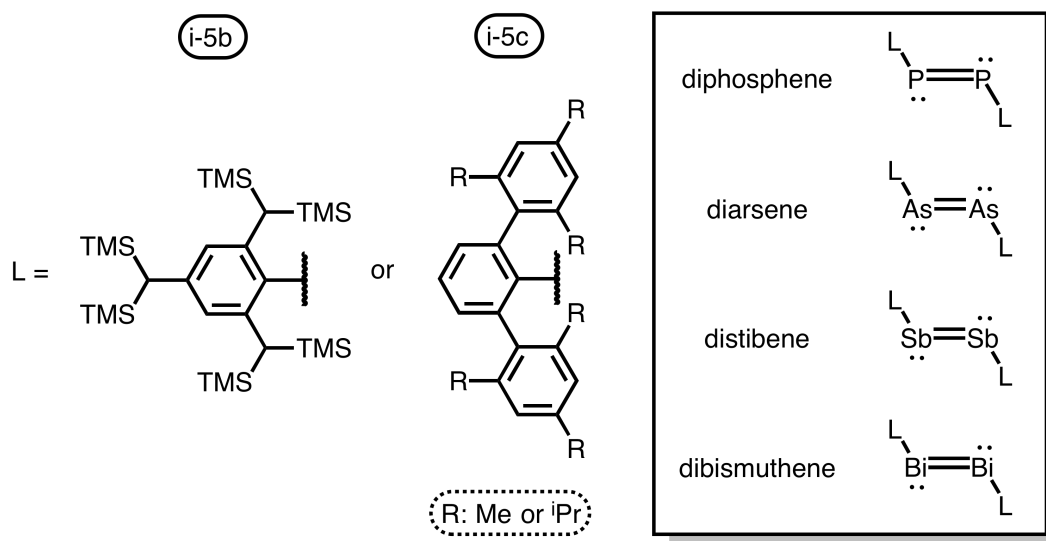

Figure 5.3: General structure of the first isolated heavier pnictene compounds. The diphosphene and diarsene compounds had already been synthesised.

Power and co-workers also produced a series of heavy dipnictenes (**figure 5.3**), utilising even larger ligands, the tertphenyls **i-5c**, discussed in **chapter 2**.[11] Magnesium was the primary reducing agent used in this work, though, for the diphosphene, potassium had to be used to avoid the formation of an internal C-H activated phosphorus(III) compound (which was the major product from their reduction attempts using magnesium).

Following this work[vii], Jones and co-workers synthesised a range of amido stabilised pnictenes, adopting an extremely bulky class of amido silyl ligand (discussed in **chapter 2**). In the case of the dibismuthene **i-5d**, ligand exchange occurred during reduction and the resulting dibismuthene is stabilised by the boryl subsitutent $\{(DAB)B\}^-$ (**scheme 5.2**).[12] One of the highlights within this is the utilisation of the soluble reducing agent $\{(DAB)B\}Li$ (where $DAB = (DippNCH)_2$, $Dipp = C_6H_3{}^iPr_2$-2,6), which had been used previously to fashion low-oxidation state pnictene compounds[viii].[13]

[vii]And most apropos to the project present in this chapter.

[viii]It was reported that other reducing agents led to complex product mixtures; this is yet another example of how small changes to the synthetic strategy can have unforeseen impacts on the obtained products.
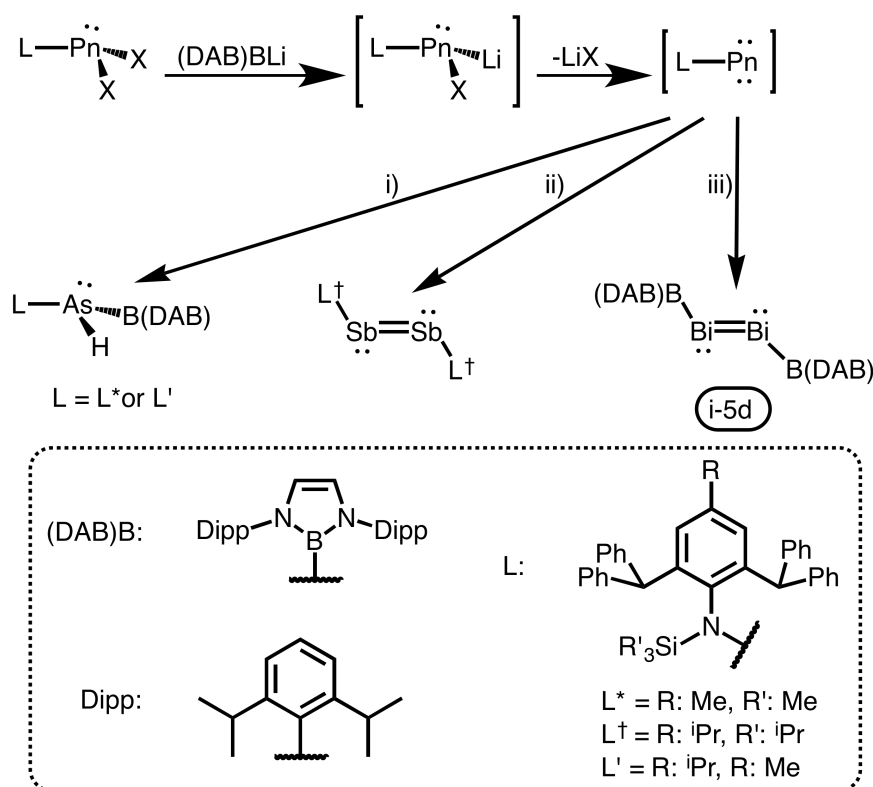
Scheme 5.2: Reduction of amido stabilised pnictogen halide precursors to a range of low-oxidation state dipnictenes. Reagents and conditions: i) trace HB(DAB), ii) dimerisation, iii) LiB(DAB), - LiL'.

During this work, it was found that slight alterations to the adopted ligand's steric profile impacted the reactivity the heavy dipnictenes. This reinforces the concept that a ligand's steric profile influences the reactivity and synthesis of low-oxidation state main-group compounds.

5.2.2   Dipnictene Reactivity

The reactivity of dipnictenes is a consquence of their low-lying frontier orbitals (HOMO-LUMO orbitals) making them ideal candidates for redox processes and reactions with electrophiles and nucelophiles. These chemical reactions can occur at three locations of a dipnictine: the Pn atom, the Pn=Pn double bond, or the Pn-R bond (**figure 5.4**).[7]
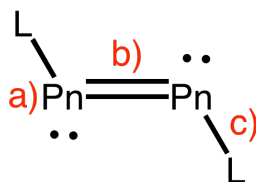

Figure 5.4: The general structure of a dipnictene and their typical points of reactivity (where Pn = pnictogen, L = ligand).

Generally when the pnictogen is phosphorus, reactions which occur at the P-P bonds (b) involve substitution and retainment of the P=P double bond. This has also been observed for the heavier pncitogens, as shown by **i-5d** (see **scheme 5.2**, above).[7]

The reactivity of low-oxidation state group 15 compounds towards small molecules is sparse, with only few examples being reported. The majority of reactivity which has been documented comes from mixed pnictogen systems, either interacting with a transition metal or some other heavy p-block element, and reactivity of diphosphenes.[1,7] Surprisingly, there are few examples of the the heavier diarsa-, distiba-, and dibismuthene reactivity, potentially due to their instability and their proclivity for oligomerisation.

The reactivity of the diphosphene **i-5a** has been extensively covered and the entirety of its reactivity is beyond the scope of this introduction.[7] A more recent example of **i-5a**'s reactivity is illustrated in **Scheme 5.3**. Here, **i-5a** is turned into the cationic species before undergoing internal C-H activation and P-P bond fission to form **i-5f**.
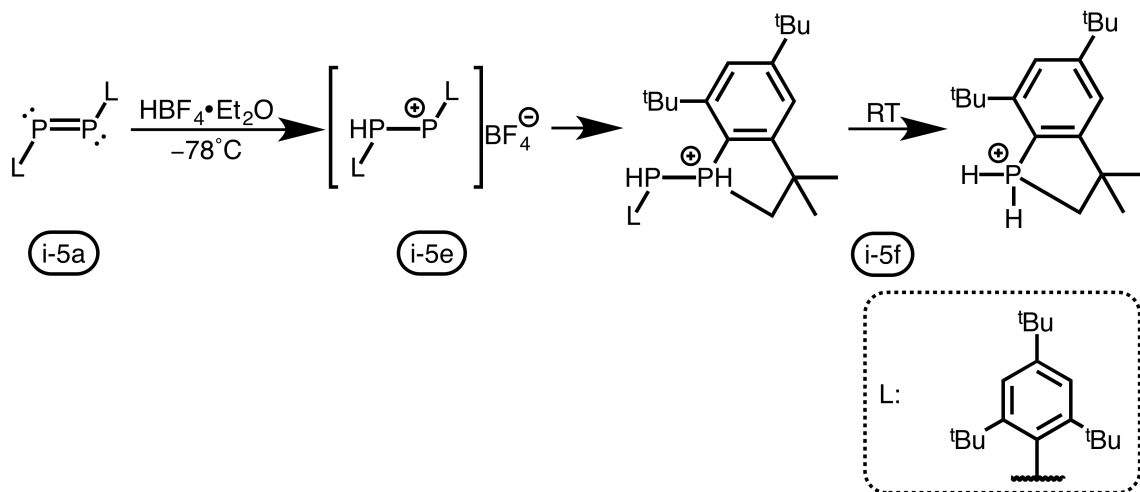
Scheme 5.3: Diphosphene **i-5a** is protonated to form the cationic compound **i-5e** which then goes on to react with itself, undergoing C-H activation and P-P bond fission at higher temperatures to form the **i-5f** species.

Dipnictenes have have been reported to react with chalcogens (group 16 elements) (**figure 5.5**).[8,14,15] The trend for this series is the requirement for harsher reaction conditions for the lighter dipncitnes (P and As) compared to the heavier dipnictenes (Sb and Bi) which react at room temperature.
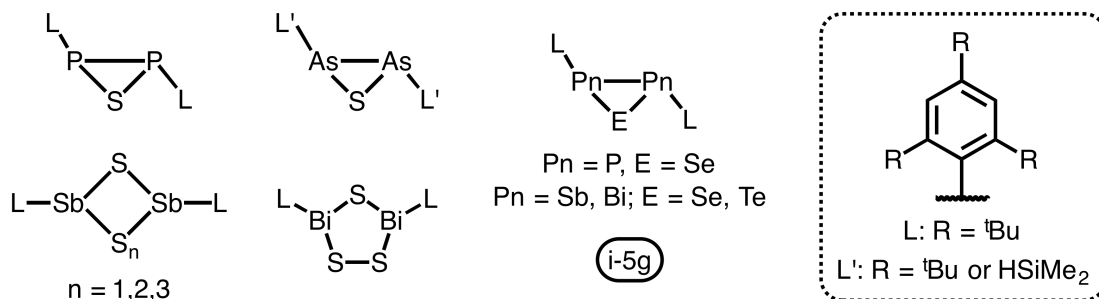
*Figure 5.5: Compounds isolated from reactions of the respective dipnictines and chalcogens. The **i-5g** constitute the heaviest heterocycles reported to-date.*

When reacted with selenium and tellurium, this series of dipnictenes either does not react or requires harsher reaction conditions, as was the case for forming the thee-membered compounds **i-5g**. These chalcogen-pnicotgen hetereocycles constitute the heaviest examples of heterocyclic compounds to date.[8]

5.2.3   Pnictogen Clusters

Main-group cluster compounds have received tremendous attention due to their containing multiple metal-metal (main-group element) bonds. Fundamentally, these compounds are comprised of chemical environments which are not readily observed in nature, displaying unique combinations of chemical properties: these cluster compounds often display reactivity not typically observed for the main-group elements under other bonding conditions.[16–20] The pnictogens - perhaps more so than the other p-block elements - tend to form cluster like compounds. This section focuses on realgar-type[ix] clusters as they are apropos to compounds discussed within the R&D section of this chapter.

Polystibides, antimony based cluster compounds, which are formed from magnesium(I) and gallium(I) compounds have recently begun to emerge within the literature.[21,22] In these cases, the magnesium(I) and gallium(I) compounds are used as soluble one-electron reductants; Schulz and co-workers took advantage of these reagents to form a series of such polystibides (some shown in **figure 5.6**).[21]

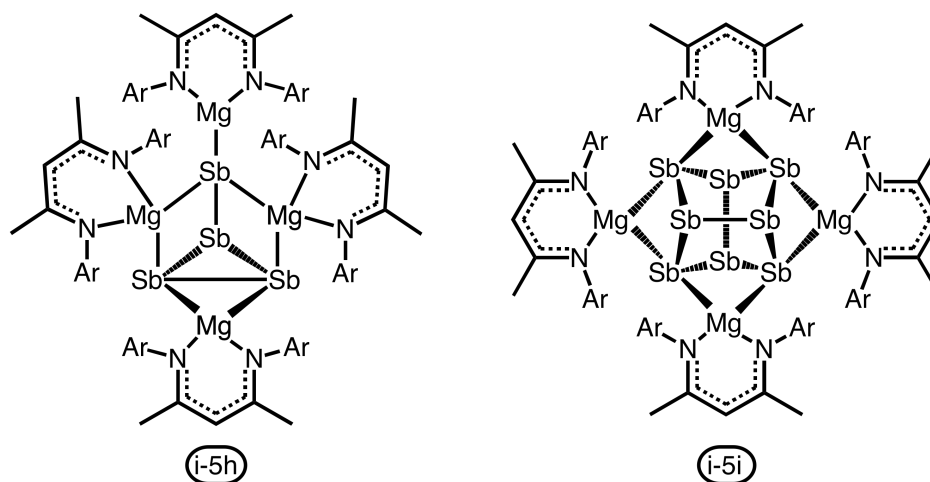[ix]referring to the cluster formation as seen in realgar α-As$_4$S$_4$.

*Figure 5.6: Illustrations of the magnesium coordinated polystibide compounds **i-5h** and **i-5i** (where Ar = HC[C(Me)N{2,6-^{i}Pr$_2$C$_6$H$_3$}]$_2$, and also HC[C(Me)N{2,4,6-Me$_3$C$_6$H$_2$}]$_2$ for **i-5i**).*

Both **i-5i** & **i-5h** are Zintl-type[x] polystibides, other examples of which, e.g. Sb$_4^{2-}$, Sb$_5^{5-}$, Sb$_7^{3-}$, and Sb$_{11}^{3-}$, are well known. The cluster **i-5h** adopts a realgar-type homoatomic structure[xi] and contains a central Sb$_8^{4-}$ unit which is stabilised by four magnesium cations: these compounds are the first examples of [Sb$_8$]$^{4-}$ polyanions.

The bonding/structure adopted by Zintl-type clusters has an impact on the electronics of the system, impacting reactivity. Such compounds are not only of fundamental interest but may display reactivity not before noted for main-group compounds.

5.3   Research Proposal

Our interest in low-oxidation state main-group systems, and recent work published related to low-oxidation state pncitogen chemistry, drove us to synthesise low-oxidation state pnictogen systems, with the chance of forming cluster type compounds.

{(^{Dipp}DAB)B}(TMS)N$^-$ has been used in the synthesis of a range of low-oxidation state compounds (discussed in **chapter 4**) but has not yet been used with pncitogens. Prior success using bulky amido ligands for the stabilisation of low-oxidation state pnictrogen compounds prompted us to use {(^{Dipp}DAB)B}(TMS)N$^-$ for similar chemistry.[12]

The objective was to utilise {(^{Dipp}DAB)B}(TMS)N$^-$ to kinetically stabilise low-oxidation state pnictogen compounds. The electronic profile of these pncitogen species should be unique in comparison to the previously synthesised amido pncitogen compounds, which were found to undergo ligand transfer, as described by Jones and co-workers.[12, 23]

[x]Main-group anionic salts.[16, 22]

[xi]Named so after the arsenic mineral realgar.

# 5.4   Results and Discussion: The Utilisation of Boryl Amido Ligands in Low-Oxidation State Group 15 Chemistry

The pro-ligands ^{Dipp}DAB(TMS/TPhS)NH (**1** & **2**) were synthesised as their respective lithium amides and then reacted with a series of pnictogen halides. From these reactions, ligand pnictogen bis-halide compounds were formed and isolated, with the general formula LMX$_2$ (where L = {(^{Dipp}DAB)B}(TMS)N$^-$, M = pnictogen, X = halide). Reduction of these compounds gave varying results; for arsenic and bismuth two low-oxidation state compounds have been isolated and will be discussed in due course.

The following sections provides the general reaction schemes for the synthesis of afore-mentioned LMX$_2$ species before giving an individual accounting for the synthesis and char-acterisation of each pncitogen compound.

5.4.1   Lithiation & General Reaction with Pnictogen Halides

1 and {(^{Dipp}DAB)B}(TMS)NLi (**Li-1**) were synthesised as described by Hadlington and co-workers.[23] Typically, the lithium amide was isolated as a crystalline material and stored within a glovebox at room temperature[xii].

2 and {(^{Dipp}DAB)B}(TPhS)NLi (**Li-2**) were synthesised in an analogoues fashion to **1**/**Li-1** (**scheme 5.4**). **Li-2** was isolated as a yellow needle-like crystalline material from a concentrated hexane solution, which had been stored overnight at –80 °C. Like **Li-1**, **Li-2** is stored in a glovebox at room temperature.


Name	R
{(^{Dipp}DAB)B}(TMS)N(H/Li) (**1/Li-1**)	Me
{(^{Dipp}DAB)B}(TPhS)N(H/Li)(**2/Li-2**)	Ph
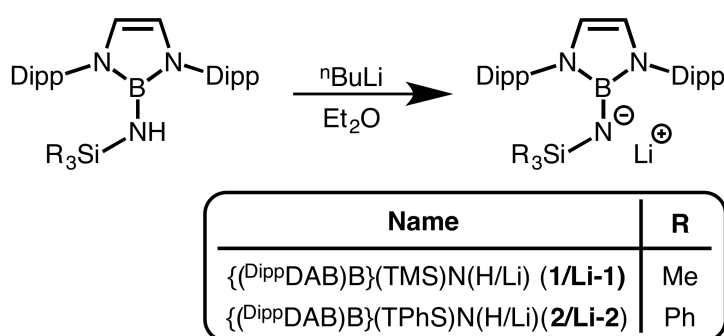
*Scheme 5.4: Lithitation of ^{Dipp}DAB(TMS/TPhS)NH (**1** and **2**, respectively) to give the respective lithium amides ^{Dipp}DAB(TMS/TPhS)NLi (**Li-1** and **Li-2**).*

[xii]This lithium amide can be stored indefinently under the stated conditions. No decomposition has yet been observed nor reported. The longest stored sample of **Li-1** is approximately two years: no decomposition has occurred based on our observations and ^{1}H NMR spectroscopic analyses.

Generally, reacting **Li-1**, as a diethyl ether/toluene solution, with a toluene solution of a pnictogen halide in 1:1 stoichiometric ratio yielded compounds of the formula LMX_2 (where $L = \{(^{Dipp}DAB)B\}(TMS)N_-$, and M = As, Sb, or Bi). Repeating these reactions in a 2:1 stoichiometry of **Li-1**:MX_3 did not yield the L_2MX compounds. The products from these reactions are the LMX_2 compounds and **1**.

Reacting **Li-2** with pnictogen halides did not yield any notable products. All reactions led to the production of the pro-ligand **2** and deposition of unknown materials with the concurrent consumption of starting reagents. Decomposition of the presumptive LMX_2 compounds[xiii] is due to steric repulsion between the ligand and the group 15 element halide. The triphenyl silyl moiety increases the proximal steric bulk of the ligand, increasing steric repulsion which results in bond fission. Further analyses of these reaction mixtures identified the presence of triphenyl silane and $(^{Dipp}DAB)BH$.
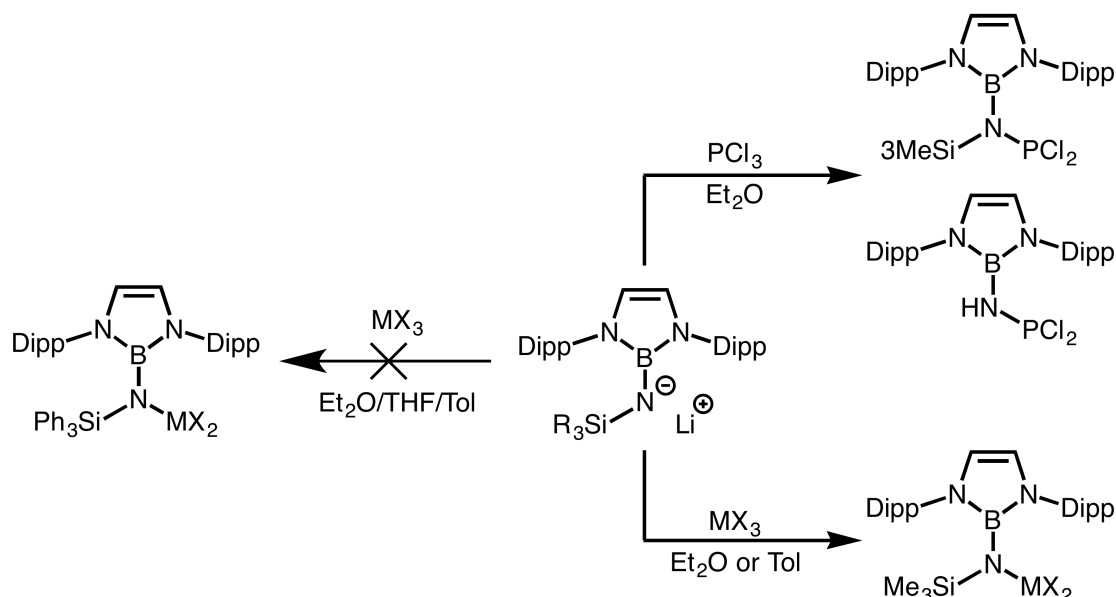
Scheme 5.5: Reaction scheme for the formation of $(\{(^{Dipp}DAB)B\}(TMS)N)MX_2$ (where M = P, As, Sb, or Bi; X = Cl or Br).

5.4.2 Phosphorus

Synthesis Using PCl_3

As per **scheme 5.5**, $[(\{(^{Dipp}DAB)B\}(TMS)N)PCl_2]$ (**3**) was successfully synthesised. Upon addition of **Li-1** to PCl_3 (as a dilute toluene mixture), the solution mixture went orange at –80 °C and became red as it was allowed to approach room temperature. Preliminary ^{1}H NMR spectroscopic analyses of this solution indicated the formation of a new major product

---

[xiii]It is possible that these compounds are transient, though there is no evidence for this occurrence.

and some minor products. It is ongoing work to successfully recrystallise **3** in order to obtain its molecular structure.

Spectroscopic Analysis of 3

The ^{1}H NMR spectrum of **3** is very similar to that of the pro-ligand **1**. The most notable differences are the splitting of the tertiary protons of the -C(H)Me$_2$ belonging to the Dipp moiey; the tentatively assigned multiplet of the primary protons of C(H)Me$_2$ belonging to the Dipp moitey; and the signals corresponding to the TMS moiety being shifted downfield. The downfield chemical shift for the TMS-assigned peaks indicates electronic de-shielding of the TMS moiety, which may be due to Si→N→PCl$_2$ electronic donation.

X-ray crystallographic characterisation of ({^{Dipp}DAB)B}NH)PCl$_2$ (4)

In our attempts recrystalise **3**, single crystals were isolated of an unexpected compound. This was revealed by X-ray diffraction to be [({^{Dipp}DAB)B}NH)PCl$_2$] (**4**) (**figure 5.7**).
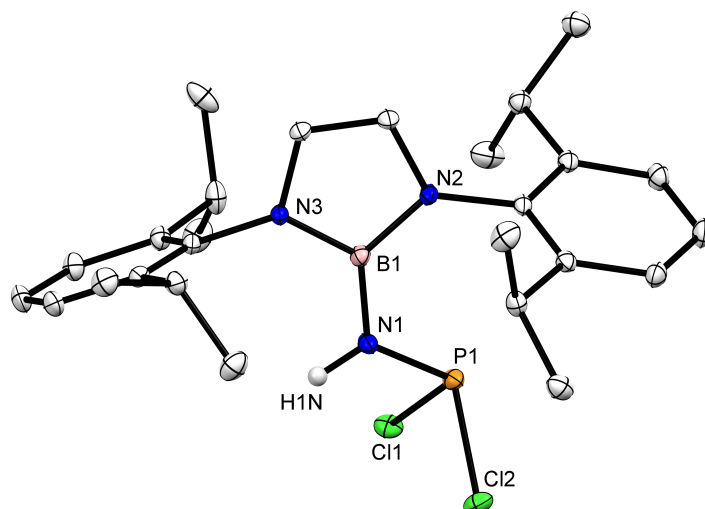
Figure 5.7: Thermal ellipsoid plot (30% probability surface) of ({^{Dipp}DAB)B}NH)PCl$_2$ (4) (hydrogen atoms omitted). Selected bond lengths (Å) and angles (°): P1-N1 1.650(2), P1-Cl1 2.100(1), P1-Cl2 2.099(1), N1-H1N 0.91(3), N1-B1 1.457(3), N2-B1 1.426(3), N3-B1 1.420(3); Cl1-P1-Cl2 96.75(3), Cl1-P1-N1 99.88(7), Cl2-P1-N1 102.66(7), P1-N1-B1 124.9(1), H1N-N1-B1 115(2), N1-B1-N3 124.9(2), N1-B1-N2 128.7(2), N2-B1-N3 106.4(2).

The molecular structure of **4** displays the phosphorus centre in its +III oxidation state and the ligand has lost its silyl moiety. The short P-N bond length of 1.650(2) Å is expected, as based on analogous compounds[xiv].[25] This short bond is a consequence of hyper-

---

[xiv]Where the sum of covalent radii for N-P is equal to 1.80 Å.[24]

conjugation of the amido nitrogen lone-pair of electrons.[26] The phosphorus centre is pyramidal, again as expected. The amido nitrogen has maintained the expected trigonal planar geometry despite reduced steric congestion. All other geometric features are as expected.

Reduction attempts

All attempts at reducing **3** (with the probable inclusion of **4**) were unsuccessful. Upon addition of the reducing agent,[xv] the solution, initially red, darkened as the reaction commenced and approached –30 °C. At this point, ^{1}H NMR spectroscopic analyses indicated a complicated mixture of compounds. Allowing the reaction to proceed to room temperature led to dissipation of the solution's colour, resulting in a pale yellow solution. The ^{1}H NMR spectrum of the final solution suggested decomposition had occurred as protonated ^{Mes}nacnac[xvi] and **1** were the prominent species identified. All attempts to isolate the species observed below –30 °C were unsuccessful.

5.4.3   Arsenic

Synthesis Using AsCl$_3$ and AsI$_3$

As per **scheme 5.5**, [({(^{Dipp}DAB)B}(TMS)N)AsCl$_2$] (**5**) & [({(^{Dipp}DAB)B}(TMS)N)AsI$_2$] (**6**) were successfully synthesised. For both cases, addition of **Li-1** to the respective AsX$_3$ compound resulted in the formation of yellow/orange solution the colour of which intensified as the reactions were allowed to approach room temperature. ^{1}H NMR spectroscopic analyses indicated the clean formation of the respective products; **5** was confirmed by X-ray crystalopgaphy.

  5 can be isolated as a red crystalline material which remains stable at room temperature within a glovebox for approximately 6 months at which point decomposition begins, albeit at a slow rate. These crystals are generally suitable for X-ray diffraction.

Spectroscopic Analyses of 5 and 6

The ^{1}H NMR spectrum of **5** is essentially the same as that observed for **3**, though the chemical shifts for the primary protons of C(H)Me$_2$ belonging to the Dipp moiety are distinct. All other NMR data are similar to those observed for the pro-ligand **1**. For **6**, again the ^{1}H NMR spectrum is similar. Generally, there is a downfield shift for all chemical shifts in comparison to the spectrum of **5**. The downfield shift may indicate the increased electron withdrawal by the AsI$_2$ fragment vs. the AsCl$_2$ fragment.

[xv][({^{Mes}nacnac}Mg)$_2$] or KC$_8$.
[xviMes]nacnac is the ligand for the reducing agent [({^{Mes}nacnac}Mg)$_2$].

X-ray Crystallographic Characterisation of ({(^{Dipp}DAB)B}(TMS)N)AsCl$_2$ (5)
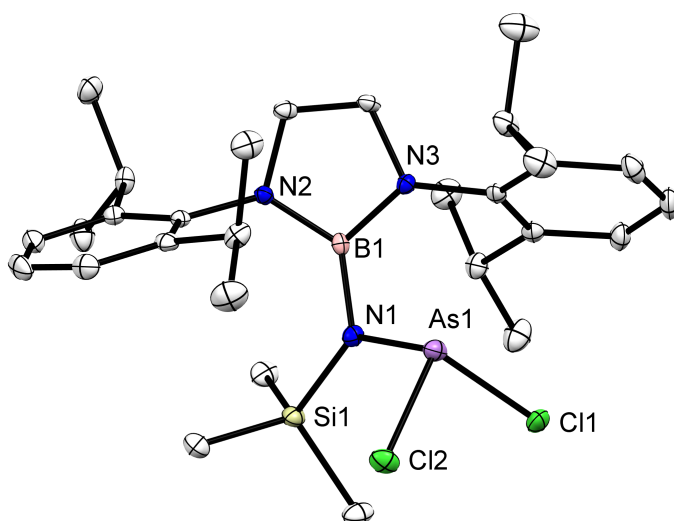
Figure 5.8: Thermal ellipsoid plot (30% probability surface) of ({(^{Dipp}DAB)B}(TMS)N)AsCl$_2$ (5) (hydrogen atoms omitted). Selected bond lengths (Å) and angles (°): As1-N1 1.815(2), As1-Cl1 2.2287(8), As1-Cl2 2.2159(8), As1-C15 3.214(3), N1-Si1 1.783(2), N1-B1 1.479(4), B1-N2 1.434(4), B1-N3 1.430(4); As1-N1-Si1 127.0(1), N1-As1-Cl1 105.21(7), N1-As1-Cl2 100.72(7), Si1-N1-B1 124.2(2), B1-N1-As1 108.8(2).

The molecular structure of [({(^{Dipp}DAB)B}(TMS)N)AsCl$_2$] (5) displays an arsenic atom in the +III oxidation state which has adopted a pyramidal geometry, as expected. It is the first example of a boryl silyl amide stabilised arsenic(III) compound. The As-N and two As-Cl bonds are in accordance with the calculated average of previously structurally characterised analogous compounds (As-N $\overline{x}$ = 1.823 Å; As-Cl $\overline{x}$ = 2.216 Å) and there is little deviation between the two As-Cl bond lengths seen in this structure.[12, 25, 27–33] A short As1-C15 distance of 3.214(3) Å, where C15 belong to the Dipp moiety of the ligand, suggests some As-aryl interaction (η_1). The sum of the bond angles at the amino nitrogen atom is close to 360° indicating a planar geometry and hence sp^2 hybridisation. Delocalisation of the nitrogen lone-pair is directed towards the arsenic atom probably leads to the relatively shorter As-N bond length[xvii] (*sum of covalent radii:* $\sum r_{cov}$(N-As)=1.91, $\sum r_{cov}$(N-As)=1.71Å).[24, 25]

Reduction Attempts

Reduction of **5** and **6** to compounds such as [({(^{Dipp}DAB)B}(TMS)N)As)$_2$] is ongoing work. Observations, so far, indicate some reaction takes place between **5** and **6** with the reducing agent [({^{Mes}nacnac}Mg)$_2$] or KC$_8$: the respective solutions becoming dark red upon reaction

---

[xvii]Known as hyper conjugation.[26]

commencement. The colour of these solutions dissipates to yellow/pale orange if allowed to stir at room temperature for more than two hours (^{1}H NMR spectroscopic analyses of this solution suggests decomposition). When below 0 °C, ^{1}H NMR spectroscopic analyses indicates the formation of some new species which display chemical shifts corresponding to the chemical environments of the expected low-oxidation state compound (*vide supra*). These shifts are the same when using **5** or **6**.

In one instance, single crystals were isolated from the reaction of **5** with [({^{Mes}nacnac}Mg)$_2$]. These crystals were determined by X-ray diffraction to be the compound [({(^{Dipp}DAB)B}(TMS)N)AsCl)$_2$] (**7**) (*vide infra*, **figure 5.9**). This compound confirmed the partial reduction of **5** (**scheme 5.6**).
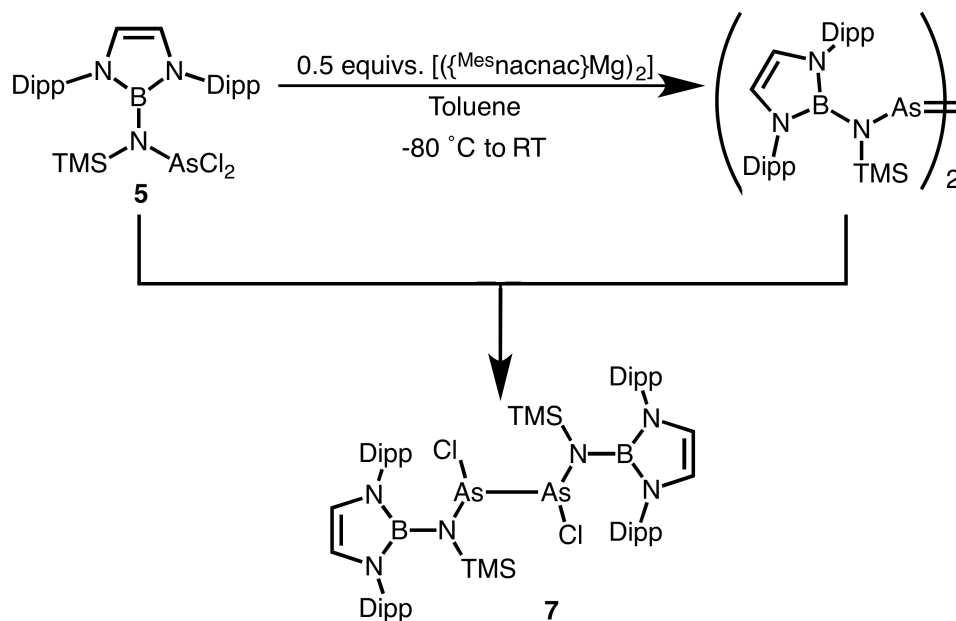
*Scheme 5.6: The reduction of **5** to form the presumptive arsene [({(^{Dipp}DAB)B}(TMS)N)As)$_2$] (this is analogues to the reduction of **6**). The formation of **7** could be due to the reaction of the product with **5**.*

We do not believe **7** represents the bulk product from these reactions, nor can we reproduce this compound without the occurrence of decomposition. Similar ^{1}H NMR spectroscopic results from our reductions of **5** and **6** preclude the likelihood that the observed major new species corresponds to **7**. It is suggested that unreacted **5** may react with [({(^{Dipp}DAB)B}(TMS)N)As)$_2$] and form **7** (unreacted **5** is always present as the reaction does not go to completion without significant decomposition). More probable is that **7** is formed from the partial reduction of **5**, though why **7** cannot be reproduced when targeted is a mystery.

X-ray Crystallographic Characterisation of [({(^{Dipp}DAB)B}(TMS)N)AsCl)$_2$] (7)

The unit cell of **7** is centrosymmetric with a two-fold axis which bisects the As-As "bond". The unit cell also contains a toluene molecule, omitted from **figure 5.9**. **7** is a bridged dimeric arsenic compound where the arsenic centre is in the +II oxidation state. It is the first example of an amido stabilised arsenic(II) halide compound.
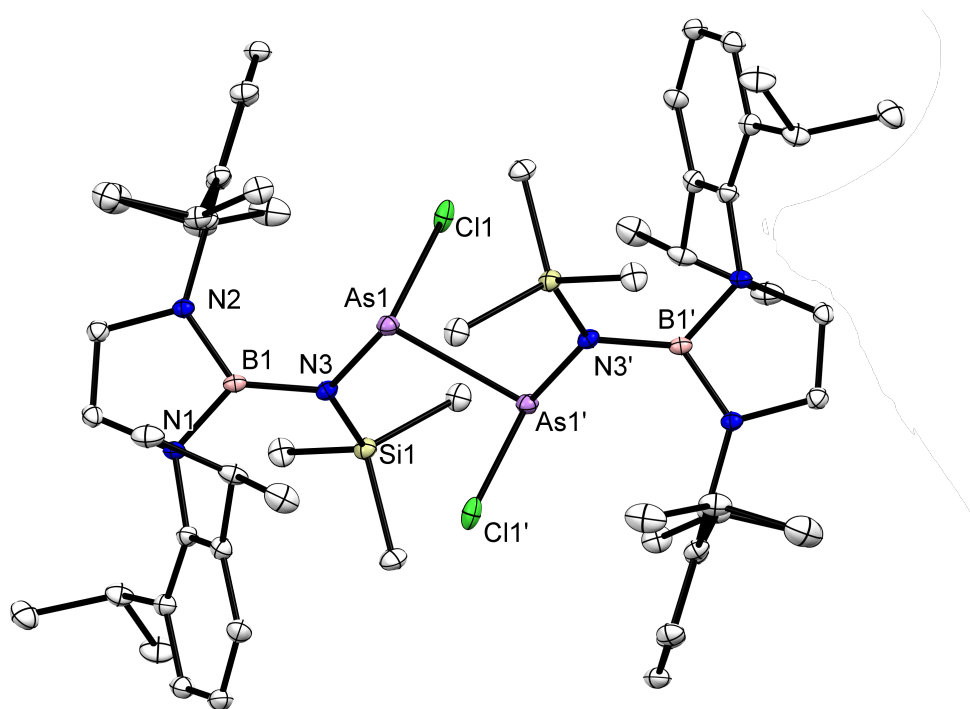

Figure 5.9: Thermal ellipsoid plot (30% probability surface) of [({(^{Dipp}DAB)B}(TMS)N)AsCl)$_2$] (7) (hydrogen atoms and a toluene molecule are omitted for clarity). Selected bond lengths (Å) and angles (°): As1-As1' 2.525(8), As1-Cl1 2.338(1), As1-N3 1.832(4), N3-Si1 1.772(3), B1-N1 1.447(6), B1-N2 1.444(5); N3-As1-As1' 101.2(1), Si1-N3-As1 127.7(2), N3-As1-Cl1 104.7(1), As1-N3-B1 112.6(3), B1-N3-Si1 119.3(3).

The molecule is in the trans conformation, most probably as to reduce steric pressure between the bulky amido ligands. The As1-As1' bond of 2.525(8) is longer than similar previously reported As-As bond lengths ($\bar{x} = 2.456$ Å), and is most probably due to steric congestion.[34–41] In comparison to **5** the As-Cl bond is longer. All other geometric features are as expected and similiar to those featured in **5**.

5.4.4   Antimony

Synthesis Using SbBr₃

As per **scheme 5.5**, [({(^{Dipp}DAB)B}(TMS)N)SbBr$_2$] (**8**) was successfully synthesised. Addition of **Li-1** to a toluene solution of suspended SbBr$_2$ produced a brown/orange[xviii] solution which became red as the reaction was allowed to approach room temperature. The ^{1}H NMR spectrum of this solution, at room temperature, indicated the formation of a major product confirmed to be **8**. A minor product was typically observed which mirrored similar chemical environments to **8**. However, unlike for phosphorus and arsenic, prolonged stirring of the reaction mixture leads to notable metal deposition as the reaction becomes dark brown/black[xix]. This compound can be isolated as single yellow-brown/red crystals from a concentrated hexane solution; these crystals are generally suitable for X-ray diffraction.

Spectroscopic Analysis of 8

The results of ^{1}H NMR spectroscopic analyses of **8** were similar to the species discussed thus far, other than its produced downfield shift of the chemical peaks. Presumably, this is indicative of increased Si→N→Sb σ bond electron withdrawal. All other data are as expected.

The ^{1}H NMR spectrum of the crude reaction mixture, which yields **8**, displays a second set of chemical shifts which reflect similar environments to **8**, though no peak was found to correspond with the TMS functional group. Based on the obtained structure for **4**, we speculate that this compound maybe the antimony compound [({(^{Dipp}DAB)B}NH)SbBr$_2$].

X-ray Crystallographic Characterisation of ({^{Dipp}DAB)B}(TMS)N)SbBr$_2$ (8)

The molecular structure [({(^{Dipp}DAB)B}(TMS)N)SbBr$_2$] (**8**) displays an antimony atom in the +III oxidation state which has adopted the expected pyramidal geometry (**figure 5.10**).

[xviii]In one instance, this reaction gave a yellow/green solution, which by ^{1}H NMR spectroscopic analyses is identical to reactions which produced a red solution.

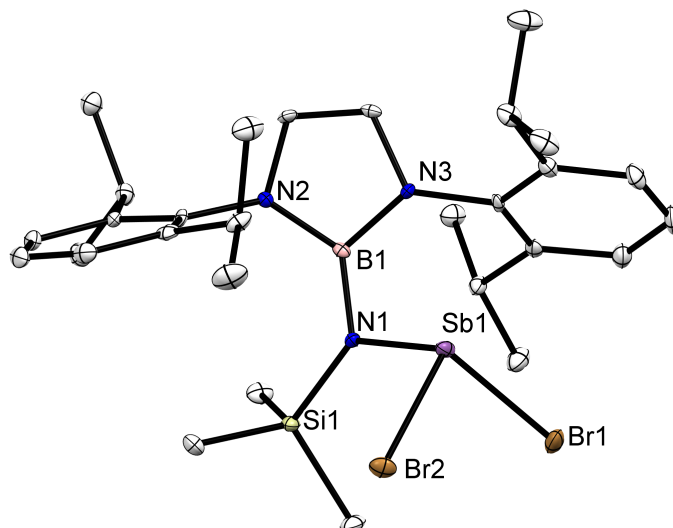[xix]Optimal conditions noted in the experimental.

Figure 5.10: Thermal ellipsoid plot (30% probability surface) of
*({(^{Dipp}DAB)B}(TMS)N)SbBr$_2$ (**8**) (hydrogen atoms omitted). Selected bond lengths (Å)*
and angles (°): Sb1-N1 2.015(3), Sb1-Br1 2.5256(7), Sb1-Br2 2.5268(6), Sb1-C15
3.221(3), N1-Si1 1.770(3), N1-B1 1.468(5), B1-N2 1.442(5), B1-N3 1.443(5); Sb1-N1-B1
108.0(2), Sb1-N1-Si1 127.1(2), Si1-N1-B1 124.8(2), N1-Sb1-Br1 103.24(8), N1-Sb1-Br2
98.28(8), Br1-Sb1-Br2 95.21(2).

Sb-N and Sb-Br bonds are marginally shorter than in comparison to the average of previously structurally characterised analogous compounds (Sb-N $\overline{x}$ = 2.038 Å, Sb-Br $\overline{x}$ = 2.544 Å).[42–47] As in **5**, the short Sb1-C15 3.221(3) Å bond indicates a weak antimony-aryl interaction (η_1). Also, as in **5**, the nitrogen donor atom displays a trigonal planar geometry and hence is sp^2 hybridisation. The lone-pair of the nitrogen may delocalise towards the antimony centre, explaining the slightly shorter Sb-N bond distance. All other geometric features are as expected.

Reduction Studies

Multiple attempts have been made to reduce **8** with little success, but work is ongoing. Addition of the reducing agents [({^{Mes}nacnac}Mg)$_2$] or KC$_8$ to a toluene solution of **8** leads to a significant colour change at below –30 °C, going from a red to a blue/purple solution. This colour persists until approximately 0 °C before metal deposition is observed. Prolonged stirring at below –30 °C also leads to metal deposition. ^{1}H NMR spectroscopic monitoring of this reaction indicates the formation of multiple products with the concurrent formation of decomposition products[xx] as the reaction continues to stir. However, a major product is observed to form which decomposes over time or at temperatures above –30 °C. It is ongoing

---

[xx]Regeneration of **1** and protonated ^{Mes}nacnac when [({^{Mes}nacnac}Mg)$_2$] is used as the reducing agent.

work to identify and isolate this compound.

5.4.5   Bismuth

Synthesis Using BiBr₃

As per **scheme 5.5**, [({(^{Dipp}DAB)B}(TMS)N)BiBr_2] (**9**) was successfully synthesised. Upon addition of **Li-1** to BiBr_3 as a toluene solution, the reaction mixture goes from a colourless solution to a red solution. As the reaction is allowed to approach room temperature the red colour of the solution intensifies. ^{1}H NMR spectorscopic analyses of the product mixture indicated the formation of a single new major product, which was later confirmed to be **9**.

This compound can be isolated as large red/purple block shaped crystals from concentrated hexane or toluene solutions. Unlike **8**, prolonged stirring does not lead to decomposition[xxi] nor does decomposition occur during recrystallisation. Along with **3**, compound **9** is indefinitely[xxii] stable over time when kept in a glovebox at room temperature. The synthesis of **9** represents the cleanest reaction of the series with no notable minor products being formed during its synthesis.

Spectroscopic Analysis

As with all the compounds belonging to this series, the ^{1}H NMR spectrum of **9** is similiar to that of the pro-ligand. Albeit, **9** displays the most downfield shifted chemical peak assigned to the TMS moiety and indicates increased Si→N→Bi σ bond electron withdrawal. This is marginally reflected in the ^{11}B{H} NMR spectrum which displays a chemical shift of δ 24.0 ppm.

Mass spectroscopic and elemental analyses confirms the formation of **9**.

X-ray Crystallographic Characterisation of ({(^{Dipp}DAB)B}(TMS)N)BiBr_2 (9)

Large red/purple crystals were always obtained from concentrated hexane/toleune solutions of **9**. These crystals are generally suitable for X-ray diffraction and allowed for the elucidation of **9**'s structure (**figure 5.11**).

[xxi]The longest this was tested for was approximately 48 hours.
[xxii]A 50 mg crystalline sample has been stored for 3 years without notable decomposition.
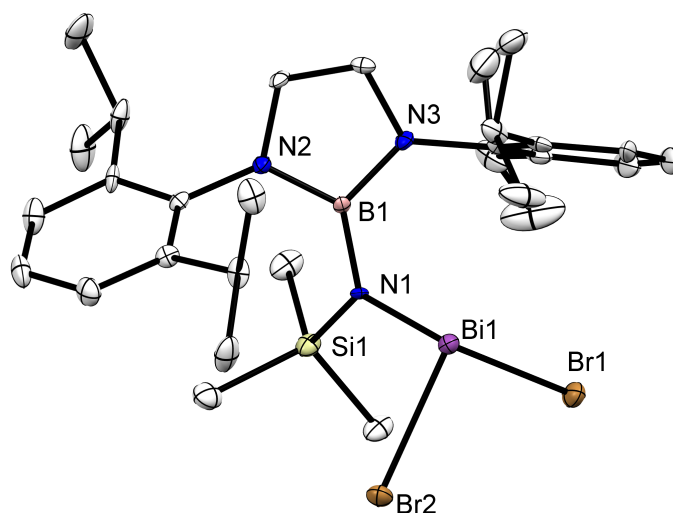
*Figure 5.11: Thermal ellipsoid plot (30% probability surface) of ({(^{Dipp}DAB)B}(TMS)N)BiBr$_2$ (**9**) (hydrogen atoms omitted). Selected bond lengths (Å) and angles (°): Bi1-N1 2.134(5), Bi1-Br1 2.6088(7), Bi1-Br2 2.642(1), Bi1-C15 3.304(9), N1-Si1 1.751(7), N1-B1 1.47(1), B1-N2 1.449(8), B1-N3 1.43(1); N1-Bi1-Br1 103.8(2), N1, Bi1-Br2 97.0(2), B1-N1-Bi1 103.8(2), Si1-N1-Bi1 123.2(5), B1-N1-Bi1 108.5(4).*

The molecular structure of **9** displays a bismuth centre in the +III oxidation state which has adopted the expected pyramidal geometry. The geometric features of **9** are similar to those seen in **5** and **8**; primarily, it also displays a short Bi1-C15 distance of 3.304(9) Å and a trigonal planar nitrogen geometry. The short aryl-carbon-bismuth distance indicates some interaction may occur between these two centres. The Bi-N and Bi-Br bonds are in accordance with the average calculated lengths of structurally charcaterised analogous compounds (Bi-N $\bar{x}$ = 2.153 Å, Bi-Br $\bar{x}$ = 2.607 Å).[12, 32, 48–50] The structural features of **9** are as expected.

Reduction Studies

Reduction studies for **9** are still ongoing. Of the series presented, our focus has been towards the isolation of the presumed low-oxidation state bismuth compounds formed during these reduction attempts. By observation, there is some reaction which occurs between **9** and either reducing agent [({^{Mes}nacnac}Mg)$_2$] or KC$_8$: the resultant solution of these reactions is purple/blue when kept below 0 °C (**scheme 5.7**). Similar observations have been made when low-oxidation state pnictogen compounds have formed.[12] Monitoring the reduction reaction by ^{1}H NMR spectroscopy indicates the formation of some new product with chemical environments which potentially corresponds to [({(^{Dipp}DAB)B}(TMS)N)Bi)$_n$]; though, there

is the concurrent formation of pro-ligand and other decomposition products. Overtime[xxiii] this new compound is believed to decompose.
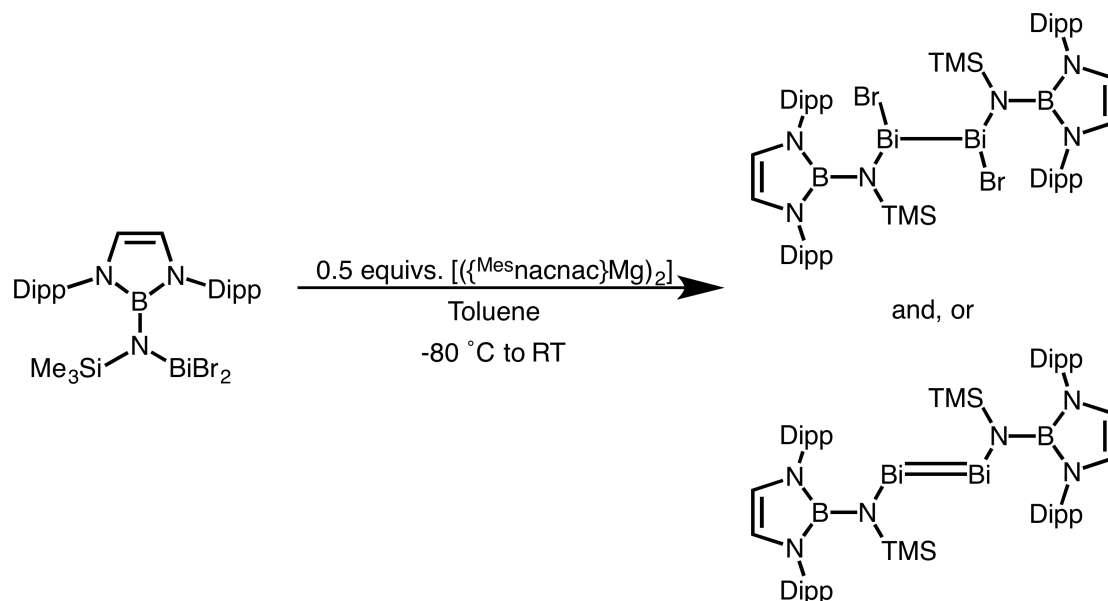
Scheme 5.7: *Synthetic scheme for the presumed low-oxidation state bismuth compounds:* $[(\{(^{Dipp}DAB)B\}(TMS)N)BiBr)_2]$ *and* $[(\{(^{Dipp}DAB)B\}(TMS)N)Bi)_2]$.

Allowing the reaction to stir and approach room temperature results in decomposition and bismuth deposition; however, when $[(\{^{Mes}nacnac\}Mg)_2]$ is the reducing agent, a black/purple/red micro-crystalline material forms in the presence of the bismuth metal. In a single instance, crystals suitable for X-ray diffraction were grown from one of these product mixtures and revealed the formation of the magnesium coordinated eight membered bismuth cluster $[(\{^{Mes}nacnac\}Mg)_4Bi_8]$ (**10**). These crystals are extremely sensitive, losing crystallinity rapidly upon placement in dried crystallographic oil[xxiv]. It is presumed this is due to a loss of solvent and not temperature related as the crystals appear to be stable at room temperature in solution over a period of 24 hours. Attempts to rationally target this compound have not yet been successful. The pure isolation/extraction of **10** has not been accomplished. Consequently, most attempts to characterise **10** have been unsuccessful and the obtained ^{1}H NMR spectroscopic data shows a complicated mixture of **1**, protonated ^{Mes}nacnac, $[(\{^{Mes}nacnac\}Mg)_2]$, and other unidentifiable species.

10 is believed to be a product of some decomposition pathway. We speculate that the reduction of **9** by $[(\{^{Mes}nacnac\}Mg)_2]$ occurs at a slower rate then the decomposition of the presumptive $[(LBi)_n]$ compound and that disproportionation occurs. Via this disproportionate pathway, activated bismuth metal forms in the presence of $[(\{^{Mes}nacnac\}Mg)_2]$ and the

---

[xxiii]Over one week of standing in solution, the product mixture gradually becomes more and more complicated.

[xxiv]Oil is dried with activated sodium metal.

two react to form **10**. However, we have no evidence to suggest this to be the case.

Characterisation of 10

The quality of X-ray diffraction data collected for **10** is not sufficient beyond identifying the presence of the compound and its connectivity[xxv]. Work is ongoing to obtain better data. Below is presented a illustration of the obtained realgar-type homoatomic bismuth cluster (a polybismuthide). **10** is homologus to the reported polystibide clusters **i-5i**.[21]
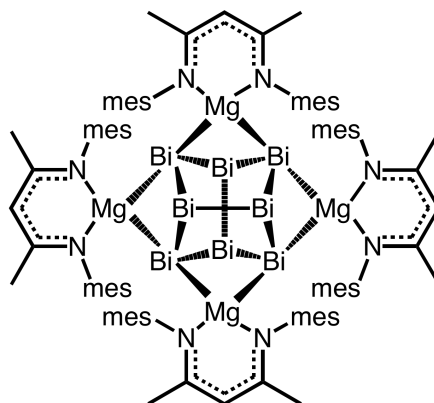

*Figure 5.12: Illustration of compound **10** as based on the preliminary X-ray diffraction results.*

Attempts to elucidate the ^{1}H NMR spectrum of this compound are on-going. The primary issue is the concurrent isolation of decomposition products which can not be extracted from the material without triggering further decomposition. Combined with this is the exceptional solubility of crystalline **10** in all commonly used hydrocarbon solvents.

5.5   Conclusion

(^{Dipp}DAB)B}(TMS)N$^-$ has been successfully bonded to the pnictogen elements: phosphorus, arsenic, antimony, and bismuth. The resulting compounds of the general formula LMX_2 are typically stable, which has allowed for their characterisation. Furthermore, the stability of these pnictogen halides has allowed us to begin exploring their potential for reduction, with the final objective to form low-oxidation state pnictogen complexes of the general formula $[(LM)_n]$. To these ends we have isolated the arsenic(II) bridged compound **7** and the unexpected magnesium coordinated polybismuthide **10**. Work continues to characterise

---

[xxv]The unit cell of **10** contains a single molecule of the cluster compound which is surrounded by solvent molecules. Disorder and heavy-metal diffraction convolute the obtained data. It is clear from the structure that the isolated crystalline material is the shown compound **10**.

the stated compounds and to isolate the presumed low-oxidation state pnictogen species observed during the reduction of this series of LMX$_2$ compounds.

5.6 Future Work

The initial success using $\{(^{Dipp}DAB)B\}(TMS)N^-$ in relation to low-oxidation state group 15 chemistry has opened up a new avenue for future work. The species synthesised thus far still hold the opportunity to access low-oxidation state group 15 compounds; though, if this proves fruitless, deviations can be made to the foundation of these boryl amides in order to access similar species. Alternative secondary nitrogen substituents may alter the steric and electronic profile of the nitrogen and prevent decomposition, thermodynamic and kinetic. The inability of $\{(^{Dipp}DAB)B\}(TPhS)N^-$ to form strong bonds with pncitogen halides suggests that silyl moieties which contain electron donating groups upon the silicon centre may lead to a stronger Si-N bond; this may be beneficial for future ligand design in relation to the aforementioned series of pncitogen complexes.

The most promising avenue of this project is to further explore the reduction of the aforementioned pnictogen halide precursors. Previous reports have suggested typical/classic reducing agents such as KC$_8$ and $[(\{^{Mes}nacnac\}Mg)_2]$, those employed in this project, may lead to complex product mixtures, which has been noted. The utilisation of Yamashita and Nozaki's lithium boryl, (THF)$_2$LiB(DAB), as a soluble reducing agent has been successful in previous work and should be considered for future reduction attempts.[12,13]

Compound **10** hints at the possibility of magnesium coordinated cluster compounds. If **10** could be successfully synthetically targeted - rather than obtained as a product of decomposition - this same synthetic method may be employed with other element halides. Failing this, the methodology presented by Schulz and co-workers, where other one-electron soluble reducing agents were used to target pnictogen zintl ions, could be adopted to form similar gallium and magnesium coordinated zintl based ions.[22]

5.7 Experimental

({(^{Dipp}DAB)B}N)PCl$_2$ (3). To a toluene solution of PCl$_3$ (0.64 ml, 7.3 mmol) was added {(^{Dipp}DAB)B}(TMS)NLi (1g, 7.6 mmol), dropwise at –80 °C. This solution was then allowed to stir at room temperature (24 °C) for 12 hrs (overnight). The solution was then filtered, volatiles were removed *in vacuo*, and the residue taken up in hexane. The solution was concentrated *in vacuo* and stored at –30 °C to afford the titled compound as red crystals (isolated crystalline yield ≈70%). M.p. = 100-102 °C; ^{1}H NMR (benzene-d^6, 400 MHz, 298 K): δ = 0.18 (s, 9H, Si-(CH_3)$_3$), 1.11 (d, J$_{HH}$ = 6.75 Hz, 12H, -C(H)-(CH_3)$_2$), 1.23-1.47 (m, 12H, *tentatively assigned* -C(H)-(CH_3)$_2$) 3.18-3.21 (m, 2H, -C(*H*)-(CH$_3$)$_2$), 3.33-3.39 (m, 2H, -C(*H*)-(CH$_3$)$_2$), 6.10 (s, 2H, -(Dipp)N-C*H*-C*H*-N(Dipp)-), 7.10-7.23 (m, 6H, Ar-*H*); ^{11}B{^{1}H} NMR (benzene-d$_6$, 128 MHz, 298 K): No signal observed; ^{13}C{H} NMR (benzene-d$_6$, 75.5MHz, 298K): δ ^{31}P{H} 131.11, 138.84; EI/MS m/z (%): EI/MS m/z (%): 188.9 (M$^+$-{(^{Dipp}DAB)B}, 33.5), 575.3 (M$^+$, 10.8).

[({(^{Dipp}DAB)B}NH)PCl$_2$] (4). Isolated as single crystals from a concentrated solution of **3** which had been allowed to stand in solution over a period of week. These crystals appeared as yellow/orange needles.

({(^{Dipp}DAB)B}N)AsCl$_2$ (6). To a solution of AsCl$_3$ (0.46 ml, 5.5 mmol) in toluene was added {(^{Dipp}DAB)B}(TMS)NLi (2.78g, 5.8 mmol) as a toluene solution, dropwise at –80 °C. This solution was then allowed to stir at room temperature (24 °C) for 12 hrs (overnight). The solution was then filtered, volatiles were removed *in vacuo*, and the residue taken up in hexane. The solution was concentrated *in vacuo* and stored at –30 °C to afford the titled compound as red crystals (isolated crystalline yield ≈70%). M.p. = 95-105 °C; ^{1}H NMR (benzene-d^6, 400 MHz, 298 K): δ = 0.21 (s, 9H, Si-(CH_3)$_3$), 1.10 (d, J$_{HH}$ = 6.51 Hz, 12H, -C(H)-(CH_3)$_2$), 1.32 (d, J$_{HH}$ = 6.80 Hz, 12H, -C(H)-(CH_3)$_2$), 3.22 (s, 4H, -C(*H*)-(CH$_3$)$_2$, splitting not observed), 6.09 (s, 2H, -(Dipp)N-C*H*-C*H*-N(Dipp)-), 7.10 (s, 2H, Ar-*H*), 7.12 (s, 2H, Ar-*H*), 7.19-7.23 (m, 2H, Ar-*H*); ^{11}B{^{1}H} NMR (benzene-d$_6$, 128 MHz, 298 K): δ = 23.06; ^{13}C{^{1}H} NMR (benzene-d$_6$, 75.5MHz, 298K): δ = 3.81 (N-*TMS*), 23.29 (Dipp-CH(CH$_3$)$_2$), 27.05 (Dipp-CH(CH$_3$)$_2$), 120.52 (N-(CH)$_2$-N), 124.90, 129.33, 138.09, 147.13 (Ar-C); IR (ATR, Nujol): $\bar{v}$ (cm^{-1}) = 758 (s), 854 (s), 907 (m), 969 (m), 1080 (m), 1119 (m), 1229 (m), 1251 (m), 1288 (m), 1325 (m), 1365 (s), 1388 (s), 1447 (s), 1462 (s), 1519 (w), 2962 (s), 2955 (s); EI/MS m/z (%): 235.2 (M$^+$-{(^{Dipp}DAB)B}, 46.7), 619.5 (M$^+$, 13.3); Anal. Calc. (%) for C$_{29}$H$_{45}$AsBCl$_2$N$_3$Si: C, 56.14; H, 7.31; N, 6.77; found (%): C, 45.85; H, 6.62; N, 5.08.

({(^{Dipp}DAB)B}N)AsI$_2$ (6). The named compound was synthesised as was **5** with the following changes: AsI$_3$ (1g, 2.2 mmol), {(^{Dipp}DAB)B}(TMS)NLi (1.10g, 2.3 mmol). The compound was isolated as a precipitate (yield ≈ 70%). ^{1}H NMR (benzene-d$_6$, 400 MHz, 298 K): δ = 0.32 (s, 9H, Si-(CH_3)$_3$), 1.135 (d, J$_{HH}$ = 7.05 Hz, 12H, -C(H)-(CH_3)$_2$), 1.415 (broad d, J$_{HH}$ = 6.80 Hz, 12H, -C(H)-(CH_3)$_2$), 3.30 (s, 4H, -C(*H*)-(CH$_3$)$_2$, splitting not observed), 6.07 (s, 2H, -(Dipp)N-C*H*-C*H*-N(Dipp)-), 7.15-7.28 (6H, Ar-*H*); ^{11}B NMR (benzene-d$_6$, 128 MHz, 298 K): δ = 22.17; ^{13}C{^{1}H} NMR (benzene-d$_6$, 75.5MHz, 298K): δ = 3.17 (N-*TMS*), 23.70 (Dipp-CH(CH$_3$)$_2$), 27.04 (Dipp-CH(CH$_3$)$_2$), 120.97 (N-(CH)$_2$-N), 124.42, 128.92,

129.46, 138.98 (Ar-C); ^{29}Si NMR (benzene-d$_6$, 80 MHz, 298 K): δ = not observed.

[({(^{Dipp}DAB)B}(TMS)N)AsCl)$_2$] (7).   The named compound was isolated from the attempted reduction of **5** to its +I oxidation state. These crystals were red needles and hand-picked away from the bulk micro-crystalline material. Not enough of the material was isolated for further analyses. All attempts to synthetically target this molecule have been unsuccessful.

{(^{Dipp}DAB)B}(TMS)N}SbBr$_2$ (8).   To a solution of SbBr$_3$ (1g, 2.8 mmol) in toluene was added {(^{Dipp}DAB)B}(TMS)NLi (1.393g, 2.9 mmol) as a toluene solution, dropwise at –80 °C. This solution was then allowed to stir at room temperature (24 °C) for 12 hrs (overnight). The solution was then filtered, volatiles removed *in vacuo*, and the residue taken up in hexane.   The solution was concentrated *in vacuo* and stored at –30 °C to afford the titled compound as yellow-red crystals (isolated crystalline yield ≈65%). M.p. = 120-122.5 °C; ^{1}H NMR (benzene-d$_6$, 400 MHz, 298 K): δ = 0.24 (s, 9H, Si-(CH_3)$_3$), 1.085 (d, J$_{HH}$ = 7.01 Hz, 12H, -C(H)-(CH_3)$_2$), 1.31 (d, J$_{HH}$ = 7.41 Hz, 12H, -C(H)-(CH$_3$)$_2$), 3.38 (sept., J$_{HH}$ = 6.65 Hz, 2H, -C(H)-(CH$_3$)$_2$), 6.07 (s, 2H, -(Dipp)N-CH-CH-N(Dipp)-), 7.09-7.25 (m, 2H, Ar-H); ^{11}B NMR (benzene-d$_6$, 128 MHz, 298 K):δ = 22.27; ^{13}C{^{1}H} NMR (benzene-d$_6$, 75.5MHz, 298K): δ = 4.69 (N-*TMS*), 23.33 (Dipp-CH(CH$_3$)$_2$), 27.08 (Dipp-CH(CH$_3$)$_2$), 120.23 (N-(CH)$_2$-N), 124.42, 125.17, 129.51, 147.26 (Ar-C); ^{29}Si NMR (benzene-d$_6$, 80 MHz, 298 K): δ = 46.9; Anal. Calc. (%) for C$_{29}$H$_{45}$SbBBr$_2$N$_3$Si: C, 46.06; H, 6.00; N, 5.56; found (%): C, 42.02; H, 7.27; N, 4.36.

({(^{Dipp}DAB)B}(TMS)N)BiBr$_2$ (9).   To a solution of BiBr$_3$ (1g, 2.23 mmol) in toluene was added ^{Dipp}DABNLi (1.122g, 2.34 mmol) as a toluene solution, dropwise at –80 °C. This solution was then allowed to stir at room temperature (24 °C) for 12 hrs (overnight). The solution was then filtered, volatiles removed in vacuo, and the residue taken up in hexane. The solution was conenctrated in vacuo and stored at –30 °C to afford the titled compound as vibrant red crystals (isolated crystaline yield ≈80%). M.p. = 123-124 °C; $_1$H NMR (benzene-d$_6$, 400 MHz, 298 K): δ = 0.27 (s, 9H, N-*TMS*, obscured by silicone grease peak), 1.07 (d, J$_{HH}$= 7.06, 12H, Dipp-CH(CH_3)$_2$), 1.27 (d, J$_{HH}$ = 7.16, 12H, Dipp-CH(CH_3)$_2$), 3.27 (s, 4H, Dipp-CH(CH$_3$)$_2$), 6.04 (s, 2H, N-(CH)$_2$-N), 7.08-7.21 (m, 6H, Ar-H); ^{11}B{^{1}H} NMR (benzene-d$_6$, 128 MHz, 298 K): δ = 24.04; ^{13}C{^{1}H} NMR (benzene-d$_6$, 75.5MHz, 298K): δ = 6.55 (N-*TMS*), 23.59 (Dipp-CH(CH$_3$)$_2$), 27.19 (Dipp-CH(CH$_3$)$_2$), 29.83 (Dipp-CH(CH$_3$)$_2$), 120.27 (N-(CH)$_2$-N), 125.52, 129.83, 138.31, 147.75 (Ar-C); ^{29}Si NMR (benzene-d$_6$, 80 MHz, 298K): δ = 16.98; IR (ATR, Nujol): $\bar{v}$ (cm^{-1}) = 755 (s), 834 (m), 900 (m), 1074 (m), 1116 (m), 1228 (m), 1325 (m), 1375 (s), 1386 (s), 1460 (s), 2341 (w), 2361 (w), 2925 (s), 2955 (s), 3053 (w); EI/MS m/z (%): 475.4 (DAB(TMS)N$^+$, 8), 843.4 (M$^+$, 0.7); Anal. Calc. (%) for C$_{29}$H$_{45}$BBiBr$_2$N$_3$Si: C, 41.3; H, 5.38; N, 4.98; found (%): C, 41.23; H, 5.56; N, 4.88.

[{^{Mes}nacnac}Mg}$_4$Bi$_8$] (10).   The named compound was isolated from a mixture of crystalline material as black/purple needle-like crystals. These crystals were suitable for X-ray diffraction, though lose their crystallinity when removed from the crude-solution mixture. Attempts are on-going to isolate this compound.

Bibliography

[1] B. D. Ellis and C. L. Macdonald, "Stable Compounds Containing Heavier Group 15 elements in the +1 Oxidation State," *Coordination Chemistry Reviews*, vol. 251, no. 7-8, pp. 936–973, 2007.

[2] C. Coulson, "Valence Oxford University Press," 1961.

[3] R. Hoffmann, "Building Bridges Between Inorganic and Organic Chemistry (Nobel Lecture)," *Angewandte Chemie International Edition in English*, vol. 21, no. 10, pp. 711–724, 1982.

[4] R. C. Fischer and P. P. Power, "π-Bonding and the Lone Pair Effect in Multiple Bonds Involving Heavier Main Group Elements: Developments in the New Millennium," *Chemical reviews*, vol. 110, no. 7, pp. 3877–3923, 2010.

[5] P. P. Power, "Bonding and Reactivity of Heavier Group 14 Element Alkyne Analogues," *Organometallics*, vol. 26, no. 18, pp. 4362–4372, 2007.

[6] M. Yoshifuji, I. Shima, N. Inamoto, K. Hirotsu, and T. Higuchi, "Synthesis and Structure of Bis(2, 4, 6-Tri-Tert-Butylphenyl)Diphosphene: Isolation of a True Phosphobenzene," *Journal of the American Chemical Society*, vol. 103, no. 15, pp. 4587–4589, 1981.

[7] L. Weber, "The Chemistry of Diphosphenes and their Heavy Congeners: Synthesis, Structure, and Reactivity," *Chemical reviews*, vol. 92, no. 8, pp. 1839–1906, 1992.

[8] T. Sasamori and N. Tokitoh, "Doubly Bonded systems Between Heavier Group 15 Elements," *Dalton Transactions*, no. 11, pp. 1395–1408, 2008.

[9] N. Tokitoh, Y. Arai, R. Okazaki, and S. Nagase, "Synthesis and Characterization of a Stable Dibismuthene: Evidence for a Bi-Bi Double Bond," *Science*, vol. 277, no. 5322, pp. 78–80, 1997.

[10] N. Tokitoh, Y. Arai, T. Sasamori, R. Okazaki, S. Nagase, H. Uekusa, and Y. Ohashi, "A Unique Crystalline-State Reaction of an Overcrowded Distibene with Molecular Oxygen: the First Example of a Single Crystal to a Single Crystal Reaction with an External Reagent," *Journal of the American Chemical Society*, vol. 120, no. 2, pp. 433–434, 1998.

[11] B. Twamley, C. D. Sofield, M. M. Olmstead, and P. P. Power, "Homologous Series of Heavier Element Dipnictenes 2, 6-Ar$_2$H$_3$C$_6$E=EC$_6$H$_3$-2, 6-Ar$_2$ (E = P, As, Sb, Bi; Ar = Mes= C$_6$H$_2$-2, 4, 6-Me$_3$; or Trip= C$_6$H$_2$-2, 4, 6-iPr$_3$) Stabilized by m-Terphenyl Ligands," *Journal of the American Chemical Society*, vol. 121, no. 14, pp. 3357–3367, 1999.

[12] D. Dange, A. Davey, J. A. Abdalla, S. Aldridge, and C. Jones, "Utilisation of a Lithium Boryl as a Reducing Agent in Low Oxidation State Group 15 Chemistry: Synthesis and Characterisation of an Amido-Distibene and a Boryl-Dibismuthene," *Chemical Communications*, vol. 51, no. 33, pp. 7128–7131, 2015.

[13] M. Kaaz, J. Bender, D. Förster, W. Frey, M. Nieger, and D. Gudat, "Phosphines with N-Heterocyclic Boranyl Substituents," *Dalton Transactions*, vol. 43, no. 2, pp. 680–689, 2014.

[14] T. Sasamori, E. Mieda, N. Takeda, and N. Tokitoh, "Reaction of an Overcrowded Distibene with Elemental Sulfur and Crystallographic Analysis of the Sulfurization Products," *Chemistry letters*, vol. 33, no. 2, pp. 104–105, 2004.

[15] T. Sasamori, E. Mieda, N. Nagahora, K. Sato, D. Shiomi, T. Takui, Y. Hosoi, Y. Furukawa, N. Takagi, S. Nagase, *et al.*, "One-Electron Reduction of Kinetically Stabilized Dipnictenes: Synthesis of Dipnictene Anion Radicals," *Journal of the American Chemical Society*, vol. 128, no. 38, pp. 12582–12588, 2006.

[16] J. D. Corbett, "Polyanionic Clusters and Networks of the Early p-Element Metals in the Solid State: Beyond the Zintl Boundary," *Angewandte Chemie International Edition*, vol. 39, no. 4, pp. 670–690, 2000.

[17] F. A. Cotton, C. A. Murillo, and R. A. Walton, *Multiple Bonds Between Metal Atoms*. Springer Science & Business Media, 2005.

[18] B. G. Cooper, J. W. Napoline, and C. M. Thomas, "Catalytic Applications of Early/Late Heterobimetallic Complexes," *Catalysis Reviews*, vol. 54, no. 1, pp. 1–40, 2012.

[19] J. P. Krogman and C. M. Thomas, "Metal–Metal Multiple Bonding in C3-Symmetric Bimetallic Complexes of the First Row Transition Metals," *Chemical Communications*, vol. 50, no. 40, pp. 5115–5127, 2014.

[20] J. F. Berry, "Metal–Metal Multiple Bonded Intermediates in Catalysis," *Journal of Chemical Sciences*, vol. 127, no. 2, pp. 209–214, 2015.

[21] C. Ganesamoorthy, C. Wölper, A. S. Nizovtsev, and S. Schulz, "Synthesis and Structural Characterization of Magnesium-Substituted Polystibides [(LMg)$_4$Sb$_8$]," *Angewandte Chemie*, vol. 128, no. 13, pp. 4276–4281, 2016.

[22] C. Ganesamoorthy, J. Krüger, C. Wölper, A. S. Nizovtsev, and S. Schulz, "Reduction of [Cp*Sb]$_4$ with Subvalent Main-Group Metal Reductants: Syntheses and Structures of [(L1Mg)$_4$(Sb$_4$)] and [(L2Ga)$_2$(Sb$_4$)] Containing Edge-Missing Sb$_4$ Units," *Chemistry–A European Journal*, vol. 23, no. 10, pp. 2461–2468, 2017.

[23] T. J. Hadlington and C. Jones, "A Singly Bonded Amido-Distannyne: H$_2$ Activation and Isocyanide Coordination," *Chemical Communications*, vol. 50, no. 18, pp. 2321–2323, 2014.

[24] A. F. Holleman and E. Wiberg, *Holleman-Wiberg Lehrbuch der Anorganischen Chemie*. Walter de Gruyter, 1971.

[25] F. Reiß, A. Schulz, A. Villinger, and N. Weding, "Synthesis of Sterically Encumbered 2, 4-Bis-m-Terphenyl-1, 3-Dichloro-2, 4-Cyclo-Dipnictadiazanes [m-TerNPnCl]$_2$,(Pn= P, As)," *Dalton Transactions*, vol. 39, no. 41, pp. 9962–9972, 2010.

[26] G. Fischer, S. Herler, P. Mayer, A. Schulz, A. Villinger, and J. J. Weigand, "Mono-, Di-, and Tricoordinated Phosphorus Attached to a N- N Unit: An Experimental and Theoretical Study," *Inorganic Chemistry*, vol. 44, no. 6, pp. 1740–1751, 2005.

[27] A. Brandl and H. Nöth, "Beiträge zur Chemie des Bors, 191. Additions-und Insertionsreaktionen von Amino-imino-boranen mit Elementtrihalogeniden der 5. Hauptgruppe," *Chemische Berichte*, vol. 121, no. 7, pp. 1321–1327, 1988.

[28] U. Braun, T. Habereder, and H. Nöth, "Lithium tert-Butyl [Phenyl (2, 2, 6, 6-tetramethylpiperidino)Boryl] Amide: A Versatile Reagent," *European Journal of Inorganic Chemistry*, vol. 2004, no. 18, pp. 3629–3643, 2004.

[29] N. Burford, T. S. Cameron, C. L. Macdonald, K. N. Robertson, R. Schurko, D. Walsh, R. McDonald, and R. E. Wasylishen, "Dissociation of 2, 4-bis (2, 4, 6-tri-tert-butylphenyl)-Cyclo-1, 3-dipnicta-2, 4-diazanes (Pnict = P, As, Sb) Imposed by Substituent Steric Strain: A Cyclobutane/Olefin Analogy," *Inorganic Chemistry*, vol. 44, no. 22, pp. 8058–8064, 2005.

[30] A. Schulz, P. Mayer, and A. Villinger, "An Unusual Reaction: a GaCl$_3$-Assisted Methyl/Chlorine Exchange in Silylated Hydrazinodichloroarsane," *Inorganic Chemistry*, vol. 46, no. 20, pp. 8316–8322, 2007.

[31] D. Michalik, A. Schulz, and A. Villinger, "Lewis-Acid-Assisted Methyl Exchange Reactions In Silylated Aminodichloroarsanes," *Inorganic Chemistry*, vol. 47, no. 24, pp. 11798–11806, 2008.

[32] A. Hinz, A. Schulz, A. Villinger, and J.-M. Wolter, "Cyclo-Pnicta-Triazanes: Biradicaloids or Zwitterions?," *Journal of the American Chemical Society*, vol. 137, no. 11, pp. 3975–3980, 2015.

[33] A. Hinz, A. Schulz, and A. Villinger, "Synthesis of a Molecule with Four Different Adjacent Pnictogens," *Chemistry–A European Journal*, vol. 22, no. 35, pp. 12266–12269, 2016.

[34] C. Jongsma and H. van der Meer, "The Structure of Arsanthrene (9, 10-Diarsaanthracene)," *Tetrahedron Letters*, vol. 11, no. 16, pp. 1323–1324, 1970.

[35] G. Becker, G. Gutekunst, and C. Witthauer, "Molekül-und Kristallstruktur des Tetrakis (trimethylsilyl)-diarsans (Trimethylsilylverbindungen der Vb-Elemente; 2)," 1982.

[36] A. L. Rheingold, D. L. Staley, and M. E. Fountain, "Pentafluorophenylarsines. The Crystal and Molecular Structures of Tetrakis (Pentafluorophenyl) Diarsine,(C$_6$F$_5$)$_2$AsAs(C$_6$F$_5$)$_2$, Tetrakis(Pentafluorophenyl)Diarsenic(III) Oxide,(C$_6$F$_5$)$_2$AsOAs(C$_6$F$_5$)$_2$, and Tris(pentafluorophenyl)Arsine," *Journal of Organometallic Chemistry*, vol. 365, no. 1-2, pp. 123–135, 1989.

[37] H. Chen, M. M. Olmstead, D. C. Pestana, and P. P. Power, "Reactions of Low-Coordinate Transition-Metal Amides with Secondary Phosphanes and Arsanes: Synthesis, Structural, and Spectroscopic Studies of [M {N(SiMe$_3$)$_2$}(μ-PMes$_2$)]$_2$ (M= Manganese, Iron), [Mn {N(SiMe$_3$)2}(μ-AsMes$_2$)]$_2$ and Mes$_2$AsAsMes$_2$," *Inorganic Chemistry*, vol. 30, no. 8, pp. 1783–1787, 1991.

[38] G. Becker, M. Schmidt, and M. Westerhausen, "Acyl-und Alkylidenarsane. VII. Tetrakis (2, 2-dimethylpropionyl) Diarsan-Darstellung und Struktur," *Zeitschrift für anorganische und allgemeine Chemie*, vol. 607, no. 1, pp. 101–108, 1992.

[39] G. Becker, W. Golla, J. Grobe, K. W. Klinkhammer, D. Le Van, A. H. Maulitz, O. Mundt, H. Oberhammer, and M. Sachs, "Element-Element Bonds. IX. 1 Structures of Tetrakis (Trifluoromethyl) Diphosphane and -Diarsane: Experimental and Theoretical Investigations," *Inorganic Chemistry*, vol. 38, no. 6, pp. 1099–1107, 1999.

[40] C. Jones and T. C. Williams, "Reactions of 2-Arsa-and 2-Stiba-1, 3-Dionato Lithium Complexes with Group 4–7 Metal Halides," *Journal of Organometallic Chemistry*, vol. 689, no. 9, pp. 1648–1656, 2004.

[41] A. Schulz and A. Villinger, "Tetrazarsoles—A New Class of Binary Arsenic–Nitrogen Heterocycles," *Angewandte Chemie International Edition*, vol. 47, no. 3, pp. 603–606, 2008.

[42] M. Lehmann, A. Schulz, and A. Villinger, "Synthesis and Characterization of 1, 3-Dihalogeno-2, 4-bis (2, 4, 6-tri-tert-butylphenyl)-cyclo-1, 3-distiba-2, 4-diazanes, [X–Sb (μ-NR)]$_2$ (X= F, Cl, Br, and I)," *European Journal of Inorganic Chemistry*, vol. 2010, no. 35, pp. 5501–5508, 2010.

[43] M. Lehmann, A. Schulz, and A. Villinger, "An Unusual Isomerization to Tetraazastiboles," *Angewandte Chemie International Edition*, vol. 50, no. 22, pp. 5221–5224, 2011.

[44] C. Hering, M. Lehmann, A. Schulz, and A. Villinger, "Chlorine/Methyl Exchange Reactions in Silylated Aminostibanes: A New Route To Stibinostibonium Cations," *Inorganic Chemistry*, vol. 51, no. 15, pp. 8212–8224, 2012.

[45] J. Li, C. Schenk, F. Winter, H. Scherer, N. Trapp, A. Higelin, S. Keller, R. Pöttgen, I. Krossing, and C. Jones, "Weak Arene Stabilization of Bulky Amido-Germanium(II) and Tin(II) Monocations," *Angewandte Chemie International Edition*, vol. 51, no. 38, pp. 9557–9561, 2012.

[46] X. Ma, Y. Ding, H. W. Roesky, S. Sun, and Z. Yang, "Synthesis and Crystal Structures of Antimony(III) Complexes with a Bis (Amino) Silane Ligand," *Zeitschrift für anorganische und allgemeine Chemie*, vol. 639, no. 1, pp. 49–52, 2013.

[47] C. Hering-Junghans, A. Schulz, and A. Villinger, "A Neutral Low-Coordinate Heterocyclic Bismuth-Tin Species," *Chemical Communications*, vol. 51, no. 72, pp. 13834–13837, 2015.

[48] D. Michalik, A. Schulz, and A. Villinger, "Dichlorocyclodibismadiazane," *Angewandte Chemie International Edition*, vol. 49, no. 41, pp. 7575–7577, 2010.

[49] C. Hering-Junghans, A. Schulz, M. Thomas, and A. Villinger, "Synthesis of Mono-, di-, and Triaminobismuthanes and Observation of C–C coupling of Aromatic Systems with Bismuth(III) Chloride," *Dalton Transactions*, vol. 45, no. 14, pp. 6053–6059, 2016.

[50] J. Bresien, C. Hering-Junghans, A. Schulz, M. Thomas, and A. Villinger, "Reactivity of TerN(SiMe$_3$)BiCl_Synthesis of an Aminobismuthenium Cation and TerN(SiMe$_3$)Bi (N$_3$)$_2$," *Organometallics*, vol. 37, no. 15, pp. 2571–2580, 2018.

Appendix

All manipulations were carried out using standard Schlenk and glove box techniques under an atmosphere of high purity dinitrogen. Diethyl ether and pentane were distilled over Na/K alloy (25:75), while THF, hexane, heptane and toluene were distilled over molten potassium. ^{1}H, ^{13}C{^{1}H}, ^{29}Si{^{1}H}, and ^{11}B{^{1}H} NMR spectra were recorded on either Bruker DPX300, Bruker Avance III 400 or Bruker Avance III 600 spectrometers at 298 K (unless otherwise stated), and were referenced to the resonances of the solvent used. Mass spectra were run using an Agilent Technologies 5975D inert MSD with a solid-state probe. IR spectra were recorded for solid samples using an Agilent Cary 630 attenuated total reflectance (ATR) spectrometer. Melting points were determined in sealed glass capillaries under dinitrogen, and are uncorrected. Micro analyses were carried out by London Metropolitan University.